Contents

89

Part I

Introduction

Abstract

Hydrogen production through water splitting thermochemical cycles powered with renewable energy represents the concrete possibility of obtaining an actually carbon free fuel. While since the 80's several thermochemical cycles have been proposed in the literature, only few of them appear today as industrially feasible. Among these, the Hybrid Sulfur (HyS) cycle is considered as particularly promising.

Such cycle involves two main steps. In a first low-temperature (below 100 °C) step, H_2O and SO_2 are electrochemically reacted to produce H_2 and H_2SO_4 in a process called *Sulfur Dioxide Depolarized Electrolysis* (SDE). The standard cell potential of SDE is about 85% lower than that of liquid water electrolysis, which may entail a significant reduction of the electrical power required. In the high-temperature thermochemical step, H_2SO_4 is thermally vaporized and decomposed into SO_3 and H_2O; subsequently, SO_3 is thermally decomposed (above 800 °C) in the presence of a catalyst to produce O_2 and SO_2, which is recycled to SDE to close the cycle.

The HyS cycle was initially conceived to be powered with high temperature nuclear heat and several technological and process challenges must be faced in order to replace the continuous nuclear source with solar energy, which is characterized by natural fluctuations. SOL2HY2 is a research project ended in November 2016 and co-funded by the Fuel Cells and Hydrogen Joint Undertaking (FCH JU) within the Seventh Framework Programme for Research and Technological Development (FP7). The project focused on applied bottle-neck solving, materials research, development and demonstration of the relevant key components of the *solar-powered HyS water splitting cycle*, i.e. the sulfur depolarized electrolyzer and the reactor for solar-powered SO_3 decomposition. The project also aimed at providing tools for the simulation and optimization of the solar HyS cycle as well as developing a techno-economic assessment of the whole process.

The present PhD project was funded by ENEA within the framework of the SOL2HY2 project and is focused on the study of the solar HyS cycle.

After a preliminary review of hydrogen production processes, in particular

of water splitting thermochemical cycles, the PhD work has been articulated in two main parts: a first part focused on the theoretical and experimental study of the high-temperature section of the cycle, and a second one focused on the process analysis and techno-economic assessment of the whole Solar-powered Hybrid-Sulfur process.

The first part is particularly devoted to the selection and development of the catalyst for the SO_3 decomposition reaction. The choice of the catalyst has taken into account the features required for the use in a high temperature adiabatic reactor subjected to daily thermal cycles, as expected for the specific application considered. Compared to other catalysts suggested in the literature, Fe_2O_3 supported by $\gamma - Al_2O_3$ pellets has exhibited, in the operating conditions of interest, better or similar performance in terms of stability and activity with a greater cost-effectiveness, lower toxicity, easier and cheaper large-scale production. Such catalyst was tested in a laboratory reactor under realistic operating conditions (temperature 925-1000 °C, pressure 1-3 atm, WHSVs 22-33 h^{-1} and feed sulfuric acid concentration 50 % w/w) and has shown a notable catalytic activity (about 70% SO_3 conversion at 1000°C and 1 atm with 50% sulfuric acid), good stability over a total of more than 100 hours on stream, even including several stand-by phases in which the catalyst was subjected to thermal cycling from operating to room temperature.

The results obtained have been processed to analyze the reaction kinetics. In order to determine the kinetic parameters of the reaction, a simple reactor model was used and the reaction rate was evaluated by assuming the SO_3 decomposition as an elementary equilibrium reaction, which led to a calculated activation energy of about 148 kJ/mol. Since the catalyst developed can be used as-is in a prototype or full scale reactor in the same range of operating conditions explored, the kinetic expression obtained is useful to design and predict the performance of an actual SO_3 decomposition reactor. Indeed, such expression was used by DLR to design the demo SO_3 decomposition reactor developed within the SOL2HY2 project.

Moreover, the catalyst production procedure was upscaled in order to provide all the catalyst used in the demo reactor (about 20 kg); in so doing, the procedure has been carefully adjusted to ensure a good support coating, and therefore catalytic activity, without being costly and time expensive in case of larger-scale production.

The PhD project also involved active participation (for a period of three months) to the latest phases of the installation of the demo plant at DLR's solar tower in Juelich, Germany. During this period, some preliminary on-sun tests were also performed in cooperation with DLR's staff. Such tests were aimed at the thermal characterization of the solar receiver-reactor system

for sulfuric acid decomposition and were carried out without catalyst in the system. The obtained results were crucial to identify issues in the original plant configuration and were used to suggested modifications to the plant layout, which were implemented by DLR in a subsequent experimental stage.

The second part of the PhD work has been focused on the process analysis and techno-economic assessment of the Solar-powered Hybrid-Sulfur cycle. In this context, the HyS process was studied block-wise in order to identify the best process options for each part of the plant. AspenPlus®flowsheets were developed for all process blocks and used to simulate the plant operation in order to determine the energy required for hydrogen production. The total energy consumption of the proposed process resulted equal to 870 kJ/mol of produced hydrogen. In particular, three energy types are required by the process: power (42%), high-temperature heat (23%) and medium-temperature heat (35%), which gives a thermochemical efficiency in excess of 19%.

Furthermore, the sizing and costing of the main equipment employed in the process has been carried out in order to allow the final economical evaluation of process. Different options for the integration the HyS plant with Concentrating Solar Thermal (CST) systems have been identified. The possibility to integrate other energy sources, such as heat obtained through sulfur burning and Photovoltaic (PV) technologies, has also been considered.

The economic performance of the solar HyS plant was assessed in several scenarios including different plant locations and combinations of (renewable and conventional) energy sources. Plant capacities in the range of 2.6 to 7.6 t/d of hydrogen were considered. Hydrogen production costs in the range 8 €/kg to about 13 €/kg have been found, with the highest values corresponding to 100% renewable hydrogen. The lowest prices are obtained with the synergistic use of PV, heat from sulfur burning process and CST technology, which leads to a promising performance of the SOL2HY2 cycle. The costs obtained are still high compared to conventional hydrogen production processes like methane steam reforming, but are in line with the current targets set by the Fuel Cells and Hydrogen Joint Undertaking (FCH-JU) for the hydrogen production by high temperature water splitting. Furthermore the cost analysis carried out is based on some conservative hypotheses. Firstly, valorization of oxygen co-produced with hydrogen is not considered. Furthermore, SO_2 and S from external sources required in some process configurations are assumed to be bought at market prices, while for some plant locations such chemicals could be available at a much lower or even at no cost.

Chapter 1

Hydrogen: production and uses

The global energy sector is currently in a transition period: after a massive exploitation of fossil resources, in order to limit their well-known ecological and economic problems, it is looking for an energy system where the contribution of renewable sources is substantial. In this scenario, Hydrogen and its uses seem to be very promising. It is a gas which burns in air producing water and heat, without other undesirable by-products. H_2 can be product both by fossil sources and renewable ones, and also by nuclear source. It can be can distributed over the network fairly easily, compatibly with end uses and with the development of suitable transport and storage technologies; finally, it can be employed for many different application, as electrical energy production both centralized and distributed, heat production and in the transport sector, with a zero or extremely small local impact. Hence, Hydrogen represents an ideal component of a future sustainable energy system; it is an incentive to widespread use of renewable sources, but in the short to medium term it can make fossil fuels compatible with environmental requirements. Being an energy carrier, H_2 can have a complementary role to that of electricity, but with the advantage that it can be stored and then transported. Consequently it can pave the way for renewable energy sources worldwide, giving to Third World Countries the opportunity of exporting energy and so allowing them greater independence from exporting states of fossil fuels [eniscuola, 2011].

1.1 Introduction to Hydrogen

Hydrogen is the most abundant element in the Universe where existing into stars, which use it as a fuel to produce energy by fusion process, and in the interstellar space. On the Earth H_2, as single molecules, exists just in little amount in the high levels of the atmosphere and volcanic fumes, because the

Earth's gravitational pull is not able of holding such light molecules. Instead, it exists in enormous amount as molecule arranged with other ones: water is a prime example. Arranged with Carbon, Oxygen and other elements, represents one of the main constituent of animal and plant worlds. In the field of organic chemistry, millions of hydrogen-based compounds, from the simplest hydrocarbon, i.e. methane, to complex molecules of proteins. Hence, Hydrogen is the third most abundant element, after oxygen and silicon, on Earth.

Officially, Hydrogen was discovered in 1766 by English chemist and physicist Henry Cavendish (1731-1810), but most likely, it had already been "discovered" many times before 1766 [chemistryexplained, 2017]. Indeed many of early chemists reported finding a "flammable gas" in some of their experiments. For example in 1671, English chemist Robert Boyle (1627-91) described experiments in which, by adding Iron to hydrochloric acid and sulfuric acid, a gas that burned easily with a pale blue flame was produced. The problem of these first discoveries was that chemists did not understand very well the nature of gases: they didn't think that many kinds of gases could exist but mistook them just for special forms of air with impurities. Cavendish discovered hydrogen over experiments like those ones performed by Boyle, with Iron metal in presence of different acids. Really, Cavendish thought that the produced flammable gas came from the Iron. Only later when chemists showed that Iron was itself an element, it was clear that the Hydrogen in Cavendish's experiment came from the acid. The name Hydrogen was attributed by the French chemist Antoine-Laurent Lavoisier (1743-94) because it was a "water former".

Hydrogen or Protium is the simplest of all elements: the first one in the periodic table, its atom (symbol H) consists of a nucleus with one proton and one electron, so its atomic number (number of protons plus neutrons in the nucleus) is 1. Even if Protium is the most common form of hydrogen, being about 99.98 percent of the Hydrogen in nature, there are other two hydrogen isotopes: Deuterium with atomic number 2, wich is about 0.015% of the Hydrogen in nature, and Tritium with atomic number 3, wich appears in small quantities in nature but can be artificially produced by various nuclear reactions.

In normal conditions Hydrogen is a diatomic molecules,H_2, with a molecular weight of 2.01594 and is a colorless, odorless, tasteless gas. Its density, 0.08999 grams per liter, is the lowest of any chemical element. H_2changes from a gas to a liquid at a temperature of -252.77°C and from a liquid to a solid at a temperature of -259.2°C [Stwertka, 2002].

It is slightly soluble in water, alcohol, and a few other common liquids. It burns in air or oxygen to produce water. It also combines readily with other

non-metals, such as Sulfur, Phosphorus, and the halogens.

At normal temperature hydrogen is a not very reactive substance, unless it has been activated by an appropriate catalyser, for example Platinum, or by an electric spark . Instead, at high temperatures it dissociates into free atoms and it is highly reactive. Atomic hydrogen is a powerful reductive agent, even at ambient temperature. It reacts with the oxides and chlorides of many metals, like Silver, Copper, Lead, Bismuth and Mercury, to produce free metals. Hydrogen reduces some salts to their metallic state, like nitrates, nitrites and sodium and potassium cyanide. It reacts with metals and non-metals to produce hydrides, like NaH, KH, H_2S and PH_3. Atomic hydrogen with Oxygen produces Hydrogen peroxide (H_2O_2). It also reacts with organic compounds to form a complex mixture of products, for istance with etilene (C_2H_4) the products are ethane (C_2H_6), and butane (C_4H_{10}). The heat released when the hydrogen atoms recombine to form the hydrogen molecules is used to obtain high temperatures in atomic Hydrogen welding .

The obvious source for forming hydrogen, is water. Nevertheless, a lot of energy is required to split a water molecule and it makes the Hydrogen production by water splitting not economical to perform .

Hower, many other methods can be used to produce Hydrogen starting from the different sources, both fossil ones like hydrocarbons and renewable ones like biomasses, which contain it.

1.2 Uses of Hydrogen: benefits and issues

The H_2 use, both as raw material and fuel, is known for several years. In the past it was long employed for filling ballons, however due to its high flammability it has been replaced by Helium.

Hydrogen is widely used in the industrial context, as raw material. Its most important use is in the manufacture of Ammonia (NH_3), where H_2 reacts with N_2 at high pressure and temperature in the presence of a catalyst. NH_3 is a very important compound because it is used for many products manifacture, like fertilizers. Hydrogen is also used for other similar processes. For example, it can be combined with Carbon monoxide to form Methanol, methyl alcohol, or wood alcohol. Like Ammonia, Methanol has a great many practical uses in a variety of industries. The most important use of methanol is in the manufacture of other chemicals, such as those used for plastics production. Small amounts of it, are used as additives to gasoline to reduce the amount of pollution released to the environment. Methanol is also used widely as a solvent in industry.

Hydrogen, in form of Tritium, is used in the manufacture of fusion bombs.

Another important H_2 application is the production of pure metals. Hydrogen gas is passed over a hot metal oxide to produce the pure metal: for example, Molybdenum can be prepared by passing hydrogen over hot molybdenum oxide.

Furthermore, Hydrogen is employed in the refinery industry in Hydrotreating/Hydrocracking plants, in the metallurgical, glass and electronics industries where, thanks to its remarkable reduction capacity, it guarantees the purity of the product. Recently, H_2 has also been used in recycling plastics, which is melted, hydrogenated and subjected to craking in order to produce lighter molecules for forming new polymers.

The Hydrogen combustion occurs with a non-luminous flame, it has not characterized by particular problems and generates polluting emissions much lower than those of other fuels, indeed the the only polluting product is the Nitrogen oxides that are formed, in little amount, due to combustion temperatures. Since the energy to supply for H_2 ignition in air is not much high, considerably lower than that required in the case of methane for example, Hydrogen is particularly suitable for being used in the low-temperature catalytic heaters.

Mixed with CO, in the range 50-70%, H_2 forms the so-called "city gas" that has been widely used as domestic gas in the most developed countries before methane became available on large scale.

Any hydrocarbon to which Hydrogen is added, improves its combustion and efficiency. For this reason, in the United States, the use of Methane with a 15% of H_2, defined Hythane, has been evaluated [Ma et al., 2010].

The Hydrogen is also ideal to be used as fuel in fuel cells. Invented in 1839 Chan [2007], the fuel cells are currently the subject of industry research, thanks to the spatial sector, which has rekindled interest in them in the 1960s after a century of oblivion. A fuel cell is an electrochemical device that, like a normal battery, transforms chemical energy into d.c. electric energy, which can be used directly to power an electric load (for example, an electric motor). The main difference, compared to a normal accumulator, is that while the electrode in a battery is itself consumed during discharge and must be regenerated over charging, in the fuel cell the electrodes are not consumed, but are only the support for chemical reactions, since the reagents (Hydrogen and Oxygen) are fed from the outside continuously. The fuel cells, like the low-temperature catalytic heaters, have the advantage to not produce, or just in little amount however, NO_x.

The area where research, about the H_2 use as fuel, has focused mostly is transport. In the context of air transport, effort has been made to exploit its high energy content and the low weight.

The liquid Hydrogen combined with liquid Oxygen, is being used for years

in NASA space programmes as propellant for Space Shuttles. A Shuttle is equipped with fuel celles that produce both electric energy and water for on-board use. H_2 use has been experimented in the field of military aviation since 1957, when the first Hydrogen-powered bomber was built in the United States. In 1988 the Soviet Union realized a Tupolev-154 fuelled by liquid Hydrogen [Serfass et al., 1991]. More recently Japan has been involved in the realization of an Hydrogen supersonic/hypersonic aereo prototype. New studies on direct steam generators and high temperature turbines, have demonstrated the possibility of using H_2 in devices operating under innovative high performance thermodynamic cycles.

In the context of automotive, the H_2 use has been tested both in internal combustion engines, where a normal combustion process occurs with the transformation of chemical energy into thermal energy and subsequent into work, and in the fuel cells, where the chemical energy of fuel is directly converted into electrical energy, which is fed to an electric engine.

Obstacle to the development of Hydrogen as an energy carrier is mainly the difficulty of transport and storage, due to its low energy density and extreme volatility, and for safety reasons associated with flammability and explosion. With regard to this latter aspect, however, a more careful analysis can reduce the concept of Hydrogen hazard [eniscuola, 2011].

This gas is less flammable than gasoline (it has a higher self-ignition temperature). It is the lightest of the elements and therefore is diluted and dispersed very quickly in open spaces. To detonate H_2 is practically impossible, except in confined spaces (to detect potentially hazardous concentrations, sensors can easily be operated with adequate security systems). Moreover when Hydrogen burns consumes very quickly, instead materials such as gasoline, diesel, LPG, or natural gas are heavier than air and, without being dispersed, remain a source of danger for much longer times. H_2,contrary to fossil fuels, is not toxic and not corrosive, and any possible leakage from storage tanks doesn't cause pollution of the ground or underground aquifers.

Many solutions have been identified for the Hydrogen storage. The liquefaction method is not the best solution in terms of "energy cost", due the very low melting temperature (about -253°C) of H_2, even if its use in addition to other technologies, could be advantageous. The most used method is the storage in high pressure cylinders (200-300 bar). Heavy industrial cylinders can be advantageously replaced by double-wall aluminum ones [Ruberti, 2000].

For consumption at homes and industries, dedicated hydrogen-pipelines or customized methane-pipelines can be use. Germany, Belgium and France have developed nearly 2000 km of hydrogen-pipelines, currently used by the chemical industry, and also in the United Kingdom, the United States and

southern Italy are already available some sections [ENEA, 2003]. The advantage of this system is given by the flow rate. Since Hydrogen produces an amount of energy per unit of weight that is 2.5 times lower than that of Methane, but is also 2.8 times faster than this last, it carries approximately the same amount of energy in the unit of time. However for the same reason, H_2 requires a a pressure of pumping 3 times higher than that for Methane. Moreover, due to its lower density, Hydrogen needs a pipelines-diameter bigger than that required by CH_4 (2 m versus 1.4 m).

Two technologies that could solve with sufficient security, convenience and cost-effectiveness are the cave storage (already experienced in the past with methane) and the use of glass balls Tzimas et al. [2003]. This latest technology is based on the use of the glass feature to be impermeable to hydrogen at room temperature, while becoming porous at some hundreds of degrees Celsius. So far this technology has been studied at a theoretical level, but it seems to offer great possibilities.

A technology suitable for the transport sector, is the adoption of carbon nanotubes, structures resulting from fullerenes technology Tzimas et al. [2003]. Already in a recent past a technique of Hydrogen absorption inside particular carbons, processed to obtain high porosity, has been developed. These are characterized by the ability to absorb hydrogen significantly, at few tens of bar and at temperature below -150 °C.

Hydrogen can be transported in the liquid form, if the system is adequately insulated in double-skin tanks with an air gap between the walls. The H_2 low chemical reactivity at low temperature, eliminates the problem of metal fractures by forming hydrides. Double wall pipes are also used, but only for short distances, due to the high production costs.

A method for the transport and storage, that has already proved its validity, is based on the property of Hydrogen to form hydrides with metals. Often the reaction occurs spontaneously at room temperature. The phenomenon proceeds in both directions and essentially depends on the H_2 gas pressure. The absorption capacity by hydrides allows, at equal volume, higher performance than that of Hydrogen liquid storage method. Hydrogen can also be accumulated by combining it with some organic compounds. Particularly the use of Toluene, with Methylcyclohexane formation by hydrogenation, is promising since both Toluene and Methylcyclohexane are known and easily transportable in safety. For the weight and size of the equipment this technique is suitable for seasonal accumulation or for use on heavy vehicles.

1.3 Production of Hydrogen

Hydrogen can be produced by a wide variety of methods, starting from different raw materials, and energy input options. Particularly, with respect to input energy resources the hydrogen production methods can be classified, as proposed by literature [Celik and Yildiz, 2017] under four main groups: electrical, thermal, biological, and hybrid methods.

1.3.1 Electrical methods

Electrolysis and plasma arc decomposition, being powered just by electrical energy, are electrical methods of Hydrogen production.

1.3.1.1 Electrolysis

Electrolysis is the most effective and well-known water splitting method, in commercial use already a few years before 1900. Pure water and electricity are the only feeds needed to produce electrolytic hydrogen. The use of renewable energy sources such as wind, solar or geothermal for a greener Hydrogen production would be theoretically desirable, but practically these technologies are nowadays not cost-effective for large-scale production. On the other hand, the use of electricity produced by fossil fuels leads to an hydrogen production cost 3-5 times greater compared to that of direct production by them (for istance hydrogen obtained by steam reforming of fossil fuel). Despite the economic uncompetitiveness electrolysis has several advantages, mainly its operation flexibility and the high purity of hydrogen produced. Purity is a very important feature for hydrogen employment in some types of fuel cells. The most important aspect of electrolysis is that it turn an energy carrier widely used and distributed, but which cannot be stored, i.e. electrical energy, in an energy carrier of high value and versatility, i.e. Hydrogen, which can be accumulated and possibly converted into the previous carrier. The device where electrolysis happens is the electrolytic cell. It consists of two electrodes, one positive and one negative, electrically connected and soaked in a current conducting liquid, the electrolyte, which usually consists of an aqueous solution of salts, acids or bases contained in a metal tub. A separator, wich internally separates the tub in two parts, completes the cell.

Basically, an electricity current is fed to the electrodes and electron movement occurs. The reaction can be written as follows:

$$H_2O + \text{electricity} \rightarrow H_2 + \frac{1}{2}O_2 \tag{1.1}$$

The commercial electrolysers consist of a number of electrolytic cells arranged in a cell stack.

The main electrolysis cell system is alkaline electrolysis which is the state-of-the-art and is a widely used method in industry [Celik and Yildiz, 2017]. Alkaline electrolysers use a aqueous KOH solution as electrolyte. It represents a mature technology, mainly suited for stationary applications and available at operating pressures up to 25 bar [Riis et al., 2006].

Inside the alkaline electrolysis cell the following reactions take place:

Electrolyte

$$4H_2O \rightarrow 4H^+ + 4OH^-$$

Cathode

$$4H^+ + 4e^- \rightarrow 2H_2$$

Anode

$$4OH^- \rightarrow O_2 + 2H_2O + 4e^-$$

The net reaction is the splitting of water (reaction 1.1)

Other technologies like polymer membrane (PEM) electrolysis and many cell systems underdevelopment exist as alternative methods.

The PEM electrolysers require no liquid electrolyte but an acidic polymer membrane is empoyed, and this feature simplifies the design significantly.

Inside a PEM electrolysis cell the following reactions take place:

Anode

$$H_2O \rightarrow \frac{1}{2}O_2 + 2H^+ + 2e^-$$

Cathode

$$2H^+ + 2e^- \rightarrow H_2$$

PEM electrolysers can potentially be designed for operating pressures up to several hundred bar, and are suited for both stationary and mobile applications [Riis et al., 2006]. The main advantages of PEM compared to alkaline electrolysers are the major safety due to the absence of KOH electrolytes, a more compact design due to higher densities and higher operating pressures.

Nevertheless for its relatively high cost, low capacity, poor efficiency and short lifetimes, the PEM electrolysers currently available are not as mature as alkaline electrolysers.

1.3.1.2 Plasma arc decomposition

Plasma is an ionized state of matter which contains electrons in an excited state and atomic species. It has a potential to be used as medium for high voltage electric current release due the presence of electrically charged particles. Natural gas (mostly methane) dissociates to hydrogen and carbonblack

as a result of thermal plasma activity. Carbonblack is in solid phase which remains at the bottom whilehydrogen is collected in gas phase. The decomposition reaction of methane to hydrogen and carbon is written as

$$CH_4 \rightarrow C_{(s)} + 2H_{2(g)} \quad \Delta H = 74.6 \text{ MJ/kmol}$$

Plasma arc decomposition can be classified as " high temperature pyrolysis " and has a potential to reduce hydrogen production cost by at least 5%, compared to large-scale steam methane reforming with carbon dioxide sequestration [Dincer and Acar, 2015].

1.3.2 Thermal methods

The thermal methods for Hydrogen production, are those requiring just thermal energy to occur; steam reforming, partial oxidation, autothermal reforming, gasification, conversion of biomass, thermolysis and thermochemical water splitting are all processes belonging to this category.

1.3.2.1 Steam reforming

The main process to produce hydrogen by hydrocarbons is the steam reforming. This process involves the conversion of light hydrocarbon and water vapor to hydrogen and carbon dioxide. Among all the possible hydrocarbons, the natural gas, made primarily of methane, is the most suitable for hydrogen production because is easy to handle, has the highest hydrogen-carbon atomic ratio (4:1), generally has low sulfur content and is relatively inexpensive. The first stage of the process is the purification of the feed, mainly used to remove Sulfur. Subsequently, the chemical reaction occurs forming a mixture of hydrogen and carbon oxide, known as 'water gas'.

For a generic hydrocarbon whose molecule consists of n Carbon atoms and m hydrogen atoms the reaction is:

$$C_nH_m + nH_2O \rightleftharpoons nCO + \left(n + \frac{m}{2}\right) H_2$$

In the case of methane the reaction becomes:

$$CH_4 + H_2O \rightleftharpoons CO + 3H_2$$

This reaction is highly endothermic and requires temperatures in the range 760-925 °C and pressure close to 2 MPa.

In the reformer also occur the"water-gas shift" (reaction 1.2) and the "methanation" (reaction 1.3) reactions :

$$CO + H_2O \rightleftharpoons CO_2 + H_2 \tag{1.2}$$

$$CO + 3H_2 \rightleftharpoons CH_4 + H_2O \tag{1.3}$$

The product gas contains approximately 74%vol of H_2, 18%vol of CO, 6%vol of CO_2 and 2%vol of CH_4. Subsequently, this mixture is before cooled in an exchanger where heat the steam headed to the reformer, and then goes in a second reactor where is added water vapor in order to convert the CO to CO_2 , by reaction 1.2. The water-gas shift is an exothermic reaction and takes place in a temperature range of 200-400 °C. Normally this reaction occurs in two stages, at high and low temperature, and reduces CO content up to about 0.2-0.4%vol. In the last step of process CO_2 is separated from the gaseous mix. The steam reforming process needs two feeds: the hydrocarbons and the heat for the endothermic reaction. The heat is totally supplied by the hydrocarbon processing whose about 45% of consumption is destined for this purpose. The hydrogen is produced both from the hydrocarbon and from the water. The steam reforming is a technologically mature process.

1.3.2.2 Partial oxidation

The partial oxidation is an other technologically mature process for hydrogen production by hydrocarbons. It is consists of the partial combustion, exothermic, of heavy hydrocarbons (e.g refinery residue oils) with oxygen to yield carbon monoxide and hydrogen. Oxygen needs to be supplied pure, since its use in air mixture would involve contamination of hydrogen with nitrogen, which is extremely difficult to separate downstream due to low boiling temperatures. In order to not supply external energy inputs, the amount of oxygen and steam must be kept under control.

For a generic hydrocarbon whose molecule consists of n Carbon atoms and m hydrogen atoms the process consists of following reactions:

$$C_nH_m + \frac{n}{2}O_2 \rightleftharpoons nCO + \frac{m}{2}H_2 + \text{heat} \tag{1.4}$$

$$C_nH_m + nH_2O + \text{heat} \rightleftharpoons nCO + \left(n + \frac{m}{2}\right)H_2 \tag{1.5}$$

$$CO + H_2O \rightarrow CO_2 + H_2 + \text{heat} \tag{1.6}$$

The reaction 1.4 is exothermic and supplies the heat for reaction 1.5, which is the same of steam reforming and so is endothermic; the remaining thermal energy is ensured by combustion of a certain amount of hydrocarbon

fed. The use of methane is not very suitable for this process with respect to heavier hydrocarbons, whose prices are lower whose and availability will increase over time.

1.3.2.3 Autothermal reforming

Autothermal reforming is a combination of both steam reforming and partial oxidation. The total reaction (reaction) is exothermic, so not require an external energy resource. However, produced amount of hydrogen by this method is lower than that of steam reforming process and needs an air separation and oxygen purification unit since purified oxygen must be fed [Celik and Yildiz, 2017].

$$C_nH_m + \frac{n}{2}O_2 + nH_2O \rightleftharpoons nCO_2 + \left(n + \frac{m}{2}\right)H_2 \tag{1.7}$$

1.3.2.4 Gasification

Solid fuels like coal or biomass can be converted to hydrogen by gasification. Particularly, Hydrogen can be produced from coal through a variety of gasification processes, e.g. fixed bed, fluidised bed or entrained flow [Riis et al., 2006]. In practice, high-temperature entrained flow processes are favoured to maximise carbon conversion to gas, thus avoiding the formation of significant amounts of char, tars and phenols.The reaction underpin the process is the following:

$$C + H_2O \rightleftharpoons CO + H_2$$

Since this reaction is endothermic, additional heat is required, as with methane reforming. The CO is further converted to CO_2 through the water-gas shift reaction (reaction 1.2). Hydrogen production from coal is commercially mature, but it is more complex than the production of hydrogen from natural gas. The cost of the resulting hydrogen is also higher. But since coal is plentiful in many parts of the world and will probably be used as an energy source regardless, it is worthwhile to explore the development of clean technologies for its use.

1.3.2.5 Decarbonization of fossil fuels by concentrated solar thermal energy

The thermal energy required for the Hydrogen production by fossil fuels can be provided, as an alternative to conventional combustion, by solar energy collected and concentrated by Concentrating Solar Thermal thecnolo-

gies. The possible processes for the decarbonization by solar energy are three:'solar cracking', 'solar reforming' and 'solar gasification'.

The solar cracking consist of thermal decomposition of natural gas, fuel oil or other hydrocarbons and is represented by following net reaction:

$$C_xH_y \rightarrow xC_{(gr)} + \frac{y}{2}H_2$$

This reaction produces a rich carbon compound in condensed phase and hydrogen in the gaseous phase.

The use of solar energy in place of combustion of fuels for reactions brings some advantages: the release of pollutants is avoided, the gaseous products are not contaminated by impurities and the energy contained in the produced fuel is increased by solar energy of an amount equal to reaction enthalpy. Nonetheless, these are still processes related to the consumption of non-renewable sources.

1.3.2.6 Biomass conversion

Energy crops, agricultural waste, both animal and vegetable ones, forestry waste from harvesting and land clearing, industrial and municipal waste, are the main resources for biomass as a fuel. In biomass conversion processes, hydrogen is normally produced together with CO_2; however biomass is accounted for being CO_2 neutral because when is burned or converted, the Carbon dioxide emitted is absorbed during photosynthesis. None of the known processes has yet reached the development level necessary to be employed on industrial scale. Currently, the pathways followed are steam gasification (direct or indirect), entrained flow gasification, and more advanced concepts such as gasification in supercritical water, application of thermochemical cycles, or the conversion of intermediates (e.g. ethanol, bio-oil or torrified wood). Gasification and pyrolysis are considered the most promising medium-term technologies for the commercialisation of H_2 production from biomass Riis et al. [2006].

1.3.2.7 Thermolysis

Direct thermolysis consists in water splitting in a single thermal dissociation step, i.e. by supplying thermal energy only:

$$H_2O + \text{heat} \rightarrow H_2 + \frac{1}{2}O_2$$

Such process requires temperatures above 2500 K. For instance, a degree of dissociation of 64% can be obtained with a temperature of 3000 K (at 1 bar) [Dincer and Acar, 2015].

The challenges of this production method are related to the extremely high temperatures required, handling of the explosive H_2- O_2 mixture and separation of the two product gases. More specifically, the existing semi-permeable membranes can be used for the separation up to temperatures around 2500 K. Therefore, the mixture needs to be cooled down in very high temperature heat exchangers before being sent to the separation process.

Baykara [2004]conducted an experimental study on water thermolysis and achieved 90% of the equilibrium conversion with a residence time of 1 ms and an operating temperature of 2500 K. After fast cooling of product gases to 1500-2000 K, H_2 and O_2 were effectively separated by using palladium membranes.

Despite the mentioned research, the issues realated to this process are still far from being solved. Therefore, direct thermolysis currently appears as not viable for industrial implementation.

1.3.2.8 Thermochemical water splitting

Thermochemical water splitting processes use high-temperature heat (500-2000 °C) to drive a series of chemical reactions that produce hydrogen.

The chemicals used in the process are reused within each cycle, creating a closed loop that consumes only water and produces hydrogen and oxygen. The high temperatures required can be achieved by using Concentrated Solar Thermal (CST) energy or waste heat from generation IV nuclear reactors.

Several solar thermochemical water-splitting cycles have been investigated for hydrogen production, each with different sets of operating conditions, engineering challenges, and hydrogen production opportunities. The International Energy Agency has completed a common criterion η for assessing the efficiency of each of these, considering the relationship between the enthalpy to form a mole of water (285.9 kJ) and the total energy needed for the decomposition process (ΣQ)

$$\eta = \frac{\Delta H^{r}_{H_2O}}{\Sigma Q} \tag{1.8}$$

includes, in addition to thermal energy, all the possible forms of energy used in the different reactions.

Particularly, in literature, more than 300 water-splitting cycles have been described. On the basis of Brown's work [Brown et al., 2003] where all the cycles have been classified and compared according to objective criteria like number of reactions, availability of employed elements, maximum temperature of process, the Sulfur-based cycles, the Ca and Br-based cycles and metal oxide cycles have been identified as the most promising processes.

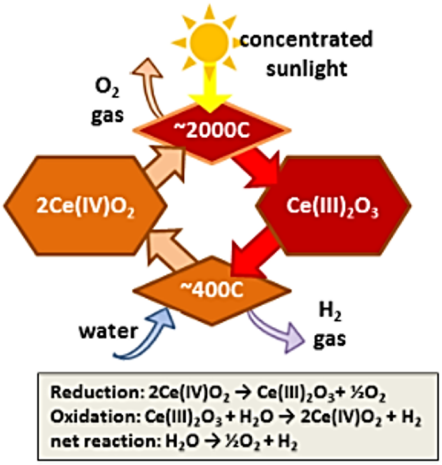

Figure 1.1: *A thermochemical cycle based on oxidation and reduction of cerium oxide particles. Reference: energy.gov [2017a]*

The general scheme of a thermochemical cycle may be expressed by following reactions:

$$H_2O + X \rightleftharpoons XO + H_2$$

$$XO \rightleftharpoons X + \frac{1}{2}O_2$$

where X represents one or more reagents that regenerate at each cycle. The net reaction is water splitting into hydrogen and oxygen. An example of thermochemical cycle powered by Solar energy is shown in Figure 1.1.

Exciting progress is continuing in this field, even if challenges remain about the research, development, and demonstration of commercially viable thermochemical cycles.

1.3.3 Biological methods

Dark fermentation, bio-photolysis, photo-fermentation and and artificil photosintesis belong to biological methods class.

1.3.3.1 Dark fermentation

Hydrogen can be produced by carbohydrate-rich substrates through the action of anaerobic bacteria, as Enterobacter, Bacillus, and Clostridium, in

environments without ligth Gürtekin [2014]. Indeed carbohydrates, mainly glucose, are the preferred carbon sources for fermentation processes, from which mainly acetic and butyric acids together with hydrogen gas are produced according to the unbalanced reaction:.

$$C_xH_yO_{z(\text{biomass})} + \text{bacteria enzyme} \rightarrow \text{organic acid} + CO_2 + H_2$$

Particularly, dark fermentation processes produce not pure H_2 but a mixed biogas containing primarily H_2 and Carbon dioxide, with eventually also lesser amounts of methane, Carbon monoxide, and/or Hydrogen sulfide. The first step of process is the hydrolysis of organic polymers to monomers, then acetogenic conversion of monomers to organic acids, alcohols, with release of hydrogen occurs. However, the requirement of organic biomass as a feedstock makes this process quite expensive. Many process conditions such as pH, hydraulic retention time (HRT), and gas partial pressure, affect highly the Hydrogen production by these bacteria, impacting on metabolic balance. The H_2 partial pressure of is extremely important for a continuous H_2 synthesis. Indeed, Hydrogen synthesis pathways are sensitive to H_2 concentrations and are subject to end-product inhibition.

1.3.3.2 Bio-photolysis

In photobiological processes, energy by solar radiation in the presence of microorganisms undergoes direct or indirect conversion into hydrogen. Cyanobacteria and green algae are able to carry out oxygen photosynthesis processes in natural conditions as well hydrogen secretion in anaerobic conditions. Production of hydrogen using these organisms may occur during direct or indirect biophotolysis of water [Moritz, 2012]. Particularly, over the direct biophotolysis, the conversion of water into oxygen and hydrogen occurs by using a key enzyme called Fe-hydrogenase which reduces protons to molecular hydrogen. Initially, solar radiation energy is captured by specific photosystems inside the chloroplasts of these microorganisms. During this process secretion of chlorophylls, accompanied by transferring the electron from the water molecule to Fe-hydrogenase via ferredoxine, occurs. Finally, hydrogenase reduces protons present in the reaction environment to molecular hydrogen. For the high sensitivity of Fe-hydrogenase to oxygen, this process occurs only in the presence of small amounts of oxygen (0.1% of the general partial pressure of gases).

The indirect biophotolysis of water is a more complex phenomenon. At first, the assimilation of CO_2 in the presence of sunlight (photosynthesis) takes place; next, in the presence of sunlight the collected organic matter is

used for secreting hydrogen with the presence of Fe-hydrogenase or nitrogenase enzyme.

1.3.3.3 Photo-fermentation

Photo-fermentation reaction consists of photonic-driven biochemical hydrogen production from water. By using photo-fermentation method, hydrogen can be produced in an aqueous media, under ambient temperature and pressure, and in presence of light-sensitive microorganisms according to the reaction:

$$C_6H_{12}O_6 + 6H_2O + \text{light} + \text{microorganism} \rightarrow 6CO_2 + 12H_2$$

Photosynthetic bacteria have long been studied for their capacity to produce significant amounts of hydrogen manly by using organic wastes in batch processes, continuous cultures, or immobilized whole cell system using different solid matrices like carrageenan, agar gel , porous glass, and polyurethane foam, as substrates [Moritz, 2012]. The advantage of this method are that oxygen does not inhibit the process. The disadvantages are: the limited availability of organic acids, the nitrogenase enzyme is slow, the process requires a relatively high amount of energy, and hydrogen re-oxidation. To increase the nitrogenase activity and decrease the energy requirements, the proper ratio of carbon to nitrogen nutrients must be maintained. Another major factor affecting the photo-fermentation process is light intensity. Although an increase in light intensity has shown some stimulatory effect on the overall hydrogen production rate of photosynthetic micro-organisms, an adverse effect was also reported on their light conversion efficiency at high light intensities. However, the light conversion efficiency can be improved by genetic manipulation of the light-harvesting antennae, thereby reducing the saturation effect of light [Moritz, 2012].

1.3.3.4 Artificial photosynthesis

Artificial photosynthesis is a bio-mimetic process mimicking the natural photosynthesis process, able to reach different objectives:

- PV-based electricity generation to support the grid system.
- Dry agriculture. Indeed with this method, carbohydrates (food), liquid fuels, chemical feed stocks, and polymers for fiber manufacture can be produced with an amount of used water thousands of times lower than that necessary for conventional agriculture. The system

has an enzyme bed reactor system which fixes CO_2 from the air (or other convenientsources) and it is powered by hydrogen and bioelectric transducers.

- Hydrogen production through the electrolytic decomposition of water into its components.

Although the technology is not mature enough to be applied to large scale manufacturing, artificial photosynthesis has a significant potential to lower global water usage and support clean energy systems by generating electricity and hydrogen from photonic energy [Dincer and Acar, 2015].

1.3.4 Hybrid methods

Photo-electrochemical method, high temperature electrolysis and the hybrid thermochemical water splitting cycles can be considered as hybrid methods of hydrogen production since are fed by different kind of energy sources.

1.3.4.1 Photo-electrochemical method

The photo-electrochemical method is electrolysis of water by using semiconductor photoelectrodes, which are electrode covered with photo-catalyst materials. During photo-catalysis, a photon hits the photo-catalyst and generates an electrone-hole pair to obtain electrical charge. In photoelectrolysis both photonic and electrical energies are converted to chemical energy (hydrogen) and for this reason it is can be classified as an hybrid method.

Particularly, the H_2 production mechanism includes five main steps [Dincer and Acar, 2015]:

1. generation of an electron-hole pair with the help of a photon that has sufficiently high energy (higher than the band gap of the p e n junction);
2. flow of electrons from the anode to the cathode generating electricity current;
3. decomposition of water into hydrogen ions and gaseous oxygen;
4. reduction of hydrogen ions at the cathode to form hydrogen in gas form;
5. separation of the product gases, processing, and storage.

Type of photon absorbing material, their crystalline structure, surface properties, corrosion resistance, and reactivity are some of the factors affecting

the performance of a photoelectrolytic system. Usually, photoelectrode stability and photonenergy to hydrogen conversion efficiency are inversely proportional: generally photoelectrodes high efficiency are not very stable in electrolyte, while chemically stable photoelectrodes show low water splitting efficiencies [Dincer and Acar, 2015].

1.3.4.2 High temperature electrolysis

The key of the high-temperature electrolysis (HTE) process is operating at temperatures higher than those of conventional electrolysis, in order to reduce the electrochemical over voltage at the electrodes. For acheiving high temperatures, in this process water is provided as superheated steam and so in addition to electric energy, also heat is required for the steam production. Operating temperatures in the range 800-1000 °C would offer the advantage of smaller specific electricity requirement than conventional electrolysis values [Jean-Pierre and Alain, 2006].The necessary electricity input is reduced corresponding to the variation of cell voltage versus temperature. Current density acceptable by the HTE cell is a function of the operating temperature and materials used for the Membrane-Electrode Assembly (MEA). The upper temperature limit is set by the materials of the HTE cell.

Two different electrolysis mechanisms can be identified [Jean-Pierre and Alain, 2006]:

- Ion O^{2-} conduction electrolysis. In this case the electrolyte considered is of the same type as the electrolyte used for Solid Oxide Fuel Cells (SOFC), i.e. zirconia stabilized with yttrium oxide (YSZ). The target operating temperature of cells is 850°C. The Figure 1.2 illustrates the working principle of O^{2-} electrolysis. Hydrogen is produced at the cathode with a fraction of steam flow not dissociated; therefore it must be separated from the residual steam.

- Proton H^{+} conduction electrolysis. The electrolyte for this technology must meet conductivity requirements at the presently envisaged operating temperature of 500°C. Materials having satisfactory conduction are being developed and still require important development work to reach industrial scale of fabrication. The Figure 1.3 illustrates the working principle of H^{+} electrolysis. The main benefits of this type of electrolysis are the production of pure hydrogen at the cathode and the use of HTR steam cycle as heat source.

Furthermore, it is possible to have different “operating modes” of an electrolyser, according to the different inlet steam and gas outlet temperatures [Jean-Pierre and Alain, 2006]:

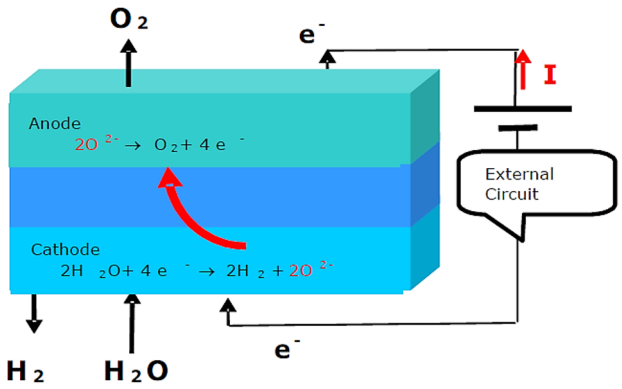

Figure 1.2: *Working principle of High Temperature Electrolysis with* O^{2-} *conduction.*

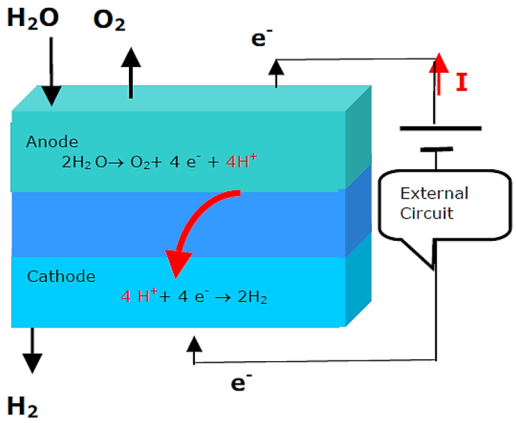

Figure 1.3: *Working principle of High Temperature Electrolysis with* H^{+} *conduction*

• the thermo-neutral mode: the energy input to the electrolyser exactly matches the energy necessary to split the water molecule at the selected operating temperature. Thus, the gas outlet temperatures are the same as the steam inlet temperature. The main interest of this mode is to operate the electrolyser under a homogeneous internal temperature, resulting in less constraints within the thin ceramic MEA.

• The auto-thermal mode: the energy input to the electrolyser exceeds the energy necessary to split the water molecule at the selected operating temperature. Thus, the gas outlet temperatures are higher than the steam inlet temperature. The electric power supplied to the electrolyser provides the excess energy released by Joule effect.

• The endo-thermal mode: the energy input to the electrolyser is less than the energy necessary to split the water molecule at the selected operating temperature. Thus, the gas outlet temperatures are lower than the steam inlet temperature.

1.3.4.3 Hybrid-thermochemical water-splitting cycles

The hybrid-thermochemical cycles operate at lower temperatures compared to water splitting cycles driven thermally (the thermochemical water splitting), combining electrical and thermal energy sources. Thermally driven chemical reactions are performed as in thermochemical water-splitting cycles while electrochemical steps are electricity driven.

The overall reaction is the decomposition of water is then

$$H_2O + \text{heat} + \text{electricity} \rightarrow H_2 + \frac{1}{2}O_2$$

An example of hybrid-thermochemical cycle is shown in Figure 1.4.

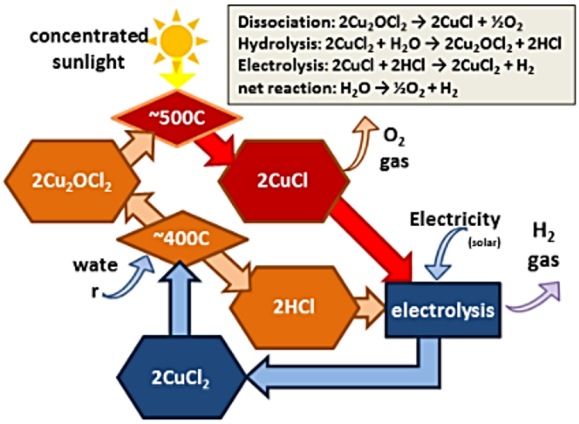

Figure 1.4: *An "hybrid" thermochemical cycle based on copper chloride thermochemistry, which includes an electrolysis step that needs some electricity input. Reference: energy.gov [2017a]*

Chapter 2

The hybrid-Sulfur cycle

The Hybrid-Sulfur cycle belongs to Sulfur-based thermochemical (and hybrid-thermochemical) cycles for Hydrogen production.

As already reported in Section 1.3.2.8, the Sulfur-based cycles have been identified as the most promising thermochemical cycles, together with those Ca and Br based and metal oxide based (Brown et al. [2003]).

Particularly the Hybrid Sulfur (HyS) cycle is considered to have a particularly high potential, as reported by the Hydrogen Initiative the US Department of Energy [Corgnale and Summers, 2011].

2.1 Sulfur-Cycles family

In the Sulfur-based cycles the key element is precisely the Sulfur in the form of sulfur dioxide or sulfuric acid. Indeed, all cycles of the sulfur family, allow to obtain the decomposition of water into hydrogen and oxygen through the following set of reactions (see Figure 2.1):

$$SO_2 + 2H_2O \rightleftharpoons H_2SO_4 + H_2 \tag{2.1}$$

$$H_2SO_4 \rightleftharpoons SO_2 + {}^1\!/_2O_2 + H_2O \tag{2.2}$$

Actually, the Reaction 2.2occurs in two steps:

$$H_2SO_4 \rightleftharpoons SO_3 + H_2O \tag{2.3}$$

$$SO_3 \rightleftharpoons SO_2 + {}^1\!/_2O_2 \tag{2.4}$$

Water, O_2 and SO_2 are the products of this reaction; the Oxygen leaves the cycle, while SO_2 is recirculated for the acid production.

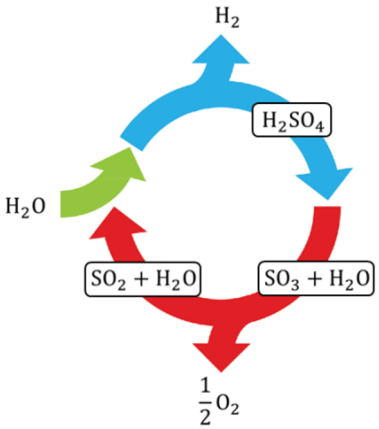

Figure 2.1: *Reaction scheme for the sulfur family of thermochemical water-splitting cycles*

While the high-temperature endothermic decomposition of H_2SO_4 is a common reaction in the Sulfur-based cycles and requires same operating conditions, instead the H_2SO_4 production from SO_2 and H_2O results from different reactions according to the specific cycle. Particularly, the cycles belonging to this family are:

1. The Westinghouse cycle or Hybrid Sulfur Cycle, which consists of the following reactions:

   $2H_2SO_{4(aq)} \rightleftharpoons 2SO_{2(g)} + 2H_2O_{(l)} + O_{2(g)} (>850\ ^\circ C)$ occurs by thermal energy

   $SO_{2(g)} + 2H_2O_{(l)} \rightleftharpoons H_2SO_{4(aq)} + H_{2(g)}\ (\sim 77\ ^\circ C)$ occurs by electric energy

2. The Ispra Mark 13, which consists of the following reactions:

   $2H_2SO_{4(aq)} \rightleftharpoons 2SO_{2(g)} + 2H_2O_{(l)} + O_{2(g)}\ (>850\ ^\circ C)$ occurs by thermal energy

   $2HBr_{(aq)} \rightleftharpoons 2Br_{(aq)} + H_{2(g)}\ (\sim 77^\circ C)$ occurs by electric energy

   $2Br_{(l)} + SO_{2(g)} + H_2O_{(l)} \rightleftharpoons 2HBr_{(g)} + H_2SO_{4(aq)}\ (\sim 77\ ^\circ C)$ occurs by thermal energy

3. Sulphur-Iodine cycle, which consists of the following reactions:

   $2H_2SO_{4(aq)} \rightleftharpoons 2SO_{2(g)} + 2H_2O_{(l)} + O_{2(g)}\ (>850\ ^\circ C)$ occurs by thermal energy

   $2HI_{(aq)} \rightleftharpoons I_{2(s)} + H_{2(g)}\ (\sim 300^\circ C)$ occurs by thermal energy

$I_{2(s)} + SO_{2(g)} + 2H_2O_{(aq)} \rightleftharpoons 2HI_{(aq)} + H_2SO_{4(aq)}$ (∼100 °C) occurs by thermal energy

In the case of Westinghouse cycle the H_2SO_4 production requires to occur only electrical energy, while in Sulphur-Iodine and Ispra-Mark 13 cycles the reaction provides the use of an halogen, respectively Iodine and Bromine, in addition to electrical energy. The use in these last two cycles of Iodine and Bromine,both corrosive and expensive elements, makes the Hybrid Sulfur Cycle the most convenient process.

It is worth to note that the Westinghouse and Ispra-Mark 13 cycles are hybrid-thermochemical cycles, requiring both electric and thermal energy to occur.

2.2 The hybrid-sulfur cycle

The Hybrid-Sulfur Cycle (HyS) or Westinghouse cycle was proposed and patented for the first time in 1975 by Brecher and Wu at Westinghouse Electric Corporation [Brecher and Wu, 1975, Brecher et al., 1977]. However since then, the cycle development required investigations and efforts of the Westinghouse engineers and scientists for almost a decade. Contemporary, the process was studied and developed also in Italy, at Ispra Research Centre, where it was known as Mark 11 cycle, and in Germany, at Nuclear Research Centre of Juelich (KFA) [Beghi, 1986]. Nevertheless, the research was interrupted for lack of interest in nuclear advanced technologies in favour of Hydrogen production methods more consolidated and so more cost-effective. After 20 years, thanks to a General Atomics study on thermochemical cycles for H_2 production , the HyS cycle has regained relevance: the Westinghouse resumed the research and the process was developed at Savannah River National Laboratory (SRNL) of United States, also becoming part of Nuclear Hydrogen Initiative (NHI) [Ryutaro et al., 2011].

The Hybrid Sulfur Cycle is a two-step process, a low-temperature electrochemical step (SDE) and an high-temperature thermochemical step. The net effect of the two reations sum is the splitting of a H_2O molecule to form H_2 and $\frac{1}{2}O_2$ as shown in Figure 2.2.

Particularly, in the electrochemical step of the HyS cycle, sulphuric acid and hydrogen are produced by sulphur dioxide depolarized electrolysis at 80-120°C, by using electric energy. In the thermochemical part, the sulphuric acid formed in electrolysis is concentrated and decomposed thermally to SO_2 and O_2. Subsequently to a gas separation step the SO_2 is circulated back to the electrolysis step for hydrogen generation. The block scheme of process is reported in Figure 2.3.

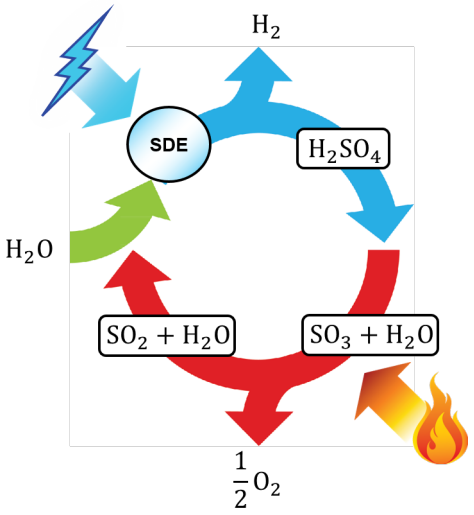

Figure 2.2: *HyS cycle*

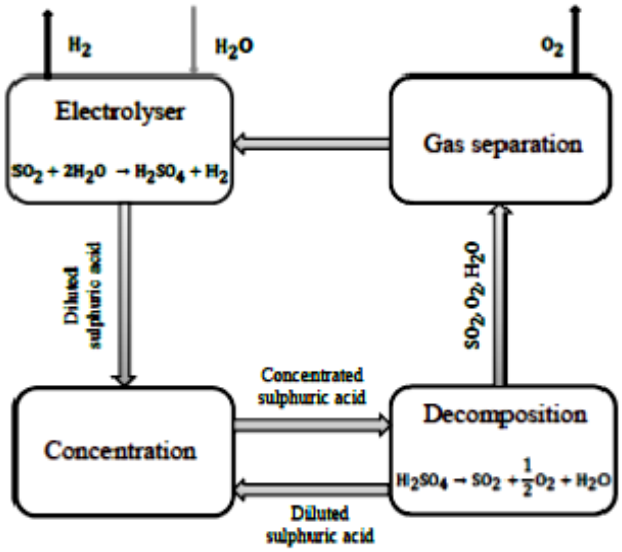

Figure 2.3: *Block scheme of HyS process*

For the concentration step of H_2SO_4 coming from the Electrolyser, a distillation process can be performed; for the SO_2 /O_2separation different options can be considered, like SO_2 absorption with water or Ionic liquid, use of selective membranes and the SO_2 liquefaction .

The most energy-demanding part of the HyS cycle is the decomposition of sulphuric acid; a high temperature is needed for fundamental thermodynamic reasons and the stabilities of sulphuric acid and sulphur trioxide. Since the decomposition of sulphuric acid requires a high-temperature input (900-1000°C), from the point of view of the continuous plant operation, it would be mainly available from nuclear power plants or similar sources. Precisely, the nuclear energy was chosen at first to power the process.

Different versions of the HyS-based cycles flowsheets have been developed and published. As an example, the Figure 2.4 shows that one proposed by SRNL [Ryutaro et al., 2011].

The SDE (EL - 01), is placed on the left. The flow 1 is the feed of H_2O to cathode (catholyte), while the flow 2 is the feed to anode (anolyte), consisting of SO_2 at 15.5 %wt in a solution of H_2SO_4 at 43.5%wt. Both streams are at 21 bar. The composition of flow 2 was set up in order that amount of dissolved SO_2 was just under the saturation point and the H_2SO_4 concentration in the stream from anode after the reaction was 50%wt. The SDE, is treated as a "black block" where a net flow of water from cathode to anode happens through a polimeric electrolyte membrane (PEM). So the electrolytic reaction happens with a SO_2 conversion of 40 % .

The produced Hydrogen goes out with the remaining water as stream 3. All the other compounds go out from anode as stream 11.

Since in the SDE a loss of pressure equal to 1 bar is presumed, the both outlet streams are at 20 bar. The SDE temperature is maintained at 100 °C by manipulating the anolyte temperature through the exchanger HX - 06.

The stream 3 goes out from cathode at 100 °C and 20 bar and is cooled in the exchanger HX - 01. The vapour flow (stream 5) is removed into KO-01 and fed to dryer where is cooled at 40°C with cooling water in order to remove all the residue of water. Hence, pure Hydrogen is obtained at 40°C and 20 bar (stream 6). The H_2O split is mixed with the feed for SDE.

Stream 11, containing SO_2 at 9.1 %wt in a solution of H_2SO_4 50.1 %wt, is split in SP - 01: its 20% is sent to H_2SO_4 decomposition section as stream 12; the other 80 % is recycled to anolyte tank (TK - 01), after being cooled at 80°C by stream 17, in the heat exchanger HX - 05.

The pressure of stream 12, outgoing from anode, decreses into three steps before being fed to vacuum column TO - 01. The throttle valve VV - 01 brings the stream at atmospheric pressure and so allows removing more than 90 % of SO_2 and any traces of oxygen into knock- out KO - 02, through

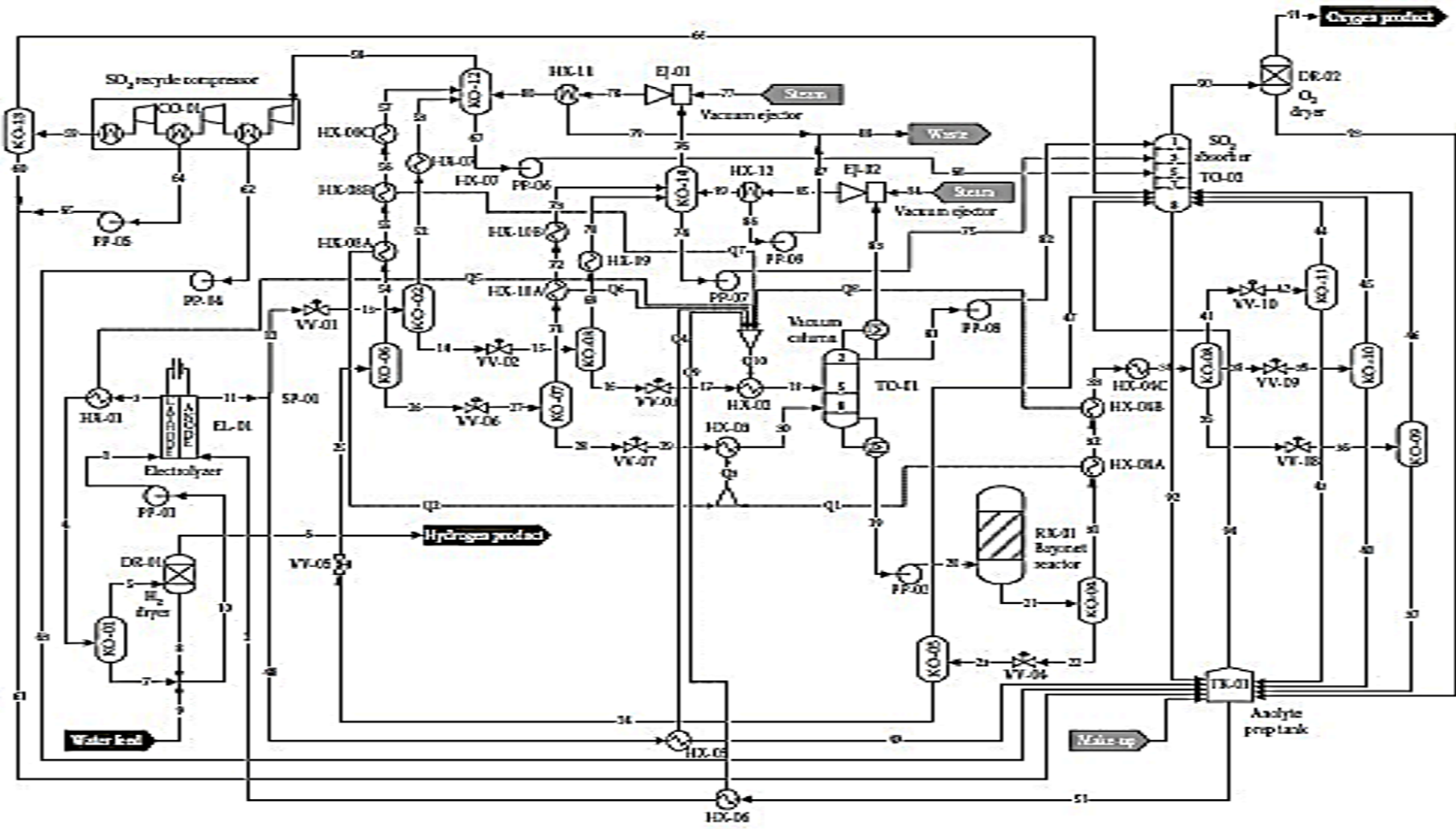

Figure 2.4: *HyS cycle proposed by SRLN. The flowsheet was relized by AspenPlus simulator.*

stream 52. In the VV-02 valve, the pressure drops just over 0,3 bar; the ejector EJ - 01 ensures the vacuum. About 90 % of remaining SO_2 and water are removed into KO-03. In the VV - 03 valve, the pressure drops up to 0,11 bar.

The stream 17, at 50.7%wt of sulfuric acid, is heated and partially vaporized in the heat exchanger HX - 02. Then the stream 18, at 94.4 °C and with a vapour fraction of about 0.37, is fed to vacuum column TO- 01. The head pressure of TO- 01 is kept at 0,09 bar by ejector EJ - 02, and since the bottom-up pressure drop is considered of 0.04 bar, the bottom pressure is 0.13 bar. The TO- 01 column has nine equilibrium stages, including a partial condenser (stage 1) and a reboiler (stage 9). Il reflux ratio is 0.1 and the vapuor fraction in the distillate is 0.001. A bottom concentration of sulfuric acid at 75 %wt is obtained by setting the distillate value at about 4.4 kmol/s. In these conditions the bottom is at 122.9 ° C and required an heat of 75,5 kJ/molH_2, which can be provided by a low pressure vapour utility. The column top is at 40 °C and required for cooling about 210,5 kJ/molH_2.

The bottom stream (19) is pumped directly to bayonet reactor (RX - 01) through PP- 02 pump, that increases the pressure to 86 bar. By a preliminary simulation was calculated that 340.3 kJ/molH_2 were needed to reactor, conceived to be powered by nuclear source, to obtain a H_2SO_4 conversion of 48.1 % and the effluent (stream 21) temperature equal to 254.7° C with a vapour fraction of 20.4% .

The stream 21 is then split in a liquid flow (stream 22) and in a vapour one (stream 31) into KO-04. The pressure of liquid is then reduced at 21 bar by means VV - 04 valve, in order to obtain the separation of 80% of dissolved SO_2 and of 99 % of O_2 (stream 47) into KO-05.

The stream 24, is the remaining liquid consisting of sulfuric acid at 59.3 %wt and 233.4°C, and it can be recycled to the vacuum column.

The stream 47, containing as already said SO_2 e O_2, is sent to absorption column TO-02 for the separation.

The pressure of sulfuric acid flow to recycle (stream 24) is reduced before being fed to vacuum column,exactly in the same three steps adopted for the stream 12 outgoing from SDE. The valve VV-05 reduces the pressure to that atmospheric, allowing to more than 99 % of SO_2 and to the traces of dissolved Oxygen to be removed into KO-06 (as stream 54), with about 22% of water. Then, the pressure drops just over 0,3 bar through the VV-06 valve. About 99 % of remaining SO_2 and water are removed inside KO-07, by used the stream 71. Finally, the pressure reaches the value of the input to vacuum column (0.13 bar), by means the VV-07 valve.

The H_2SO_4 flow at 67.1 %wt (stream 29) is heated and vaporized partially into exchanger HX - 03.

The vapour from reactor (stream 31) is cooled at 40 ° C and partially condensed in three stages (inside the exchangers HX - 04A , HX- 04B , and HX- 04C), and then is split in a vapour phase and two liquid ones into knock-out KO-08. The lightest liquid phase consists of H_2O with 27.3 % wt of SO_2 and a little amount of O_2; while the heaviest phase is liquid SO_2 with 3.7 wt % of water and a little amount of Oxygen. The three effluents from KO-08, go from 86 to 21 bar by means VV-08, VV-09 and VV-10 valves, and it results in further phase changes.

So, the vapour phases are separated from liquid ones into knock-out KO-09, KO-10, and KO-11, and fed to bottom of absorption column of SO_2; while the liquid phases are sent to anolyte tank.

Considering the acid Concentration section in the flowsheet, the stream 85, the effluent of second ejector (EJ - 02), is cooled at 40 ° C with cooling water in the exchanger HX-12 and the condensed flow (stream 86) is pumped to waste through the PP-09 pump. This helps to guarantee that all pollutants that can be introduced with the vapuor (stream 84) are eliminated from the system.

The other vapours (stream 89) are sent to knock-out KO-14, where the pressure is maintened at 0,3 bar by EJ-01 ejector. The equipment KO-14 also receives the partially condensed vapours from knock-out KO-03 (stream 70) and KO-07 (stream 73), after being cooled at 40 ° C by cooling water inside the exchangers HX-09 and HX-10B.

The aqueous phase removed by means KO-14 (stream 74) is pumped to SO_2 absorpsion column by using PP-07 pump. The EJ-01 effluent (stream 78) is cooled with cooling water at 40 °, into HX -11 and the condensed flow is sent to waste.

The remaing vapours (stream 80) are sent to a knock-outat atmospheric pressure (KO -12). KO-12 receives also the partially condensed vapours from knock-out KO-02 and 06. particularly, the vapuors from KO - 02 (stream 52) are first cooled with cooling water in HX-07, while the vapours from KO-06 (stream 54) are cooled at 40 ° C in the three exchangers HX-08A ,HX - 08B and HX-08C. The stream 67 from KO -12 is a 4.8wt% solution of SO_2 in water and is pumped to SO_2 absorption column by PP - 06 pump.

The vapour stream 58 is a flow of wet $SO_2$with about 0.3 %mol of O_2 and is compressed to 21 bar, by a three- stage compression (CO- 01), before being fed to the column bottom for SO_2absorpsion. At first the pressure is increased to 2.78 bar. About 5 %vol of condensed stream, consisting in a 12.9 %wt SO_2 solution, is removed by stream 62 and sent to anolyte tank via PP-04. Then the pressione is increased to 7.65 bar; much of the effluent of this stage is condensed into intercooler and is removed by knock out as liquid SO_2 containing just 0.8%wt of water and Oxygen in trace. This stream is

sent to Anolyte Prep Tank by PP - 05 pump.

The effluent partially condensed from the last compression stage (stream 59) is fed to knock- out KO-13. Less than 1%vol of stream fed to CO- 01 (stream 58), remains as vapour phase (stream 66) and is fed to the absorption column bottom and little more than twice that amount is removed as condensed stream (60) and sent to Anolyte Prep Tank.The stream 66 consists in 65 %vol of O_2 and 35 %vol of SO_2, while the stream 60 is SO_2 at 99.9 %wt with little amount of Oxygen and water.

The SO_2 absorption column has eight equilibrium stages; it works out at 21 bar with a negligible loss of pressure.

The stream 81 from vacuum column, consisting of water at 99.9 %wt and SO_2 at 0,1 % at 40 ° C, is fed to upper stage of absorption column, by using the PP-08 pump.

The stream 75 from KO-14, consisting of water at 98.7 %wt and SO_2 at 1,3 %wt at 41 ° C is fed at third stage of column.

The effluent of the first ejector is sent to knock-out and its condensed phase (stream 68), consisting of water at 95.2 %wt and SO_2 at 4.8 %wt at 40 ° C, is sent to stage 5 of column. The vapours coming from the five knock-out and Anolyte Prep Tank are fed to the column bottom. SO_2 is removed from vapour phase that crosses the absorber, by meeting water with progressively less dissolved SO_2.

The stream 90 is 98.7 %vol of O_2 at 41°C and 21 bar, with 0.5% of water and 0.8 % of SO_2. It is fed to dryer (DR - 02), where SO_2 and H_2O are removed (stream 93) and sent to Anolyte Prep Tank; the stream 91 consists of pure Oxygen at 40°C and 21 bar. The stream 92 contains 14.1 %wt of SO_2 in water at 82 °C and 21 bar, with traces of O_2 and H_2SO_4 and is sent to Anolyte Prep Tank. All the SO_2 produced by acid decomposition, in addition to that recovered by SDE effluents go to Anolyte Prep Tank.

The resulting liquid (stream 51) is a 43.5 %wt H_2SO_4 solution, containing 15.5 %wt of SO_2 at a temperature of 84.7°C and a pressure of 21 bar. This is fed to the SDE anode after the regulation of temperature in the exchanger HX-06 (by exchange with the stream 17 inside HX-02). The anolyte (stream 2) is at 78.8°C.

To Anolyte Prep tank is sent a sulfuric acid make up in order to to compensate for the losses of sulfur dioxide and water at ejector. This plant is set up to produce 1 kmol/s of Hydrogen.

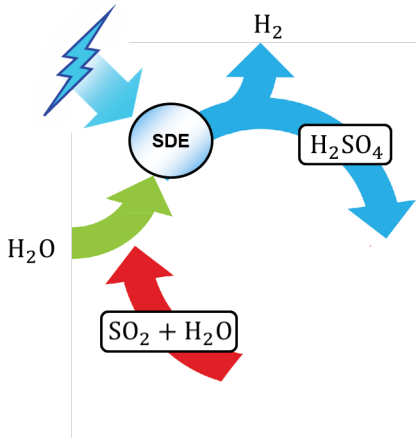

Figure 2.5: *Outotec Open Cycle process*

2.3 Outotec open cycle

The Outotec Open Cycle process (OOC) has been developed by Outotec Corporation and Aalto Foundation University. It can represent an attractive alternative for Hydrogen production when a SO_2 source is available, as it involves only one stage (SDE) and does not require sulphuric acid decomposition (2.5).

In the original concept, Hydrogen was basically a by-product [Lokkiluoto et al., 2012]. Indeed the process was not originally developed to produce Hydrogen, but to remove SO_2 from gaseous effluents of the metallurgical industry and valorise it into a commodity, i.e. H_2SO_4 . Hence, the Hydrogen production was coupled with metallurgical or other operations: a part of SO_2 obtained by metallurgical processes, and usually oxidized to produce the SO_3 employed for the sulfuric acid production, could be sent to the electrolyzer to produce sulfuric acid and Hydrogen (Figure 2.6) . With a worldwide production of sulfuric acid of 200-250 Mta, the by-product Hydrogen opportunity with this process is 4-5 Mt/a (˜35-45 PJ assuming hydrogen LHV energy value) [Lokkiluoto et al., 2012].

As already said, SDE stage is a common step in both HyS and the new Outotec open cycle process. However Outotec Open Cycle is ”open” because the sulphuric acid is a co-product of process and it is not reused to produce SO_2 (which is an external source) like in the HyS cycle which is instead “close”.

The OOC has many technical and economical advantages as the low Investment and O&M (Operation & Mainteinance) costs, and the low process

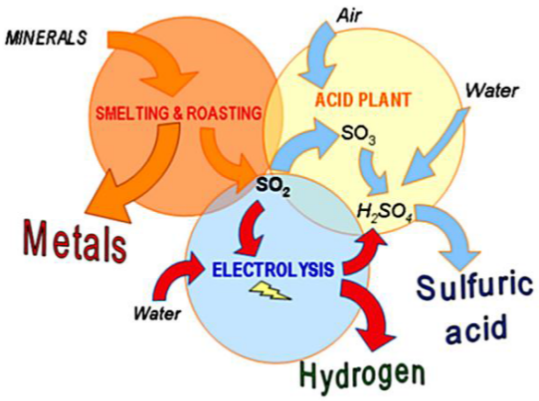

Figure 2.6: *The Outotec Open Cycle concept.*

temperatures. Furthermore it presents high flexibility in responding to the local demand of Hydrogen and the revenues from acid sales can provide substantial economic benefits when comparing hydrogen production costs [Lokkiluoto et al., 2012].

However, OOC for Hydrogen production suffers from limitations due to the close link between H_2 production to SO_2 availability and H_2SO_4 production. Moreover, the open flows not allowing the complete closed cycle, require the integration between SDE and H_2SO_4 decomposition plants. Hence, it is extremely important to decouple the H_2 production and that one of H_2SO_4 because their demands could be different. This requires an additional high-temperature part of the process where sulfur dioxide is produced by the decomposition of sulfuric acid, like in the traditional HyS cycle.

A solution could be realize an HyS-type thermochemical cycle partially open (Figure 2.7), in which the SO_2 availability to produce Hydrogen is ensured by H_2SO_4 decomposition process, like in the Convential HyS cycle, process and by external source, like in the Outotec Open Cycle®.

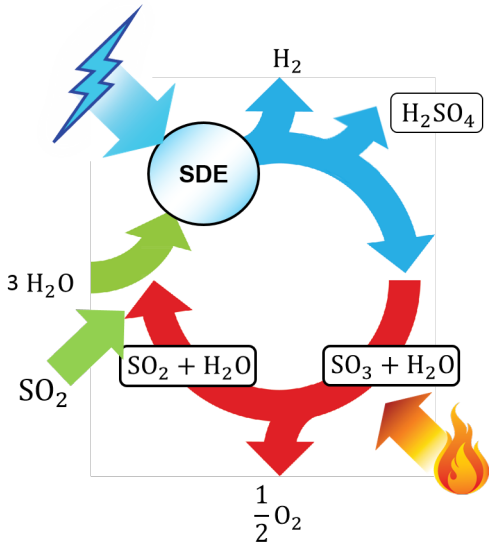

Figure 2.7: *HyS-type thermochemical cycle partially open*

Chapter 3

The European project SOL2HY2

3.1 Objectives of the SOL2HY2 project

SOL2HY2 (Solar to Hydrogen Hybrid Cycles) was a research project, started on 01/06/2013 and ended on 30/11/2016, co-funded by the Fuel Cells and Hydrogen Joint Undertaking (FCH JU) within the Seventh Framework Programme for Research and Technological Development (FP7) [sol2hy2.eucoord, 2017].

The project was aimed at relise a solar-powered version of Westinghouse cycle, which was instead designed to be fed by nuclear energy [Brecher et al., 1977]. Particularly, it focused on applied bottle-neck solving, materials research, development and demonstration of the relevant-scale key components of the solar-powered HyS water splitting cycle complemented by their advanced modeling and process simulation including conditions and site-specific technical-economical assessment optimization, quantification and benchmarking.

Besides providing key materials and process solutions, for the first time the whole production chain and flowsheets have been connected with multi-objective design and optimization algorithms ultimately leading to hydrogen plants and technology "green concepts" commercialization.

The consortium consisted of key materials suppliers, process development SME and industry, RTD performers and a University, namely:

- EnginSoft, a consulting company operating in the field of computer aided engineering, virtual prototyping and advanced simulation ;
- Aalto Korkeakoulusäätiö (Aalto University Foundation), operating as Aalto University, formed by merging Helsinki University of Technology

(TKK), Helsinki School of Economics and University of Art and Design Helsinki

- Deutsches Zentrum für Luft- und Raumfahrt e.V. (abbreviated DLR), the German Aerospace Center having four future-oriented fields of research activities: aeronautics, space flight, transport research, and energy technology;

- ENEA, the Italian National Agency for New Technologies, Energy and the Sustainable Economic Development - a public undertaking operating in the fields of energy, the environment and new technologies to support competitiveness and sustainable development.

- Outotec Corporation, which develops and provides technology solutions for the sustainable use of Earth's natural resources.

- Erbicol SA, specialized on manufacturing of extra hard materials like ruby for the watch industry, white sapphire disks, cylinders and pistons for micro-pumps, plates for scrapers, as well as micro-magnets in rare earth materials for the watch industry and other industries. For more than 10 years Erbicol is also active in the production of silicon infiltrated SiC foams.

- Oy Woikoski AB, the oldest specialized gas producer and distributor in Finland.

3.2 Main concepts of SOL2HY2 process

The main objective of the SOL2HY2 project was the production of Hydrogen through the use of a HyS-type thermochemical cycle. The possibility of using a partially or completely open version of the cycle, such as the new Outotec Open Cycle® process [Lokkiluoto et al., 2012], has been also envisaged.

As already explained in previous Chapter 2, conventional HyS makes use of SO_2 and H_2SO_4 in a closed cycle starting from water and generating H_2 and O_2 according to the following two reactions:

$$SO_2 + 2H_2O \rightleftharpoons H_2SO_4 + H_2 \tag{3.1}$$

$$H_2SO_4 \rightleftharpoons H_2O + SO_2 + {}^1/_2O_2 \tag{3.2}$$

where, the reaction 3.2 develops in turn as two distinct reactions:

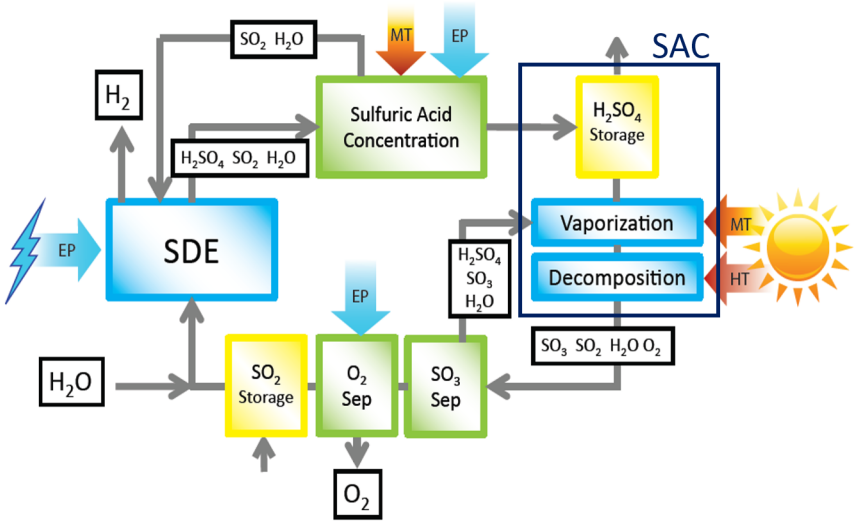

Figure 3.1: *Simplified block diagram of the HyS process considered here. The main energy input type required by the different process blocks is highlighted (MT: medium temperature heat; HT: high temperature heat; EP: electric power). Reference: Liberatore et al. [2016].*

$$H_2SO_4 \rightleftharpoons SO_3 + H_2O \quad \sim 400°C \tag{3.3}$$

$$SO_3 \rightleftharpoons SO_2 + {}^1/_2O_2 \quad > 800°C \tag{3.4}$$

OOC involves only the low temperature reaction of Sulfur dioxide Depolarized Electrolysis (SDE) (reaction 3.1), without sulfuric acid (SA) decomposition (reaction 3.2).

The SO_2 feed required by OOC can be obtained from waste streams of flash smelting, sulfide roasting, sulfur combustion or any other similar operation.

A simplified block diagram of the process considered in SOL2HY2 process is presented in Figure 3.1, where the main energy input types required by the different process blocks are highlighted.

The effluent anolyte SA solution from the SDE is concentrated before being evaporated and heated at 1000 °C. The gas stream at 1000 °C, which is composed almost only of $SO_3$and H_2O, is fed to an adiabatic reactor where SO_3 is decomposed in SO_2 and O_2. For simplicity the operations of evaporation, heated at 1000°C and decomposition, will be considered in this work, belonging to a section defined as Sulfuric Acid Cracking (SAC) .

The conversion of decomposition reaction is thermodynamically limited so the separation and recycling of unreacted SO_3 to the reactor's feed is required. Finally, the produced SO_2 is separated from O_2 by refrigerated compression and recycled to SDE. For several self-evident reasons, if possible, the chemical plant should be operated continuously; however, the use of the intermittent solar source to power the process requires a part of the plant to work discontinuously 8 h per day, when the solar radiation is available. SA and SO_2 storage tanks are used as a buffer to decouple the operating regimes of the continuous and discontinuous part of the chemical plant.

The process requires three main types of energy input: power, medium temperature (<550°C) heat and high-temperature (>600°C) heat.

In the context of SOL2HY2 process, the heat required to power the HyS cycle was conceived to be provided by Concentrating Solar thermal (CST) thecnologies.

For electric power needed in the process, the easiest option is the use of the electric grid. Nevertheless, in order to increase the fraction of renewables in the energy input, also the installation of a power block coupled with Concentrating Solar Power (CSP) plant was considered.

3.2.1 Concentrating Solar energy systems

The solar energy source is notably abundant, but it does not result very much concentrated. Hence, for its industrial use, a system able not just of capturing the radiation but also of concentrating it is needed. Very important in these kind of systems is the "concentration ratio" , that is the ratio between intensity of irradiation in the focal area of the system and the intensity of solar irradiation. The unit of misure of concentration ratio is the "Sun" or "numbers of Suns".

The Concentrating Solar energy systems focus the direct solar irradiation by means mirrors and are classified on the basis of the temperatures reached by heat tranfer fluid (HTF) and of concentration ratio. Particularly, for industrial plants these can be classify as:

- linear parabolic concentrators (CPL) systems
- punctual parabolic concentrators or parabolic dish systems
- solar tower systems
- duble concentration systems

The CPL are characterized by operating temperatures of HTF in the range 150- 550 °C and by a concentration ratio in the range 30-100 Suns [Kodama

and Gokon, 2007]. They have a parabolic reflective surface that focuses the sun rays on a focal line where a receiver tube is located. In the receiver tube of CPL, a fluid which absorbs energy and transports it into a storage tank,useful in the period of low or no sunshin, flows. The storaged thermal energy can be transformed into electricity through Rankine cycles in turbomachines. The HTF of the latest generation are the molten salts that can reach temperatures up to 550°C against the 400°C of mineral and synthetic oil. The most used mixture of molten salts consists of $NaNO_3$(60%wt) and KNO_3 (40%wt), both widely employed for fertilizer production and so available in great amount and low costs. Under normal operating conditions of the solar field, the salts temperatures are in the range 290-550 °C, they are not flammable and toxic, have an high heat transfer coefficient, high thermal capacity, high density and low operating pressure. The use of molten salts for heat storage insead of diathermic oil, used in the past, allows to work at higher temperatures, to improve performance and to simplify the plant design. With this thermal storage system the solar plant can work out continuously, 24 hours a day.

As regard to the parabolic dish systems the HTF operating temperatures are in the range 300-1500 °C (2000° for some laboratory applications) and the concentration ratio is in the range 1000-5000 Suns. These systems are composed by a parabolic mirror which reflects the solar radiation in focal point, where a receiver is placed.

The solar tower systems are characterized by operating temperatures of HTF in the range 500-1000 °C and the concentration ratio is in the range 500-5000 Suns. These systems consists of linear mirrors, namely heliostates, equipped with a dual axis solar tracking system. The heliostates reflect sunlight and concentrate it by overlapping reflections on a receiver placed on the tower top [Kodama and Gokon, 2007].

Recently developed are the double solar concentration systems, which consist of a field of heliostats, a reflector placed on a tower and a receiver placed on the ground coupled to a second concentrator (CPC). The focal point of the upper hyperboloid reflector coincides with the target of the heliostats. The CPC allows to further improve the concentration of solar energy. The concentration factor of these systems is in the range 5000 to 10000, and the receiver on the ground can reach temperatures above 1300 ° [Kodama and Gokon, 2007].

The solar radiation capture and concentration system presents losses of different nature that cause often considerable reduction of the power made available to the receiver compared with that picked up. The greatest losses are due to not perfect pursuit of the sun position , geometric and or optical imperfections of the collectors, presence of dark areas.

The global yield of a solar receiver can be defined as the ratio between the

really absorbed energy and the solar energy by concentrator (the conductive and convective losses are not considered):

$$\eta = \frac{aIC - \varepsilon\sigma T^4}{IC}$$

where I is the solar radiation intensity [W/m^2], T is the operating temperature of receiver [K], C is the concentration ratio [sun], σ is the Stefan-Boltzmann constant [W/(m^{2}K^4)], a and ε are respectively the absorption and emissivity coefficients of the riceiver [Kodama and Gokon, 2007].

3.2.2 Power block

The possibility to include the power block in the CSP plant was also considered in the SOL2HY2 process.

A power block can reduce or avoid the use of grid power or even allow for a net export of power to the grid (i.e co-production of H_2 and power).

When this option was envisaged in the process, power generation has been assumed to be carried out by a steam cycle since coupling of this technology with molten salt CSP plants is already demonstrated and used in existing power plants. Furthermore, this choice allowed part of the steam produced with the MS steam generator to be used as heat transfer fluid for the chemical plant and provided heat for SA concentration and vaporization.

A scheme of the Rankine cycle considered for the power block is shown in Figure 3.2.

In more detail, two different process configurations were considered Liberatore et al. [2016]:

1. the molten salt sensible heat is partly transferred to the Rankine cycle and partly used to produce high pressure steam as thermal fluid for the chemical process (SA vaporization and concentration units), through the heat exchangers HEX-VAP and HEX CONC;

2. the molten salt heat is totally used to produce high pressure steam for generating electricity through the steam turbines.

In this second process configuration the heat demand of the SA evaporation and concentration units is directly satisfied by the heat exchange with hot molten salts, without the intermediate exchange with high pressure steam. The first process option can be split in two operation modes: during the daily 8 hours of operation of the CSP, both the SA vaporization and concentration units work and are powered by the high and medium pressure steam (Case 1a), while in the remaining 16 hours operation only the SA concentration

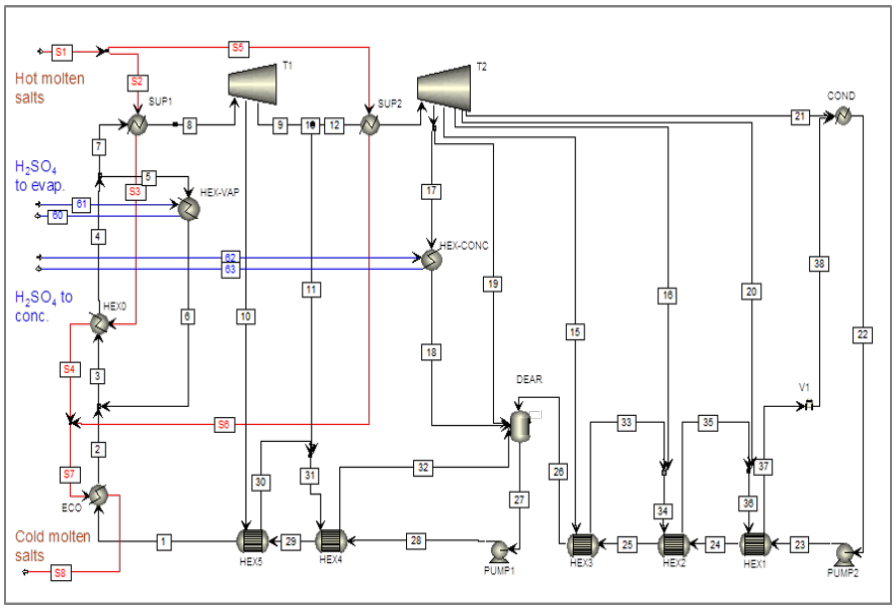

Figure 3.2: *Process scheme of the Rankine cycle powered by molten salts sensible heat. In Case 1a (8 hours solar operation) both the heat exchangers HEX-VAP and HEX-CONC work, while in Case 1b (16 hours operation) only the HEX-CONC is in operation. In Case 2 the heat exchangers HEX-VAP and HEX-CONC are not present. Reference: Liberatore et al. [2016].*

unit is active and its energy need is fulfilled by the medium pressure steam (Case 1b).

Furthermore, some common improvements to the Rankine cycle (reheating and regenerative steps) have been introduced with the aim of increasing the cycle thermal efficiency. In particular in this reheating variation, the steam turbine is split in two stages, working in series, and the steam, after the first expansion stage, is re-heated up to the maximum temperature (540°C), removing the moisture produced at the final stages of the expansion process. Moreover, according to the regenerative cycle, the working fluid, on its way from the condenser to the boiler, is pre-heated by indirect contact with the inter-stage steam bled from the turbine.

3.3 Objectives of the thesis

The PhD project started on November 2014 and has been funded by ENEA within the European project SOL2HY2. As already explained in greater detail in the previous paragraph 3.1, the objective of European project was to design for the HyS-Sol cycle a process scheme technically, environmentally and economically optimal and to realize the demonstratives of two main components, i.e. the sulfuric acid decomposer and electrolyzer.

In this context, the envisaged activities within the PhD way were generally:

- Analysis of Hybrid-Sulfur cycle and definition of an optimal flowsheet
- Theoretical and experimental study of sulfuric acid decomposition in a lab-scale reactor
- Attendance to on-sun testing of the demonstrative solar-powered reactor for sulfuric acid decomposition (this DEMO plant was set up in Juelich, at Solar Tower of DLR)
- Analysis and optimization of the interface between chemical plant and solar field

Specifically, starting from the theoretical study of HyS cycle, the work carried out in the three years has been characterised by:

- Theoretical and experimental assessement of high temperature SA decomposition and in particular:
  - Choice and development of catalyst for SO_3 decomposition

  - Catalyst testing
  - Kinetic analysis of decomposition on selected catalyst
  - Active contribution to the completion of DEMO plant for SA decomposition installation and attendance to some preliminary on-sun tests (during a stay of three months in Jülich)

- Analysis of HyS-Sol process with thecnical-economical evaluation, by starting from single process units as follows:

  - Concentration section: study and flowsheeting of possible configurations, with identification of the most suitable one
  - SAC and SO_3 separation sections: study and flowsheeting of possible configurations, with identification of the most suitable one
  - SO_2/O_2 separation section: study and flowsheeting of possible configurations, with identification of the most suitable one; in this context a detailed literature survey has been carried out on the use of Ionic Liquids for separation processes
  - Definition of the final block diagram for SOL2HY2 process with sizing and cost estimates of main equipment employed, and global consumptions and efficiencies evaluation

- Evaluation of different integration configurations between chemical and solar plants, considering also the possibility to integrate other energy source thecnologies in addition to Concentrating Solar thermal ones, i.e. Sulfur burning and Photo Voltaic (PV). This analysis has ended with identification of the best configuration, in term of Hydrogen cost and share in no-fossil energy of total power used in the process.

Part II

Experimental section

Chapter 4

Development of a catalyst for sulfur trioxide decomposition

Sulfuric acid decomposition (reaction 3.2) is the sum of two different reactions, 3.3 and 3.4. In particular the latter, i.e. the SO_3decomposition, is an endothermic reaction presenting a great kinetic barrier, hence high temperatures and the use of a catalyst are required to ensure reasonable reaction yields [Brutti et al., 2007].

A significant part of the activities carried out in this PhD project were related to the development and characterization of a suitable catalyst for SO_3 decomposition and are reported in this Chapter. The work started from a literature survey on catalysts proposed for SO_3 decomposition, in order to identify the most suitable for use in the solar-powered HyS process. For the selected candidate materials, production methods were set up and sample produced for testing. The performance results in terms of stability and activity have been compared and allowed to select the most suitable option. Subsequently, the production method of the selected catalyst has been further improved for the production of bigger quantities, required for the use in a pilot-scale reactor realized by DLR within the SOL2HY2 project.

Up to 150 hours-on-stream stability tests were carried out in relevant operating conditions by subjecting the catalyst to daily thermal cycles, which are typical in the case of solar-heated reactors. Furthermore, an experimental campaign aimed at assessing the catalyst activity under different operating conditions was carried out and allowed to derive an expression for the rate of the SO_3 decomposition reaction. The reaction kinetics obtained in this study have been used by DLR researchers to size the decomposition reactor of the pilot plant.

4.1 Literature survey on catalysts for sulfur trioxide decomposition

4.1.1 Active phase

In general, the materials proposed in literature as active phase for SO_3 decomposition reaction, may be grouped in noble metals and metal oxides.

With regard to catalytic activity, supported noble metals are presumably the best choice [Brittain and Hildenbrand, 1983].

In fact, the investigation of Ishikawa et al. [1982], showed that Pt supported on Al_2O_3 pellets (1-2 mm of diameter) gave a SO_3 conversion close to the equilibrium at temperatures from 1073 to 1173 K.

Brutti et al. [2006] carried out a comparaison between palladium and both iron (III) oxide and non-catalysed systems. Nanoparticles of Pt, Pd, Rh, Ir were investigated (on supports ofTiO_2 and Al_2O_3pellets) by Rashkeev et al. [2009].

However, the cost of all of these proposed metals is a limiting factor, especially when a massive use is required. To overcome this problem single or mixed metal oxides have been widely proposed as alternative active phases.

Tagawa and Endo [1989] compared several metal oxides andCr_2O_3 was the one that showed the best behaviour, similar to that one of Pt, even if it presented leaching problems.

An alternative good choice is represented by Fe_2O_3[Barbarossa et al., 2006, Tagawa and Endo, 1989].

Furthermore, in order to improve both catalytic activity and the operative temperature range compared to those of single metal oxides, several systems with mixed oxides were studied.

$Fe/Cu/Al_2O_3$ were investigated before by Kovalev et al. [1986] and later by Abimanyu et al. [2008].

Test on Fe-Cr oxides (supported on Al_2O_3) were carried out by Kovalev et al. [1991]. More recently also Banerjee et al. [2008] carried out a study on Fe-Cr mixed oxides ($Fe_{2(1-x)}Cr_{2x}O_3$) .

CuO/Cr_2O_3 and CuO/Fe_2O_3 ,active up to 725 °C, seemed to be more performing than Pt/TiO_2 above 800 °C in a work of Ginosar et al. [2009].

Also $Ce_{0.8}Cu_{0.2}O_2$showed an activity higher than Pt above 800 °C [Zhang et al., 2015].

4.1.2 Catalyst support and carrier

Both in the case of noble metals or metal oxides, the use of substrate for the active phase was widely adopted (as was highlighted by previous literature

references) because leads clear benefits. Indeed in case of noble metal, it reduces the active phase amount, consequently the cost, and minimizes the poisoning issue by sulphur. With regard to oxide or mixed oxides catalysts, instead the main advantage is that by depositing them on a substrate, the possibility to regulate the granulometry and the thermal transfer properties of the catalytic bed is ensured. Indeed metal oxides present thermal-insulating properties, therefore, it could be difficult to properly heat a catalytic zone by an external power source. Another advantage of using the substrates is the possibility to shape them (as, for instance, foams or honeycombs) in order to fit the material in proper designed reactors.

Norman et al. [1982] highlighted that Al_2O_3 was not a good support for Platinum specie due the metal poisoning issue by sulphur; $BaSO_4 - TiO_2$, TiO_2, ZrO_2, and SiO_2 were, in order of feasibility, better choices.ZrO_2 was also employed as support for Pt by Gelbard et al. [2005] for pressurized SAC (Sulfuric Acid Concentration) test.

Kwak et al. [2006] investigated the SiC catalytic activity, which is extremely low, if not negligible, at all temperatures (in comparison with the decomposition rate without catalyst). Lee et al. [2013] interestingly showed that SiC could stabilize Pt/Al_2O_3 respect to sulfatation. A particular emphasis was put on SiSiC supported catalyst during the last European project "Hycycles", which was, among other issues, focused on a SAC decomposer placed into a direct solar irradiated reactor [Roeb et al., 2013]. Iron (III) oxide powder was supported on a SiSiC honeycomb, catalytic activity, investigated up to 900 °C and 4 bar of total pressure, was comparable with Fe_2O_3 pellets [Giaconia et al., 2011], and was also higher when silicon carbide was coated with mixed oxides such as Fe_2O_3/Cr_2O_3 and Fe_2O_3/CuO[Karagiannakis et al., 2012].

4.2 Choice of the catalyst

4.2.1 Active phase

The catalys developed for the SOL2HY2 project has been chosen on the basis of a series of considerations. Particularly to be suitable for the massive production required, the catalyst had to be not only cost-effective, environmentally friendly and satisfactorily active, but it also had to be suitable for cheap, simple and easily scalable preparation methods.

Considering that according to literature informations the active phase of catalyst could be chosen between both some noble metals and some oxides, but the use of noble metals is disadvantaged due to its high cost, the choice

has focuses on metal oxides.

Iron oxide presents a lower toxicity and is more cost effective than Cu and Cr based oxide, along with a good catalytic activity above 780° [Norman et al., 1982]. Furthermore, the main advantage to use Cu and Cr-based oxides it is the possibility to work at low temperatures (less than 800°C), but it was not relevant for SOL2HY2 process wich worked at higher thermal levels.

Moreover, even if other metal oxides (in particular mixed oxides) have a better catalytic activity, the use of iron oxide allows an easier preparation method, leading to minor cost and time in large scale preparation processes.

For all these reasons, Fe_2O_3 has been chosen as active catalytic material for the SO_3decomposition reactor of SOL2HY2 pilot plant.

4.2.2 Catalyst support and carrier

Based on the information obtained through literature survey, both SiC and Al_2O_3 where took in account and tested as catalyst substrates [Turchetti et al., 2015, Sau et al., 2015] .

The tests were aimed at identifying simple preparation methods, still obtaining an acceptable catalytic activity and good stability (higher than 100 hours-on-stream in laboratory tests) under concentrated SA flow at high temperatures and daily thermal cycling. Several kinds of deposition methods were used, testing:

- precoating techniques, using Al_2O_3 before Fe_2O_3 , and $Fe_2(SO_4)_3$;
- direct, also multiple, impregnation techniques using Fe_2O_3 , $Fe_2(NO_3)_3$ and $Fe_2(SO_4)_3$;
- calcinations of samples at different temperatures.

All the samples prepared according to the different methods, and the tests results obtained in terms of stability and catalytic activity for each of them are summarized in Table 4.1.

On the basis of results $\gamma - Al_2O_3$ has been selected as support for decomposition catalyst because, among those that fulfilled the criteria of both good stability and good catalytic activity (as will be clearly show in the Chapter 5), required the simpler preparation method.

Hence the catalyst chosen, i.e. Fe_2O_3 supported by $\gamma - Al_2O_3$pellets which as of now will be briefly named as $Fe_2O_3/\gamma - Al_2O_3$, has been prepared by alumina impregnation with iron (III) nitrate. The $Fe(NO_3)_3$ employed for preparation was provided by VWR CHEMICALS in the form of nona-idrate nitrate (thecnical grade) while $\gamma - Al_2O_3$cylindrical pellets (2

Table 4.1: *Samples description and tests results in terms of stability and activity.*

Catalyst N.	Support type	I impregnation	I calcination	II impregnation	II calcination	Stable	Active
1	SiC	Fe_2O_3	950 °C			NO	YES
2	SiC	Al_2O_3	1500 °C	$Fe_2(SO_4)_3$	1500 °C	YES	NO
3	SiC	Fe_2O_3	1150 °C	$Fe_2(SO_4)_3$	1150 °C	YES	YES
4	SiC	Al_2O_3	1500 °C	$Fe_2(SO_4)_3$	1050 °C	YES	YES
5	Al_2O_3 foam	$Fe_2(SO_4)_3$	1100 °C			NO	YES
6	Al_2O_3 foam	Fe_2O_3	1150 °C	$Fe_2(SO_4)_3$	1150 °C	NO	YES
7	Al_2O_3 pellets	$Fe(NO_3)_3$	1050 °C			YES	YES

mm in diameter x 3 mm in height) was a commercial product of Alfa Aesar (Italy).

The chosen size for pellets, has ensured an high surface area and minimum pressure drops (Figure 4.1) .

The pressure drops per unit lenght have been calculated with the Ergun Equation:

$$\frac{\mathrm{d}P}{\mathrm{d}z} = -\frac{G}{\rho D_p}\left(\frac{1-\phi}{\phi^3}\right)\left[\frac{150\,(1-\phi)\,\mu}{D_p} + 1.75G\right] \tag{4.1}$$

where P is the pressure [Pa], z the packed bed length [m] , G the surface mass velocity of inlet stream [kg $s^{-1}\,m^{-2}$], ρ the density [kg/m^3], D_p the diameter of catalyst particles [m], ϕ the void fraction (considered equal to 0.41) and μ the dynamic viscosity of the gas phase.

For this expression since the catalyst has been employed in the form of cilindrical pellets, like D_p an "equivalent spherical diameter" as has been calculated as the diameter of a perfect sphere having the same volume of the cylindrical pellet; the result is given by the following expession:

$$D_p = 2\,r_{sphere} = 2\left(\frac{3}{4}r_{cylinder}^2 h_c\right)^{\frac{1}{3}} = 2\left(\frac{3}{4}\left(\frac{0.002}{2}\right)^2 0.003\right)^{\frac{1}{3}} = 2.62\,\mathrm{mm}$$

4.3 Development of the catalyst preparation method for larger-scale production

The procedure followed in laboratory for preparing the small amount of $Fe_2O_3/\gamma - Al_2O_3$ during the preliminary tests for the selection of most suitable catalyst (see previous paragraph 4.2.2, Table 4.1.) has been obviously

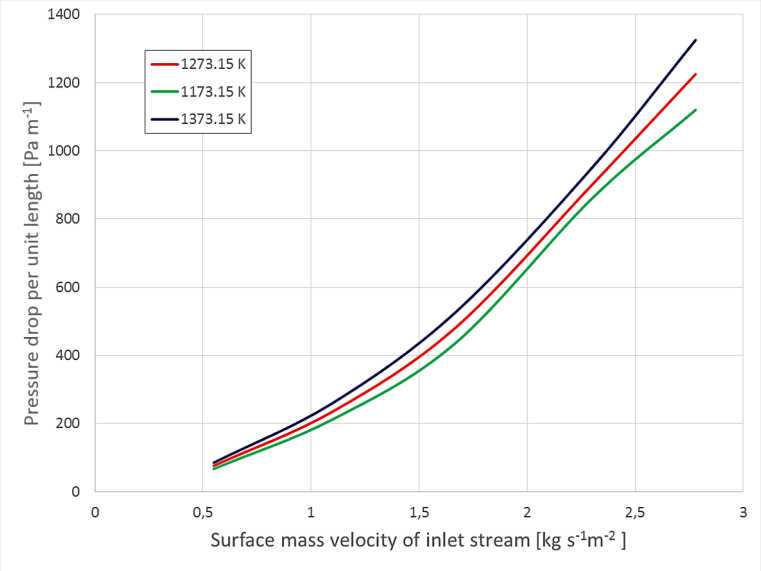

Figure 4.1: *Pressure drop per unit length vs Surface mass velocity of inlet stream at different temperatures. The values of temperature and Surface mass velocity have been chosen in range of interest for SOL2HY2 process.*

readopted for producing the catalyst large amount to ship to DLR (about 20 kg).

The preparation procedure is illustrated in Figure 4.2.

Exactly as in the case of small amount, a direct impregnation has been the first step planned: the iron nitrate was added to alumina with a weight ratio of 1.5:1 in a stirred flask at 60°C for about forty five minutes. After this impregnation phase, the catalyst has been decomposed inside an oven, at about 300°C for about 4 hours . Finally the solid has been calcined by setting before a ramp from ambient temperature to 1050 °C, with heating rate of 3 °C/min, and then an isotermal (1050°C) of 12 hours. The calcination up to 1050°C was necessary in order to obtain a material feasible for solar reactor working at high temperatures (1000°C).

During the first days of manifacture, by visual analysis it turned out that the appearance of the impregnated pellets was different with respect to the catalyst prepared in the scale of few grams. In particular, the red surface layer is not homogenous, and white and pink spots were detectable (Figure 4.3).

Hence in order to understand the reason for the apparent different product obtained scaling up the method, these pellets were analysed by X-rays diffraction (XRD) technique in the angular range $4° < 2\theta < 40°$, using a Seifert

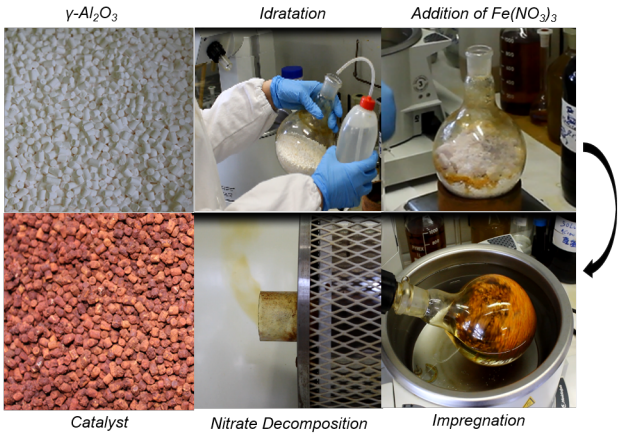

Figure 4.2: *Large amount of catalyst-preparation-procedure*

Figure 4.3: *Catalyst produced by following the procedure set up on small amount*

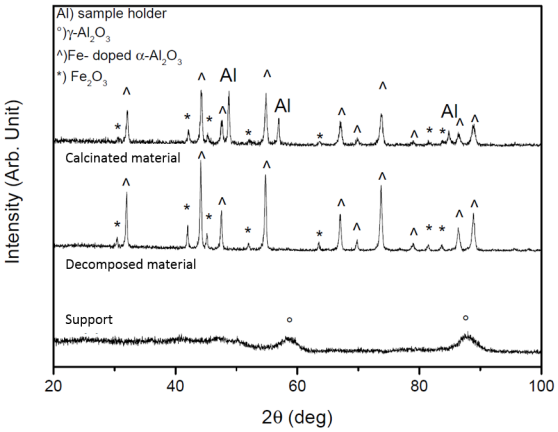

Figure 4.4: *XRD spectra of the powered catalyst produced by following the procedure set up on small amount*

Figure 4.5: *Catalyst produced by repeating twice the procedure set up on small amount.*

Pad VI apparatus equipped with Mo Kα radiation and a LiF monochromator on the diffracted beam. Actually, the white/pink substance resulted to be iron (III) oxide plus $\alpha - Al_2O_3$, where aluminium atoms are partly replaced with iron (likely Fe(III)), mixed with the expected Hematite (Figure 4.4). The substrate is confirmed as $\gamma - Al_2O_3$.

To be sure to carry out a preparation wich guaranteed the maximum coverage (detectable visually) of the substrate with active phase and therefore the best activity all the preparation procedure (figure 4.2) was repeated a second time.

The final catalyst is shown in Figure 4.5.

Finally, in order to check the feasibility of the final synthesis procedure

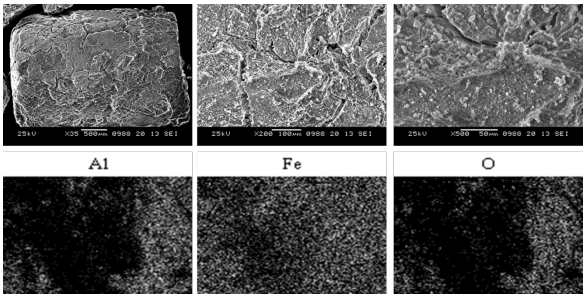

Figure 4.6: *SEM images (above) at different magnifications and elemental EDX mapping (below) of the pellets after the preparation procedure and before their usage for sulphuric acid decomposition.*

Figure 4.7: *XRD spectra of the powered catalyst before the experimental campaign.*

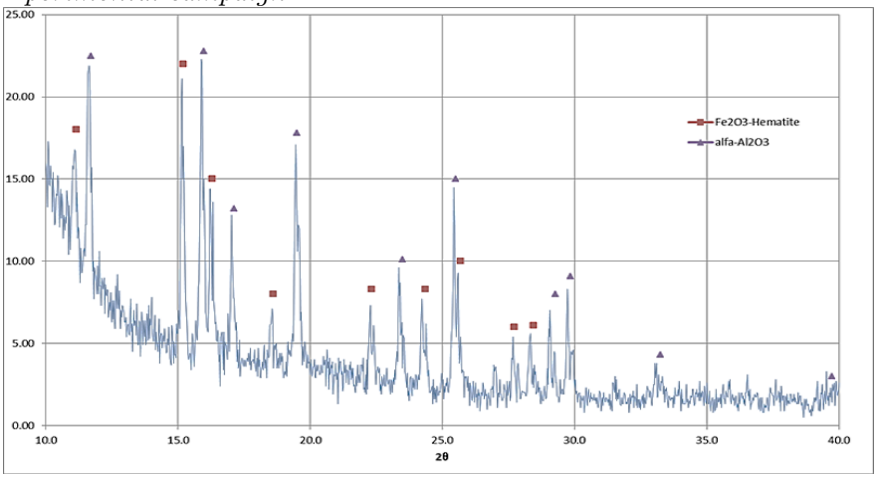

a SEM/EDX analysis was carried out also on these final pellets , by using a SEM Jeol JSM-5510LV equipped with an EDX probe IXRF EDS-2000. As Figure 4.6 shows, the active phase (brighter granules) is homogenously distributed over the alumina surface. Moreover, an XRD analysis on the powered catalyst was performed to certify that the starting support material was really $\gamma - Al_2O_3$ (Figure 4.7).

Chapter 5

Catalyst testing

The $Fe_2O_3/\ \gamma - Al_2O_3$ has been long tested in laboratory. Initially were carried out tests on catalyst stability to confirm its good performance in the operating conditions of SOL2HY2 DEMO plant. Finally, an experimental campaign for evaluating the values of catalyst activity at different operating conditions (temperature, flow rate and pressure) was carried out in order to assess the kinetics of decomposition reaction.

5.1 Materials and methods

The experimental tests were carried out in a laboratory plant, which is schematically shown in Figure 5.1.

Catalyst samples (about 2.10 g in each test) were placed in a quartz tubular reactor with internal diameter of 1.5 cm and length of 1 m. The catalytic bed was always kept at the centre of the oven by filling the above and below dead space in the reactor with inert quartz pellets. To reach the required operating temperatures, the reactor was put in a ceramic oven equipped with a PID controller, provided by CARBOLITE.

The reactor was fed from the top with a 50%wt Sulfuric acid solution, prepared by dilution of commercial 96% wt acid (Carlo Erba, reagent grade) with deionized water. The feed flowrate was controlled with a KNF LAB membrane pump. In the reactor first the sulfuric acid was vaporized and decomposed into H_2O and SO_3 and then SO_3 was decomposed into SO_2 and O_2. The outlet stream from the reactor was cooled at room temperature in order to condense water and unreacted SO_3 as an aqueous sulfuric acid solution and separate it from process. The remaining gas stream was bubbled in a concentrated hydrogen peroxide solution (Carlo Erba, 50% wt) to trap the produced SO_2. Finally, the gas stream was dehydrated through a Silica

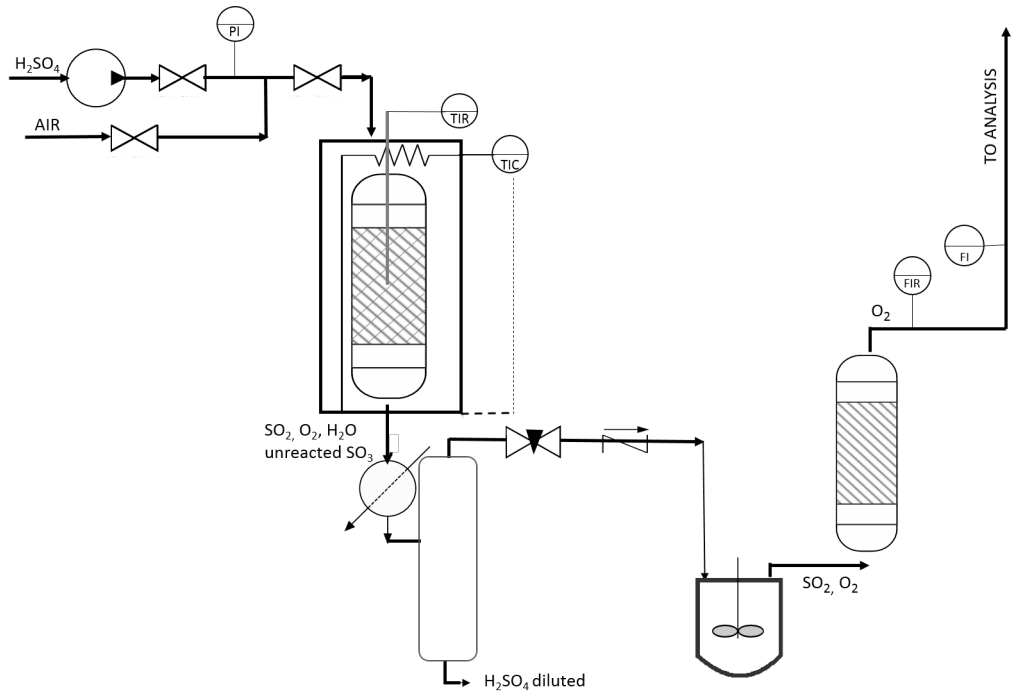

Figure 5.1: *Scheme of the laboratory plant for* H_2SO_4 *decomposition.*

Table 5.1: *Type of experiments carried out and their operating conditions.*

TYPE OF TEST	P(atm)	T_{oven}(K)	WHSV(h^{-1})
Catalyst stability	1	1273	22
Pressure effect on reaction	1; 2; 3	1273; 1233; 1198	22
H_2SO_4 flowrate effect on reaction	1	1273; 1233; 1198	22; 32

gel (Carlo Erba, Italy) packed bed and sent to a Bronkhorst mass flow meter to measure the flowrate of the produced Oxygen.

The temperature inside the catalytic bed was measured with a stainless steel thermocouple protected with an alumina coating and recorded with a MV1000-Yokogawa device. The operating pressure was manually controlled by a needle valve placed downstream of the condenser.

Before each daily set of tests, the catalyst was maintained overnight at room temperature and then heated up at the required temperature at a rate of 15 °C/min. This procedure also allowed to test the catalyst stability to daily thermal cycles, which are typical of solar-powered processes. When the operating temperature was achieved, pressure and sulfuric acid flowrate were set to obtain the desired combination of operating conditions and about 30 min allowed to reach stable operation; after that, the test was continued for about 1.5 h while recording all measured variables. At the end of the daily set of experiments, the system was purged by flowing air and then the reactor was left to cool down.

A summary with the different tests performed and operating conditions adopted is reported in Table 5.1, where the Weight Hourly Space Velocity (WHSV) is defined as the ratio of the inlet sulfuric acid mass flowrate divided by the catalyst mass. For each test, the experimental SO_3 conversion ($X_{SO_3}^{exp}$) was calculated as follows:

$$X_{SO_3}^{exp} = \frac{2F_{O_2}^{out}}{F_{SO_3}^{0}}$$

where $F_{O_2}^{out}$ is the outlet flowrate of the produced oxygen and $F_{SO_3}^{0}$ the inlet sulfur trioxide flowrate, which is readily calculated from the feed flowrate assuming full decomposition of sulfuric acid in H_2O and SO_3.

5.2 Results and discussion of stability tests

As already anticipated in the previous paragraph (Table 5.1), the tests for evaluating the catalyst stability over the time, have been carried out at 1000 °C, atmospheric pressure and WHSV= 22 h^{-1}(about 1 ml/min of SA 50%wt

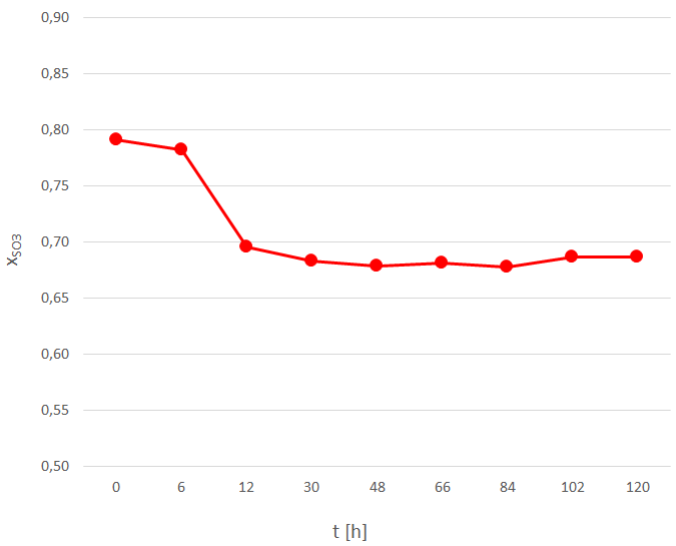

Figure 5.2: SO_3 *conversion over the time at 1273.15 K, 1 atm and WHSV about 22* h^{-1}.

solution). The value of temperature for stability test has been chosen other than 850°C, wich is much more used in literature [Brutti et al., 2006, Barbarossa et al., 2006, Ginosar et al., 2009, Karagiannakis et al., 2011, Roeb et al., 2013, Giaconia et al., 2011], for simulating the real condition inside SOL2HY2 plant. Also P and WHSV have been chosen by considering the nominal operating condition of pilot plant (P=1 atm and F_{SA}=1 l/min), taking obviously into account (for the feed flowrate) that the demo reactor is about 1000 times bigger than that employed in laboratory. As shown in (Figure 5.2), catalyst stability was monitored for about 120 working hours.

After an initial deactivation the catalyst activity kept fairly stable after about 12 h on stream, with conversion values close to 70% . This value has resulted almost satisfactory in comparison to the equilibrium conversion value for the decomposition reaction in the same operating condition, i.e. about 94% (see Figure 9.1 in the Chapter 9) .

In order to explain this initial deactivation a SEM/EDX analysis was carried out on the catalyst after the experimental campaign. In Figure 5.3 no particular sintering phenomena are detectable compared to case of not yet used catalyst (Fig. 4.6). On the other hand, the elemental mapping pictures indicate some depletion of Fe from the surface of the support; this effect, confirmed by an XRD analysis (Fig. 5.4) accounts for the initial decrease of catalytic activity. Moreover, sulphur is accumulated on the catalyst surface, although in small quantity.

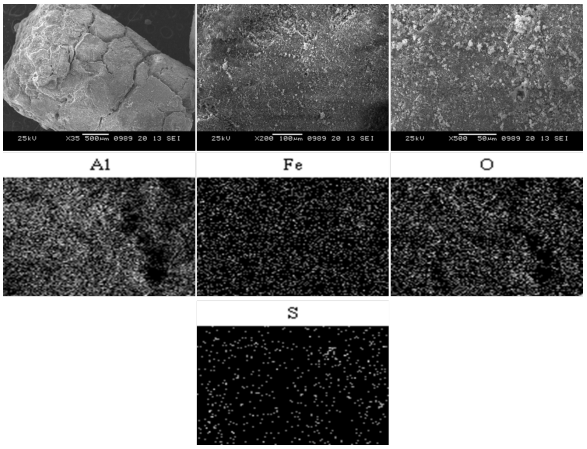

Figure 5.3: *SEM images (above) at different magnifications and elemental EDX mapping (below) of the pellets after their usage for sulphuric acid decomposition (more than 100 hours)*

As just said, in Fig. 5.4 is reported the XRD spectra of the powered catalyst. Although the starting support material was certified $\gamma - Al_2O_3$ (Fig. 4.7), the high temperature used to calcinate led to the almost exclusively presence of the α phase. Actually, this transition (through other Al_2O_3 phases) is described in the scientific literature [Lamouri et al., 2017, Legros et al., 1999]. The XRD patterns before and after the test campaign only differ for a certain depletion of hematite, in accordance with the EDX analysis.

5.3 Analysis of reaction kinetics

5.3.1 Literature survey on the kinetics of sulfur trioxide decomposition

Astholz et al. [1979] were among the first to study the kinetics of the Sulfur trioxide decomposition reaction at temperature from 1700 to 2500 K and high deegre of diluition by using of Ar as carrier gas. They treated the mechanism in terms of a unimolecular kinetic where the limiting stady was the split of a bond S-O in the sulfur trioxide, by loss of an isolated atom of oxygen. This process required overcoming a very high energy barrier and so involved a slow unimolecular kinetics. Final kinetic equation suggested was:

$$\frac{d\left[SO_2\right]}{dt} = k_I \cdot \left[SO_3\right], \ \text{mol} \cdot \text{cm}^{-1} \cdot \text{s}^{-1}$$

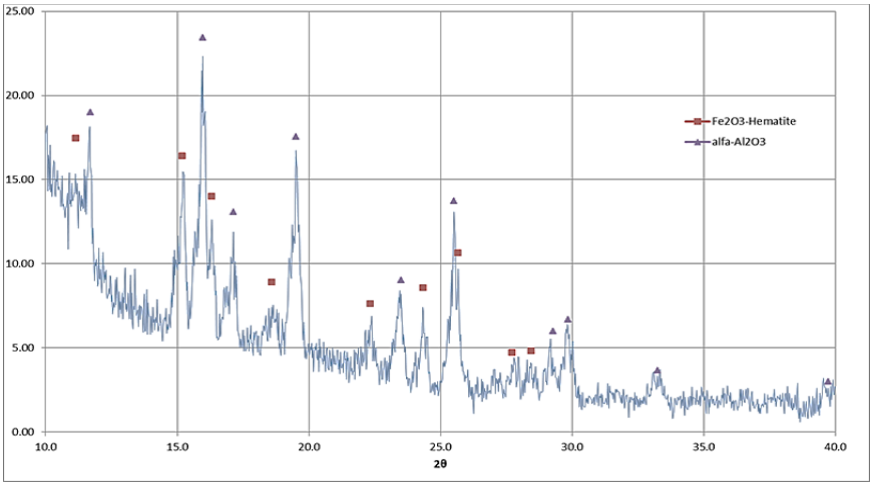

Figure 5.4: *XRD spectra of the powered catalyst after the experimental campaign*

where k_I was the pseudo-first order rate costant, given from:

$$\frac{k_I}{[\mathrm{Ar}]} = 10^{15.5\pm0.2} \cdot \exp \frac{-\left(265000 \pm 11000\right)}{RT},\ \mathrm{cm}^3 \cdot \mathrm{mol}^{-1} \cdot \mathrm{s}^{-1}$$

Also Lüpfert [1996] and Yilmaz et al. [2006] carried out the kinetic study of SO_3 decomposition reaction and provided values of rate constants substantially in agreement with those misured by Astholz et al. [1979], although at different temperature range: respectively higher ,1023-1373 K , and lower ,1000-1400 K. All the authors mentioned above not considered the presence of a catalyst in the reaction. Insted, study of catalytic activity of oxides of Ce(IV), Cr(III), Fe(III), Al, Ni, Cu and Pt, at 600-950°C in a fixed bed reactor, was carried out by Tagawa and Endo [1989] to find some suitable catalysts for the decomposition of sulfuric acid for generating oxygen in thermochemical water splitting process. The reaction mechanism considered was the following :

$$MO + SO_3 \rightleftharpoons (MSO_4) \rightleftharpoons MO_2 + SO_2$$

$$MO_2 \rightleftharpoons MO + \frac{1}{2}O_2$$

where MO and MO_2 were the reduced and the oxidized form of the metal oxide catalyst, respectively, and (MSO_4)a transient state. They assumed that the decomposition obeyed the first order rate equation with respect to SO_3 concentration

$$r = k \cdot (1 - x)$$

More recently Giaconia et al. [2011] to assess the decomposition with iron(III) oxide-based catalysts assumed a first-order kinetic law for the reaction:

$$r = k_c \cdot P_{SO_3}$$

where kc is the "intrinsic" reaction rate constant and the P_{SO_3} the SO_3 partial pressure.

5.3.2 Matematical model for the analysis of experimental data

To determine the kinetic constants of the SO_3 decomposition reaction on the selected catalyst, a simple reactor model was used. The approach is similar to the one used in a previous paper [Turchetti et al., 2016]. The laboratory reactor employed for the experimentation was modelled as an isothermal and isobaric Plug Flow Reactor (PFR). Based on these assumptions, SO_3 mass balance can be expressed as:

$$F^0_{SO_3} \frac{\mathrm{d}X_{SO_3}}{\mathrm{d}M} = r^m_{SO_3} \tag{5.1}$$

where $r^m_{SO_3}$ is the specific rate of SO_3 consumption per unit catalyst mass and M is the mass of catalyst in the reactor.

The reaction rate was evaluated by assuming the sulfur trioxide decomposition as an elementary reversible reaction, which leads to the following expression:

$$r^m_{SO_3} = -k_m P y_{SO_3}(1 - \eta_{STD}) \tag{5.2}$$

In Equation 5.2 k_m is the kinetic constant per unit catalyst mass, P the total pressure, y_{SO_3} the molar fraction of SO_3 and η_{STD} is defined as follows:

$$\eta_{STD} = \frac{y_{\mathrm{SO_2}} y^{1/2}_{\mathrm{O_2}}}{y_{\mathrm{SO_3}}} \left(\frac{P}{P_{\mathrm{ref}}}\right)^{1/2} \frac{1}{K_{STD}}$$

where K_{STD} is the thermodynamic constant of the sulfur trioxide decomposition reaction, $P_{\mathrm{ref}} = 1$ bar the reference pressure and y_i the molar fraction of component i. It is worth noting that far from chemical equilibrium, i.e., when $\eta_{STD} \ll 1$, Equation 5.2 approaches first-order irreversible kinetics respect to SO_3, which are often assumed in previous works dealing with sulfur trioxide decomposition.

By substituting Equation 5.1 in the equation 5.2 and integrating, the following expression is obtained that allows to calculate the kinetic constant from the SO_3 conversion observed in an experimental test:

$$k_m = \frac{F^0_{SO_3}}{P\,M} = \int_0^{X^{exp}_{SO_3}} \frac{\mathrm{d}X_{SO_3}}{y_{SO_3}(1-\eta_{STD})} \tag{5.3}$$

The integral in Equation 5.3 was calculated numerically considering that the PFR assumption allows to set

$$y_i = \frac{F_i}{\sum F_i}$$

and the flowrates of each component, F_i, are straightforward functions of X_{SO_3} and feed composition.

5.3.3 Results

The activity of $Fe_2O_3/\ \gamma - Al_2O_3$ has been evaluated at different operating conditions (as indicated in Table 5.1). The results of experimentation in terms of X_{SO_3} have been used as input to the Matematical model introduced in the previous paragraph (5.3.2), with the aim to assess the decomposition kinetics.

In order to study the thermal effect on the rate constant, the oven temperature was varied in a range 1198.15-1273.15 K.

In Figure 5.5 the resulting Arrhenius plot, at P=1atm and WHSV$\approx 22 h^{-1}$ which were the operating conditions closer to those of SOL2HY2 process design, is reported.

Tests were carried out, at the same previous temperatures , also by varing the pressure between 1 and 3 atm. The results showed that the pressure had influence on apparent rate constant : k^m_{STD} lower values were obtained for higher operating pressures (Figure 5.6).

By using as input of kinetic model the conversion data of [Giaconia et al., 2011], the only ones available in literature at different pressures, the same trend of rate constant with pressure has been confirmed even on other catalytic systems (Fe_2O_3 pellets and Fe_2O_3on SiSiC) and lower temperatures (800 - 850 °C).

By reporting data of Figure 5.6 in an Arrhenius plot parametric with respect to pressure, to identify the kinetic parameter at the different operating conditions was possible.

Particularly, fitting all the results simultaneously via expression 5.4

$$k_m = k^0\,|_{P_i} \cdot \exp\left(-\frac{E_a}{\mathrm{RT}}\right) \tag{5.4}$$

with k^0 = pre-exponential factor at the pressure system P_i, E_a = apparent activation energy and R is gas constant, and by forcing E_a to be constant

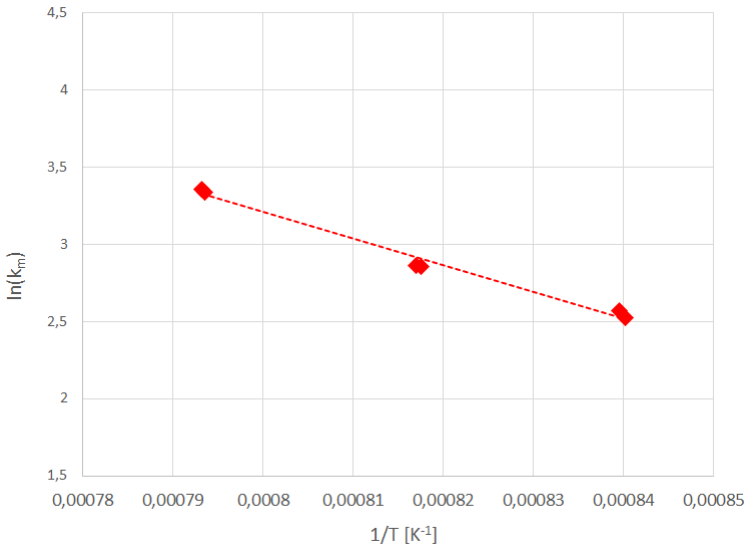

Figure 5.5: *Arrhenius plot at 1 atm and WHSV about 22* h^{-1}

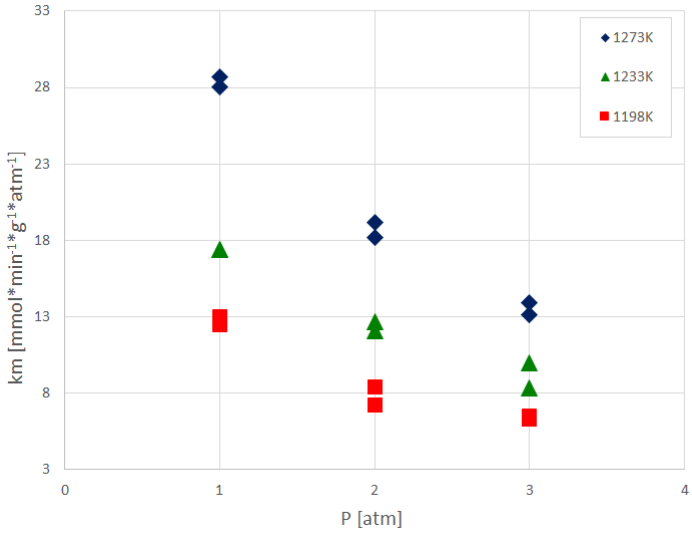

Figure 5.6: *Effect of pressure on rate constant, at WHSV about 22* h^{-1}.

Table 5.2: *Kinetic parameters at different pressure and WHSV about 22* h^{-1}

P (atm)	$k^0(\text{mmol} \cdot \text{min}^{-1} \cdot \text{g}^{-1} \cdot \text{atm}^{-1})$	$E_a(\text{kJ} \cdot \text{mol}^{-1})$
1	$3.7{\cdot}10^7$	148
2	$2.4{\cdot}10^7$	148
3	$2{\cdot}10^7$	148

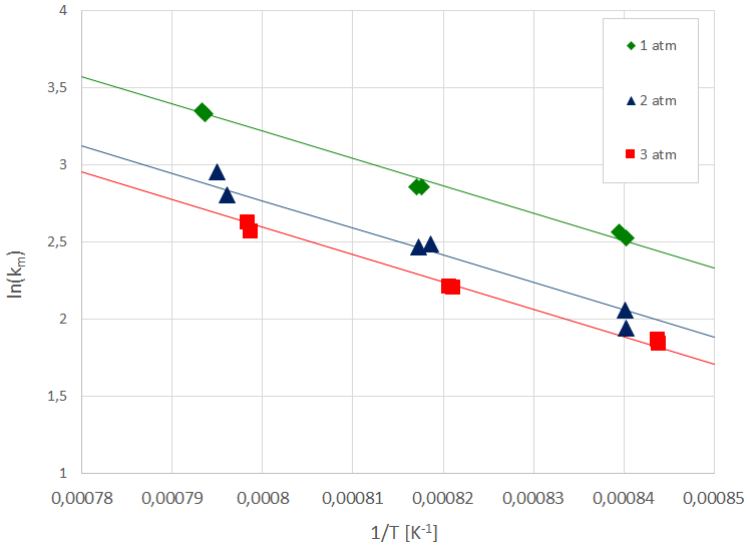

Figure 5.7: *Arrhenius plot for different pressure, WHSV about 22* h^{-1}.

for all tests, different (optimal) values of k^0 resulted at each pressure (Table 5.2) and the corresponding lines (continuous lines) have been drawn in the Figure5.7.

The kinetic parameters determined, were used as reference by DLR to size the adiabatic reactor of SOL2HY2 solar plant.

Furthermore, the effect of sulfuric acid input flow rate on conversion reaction was investigated. The results, in Figure 5.8 , showed that X_{SO_3} decresed with WHSV increasing, in accordance with other trend known in literature although for different catalytic systems and operating conditions (Tagawa and Endo [1989], Giaconia et al. [2011].

In the same Figure 5.8, the experimental values of conversion are compared with those calculated, at the same operating conditions, by the estimated kinetic parameters (continuos lines). The quite good agreement that can be observed, indicates that the model adequately describes the behavior of the reactor.

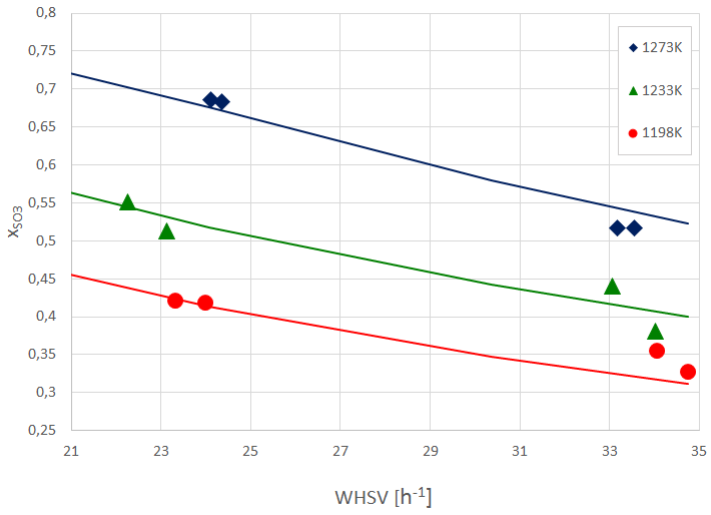

Figure 5.8: *Effect of Sulfuric acid flow rate on conversion at 1 atm.*

Finally in order to evaluate the performance of $Fe_2O_3/\ \gamma - Al_2O_3$, a comparation with other catalysts suggested by literature was carried out.

Particularly,Fe_2O_3 pellets and Fe_2O_3 supported by SiSiC, proposed by Giaconia et al. [2011] have been considered. Other literature references were excluded because their catalytic system was based on noble metals (certainly more effective but too expensive) or on materials convinient to operate mainly at temperatures lower than 800°C.

Conversion data from Giaconia et al. [2011] paper were extrapolated so that operating conditions (in terms of WHSV, sulfuric acid concentration and pressure) were the same used in the present work; these values were employed as input of kinetic model to calculate the rate constants. Since many conversion values on Fe_2O_3 pellets and Fe_2O_3 supported by SiSiC were available between 775 and 850 °C , the comparison has been performed considering two temperatures in this range (800 and 825°C). The rate constants on $Fe_2O_3/\ \gamma - Al_2O_3$ (provided by experimental test between 925 and 1000°C), were calculated by using kinetic parameter values mentionated above (k^0= 3.699·10^7 mmol min^{-1} g^{-1} $atm^{-1}$and E_a= 147.636 kJ mol^{-1}).

The results in Figure 5.9, showed that the $Fe_2O_3/\gamma - Al_2O_3$ performance was better than that of Fe_2O_3 pellets and, within the experimental error, similar to that of Fe_2O_3 supported by SiSiC.

It is worth noting that Iron (III) nitrate on Silicon Carbide was prepared by a more complex and costly method [Giaconia et al., 2011] than that used for Iron (III) nitrate on Alumina in SOL2HY2 application. Furthermore, the

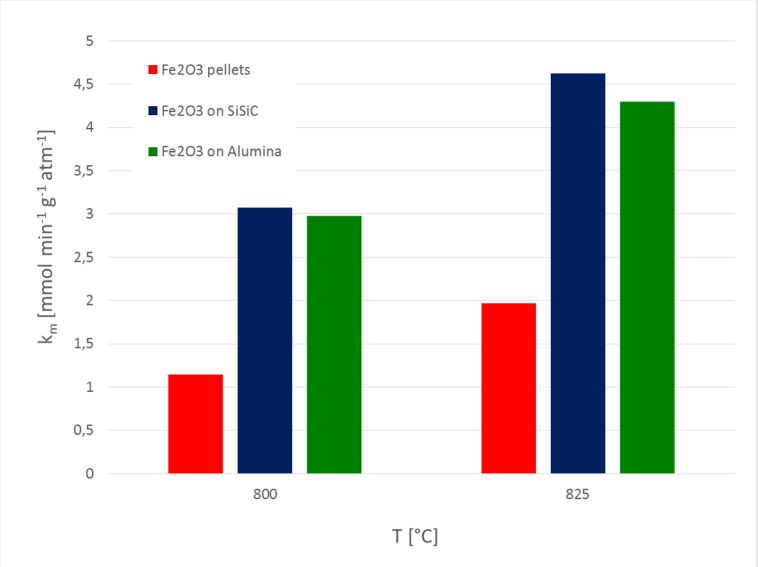

Figure 5.9: *Rate constant of different catalytic systems at 800 and 825 °C and 1 atm.*

calcination step in the case of $Fe_2O_3/\gamma - Al_2O_3$ was performed at a temperature higher than that used in the Fe_2O_3 supported by SiSiC, 1050 °C against 900°C, due to the SOL2HY2 process needs (i.e. to obtain a material feasible for solar reactor working at 1000°C). This could affect adversely the activity of $Fe_2O_3/\gamma - Al_2O_3$, due to major sintering iusses, but its performance have proved however to be satisfactory.

Hence, in comparison with other catalysts suggested by literature, $Fe_2O_3/\gamma - Al_2O_3$ exhibited better or similar performance with a greater cost-effectiveness, lower toxicity and the guarantee of easier large-scale production.

Chapter 6

Setup and thermal characterization of a pilot plant for SA decomposition

One of the main objectives of the SOL2HY2 project was the design and development of a demo plant for sulphuric acid cracking (SAC) powered by solar energy. The effective coupling of solar thermal energy to the medium temperature evaporation (Reaction 3.3) and the high-temperature SO_3 decomposition has represented a crucial point in this context.

Within the project, DLR was in charge of the design, construction and operation of a SAC pilot plant (higher than 100 kW thermal power) to be installed in its solar tower facility located in Jülich (Germany). The work carried out within this PhD project has contributed to the SAC design and demonstration activities through

- the development, kinetic characterization and production of the catalyst for SO_3 decomposition to be loaded in the reactor (Chapter 4 and 5)

- active participation to DEMO plant installation and preliminary testing during a secondment that took place from 14 September to 14 December 2015.

This chapter reports about the activities carried out during the secondment period at DLR, which mainly involved cooperation with resident staff for the preparation and installation of the temperature measurement system, calibration of part of the analysis equipment and the preliminary on-sun thermal characterization of the whole system.

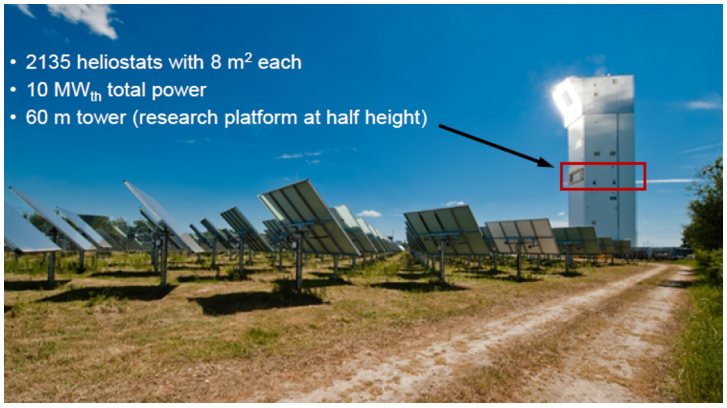

Figure 6.1: *Solar tower and heliostates field in Juelich. Reference of picture: Thomey et al. [2016]*

6.1 Description of the pilot plant

The demo plant has been designed and realised by DLR in its solar tower facility (Figure 6.1) located in Juelich, Germany.

The design builds on experimental experience obtained within the framework of previous research projects [Noglik et al., 2009, Thomey et al., 2012], in which a solar reactor for SA decomposition was developed and tested on lab-scale inside a solar furnace. In this previous reactor, evaporation and SO_3 decomposition took place inside two separate chambers containing a directly irradiated porous ceramic structure (volumetric receiver), each closed by a quartz glass window. The results obtained in the solar furnace experiments showed that, due to kinetic limitations in the inlet section of the catalytic bed and heat transfer limitations in the depth of the honeycomb, the first few centimeters of the bed acted as a solar receiver, heating up the incoming gases, while the remaining part of the bed could be practically considered as an adiabatic reactor [Botero et al., 2016].

Based on such results, the solar receiver and the reactor were kept separate in the design of the new on-sun demonstration plant, which also allowed to validate and later optimize each of these units independently.

A simplified scheme of the DEMO plant is shown in Figure 6.2.

The feed to DEMO plant is a liquid sulphuric acid flow, 1 ml/min at 50 wt%, which is injected by a peristaltic pump at the bottom of an electrical evaporator, where it vaporises. The evaporator consists of six vertical steel tubes electrically heated from outside with a power of about 60 kW. Tubes are protected against corrosion by boiling sulphuric acid, using SiC tubes filled with SiC foam structures to enhance heat transfer [Romero et al., 2014].

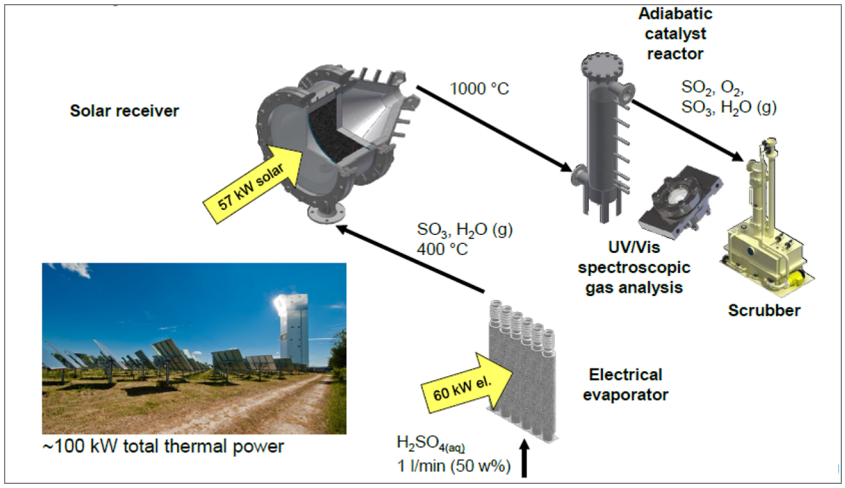

Figure 6.2: *Initial configuration of pilot plant for sulfuric acid cracking. Reference: Thomey et al. [2016].*

The acid vapour from the evaporator, with an expected temperature of about 400 °C, is collected in a steel manifold and sent to the solar receiver through a Joule heated steel pipe.

An 1-dimensional thermodynamic analysis, a CFD modelling and a ray-tracing analysis of the solar field in Juelich, were carried out to define geometry (diameter of aperture of 0.4 m), operating parameters (design point: 57 kW on aperture) and the mechanical design of the solar receiver [Niehoff et al., 2016]. Concentrated solar radiation enters the system through a planar quartz glass window mounted in a steel flange which is protected by water cooled secondary optics. The radiation heats a SiC foam absorber made up of several sections.

The acid vapour goes to the space between window and solar absorber and is superheated to a design temperature of 1000 °C while flowing through the foam structure. This hot gas is then fed to the adiabatic reactor.

The adiabatic reactor was designed by considering the kinetics of SO_3 obtained as shown in Section 5.3. It consists of a steel vessel with a packed bed of up to 50 l volume of catalyst (as already said in previous pharagraphs the catalyst is Alumina pellets coated with Iron(III) oxide). The superheated sulphuric acid gases vertically pass through the catalyst bed producing Sulfur dioxide. Considering a good chemical conversion of about 70 % (in the same operating condition the equilibrium conversion of SO_3 decomposition reaction is about 81%, see Figure 9.2 in Chapter 9), the temperature should decrease to a design temperature of 800 °C due to the endothermic reaction.

Finally a scrubber is placed downstream of the reactor to neutralize the

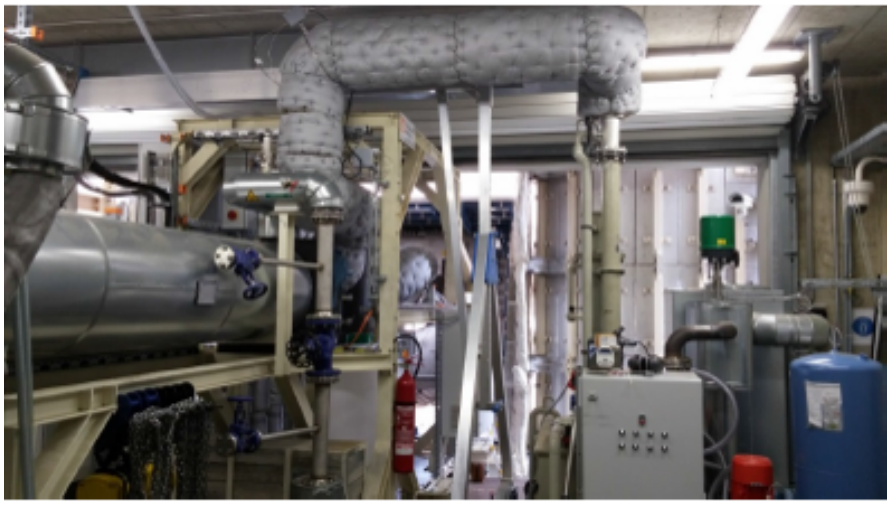

Figure 6.3: *Picture of set up DEMO plant. Reference: Thomey et al. [2016]*

acidic gases produced by chemical absorption in a NaOH solution.

6.2 Thermal characterization tests

When the plant was ready for the start-up (a picture of set up plant is shown in Figure 6.3), some preliminary on-sun tests were performed for the thermal characterization of the solar receiver-reactor system for sulfuric acid decomposition. Indeed these tests were carried out without catalyst and final conversion evaluation, but with the main objective of monitoring the temperature values in the plant detected by temperatures measurement system.

For this purpose, the thermocouples of temperature measurement system were installed in each plant section: evaporator, receiver, reactor, scrubber and piping.

The preliminary tests have been carried out by gradually approching the value chosen for each operational specification, i.e. flow rates, power to collected on the receiver and numbers of heliostates of solar field employed to reach the power set up, and are the following:

- 02/10/2015: test with air and steam (some of the operational specifications are reported in Figure 6.4)

- 11/10/2015: test with air and steam (some the operational specifications are reported in Figure 6.5)

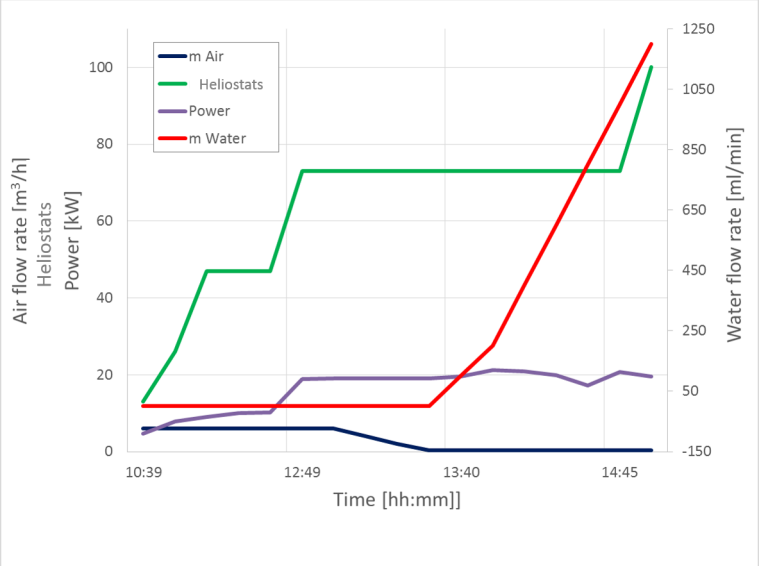

Figure 6.4: *Trend of some operational specifications during the test of 02/10/2015. Diagram prepared in cooperation with DLR.*

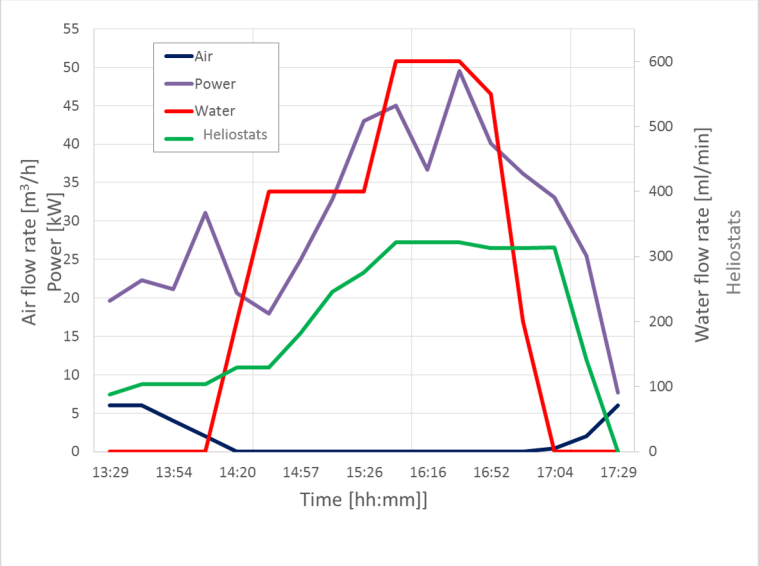

Figure 6.5: *Trend of some operational specifications during the test of 11/10/2015. Diagram prepared in cooperation with DLR.*

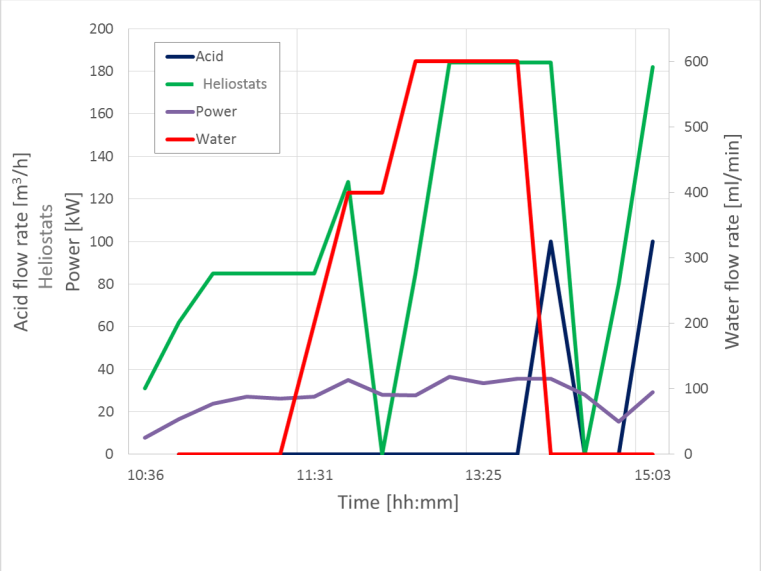

Figure 6.6: *Trend of some operational specifications during the test of 27/10/2015. Diagram prepared in cooperation with DLR.*

- 27/10/2015: test with steam and acid (some the operational specifications are reported in Figure 6.6)

6.3 Results and discussion

Temperature trends related to the main sections of plant, collected and processed during these preliminary on-sun tests, are reported in the Figures 6.7,6.8 and 6.9.

As regard to test with air and steam of 02/10/2015, the results in Figures 6.7 shown that the temperature in each of the six evaporator tubes (Evaporator 1, Evaporator 2, etc..) reached and stabilised over the test period around values of 400 °C. This is exactly what was expected according to the preliminary simulations performed to design the evaporator [Romero et al., 2014]. Hence, the evaporator design could be considered complying with the plant operational needs.

Regarding to the temperatures trend into receiver, the results showed that the temperatures reached over the test period in the absorber side were in the range 800-1000°C. This is a satisfactory result considering the termal level required in the plant for the decomposition reaction (1000°C), also bearing in mind that this temperature could be potentially increased by varying some operational specifications (increasing the value of power and so the numbers

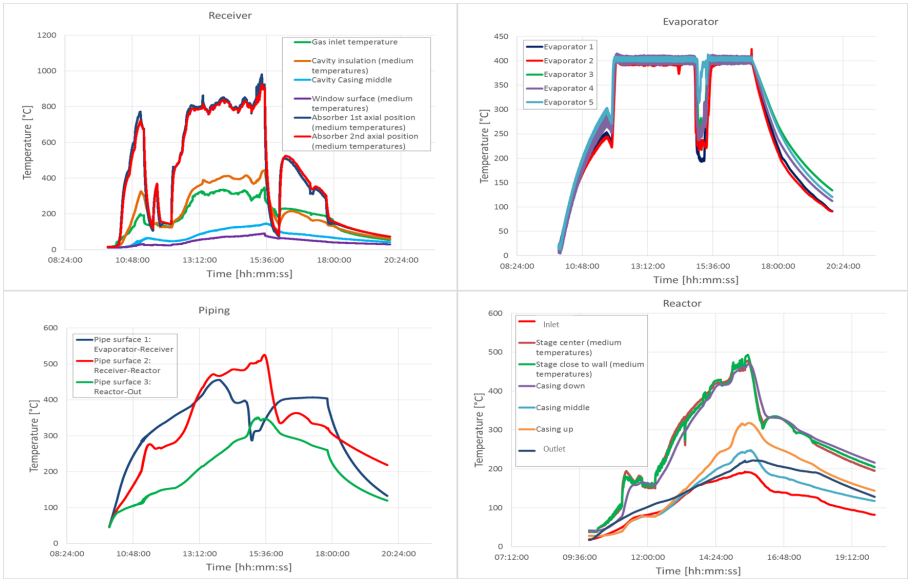

Figure 6.7: *Temperature trends collected during the on-sun test of 02/10/2015, related to main sections of plant. Diagram prepared in cooperation with DLR.*

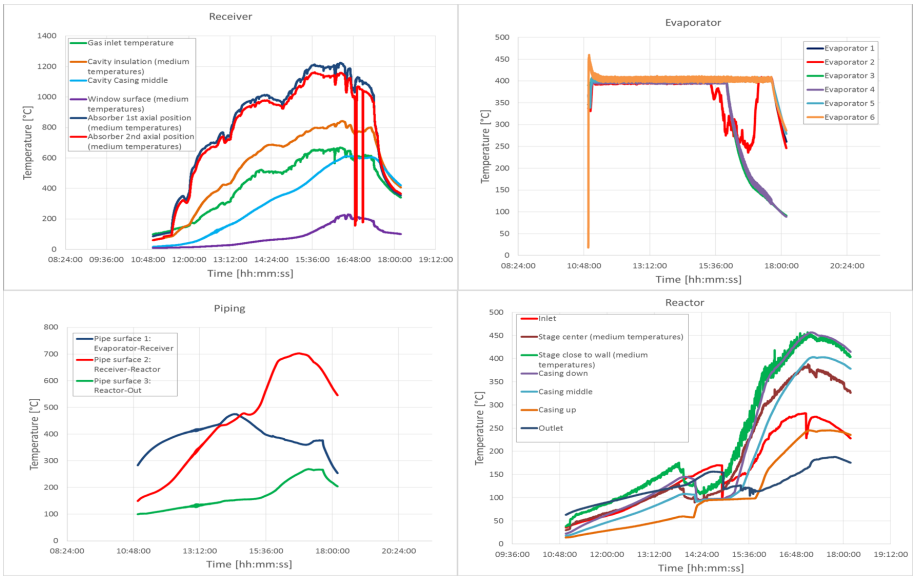

Figure 6.8: *Temperature trends collected during the on-sun test of 11/10/2015, related to main sections of plant. Diagram prepared in cooperation with DLR [Niehoff et al., 2016].*

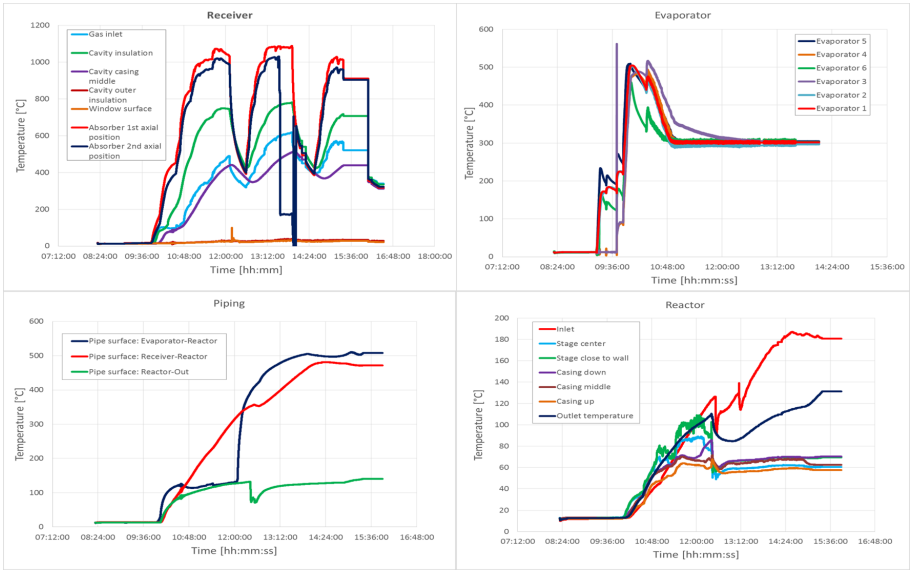

Figure 6.9: *Temperature trends collected during the on-sun test of 27/10/2015, related to main sections of plant. Diagram prepared in cooperation with DLR.*

of heliostats).

The temperature trend on the quartz glass window of receiver was lower; this is normal if it is considered that in the plant design this window is mounted in a steel flange which is protected by water cooled secondary optics. It meant that the cooling system worked well.

The temperature of inlet stream to receiver reached and stabilised over the test period around value of 300 °C, lower than value of 400°C in the evaporator, keeping the trend detected into piping section between evaporator and receiver (Pipe surface 1), where heat losses so occurred.

Crossing the piping between receiver and reactor (Pipe surface 2), the outlet stream from receiver section of process could meet a maximum temperature of about 700°C; this higher temperature was obviously determained by the influence of irradiate heat from absorber.

However moving into reactor, the results showed that the maximum temperature met by stream was of about 450°C. This temperature was detected the reaction section closer to wall and so overlooking the absorber, while the temperatures reduce moving inside the reactor. Since the minimum temperature required to ensure the activity of SO_3 decomposition reaction catalyst equal to about 780°C [Norman et al., 1982]), these results revealeted that the temperatures trend in the reactor was not appropriate for the decomposition reaction.

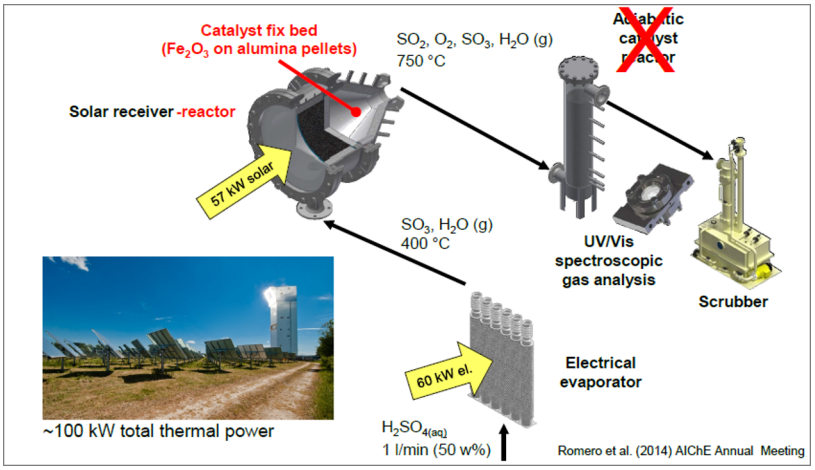

Figure 6.10: *Final configuration of pilot plant for sulfuric acid cracking. Thomey et al. [2016].*

By looking at the results of the other two tests (Figures 6.8 and 6.9) more on less similar temperatures trends could be detected. However, it is worth to note that the temperatures reached into receiver were higher than those of first test (lower than 1000°C), particularly around 1200°C for the test with air and steam of 11/10/2015 and around 1100°C for the test with steam and acid of 27/10/2015. This depends from the increasing of value set for the power to plant (and so of heliostates number), as can be seen comparing the operational specifications in Figures 6.5 and 6.6 with those in Figure 6.4.

However, the results showed that the temperatures recorded into reactor also in these two last tests, seemed to be much lower than that expected: less than 500°C in the test with air-steam (Figure 6.8) and even lower than 200°C in the tests with steam-acid (Figure 6.9).

It meant that a different configuration of plant decomposition section was required to avoid catalyst deactivation.

On the basis of preliminary tests results, DLR has hence re-iterated the design of the system by placing the catalyst bed closer to the receiver, where high temperatures were reached (about 1000°C, as shown in the figures 6.7,6.8 and 6.9).

The new configuration is reported in Figure 6.10.

Finally, an experimental campaign in actual reaction conditions was carried out in the DEMO plant last April 2016 [Thomey et al., 2016] .

Part III

Process analysis and techno-economic assessment

Introduction to process analysis and techno-economic assessment

As anticipated in the Chapter 3 talking about the Objectives of thesis, the analysis of HyS-Sol process with techno-economic evaluation has represented an important part of PhD activity.

For this purpose, starting from the informations about conventional HyS cycle, in the first place a simplified block diagram for the solar-powered process (already presented in the previous Chapter 3) has been developed, and it is shown in Figure 6.11,where the main energy input types required by the different process blocks are highlighted.

The effluent anolyte SA solution from the SDE is concentrated before being evaporated and heated at 1000 °C. The gas stream at 1000 °C, which is composed almost only of $SO_3$and H_2O, is fed to an adiabatic reactor where SO_3 is decomposed in SO_2 and O_2.

Since the conversion of decomposition reaction is thermodynamically limited, the separation and recycling of unreacted SO_3 to the reactor's feed is required. Finally, the produced SO_2 is separated from O_2 by refrigerated compression and recycled to SDE.

For several self-evident reasons, if possible, the chemical plant should be operated continuously; however, the use of the intermittent solar source to power the process requires a part of the plant to work discontinuously 8 h per day, when the solar radiation is available. SA and SO_2 storage tanks are used as a buffer to decouple the operating regimes of the continuous and discontinuous part of the chemical plant.

The main units identified in this simplified scheme, i.e. SDE, Concentration section, SAC, SO_3 and SO_2/O_2 separation sections has been then individually studied and developed.

Particularly for each of them starting from analysis of their general aspect, the different possible process schemes have been identified and compared

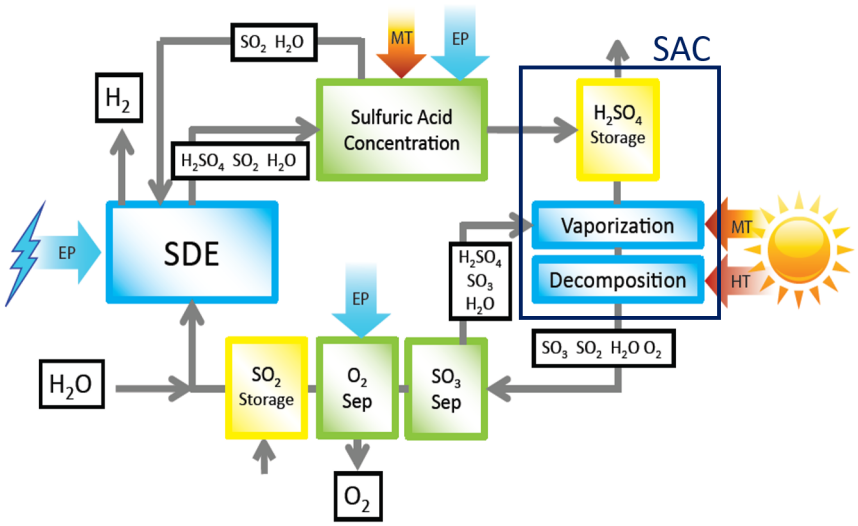

Figure 6.11: *Simplified block diagram of the HyS process considered here. The main energy input type required by the different process blocks is highlighted (MT: medium temperature heat; HT: high temperature heat; EP: electric power). Reference: Liberatore et al. [2016].*

(where it was possible) to select the most suitable one. Finally, the flowsheet of the selected process for the unit in question has been developed .

By this assessment, the definition of the final block diagram for the whole HyS-Sol process with global energy requirements and efficiencies evaluation was possible. In this context, the main process equipment were sized and costed for the final economic assessement.

Indeed to complete the work, the evaluation of different integration configurations between chemical and solar plants has been addressed with the identification of the best configuration in term of Hydrogen cost and share in no-fossil energy of total power used in the process. Particularly over the course of this assessement, also the possibility to integrate other energy source thecnologies in addition to Concentrating Solar thermal ones, i.e. Sulfur burning and Photo Voltaic (PV) has been envisaged.

Chapter 7

Sulfur dioxide depolarized electrolysis

As already pointed out, one of the fundamental steps in the HyS cycle is the Sulphur dioxide Depolarized Electrolysis, in which sulfur dioxide produced in the high-temperature step of the process is electrochemically reacted with water to produce hydrogen and sulfuric acid:

$$SO_2 + 2H_2O \rightarrow H_2 + H_2SO_4$$

Despite its importance in the cycle, the SDE block of the HyS process is outside of the scope of this PhD work, which was mostly focused on the high-temperature block of the process. However, this chapter reports general information on the SDE technology and on its current developments as well as performance data of the SDE unit developed within the SOL2HY2 project, which were used in this work to determine the energy requirements of the SDE process block. Such information was derived from the literature or directly provided by the Research Grouping Aalto Korkeakoulusäätiö (Aalto University Foundation), which was in charge of the development of the SDE demo unit within the SOL2HY2 project.

7.1 General aspects of SDE

Compared with liquid water electrolysis, SDE is characterized by a much lower standard potential (0.16 V vs 1.23 V, see Table 7.1) and could therefore require a much lower electricity consumption for the production of hydrogen. Furthermore, liquid water electrolysis requires high over-voltages (practical operating voltages reach up to 1.8-2.2 V[Gorensek et al., 2009], resulting in an even higher electricity demand

Table 7.1: *Summary of electrodic reactions involved in water electrolysis and SDE.*

Electrolysis	Electrode	Reaction	E^0[V]
Water	Anode	$2H_2O \rightarrow O_2 + 4H^+ + 4e^-$	1.23
	Cathode	$2H^+ + 2e^- \rightarrow H_2$	0
SDE	Anode	$SO_2 + 2H_2O \rightarrow H_2SO_4 + 2H^+ + 2e^-$	0.16
	Cathode	$2H^+ + 2e^- \rightarrow H_2$	0

Moreover, due the high operation voltage at the anode, the use of quite expensive construction materials is needed and this increses additionally the H_2 production costs.

On the other hand, in the case of SDE significantly lower over-voltages may occur and practical operating voltages in the range 0.5-1.2 V can be expected [Gorensek et al., 2009], depending on the current density and other operating conditions [Staser and Weidner, 2009, Lu and Ammon, 1982, O'Brien et al., 2010]).

The structure of a SDE cell, such as those of polymer electrolyte membrane (PEM) water electrolysers and PEM fuell cells, consists of two electrodes and a proton polymer electrolyte membrane, usually Nafion, which separates the anode stream (anolyte) and cathode stream (catholyte) as presented in Figure 7.1 . The anolyte is a diluted H_2SO_4 solution in which SO_2 is dissolved, while the catholyte can be water [Gorensek, 2011] or a sulphuric acid aqueous solution [Aalto-University, 2014].

As summarized in Table 7.1, at the anode SO_2 is oxidized to H_2SO_4 with the production of protons and electrons. While protons can cross the PEM, electrons are rejected and reach the cathode through the electric circuit of the cell; here they meet the protons to form hydrogen.

7.2 Development of SDE technology

Over the years, research on SDE systems focused mainly on the selection of materials and catalysts for the anode. Among different catalysts proposed [Xue et al., 2014, Colon-Mercado and Hobbs, 2007, Kriek et al., 2014, O'Brien et al., 2010], Pt [Lu, 1983] and Au [Quijada et al., 2000] were mostly considered. Since whole Pt coatings are very expensive and SO_2 strongly adsorbs on Pt surface sites, leading to increased anodic overpotentials [O'Brien et al., 2010, Quijada et al., 2000], Au has been selected as anodic catalyst within the framework of SOL2HY2 project Santasalo-Aarnio et al. [2016a]. Because the cathode reaction can occur on various different surfaces in sulfuric acid

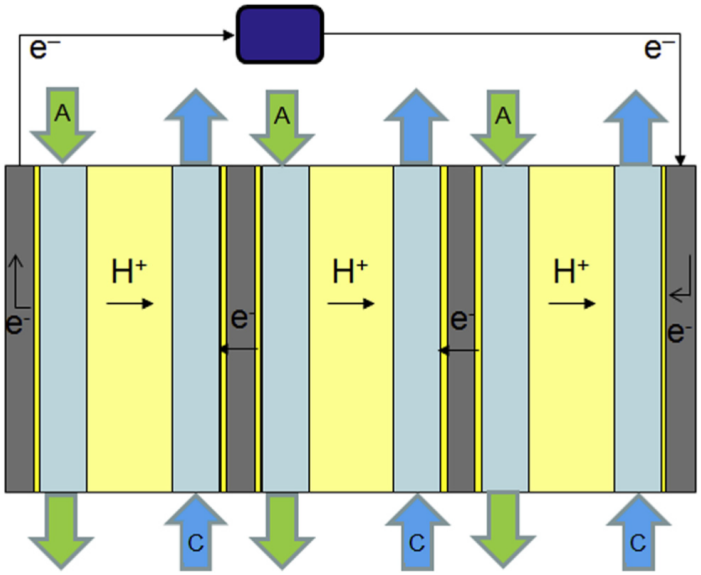

Figure 7.1: *PEM SDE module with 3 cells. The flows of anolyte and catholyte are marked with A and C, respectively. The yellow-shaded area represents the nafion membrane. Reference: Santasalo-Aarnio et al. [2016a].*

media, including polycrystalline Pt and Au electrodes [Mukouyama et al., 2008], Au can be used as catalyst for both electrodes in SDE application.

For industrially relevant H_2 production rates, the single cell configuration must be scaled either by increasing the cell geometric size or connecting the cells in series (a SDE stack with 3 unit cells is in Figure 7.1) with an increase of operating voltage of the stack.

Bipolar plates, already used in PEM fuel cells and electrolysers, have been considered to connect the cells in series: the anode reaction takes place on one side of the plate and the produced electrons are conducted through the plate to other side that acts as the cathode of the following unit cell (Fig. 7.1).

Great relevance is assumed by the choice of materials for these bipolar plates, that should offer high corrosion resistance and surface conductivity, good heat transfer properties, simplicity of manufacture and cost-effectiveness. Carbon based materials have been widely used in PEM fuel cells for the optimal combination of thermal and electrical properties in addition to low weight which is vital for transport application [Antunes et al., 2011]. On the other hand stainless steel based materials have been also considered for their cost efficiency and plasticity [Davies et al., 2000, Lee et al., 2005].

Since for stationary applications like the electrolysers, the relevance of stack weight is low but extremely important is mechanical strength and durability, the stainless steel plates have been preferred.

Initially, on the basis of an accurate literature survey, two different SS substrates 316L and 904L were identified for application in the SOL2HY2 project and analysed to evaluate their thermodynamically suitability in SDE conditions [Santasalo-Aarnio et al., 2016a]. Results have showed that 904L provided sufficient thermodynamic stability in operating SDE electrolyte concentration (10-40% wt of SA solution both SO_2 saturated and no SO_2 saturated) and temperature range (20°C-70°C).

To enhance corrosion resistance, both some additives (Fe, Ni and Cr also small amounts of Mo, Cu, Mn and Si) have been added to steel and the bipolar plates have been coated by thin Au layers, wich assume a dual function: providing electrocatalytic surface for both electrode reactions and improving the stainless steel support corrosion tolerance. Hence the stability and performance of the coated bipolar plates were tested in a bench-scale electrolyser setup, whose detailed description is reported in the work of Lokkiluoto and Gasik [2013]. The results have confermed that these plates could be utilized as economic catalyst for SDE, with moreover a satisfying corrosion resistance in SDE operation [Santasalo-Aarnio et al., 2016a].

It is worth to note that differently from previous demonstrations for SDE stacks, performed by using pressurized liquid electrolyte [Summers, 2008] or ambient gas-phase reagents [Stone et al., 2011], in the SOL2HY2 process a liquid fed for SDE stack at ambient pressure, has been considered [Gasik et al., 2017]. To optimize the H_2 production of the stack, several parameters have been observed from the whole stack and from individual unit cells in order to understand the mechanisms inside the SDE during operation. Particularly, the electrolyte flow in stack design presents especial interest due to importance to separate the anode and cathode reactants: the separator PEM membrane has water-filled channels permitting hydrated proton transport [Mauritz and Moore, 2004] and balancing the sulfuric acid concentration between electrolytes. Along these channels also other small uncharged molecules (like SO_2) can diffuse and reach the cathode, where possible parasitic reactions may occur; the most common parasitic reactions are SO_2 reduction to S and H_2S [Santasalo-Aarnio et al., 2016b]. For ensuring efficient SDE operation, these side reactions should be avoided and especially in stack design, this issue becomes more significant due to increase of the membrane electrolyte interface.

In this regard, two different anolyte flow options were tested and their schematics are presented in Figure 7.2 : the direct flow of the electrolyte with constant SO_2 concentration to each unit cell (Z-configuration) and the

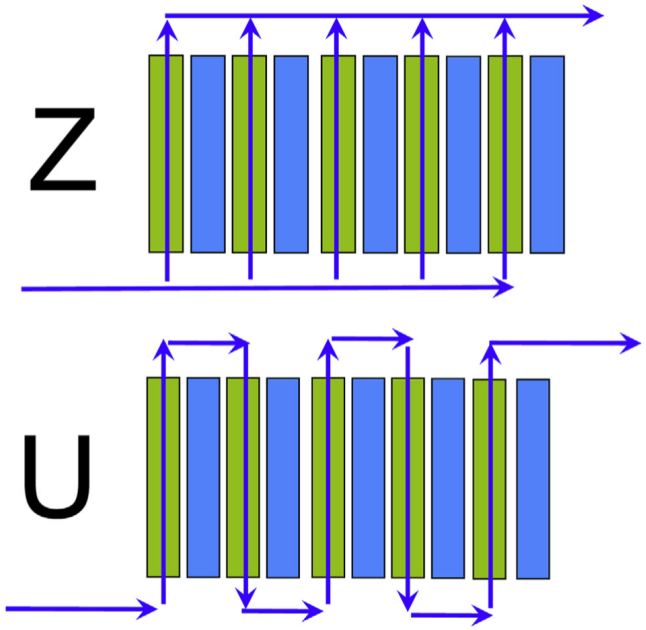

Figure 7.2: *Different anolyte flows in the SDE stack: in the Z configuration the same anolyte will be directed to each cell, in the U-configuration the output of the cell is input to the next unit cell and* SO_2 *concentration decreases in each cell. Green blocks correlate to anolyte streams, blue catholyte streams (always Z-configuration). Reference: Gasik et al. [2017]*

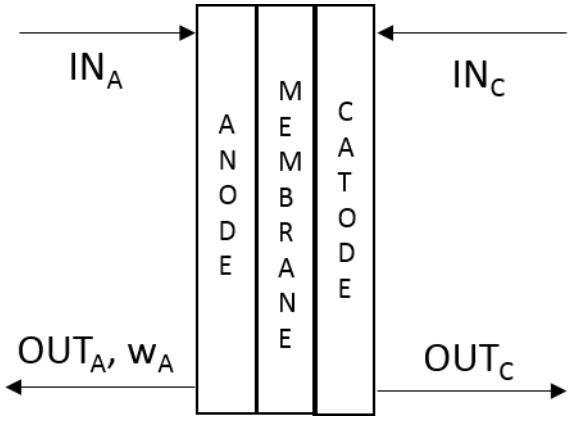

Figure 7.3: *Block related to elecrolytic section with inlet and outlet flows.*

serpentine flow where electrolyte enters each unit cell one at a time possible reducing SO_2 concentration in each cell (U-configuration).

Results revealed that the U-configuration offers 40% increased efficiency compared with the Z-configuration, indicating that as expected the anolyte flow design presents a great influence on the performance of the stack. However, the main drawback of U-configuration is the increased SO_2 carry-over to the cathode promoting side reaction and in long term operation lowering the stack efficiency. These both phenomena are due to larger residence time of the SO_2 containing electrolyte in the stack.

To ensure prolonged stack operation, the environment of individual unit cells was further studied and the results implied that none of the unit cells experienced high voltage that could damage the coatings on the bipolar plates. Nevertheless, additional optimization of the stack will be required to reach the efficiency of a single cell and to avoid SO_2 carry-over to ensure long time operation.

7.3 Process simulationsof the electrolyser

For the purpose of process flowsheeting, a simple model of the electrolyser indicating the mass balances was used, and it is schematized in Figure 7.3.

The anode inlet stream (IN_A) consists of SO_2, H_2O and H_2SO_4. The catode inlet stream (IN_C) is an aqueous solution of H_2SO_4 while the catode outlet stream (OUT_c) consists of H_2SO_4,H_2O and H_2.

The anode outlet stream (OUT_A) is a sulfuric acid solution charachterised by a SA weight concentration w_A. Particularly, this stream represents the inlet flow to Concentration Section of SOL2HY2 (stream named “FEED” and

Table 7.2: *Data related to electrolyzer provided by Aalto University Foundation*

w_A [%wt]	ΔV_{SDE} [Volt]	Electrical Power [kJ/mol of produced H_2]
13	1.25	259
20	1.34	275

characterised by the SA weight concentration w_{in} in the Chapter 8). Furthermore, the temperature and pressure values of OUT_A are respectively 25 °C and 1 atm according to the operating conditions set up in the configuration developed by Aalto University Foundation for SOL2HY2 project.

The SDE performance and particularly the value of electric potential to Electrolyser (ΔV_{SDE}) from which derives the electrical consumption are affected by anolyte composition.

In this context, in table 7.2 are reported the values of ΔV_{SDE} and of electrical power for mole of produced $H_2$for two values of w_A, i.e. 13 and 20 %wt which were considered the best choices from an operational point of view for the global process. These performance data have been provided by Aalto University Foundation and their knowladge has been necessary for the consumptions and efficiencies evaluation of SOL2HY2 process.

Chapter 8

Sulfuric acid concentration

8.1 Process screening

Sulfuric acid is rather diluted in the outlet anolyte solution of the SDE. In order to reduce the requirements for high temperature heat, such solution must be concentrated before sent to SAC section.

In order to realize the sulfuric acid concentration the only possible solution was represented by distillation process. Based on the result of a preliminary considerations on the number of theoretical stages required, an exhaustion column of three stages has been set.

With the purpose to increase as much as possible the process efficiency, have been developed strategies of heat recovery. In this context three methods were considered:

1. the preheating of feed with column residue (Fig. 8.1);
2. the preheating of feed firstly with steam from the column top and then with column residue (Fig. 8.2);
3. thermo-compression of overhead steam (Fig. 8.4): to exploit the latent heat of the steam from the column top (stream 5 in Fig. 8.4), this vapour has been compressed to 2.3 atm and employed for preheating the feed of column (stream 2 in Fig. 8.4) up to a temperature different depending on both initial and final acid concentration considered.

These methods were compared in terms of energy demand. The first two methods were not chosen for the final flowsheet, because the thermo-compression procedure of the vapour from the column top, required the minor external input of energy as the Figure 8.3 shows. In this figure a case study with SA final concentration = 0.75 (wt/wt) is shown, but the same trend resulted for all the other specifications.

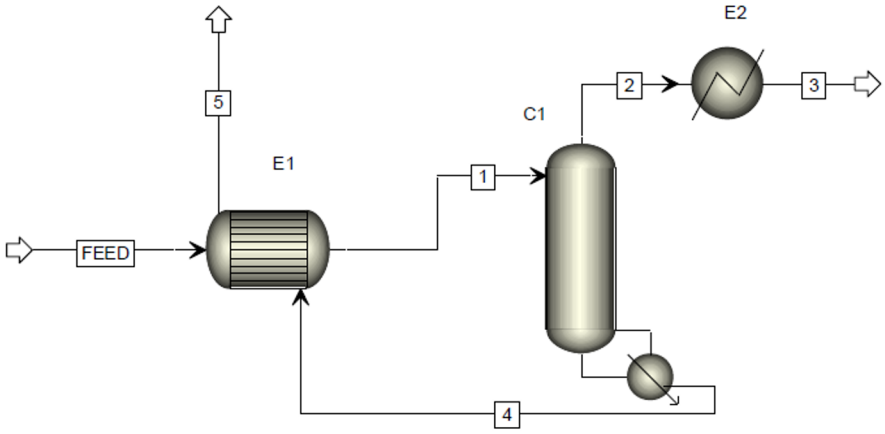

Figure 8.1: *Scheme of preheating with the column residue*

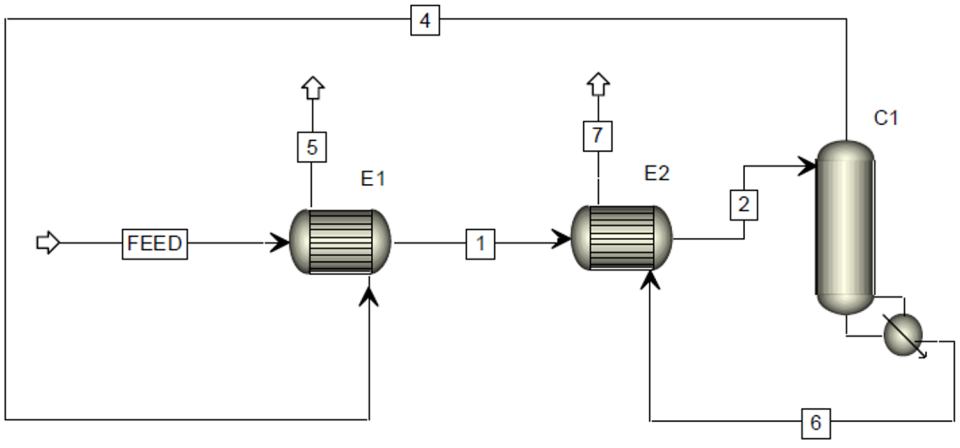

Figure 8.2: *Scheme of preheating with steam from the column top and with column residue*

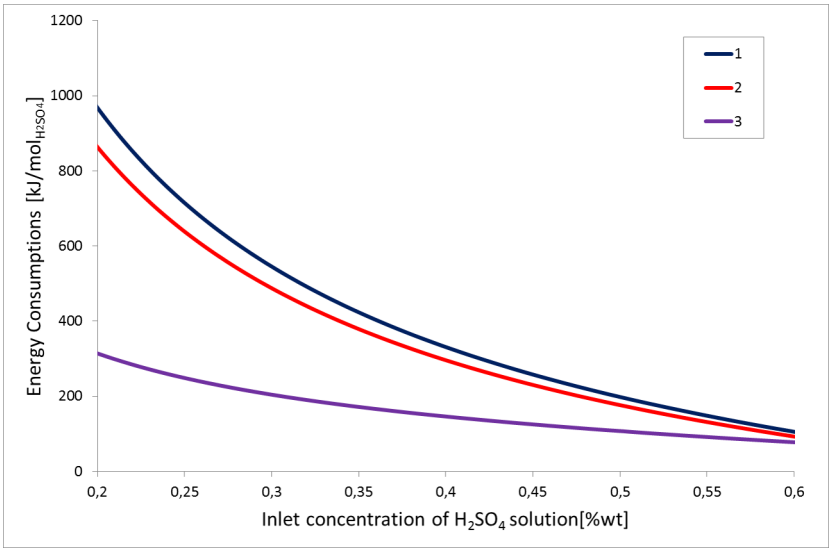

Figure 8.3: *Consumptions comparison between different configurations for the concentration section: 1) Preheating of feed with column residue, 2) Preheating of feed with steam from the column top and with column residue, 3) Thermo-compression of overhead steam. SA final concentration = 0.75*

8.2 Flowsheet development

For the simulations carried out by using Aspen Plus®, $1\text{mol} \cdot \text{s}^{-1}$of H_2SO_4 coming from the SDE at 25°C and 1 atm, has been set as input to concentration section (FEED in Fig. 8.4). In addition to this stream a recycle of SA with low composition (about 35%wt) coming from SAC section is introduced (stream R-SAC in Figure 8.4 wich is the same of stream 13 in Figure 9.5).

The energy consumptions have been evaluated at two different values ofH_2SO_4 final concentation w_{out} (50 and 75 %wt), considering a range of 13-20 %wt for the H_2SO_4 initial concentration w_{in}.

The acid final concentration values have been choosen considering the effect on energy consumptions both for the concentration step and for the following decomposition section. Indeed, the consumptions related to concentation unit grow with increasing final concentration, while an opposite trend results for consumptions of the SAC. Hence, values of 50 and 75 %wt represented a good compromise.

The final flowsheet relating to the concentration section, realized and processed in Aspen Plus®, is shown in Figure 8.4 .

The results in terms of eletric and thermal consumptions at the different specific conditions are listed in Table 8.1 and the trend of global consumptions

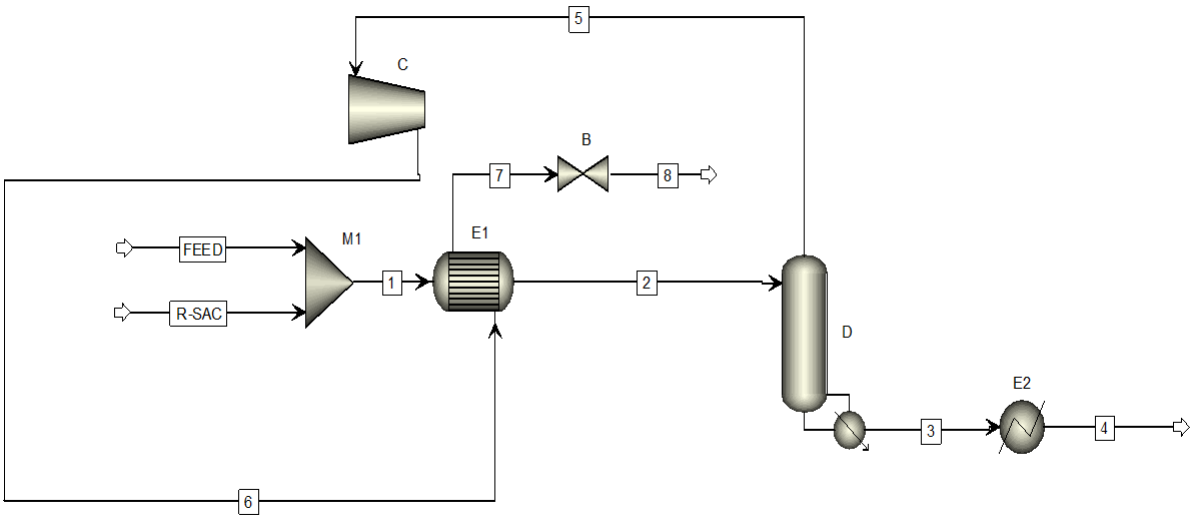

Figure 8.4: *Flowsheet of Concentration section*

is also plotted in Figure 8.5.

Clearly the energy demand for the concentration process increases as the difference between the inlet and outlet sulfuric acid concentrations increase.

Table 8.1: *Energy consumptions for Concentration section*

w_{in} [%wt]	w_{out} [%wt]	W_{C} [kJ/mol SA]	Q_R [kJ/mol SA]	C_{tot} [kJ/mol SA]
13	75	120,45	133,67	434,795
14	75	116,94	121,43	413,78
15	75	113,15	112,74	395,615
16	75	109,58	104,01	377,96
17	75	107,19	95,19	363,165
18	75	104,66	89,95	351,6
19	75	102,02	82,9	337,95
20	75	100,66	77,57	329,22
13	50	107,47	114,68	383,355
14	50	102,21	103,36	358,885
15	50	98,85	93,64	340,765
16	50	94,83	85,54	322,615
17	50	92,16	77,41	307,81
18	50	88,72	70,92	292,72
19	50	86,65	66,05	282,675
20	50	84,66	59,53	271,18

w_{in}weight compositions of input (FEED in Fig. 8.4)
w_{out} weight compositions output (stream 4 in Fig. 8.4)
W_{C}: net work of compressor C;
Q_R: reboiler heat of column D;
C_{tot}: total consumption calculated as $\frac{(W_{\mathrm{C}}+Q_R)}{0.4}$.

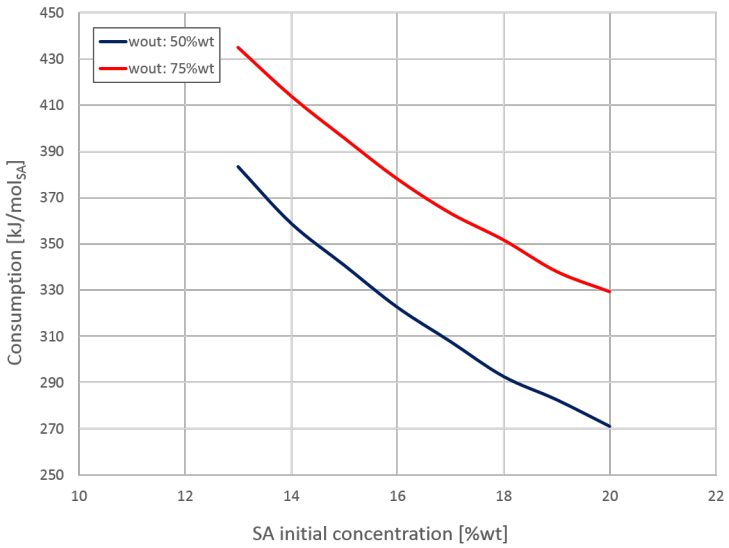

Figure 8.5: *Trend of global consumptions for the Concentration section with the SA initial concentration considering two SA final concentration, i.e. 50 and 75 %wt.*

Chapter 9

Sulfuric acid decomposition and Sulfur trioxide separation

9.1 General aspect

Due to thermodynamic limitations, the SO_3 decomposition reaction carried out in the SAC

$$SO_3 \rightleftharpoons SO_2 + \frac{1}{2}O_2 \;\; \Delta H(298\,K) = 98.9\,{}^{kJ}/_{mol} \tag{9.1}$$

does not attain complete conversion and SO_3 can be present in the outlet reactor stream also in a considerable amount.

The actual SO_3 conversion depends also on reaction kinetics; however, its maximum value is limited by thermodynamic equilibrium conditions, which in turn depend on temperature, pressure and composition of the reactor feed. Indeed, a mixture of steam and SO_3 is fed to the SAC, whose composition depends on the concentration level fixed in the SA concentrator and the presence of recycle streams.

As a reference, the equilibrium SO_3 conversion is plotted in Figure 9.1 as function of reactor feed composition at different temperatures and 1 bar (which is representative of the operating pressure for SOL2HY2 SAC reactor). It can be seen that, since Reaction 9.1 is endothermic, obviously the equilibrium conversion increases with temperature; furthermore, although H_2O is in fact an inert in SAC, since reaction occurs with an increase of moles, an increase of H_2O concentration in the reactor feed is beneficial for SO_3 conversion at equilibrium. Fig. 9.1 is a good reference if the decomposition reaction is carried out in a reactor approaching isothermal conditions.

Actually, the SAC demonstrator that is being developed in the SOL2HY2 project is constituted by a solar heater followed by an adiabatic reaction

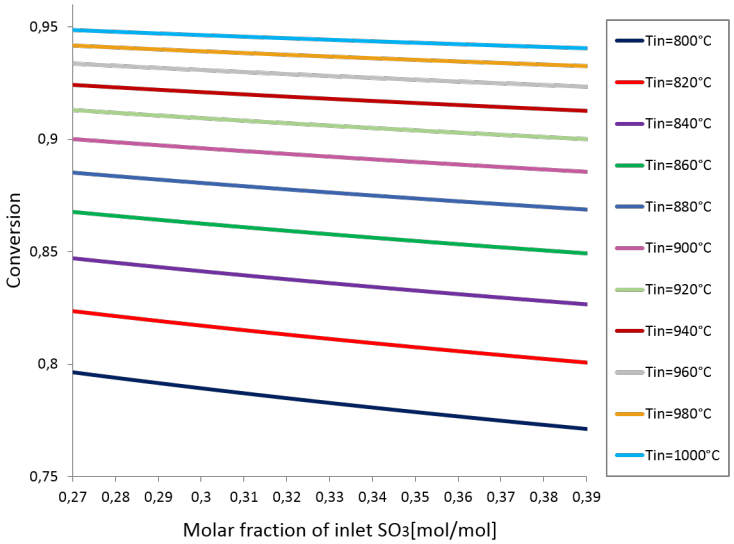

Figure 9.1: *Equilibrium conversion for isotermal* SO_3 *decomposition. Parametric curves for different inlet temperatures.*

chamber (Chapter 6). This type of reactor is likely to be characterized by a significant difference between the inlet and outlet temperature; therefore, Figure 9.2 shows SO_3 conversion in an adiabatic equilibrium reactor as a function of reactor feed composition with several curves corresponding to different inlet temperatures.

Obviously for the SO_3 decomposition reaction, the efficiency of an isotermal reactor is higher than that of an adiabatic reactor; indeed for example by comparing the Figures 9.1 and 9.2 can be seen that considering the same reactor feed composition of 0.27 $^{\text{mol SO}_3}/_{\text{mol tot}}$a SO_3 conversion of about 0.95 can be obtained by operating at 1000°C in an isothermal reactor, while with an inlet temperature of 1000°C in an adiabatic reactor the SO_3 conversion theoretically resulting is equal to 0.62.

However for technological and constructive semplicity, in the design of the SAC demonstrator as said above, an adiabatic reaction chamber was envisaged. For this reason also for the flosheeting of the Sulfuric acid decomposition section, an adiabatic equilibrium reactor has been considered as it will be seen in the next paragraph.

After the reaction step the unreacted SO_3 must be separated together with H_2O downstream of SAC and recycled to the SAC feed in order to increase the overall conversion and save energy. Furthermore, separation is clearly needed to obtain SO_2 to be recycled to the SDE.

Due to the high difference in dew point of sulphuric acid vapour compared

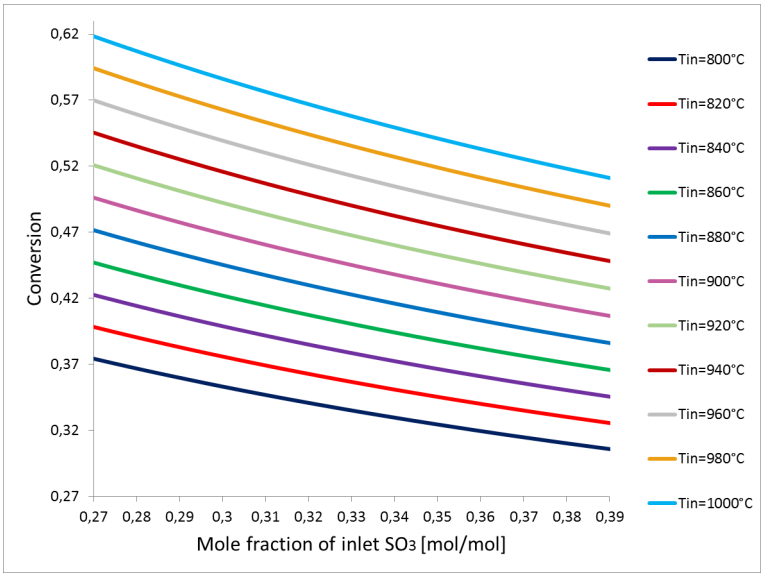

Figure 9.2: *Equilibrium conversion for adiabatic* SO_3 *decomposition. Parametric curves for different inlet temperatures.*

to SO_2 and O_2 , separation of SO_3 and H_2O downstream of SAC is in principle simple, cooling to ambient temperature being theoretically sufficient to obtain an almost complete separation.

According to the design of SAC DEMO PLANT (Chapter 6), the outlet stream of SAC containing SO_2 and O_2, unreacted SO_3 and H_2O is at close-to-ambient pressure and temperature in the range 700°C-800°C.

Upon cooling, SO_3 and H_2O react in the gas phase according to the following exothermic reaction:

$$SO_3 + H_2O \rightleftharpoons H_2SO_4 \tag{9.2}$$

Reaction 9.2does not require a catalyst and can be considered as instantaneous, so that the reaction extent can be calculated by assuming equilibrium conditions. Figure 9.3 shows the decomposed fraction of H_2SO_4 at ambient pressure as a function of temperature. It can be seen that above 600°C H_2SO_4 is completely decomposed as SO_3 and H_2O, while around its normal boiling point, i.e. between 300 and 350°C, SA is mainly present in the undissociated form. Therefore, for process and calculation and energy balances, the cooling operation of the outlet stream can be conceptually divided in three steps:

1. From 700-800 °C to SA dew point, by subtracting sensible and reaction heat from the gas

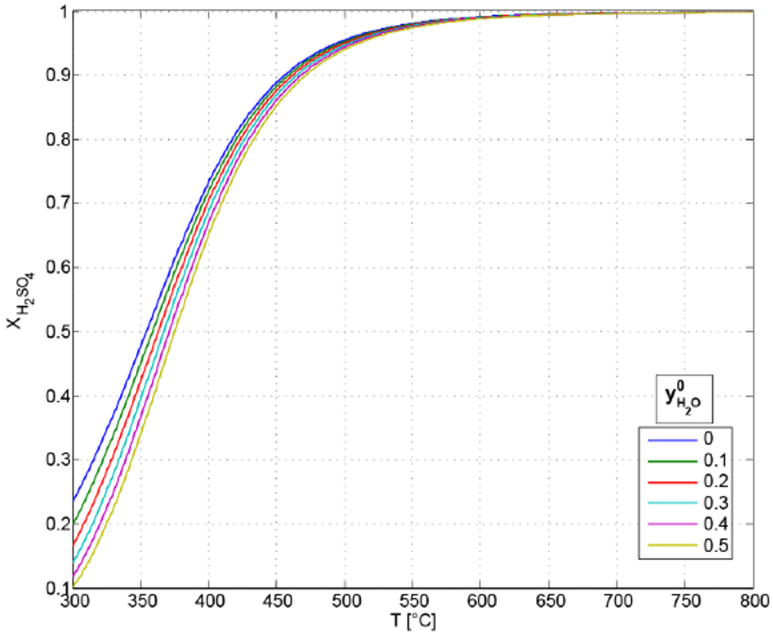

Figure 9.3: *Conversion of the gas phase sulfuric acid decomposition reaction. Parametric curves correspond to different initial water mole fractions.*

2. From dew point to bubble point, by subtracting the latent heat of condensation of H_2SO_4
3. Liquid SA cooling to the final temperature, by subtracting sensible heat from the liquid (small amount compared to the first 2 steps).

Clearly, for the sake of the process efficiency, as much heat subtracted to separate SO_3 and H_2O as possible should be recovered within the process. The simplest approach in this case could be to use this heat to vaporize/pre-heat the SAC feed.

For this reason, the SO_3 separation has been analysed in combination with SAC and an integrated flowsheet including the two process blocks has been developed, as it will be seen in the next paragraph.

9.2 Flowsheet development

As already said, for flowsheeting calculations an adiabatic equilibrium reactor has been envisaged.

Some specifications have been assumed according to the design proposed by DLR for the DEMO plant:

- the temperature of outlet reactor stream was set at 800°C;
- for reaching the decomposition temperature a Solar Tower (ST) was envisaged;
- the temperature of ST was set at 1000°C.

In order to obtain a temperature of 800°C for the outlet reactor stream, the conversion in the adiabatic equilibrium reactor was set up equal to 42%.

Furthermore, inner heat recovery was envisaged with the purpose to increase the global efficiency as much as possible.

The thermal recovery has been obtained by exploiting the hot stream outgoing from the decomposition reactor, i.e by sending it as counter-current hot fluid in some FEED pre-heating stages up to reach the decomposition temperature of 1000°C. In this context, a pinch analysis was performed to define how realizing the heat exchange between the FEED (cold fluid) and the the reaction product (hot fluid) in order to obtain the maximum heat recovery. In the Figure 9.4 the pinch analysis is reported, by considering for the SA composition FEED a value of 75%wt .

The conceptual integrated flowsheet for the SAC and SO_3separation sections, developed by process simulator Aspen Plus®, is shown in Figure 9.5 .

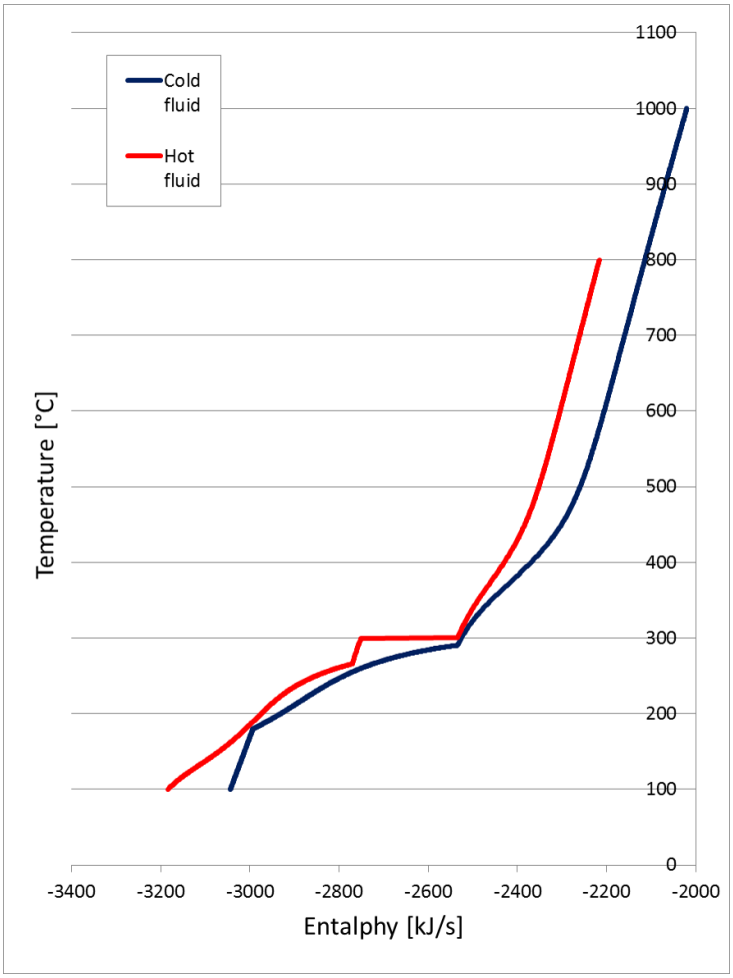

Figure 9.4: *Pinch analysis considering SA solution at 75%wt as FEED*

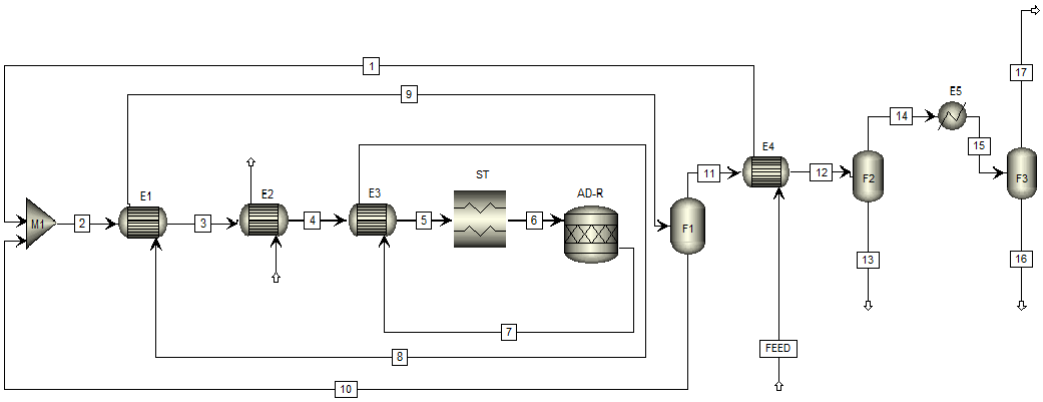

Figure 9.5: *Integrated flowsheet for SAC and* SO_3 *Separation. In the flowsheet ST is the Solar Tower, AD-R is the Adiabatic Reactor, E1,E2..E5 are heat exchangers, F1, F2 and F3 are flash and M1 is a mixer.*

The feed coming from liquid SA storage (FEED) is preheated in heat exchanger E4 by reaction product coming from other two previous cooling stages (E3 and E1); subsequently, the heated feed (stream 1) is mixed with the stream 10 which is SA condensed and separated from the product steam in F1. Temperature in separator F1 is adjusted to obtain a recycle stream with the same SA concentration as the stream1.

The mixture (stream 2) is vaporized by using both part of heat recovered from the reactor products (E1) and by using heat provided from an external source, i.e. medium temperature solar plant (this step is represented as E2). Then the totally vaporized stream 4 is heated up to the temperature of 1000°C by using heat of reactor products (in E3) and the heat picked up from a solar tower (ST). The stream from ST is fed to an adiabatic reaction chamber (AD-R).

Downstream of the adiabatic reactor, products are cooled down to ambient temperature in four cooling steps, in the order E3, E1, E4 and E5.

Starting from the stream 9 coming from the second cooling stage, three liquid currents are separated:

- stream 10 in F1, which is SA at the same composition as the feed and is recycled and mixed with stream 1 in M1;

- stream 13 in F2, which is SA at 30%wt and can be stored and used elsewhere in the plant (anolyte preparation) or recycled upstream of the SA concentration unit

Table 9.1: *Energy need for SAC/SO_3separation. The heat recovery was obtained by exploiting the hot products of decomposition reactor. The external energy was provided by concentrating solar thermal energy thecnologies.*

"FEED" COMPOSITION	HEAT RECOVERY [kJ/s]				EXTERNAL ENERGY REQUIRED [kJ/s]	
	DUTY(E1)	DUTY(E3)	DUTY(E4)	TOTAL	DUTY(E2)	DUTY(ST)
75%wt	288.07	318.63	11.03	617.7	206.09	196.37
50%wt	163.39	238.682	4.33	406.4	395.75	197.11

- stream 16 in F3, which is water (with SO_2 and SA traces) and is directed to a water storage tank and recycled where needed in the plant

The final effluent of this section (stream 17) contains SO_2 and O_2 , and is directed to the SO_2 / O_2 separation block.

The simulations by Aspen Plus have been performed considering two different FEED concentations: 50 and 75 %wt of SA.

The results in therm of energy need in the process are reported in Table 9.1

As it can be seen, by starting from a SA solution at 75 %wt an higher termal recovery could be realized and so a smaller energy demand from outside with an higher global efficiency were detected than those for a FEED composition equal to 50%wt of SA.

Furthermore, the specifications of each stream involved in the process flowsheet (Figure 9.5) are listed in Table 9.2, for a SA concentration in the FEED of 75%.

Table 9.2: *STREAM table related to flowsheet in Figure 9.5, by considering a FEED at 75%wt of SA.*

STREAM	FEED	1	2	3	4	5	6	7	8	9	10	11	12	13	14	15	16	17
T [°C]	30	71.6	123.7	262	289.3	577.2	1000	800	300	165	165	165	97	97	97	30	30	30
P [°C]	1	1	1	1	1	1	1	1	1	1	1	1	1	1	1	1	1	1
Vap. Frac	0	0	0	0.55	1	1	1	1	1	0.55	0	1	0.99	0	1	0.35	0	1
Mass Flow [kg/h]	469.8	469.8	1059.9	1059.9	1059.9	1059.9	1059.9	1059.9	1059.9	1059.9	590.1	469.8	469.8	0.8	469	469	186	283
Mass Frac																		
H_2O	0.25	0.25	0.25	0.25	0.26	0.39	0.39	0.39	0.32	0.31	0.25	0.39	0.39	0.69	0.39	0.39	0.95	0.01
H_2SO_4	0.75	0.75	0.75	0.75	0.71	0.01	0	0	0.38	0.42	0.75	0	0	0.3	0	0	0	0
SO_3	0	0	0	0	0.03	0.6	0.611	0.34	0.03	0	0	0	0	0	0	0	0	0
SO_2	0	0	0	0	0	0	0	0.22	0.22	0.22	0	0.49	0.49	0.01	0.49	0.49	0.05	0.79
O_2	0	0	0	0	0	0	0	0.05	0.05	0.05	0	0.12	0.12	0	0.12	0.12	0	0.20

Chapter 10

Sulfur dioxide and oxygen separation

10.1 General considerations

Removal of SO_2 from gaseous streams is a widely studied topic, especially with regards to the purification of combustion effluents, where SO_2 is formed upon oxidation of sulphur compounds contained in virtually any fuel. Therefore, in this context several processes are available depending on the inlet and target SO_2 concentrations. However, virtually all of these processes are conceived as purification operations, i.e. are suitable to treat streams in whichSO_2 is present in small amounts (few percent on mole basis) and final concentration levels in the tens of ppm range must be achieved. Due to the high concentration of both components, the separation between SO_2 and O_2 required in the hybrid sulfur process (molar ratio 2:1, saturated with water vapour) is rather a bulk separation process.

Furthermore, since the SO_2 / O_2 separation unit in the SOL2HY2 process links two parts of the plant that operate one continuously (electrolysis and concentration steps) and the other one discontinuously (SAC and SO_3 separation), depending on separation operating regime two process configurations were possible:

- SO_2 / O_2 separation unit works in a continuous regime like SDE and concentration step (Figure 10.1);
- SO_2 / O_2 separation unit works in a discontinuous regime like the SAC and SO_3 separation (Figure 10.2).

While in the first configuration the outlet stream from SAC, SO_2 separation can not be directly fed to the separation unit but have to be compressed and

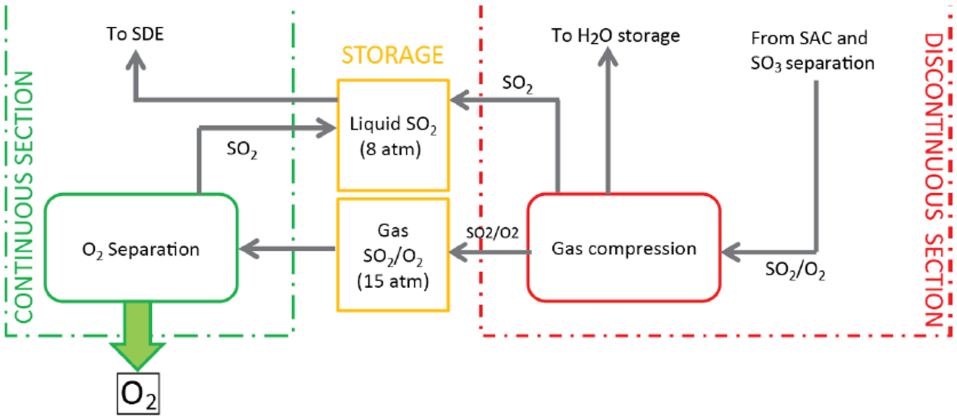

Figure 10.1: *Configuration with separation operating continuously*

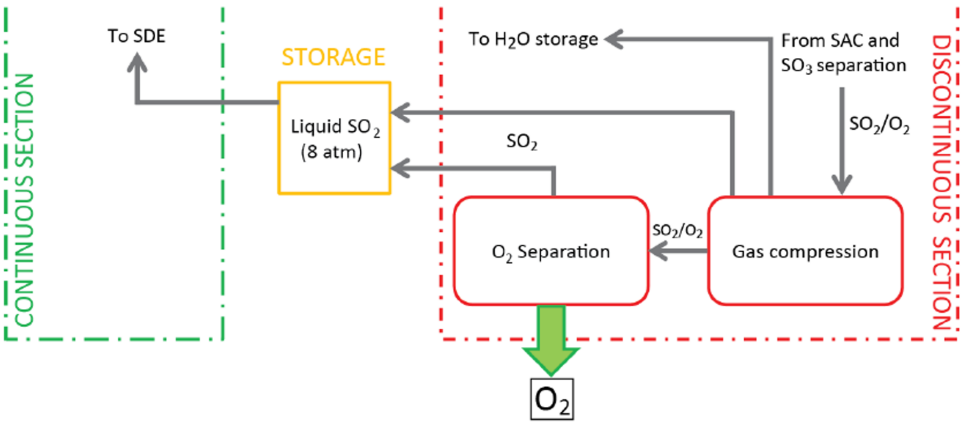

Figure 10.2: *Configuration with separation operating discontinuously*

stored to allow mismatching of the operating regimes, in the second one no intermediate storage is required and so one gas storage tank is saved. For this reason, the discontinuous option has been preferred in SOL2HY2 process.

Hence, the options that could be considered for a separation bulk and operated discontinuously were mainly:

- absorption with water;
- absorption with ionic liquids (ILs);
- membrane separation;
- SO_2 liquefaction.

Moreover, whichever method is used, in order to perform a successful separation, two specifications had to be kept as high as possible:

- the SO_2 recovery: that is the fraction of SO_2tained in the inlet stream which is recovered with the separated SO_2 stream. The complement to 1 of the SO_2 recovery is the SO_2 slip, i.e. the fraction of SO_2 which is lost with the O_2 separated stream;
- theO_2 purity:O_2 molar fraction in the separated O_2 stream.

Indeed a low SO_2 recovery requires high SO_2 makeup, which is clearly not economically acceptable. Furthermore, SO_2 contamination requires further treating of the final O_2 stream to recover a marketable or, if the obtained O_2 stream is vented, an environmentally compatible co-product. For this last reason also a great O_2 purity is important to be aimed.

It is worth noting that, in this operation, SO_2 purity is not as important as O_2 purity is because small amounts of O_2 in the SDE anolyte feed do not cause any significant problems, even if a small reduction of the cycle efficiency may be caused by non-electrolytic SO_2 oxidation in the liquid phase. In the design of this separation unit, focus has been put on SO_2 recovery, which is more important for the HyS cycle, rather than O_2 purity. However, meeting the specification on recovery will also ensure a low SO_2 contamination of the O_2 stream.

10.2 Process screening

10.2.1 Absorption with water

One of the wet processes to removeSO_2 from gaseous stream is water absorption. This is probably one of the simplest choices, which employs a safe

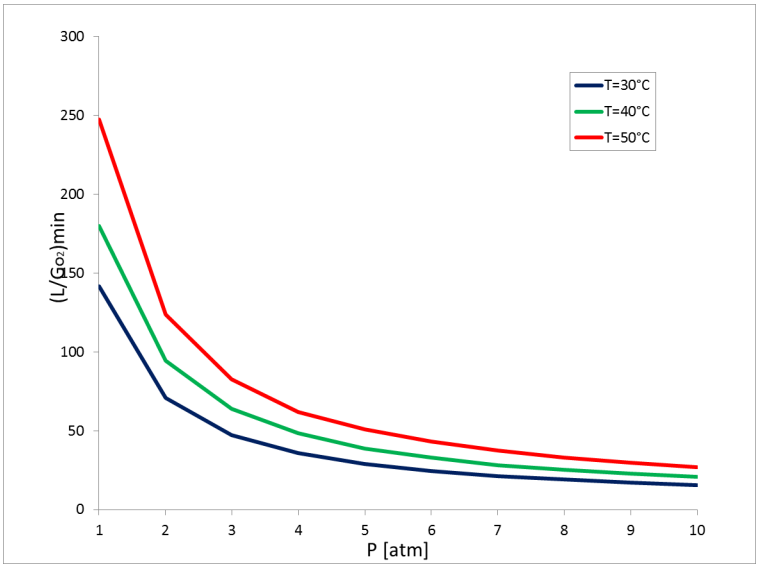

Figure 10.3: *Minimum liquid rate* $\left[\frac{mol_{H_2O}}{mol_{O_2}}\right]$ *for* SO_2 *absorption as a function of operating pressure.*SO_2 *recovery has been set to 99%.*

and relatively cheap solvent. Furthermore, water absorption was already included as SO_2 /O_2 in the flowsheets of nuclear-powered HyS cycle [Gorensek, 2011]. In this process, the gaseous stream is contacted with liquid water and, due to significantly higher solubility of SO_2 in water compared to O_2, SO_2 is preferentially transferred to the liquid phase and removed from the gas.

Liquid absorption is a conventional operation in the chemical industry, which is usually carried out in absorption towers where the gas stream if fed from the bottom and the liquid phase flows in counter-current from the top. Gas-liquid contact is ensured by the use of appropriate column internals like sieved plates or packed beds. Once the SO_2 recovery to be achieved is fixed, the minimum liquid water flowrate required to meet the specification can be calculated based on thermodynamic and mass balance considerations. The minimum specific water flowrate required to obtain a 99% SO_2 recovery is reported in Figure 10.3 as a function of the column operating conditions. In Figure 10.3 the specific water flowrate is referred to O_2 in inlet stream; this value must be halved in order to refer to SO_2 . Either an increase of pressure or a decrease of temperature favour the absorption process, so that a lower amount of water is required; however, significant minimum amounts of water are required. The actual value of water flowrate depends also on the number of theoretical separation stages realised in the absorption column: the higher the number of stages, the closer the water flowrate to the

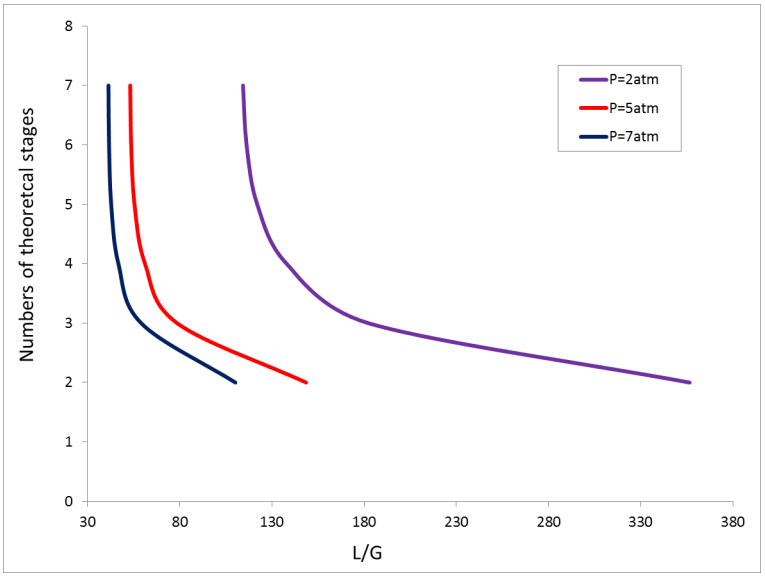

Figure 10.4: *Numbers of theoretical stages needs to attain 99%* SO_2 *recovery. Inlet streams at 40°C.*

minimum value. Figure 10.4 reports the number of theoretical stages needed to attain 99% SO_2 recovery as a function of the specific water flow. As the specific water flows approaches the minimum value, the number of required stages increases to infinity. It can be seen that, for all pressures, a number of 5-7 theoretical stages is sufficient, since a higher number does not allow to obtain any significant advantage. However, the actual number of stages will be higher because of mass transfer limitations. It is worth noting that Figure 10.4 is obtained by assuming a temperature of 40°C for both inlet streams and accounting for the moderate temperature increase caused by the heat of solution of SO_2. Due to the high amounts of water required, if water absorption is implemented for SO_2 separation, a regeneration step will probably also be needed. Regeneration is obtained in a second column operating at lower pressure and/or higher temperature. However, possibly not all the liquid flow coming from the absorption column needs to be regenerated because a SO_2 -saturated water stream is required as anolyte feed in the SDE.

10.2.2 Absorption with ionic liquids

10.2.2.1 Literature survey

Recently, ionic liquids (ILs) have been proposed as a possible, more efficient alternative to water for SO_2 absorption in the HyS process Shin et al. [2012]. Indeed, these particular liquids, whose use is spreading in several

different fields, possess very interesting properties that make them very good candidates to be used in such operation; namely, they exhibit:

- very powerful solvent properties. In some cases, the uptake for gases such as CO_2 and SO_2 can exceed 1 mol of gas per mole of ionic liquid. This allows to operate absorption with much lower liquid flowrates and/or lower operating pressures;

- thermal stability over a reasonably wide temperature range, which allows to operate solvent regeneration by a temperature swing process;

- extremely low vapor pressure, so that they are virtually non-volatile and losses by evaporation are negligible.

This is a very important, especially regarding the regeneration step: solvent evaporation causes additional costs for solvent makeup, product contamination and possible environmental issues. This is also the reason why ionic liquids are considered as "green" solvents. On the other hand, possible drawbacks associated with the use of ionic liquids in this process are:

- high viscosity: values from 10 to 500 cP, with strong temperature dependence are reported. Higher viscosities are associated with higher pumping energy requirements; however, if the use of ionic liquids allows operating at lower pressures, the energy saved for gas compression exceeds the increased pumping consumption;

- high cost: ionic liquids are in general very costly, especially if compared to a very cheap solvent such as water. However, much lower initial amounts and makeup are required for this type of liquid;

- "unconventional" nature. There is no consolidated experience in large scale industrial applications of this type of fluids.

Several ionic liquids have been studied for SO_2 absorption, and not only for the specific application in the HyS process. Most of them are reported in Table 10.3 and a list of all ionic liquids considered in this literature survey, both for Absorption with Ionic Liquids (ILA) and Supported Ionic Liquid Membranes (SILMs); the meaning of the abbreviations used for each IL name is contained in Tables 10.1and 10.2.

In their study, Kim et al. [2007] investigated the absorption and desorption process of SO_2 by ionic liquid for the recycle of SO_2 into sulfuric acid generation reaction in the thermochemical Sulfur-Iodine cycle. At 1 atm and 50°C, fixing [BMIm] as cationic part, the anions $[Cl]^-$, $[OAc]^-$, $[MeSO_3]^{2-}$,

Table 10.1: *ILs considered in this script*

Short name	Full name
[BMIm] [Cl]	1-butyl-3-methylimidazolium chloride
[BMIm] [OAc]	1-butyl-3-methylimidazolium acetate
[BMIm] [BF_4]	1-butyl-3-methylimidazolium tetrafluoroborate
[BMIm] [$MeSO_4$]	1-butyl-3-methylimidazolium methyl sulfate
[BMIm] [$MeSO_3$]	1-butyl-3-methylimidazolium methyl sulfite
[BMIm] [PF_6]	1-butyl-3-methylimidazolium hexafluorophosphate
[BMIm] [HSO_4]	1-butyl-3-methylimidazolium hydrogen sulfate
[EMIm] [$EtSO_4$]	1-ethyl-3-methylimidazolium ethyl sulfate
[$OH(CH_2)_2NH_3$][formate]	2-hydroxyethylammonium formate
[$OH(CH_2)_2NH_3$][lactate]	2-hydroxyethylammonium lactate
[$OH(CH_2)_2NH_3$][acetate]	2-hydroxyethylammonium acetate
[$(OH(CH_2)_2)_3NH$][formate]	tri-(2-hydroxyethyl)ammonium formate
[$(OH(CH_2)_2)_3NH$][lactate]	tri-(2-hydroxyethyl)ammonium lactate
[$(OH(CH_2)_2)_3NH$][acetate]	tri-(2-hydroxyethyl)ammonium acetate
[$(OHCH_2OCH_2NH_2$][formate]	2-(2-hydroxyethoxy) ammonium formate
[$(OHCH_2OCH_2NH_2$][acetate]	2-(2-hydroxyethoxy)ammonium acetate
[$(OHCH_2OCH_2NH_2$][lactate]	2-(2-hydroxyethoxy)ammonium lactate
[P_{66614}][Tetz]	trihexyl(tetradecyl)phosphonium tetrazole
[P_{66614}][Im]	trihexyl(tetradecyl)phosphonium imidazole
[P_{66614}][Triz]	trihexyl(tetradecyl)phosphonium triazole
[P_{66614}][DCA]	trihexyl(tetradecyl)phosphonium dicyanamide
[TMG][lactate]	1,1,3,3-tetramethylguanidinium lactate
[MEA][lactate]	monoethanolaminium lactate
[N_{2222}][lactate]	tetraethylammonium lactate
[BMIm]L	1-butyl-3-methylimidazolium lactate
[TMG][PHE]	1,1,3,3-tetramethylguanidinium phenol
[TMG][TE]	1,1,3,3-tetramethylguanidinium 2,2,2-trifluoroethanol
[TMG][Im]	1,1,3,3-tetramethylguanidinium imidazole

Table 10.2: *ILs considered in this script*

PMIm	1-propyl-2-methylimidazole
DMIm	1,2-diethyl-4(5)-methylimidazole
$PEG_1 - Im$	1-polyethylenglicol-imidazole
$PEG_1 - MIm$	1-polyethylenglicol-methylimidazole
$PEG_2 - Im$	1-dipolyetilenglicol-imidazole
$PEG_2 - MIm$	1-dipolyetilenglicol-4(5)-methylimidazole
$[C_4Py][SCN]$	1-butylpyridinium thiocyanate
$[EMIm]\,BF_4$	1-ethyl-3-methylimidazolium tetrafluoroborate
$[HMIm]\,[BF_4]$	1-hexyl-3-methylimidazolium tetrafluoroborate
$[BMIm]\,[Tf_2N]$	1-butyl-3-methylimidazolium bis(trifluoromethylsulfonyl)imide
[MIm] [acetate]	1-methylimidazolium acetate
[BIm] [acetate]	1-butylimidazolium acetate
$[N_{2224}]$[acetate]	triethylbutilammonium acetate
$[N_{2224}]$[propionate]	triethylbutilammonium propionate
$[N_{2224}]$[dimalonate]	triethylbutilammonium dimalonate

$[MeSO_4]^-$, $[BF_4]^-$, $[PF_6]^-$ and $[HSO_4]^-$, showed in this exact order, a reducing effect of SO_2 absorption capability. Indeed, $[BMIm]\,[Cl]$ presented the largest amount of SO_2 absorbed and could be the most promising absorbent even if it was shown vulnerable to high temperature around 250°C. Also the second largest SO_2 absorbing ionic liquid, $[BMIm]\,[OAc]$, was not stable at the temperature around 200 °C. Solubility of oxygen, which could be expected as negligible because of the non-polarity of its molecule, was compared whit that of SO_2 using $[EMIm]\,[EtSO_4]$ as absorbent. Indeed, the amount of absorbed oxygen was found to be lower than that of SO_2 by one order of magnitude.

The same authors conducted cycles of absorption and desorption by temperature swing in another study [Kim et al., 2008], again by using $[EMIm]\,[EtSO_4]$, which was selected after a screening process with criteria of thermal stability, cost, and absorption capability. Reversibility SO_2 absorption and high SO_2 solubility was verified even with different desorption temperatures. At 50 °C and 0.7 atm, $[EMIm]\,[EtSO_4]$ absorbed 0.95 gmol SO_2/gmol IL and fully desorbed SO_2 at higher temperature (from ∼100° C). The desorption rate observed depended on the operating temperature; full desorption was achieved both for test at 100°C and 130°C, while opereting at 70°C absorption was not complete.

Many of the ILs mentioned above, were compared by Lee et al. [2008]. They concluded that $[BMIm]\,[MeSO_4]$was the most appropriate absorbent

because:

- it was thermally stable with non-volatility up to 300 °C;
- it absorbed high amounts of SO_2 as 1.38 mol SO_2 per mole of ionic liquid at 35 °C and 1 atm;
- absorption proved reversible with the highest initial absorption rate.

Furthermore Shin et al. [2012] proposed a HyS flowsheet using [EMIm] [$EtSO_4$] as ionic liquid absorbent to separate SO_2 from O_2. The authors claimed that [EMIm] [$EtSO_4$] was chosen among various candidate ionic liquids due to a relatively low cost and easiness of massive synthesis.

$[Tf_2N]^-$,as anionic part of ILs, was analysed linked to two different cations: $[HMIm]^+$and $[HMPy]^+$by Anderson et al. [2006]. From tests at 25°C was clear that the solubilities of SO_2 in [HMPy] [Tf_2N] and [HMIm] [Tf_2N]were similar: this confirmed that the most significant effect on gas solubility in a IL is often gave by the anion. Other measurements of solubility were carried out at 40 and 60 °C and compared with those related to CO_2. It resulted that SO_2 was over an order of magnitude more soluble than CO_2 : for istance, Henry's law constant at 25°C in [HMIm] [Tf_2N] was 1.64 bar for the sulfur dioxide against 32.8 bar for the carbon dioxide. To validate it, also the enthalpy and entropy of absorption were calculated and resulted that the force of interaction between SO_2 and [HMIm] [Tf_2N] was twice that of CO_2 and the same IL. Drawing on the data produced by Wu et al. [2004] on the SO_2-[TMG][lactate] system, Anderson et al. [2006] showed that [HMIm] [Tf_2N] had a good absorption capacity. Indeed, even if in the case of [HMIm] [Tf_2N]the absorption was only physical while for [TMG][lactate] also a chemical interaction was to be considered (as evidenced by IR spectroscopy), the Henry's law constants at 40 °C were not really different (2.3 vs 1.2 bar respectly).

For their study on the SO_2 absorption, Yuan et al. [2007] synthesized and characterized a series of hydroxyl ammonium ILs. These liquids were prepared by neutralizing ethanolamine in ethanol with different acids. Their absorption capacity were investigated at atmospheric pressure by varying both cationic and anionic part, particularly 2-hydroxyethylammonium, tri-(2-hydroxyethyl) ammonium and 2-(2-hydroxyethoxy)ammonium as cations and lactate, acetate and formate as anions were investigated, respectively. Moreover, the regeneration of ILs was also conducted by increasing temperature or operating under vacuum. The experimental results showed that absorption at 298.2 K and 101.3 kPa required about 1 h to reach the equilibrium state and the maximum SO_2 solubilities in these ILs were quite high. It was very important to note that the effect of cations on the solubilities of

SO_2 followed the sequence 2-hydroxyethylammonium >tri-(2-hydroxyethyl) ammonium > 2-(2-hydroxyethoxy)ammonium while that of anions was lactate > acetate > formate. Accordingly, the 2-hydroxyethylammonium lactate showed the highest capacity for absorption of SO_2, with an equilibrium mole fraction of 0.51. By changing the operative conditions, authors showed that the SO_2 solubilities in all synthesized ILs were negligible at the atmospheric pressure when the temperature rised to 353.2 K and it was possible to regenerate SO_2-saturated ILs in vacuum conditions at 298.2 K within 2 hours. As an example, cycles of SO_2 absorption and desorption in tri-(2-hydroxyethyl)-ammonium lactate were carried out. These recycling experiments were repeated for four times, and the decrease of the absorption ability was very little. To understand the mechanism of absorption, FTIR spectra of SO_2-absorbed ILs were compared with those of SO_2-free ILs. It could be deduced that the SO_2 molecule attacked the group of -NH in the cation of the ILs creating the N-S bond and that simultaneously the carboxylate was turned to carboxylic acid. The absorbed SO_2 is released by breaking down the N-S bond operating under vacuum or by heating. The authors concluded that the absorption of SO_2 using these ILs follows both a physical and chemical mechanism, so that the solubilities of SO_2 in these ILs are lager than in other commonly used solvents.

The sulfur dioxide and ammonia absorption ability of task-specific ionic liquids[1] (TSILs) - all gaunidium-based ILs (GBILs) : $[TMG][BF_4]$, $[TMG][Tf_2N]$, $[TMGB_2][Tf_2N]$, $[TMGPO][BF_4]$ and $[TMGPO_2][BF_4]$- was investigated by Huang et al. [2008]. The authors evaluated that operating at room temperature and 1 bar, up to 2 moles of gas could be absorbed per mole of ionic liquid. Subjecting the ILs to many cycles of absorption-desorption (the desorption was obtained by heating or lowering of the pressure) no change in absorbing capacity of the ionic liquids was observed. The standard enthalpy of absorption was analysed and was found to be in the range -21 to -37 $kJmol^{-1}$, indicating a moderate association between gas and liquid.

Shang et al. [2011] synthesized other three guanidinium-based ionic liquids and investigated their absorption and desorption capacity of sulfur dioxide. The gas absorptions were carried out under atmospheric pressure and at various temperatures while the desorptions at 40 and 100 °C under vacuum. It was seen that the amount of SO_2 in the GBILs increased linearly with time reaching the equilibrium within 30 min and the saturated molar ratio of SO_2 to GBILs varied from 2.24 to 3.16 operating at 40 °C. The absorption

[1]The task-specific ionic liquids are ILs synthesized to absorb a specific gas; in the case of SO_2 the TSILs have been experimentally demonstrated to absorb more than conventional ILs from gas mixtures with low SO_2 concentration.

capacities and rates decreased significantly with increasing temperature, for example [TMG][TE] reached an equilibrium absorption capacity of 4.13 at 20 °C and of 1.43 at 90 °C. Operating for the absorption phase at 20 °C and atmospheric pressure and for the desorption phase at 100 °C under vacuum, it was shown that equilibrium absorption capacity of [TMG][TE] was the largest among three GBILs absorbents and about 1.60 times as high as that of [TMG][PHE]; instead [TMG][Im] showed the most desirable desorption capacity. Moreover this last IL seemed to be the strongest absorbent within temperature range between 40 and 70 °C. Comparing the maximum SO_2 absorption capacity of these GBILs at atmospheric pressure - from 2.24 to 3.17 at 40 °C- with those of other ILs, for example [TMG] [lactate] -1.7 at 40 °C and 1.2 bar- the authors suggested that the GBILs studied in their work could be regarded as a type of very effective SO_2 absorbent, with great potential in SO_2-containing gas mixtures purification. Finally, by using FTIR and H-NMR spectroscopy techniques, spectra of SO_2-free and SO_2-absorbed were analyzed. The combination of FTIR and 1H NMR spectra of SO_2-free and SO_2-absorbed [TMG][PHE] indicated the chemical interaction between amino of the TMG moiety and SO_2. However, the authors concluded that generally the physical absorption predominated over the chemical one at 20 °C for all three GBILs , and played an important role at higher temperatures (up to 70 or 90 °C).

Jin et al. [2011] determined the solubilities of SO_2 in [TMG][lactate] and [MEA][lactate] comparing these with those in more conventional ILs [bmim][BF_4] and [bmim][PF_6]. Previous studies of other authors (Wu et al. [2004], Huang et al. [2006],Yuan et al. [2007], Ren et al. [2010]) suggested that [TMG][lactate] and [MEA][lactate] were the most promising TSILs in purification of SO_2-containing gas, such as flue gas. Hence, the choice of Jin et al. [2011] to employ them as task-specific ILs in their work. The SO_2 solubilities were studied at temperatures ranging from 293.15 to 333.15 K and SO_2 partial pressures ranging from 0.344 to 101.25 kPa and correlated by a modified Redlich Kwong equation of state. The results showed that the solubilities both in [TMG][lactate] and [MEA][lactate] decreased slowly when pressure decresed, at high pressures (>6 kPa), and decreased more notably with decresing pressure, at low pressures (<6 kPa); however these values of solubility remained much higher than zero, even at the relatively low pressures. For example, with [TMG][lactate] was obtained a solubility of 0.382 mol fraction at pressure 0.709 kPa, and with [MEA][lactate] at 0.344 kPa, a value of solubility of 0.354 mol fraction. Regarding [bmim][BF_4] and [bmim][PF_6], the authors saw that the SO_2 absorption capacities increased with an increase in pressure. Furthermore, at high partial pressures of gas, these ILs could absorb SO_2 effectively, while at low partial pressur they could absorb sulfur

dioxide with very low solubilities. For example, at 101.325 kPa, the solubilities of [BMIm][BF_4] and [BMIm][PF_6] were 0.586 and 0.540 in mole fraction, respectively; at 0.344 kPa, the solubilities were 0.010 and 0.005 mol fraction, respectively. These results indicated that both task-specific ILs and normal ILs had good performances for absorption of pure SO_2 or feed gas streams with high contents of SO_2 , whereas only task-specific ILs could excellently absorb SO_2 from flue gas containing very low contents of SO_2 . Jin et al. [2011] in agreement with what was already suggested by other authors (Wu et al. [2004], Ren et al. [2010]) , explained that behaviour saying that there was only physical interaction between normal ILs and SO_2, while the absorption by task-specific ILs was due to both physical and chemical interactions. Chemical interaction, which is much stronger than physical interaction, is not influenced significantly by pressure; physical interaction is greatly dependent on pressure, which normally obeys the Henry's law. Therefore, in this last case when the partial pressure of SO_2 decreases, the solubility of SO_2 also decreases linearly. So, analysing the previous results in view of what has just been explained, the authors concluded that conventional ILs absorbed SO_2 only phisically; instead in the case of TSILs there were both chemical interaction and physical interactions at high SO_2 pressure and predominantly chemical interaction at low pressures.

Tian et al. [2014] used other two kinds of ionic liquids based on lactate anion to absorb SO_2 at high temperatures (from 100 to 120 °C): [N_{2222}][lactate] and [BMIm][lactate] . The ILs showed high absorption capacities: the mole ratio of SO_2 to IL at 100° C was 1.229 for [N_{2222}][lactate] and 1.102 for [BMIm][lactate], and remained over one also at T >100 °C in the case of [N_{2222}][lactate]. Cycles of SO_2 absorption/desorption were carried out: the absorption steps at 110 °C for 60 min, and the desorption steps at the same temperature for 360 min. The results showed that negligible losses of absorption capacity were found for the ILs during the reuse cycles; as an example the rates mol SO_2/mol [BMIm][lactate] of the 5 cycles were 1.033, 1.031, 1.043, 1.045, 1.029 after the absorption. Furthermore by using FT-IR, 1H NMR and 13C NMR spectra , the absorption mechanism was studied; the analysis indicated that there were strong chemical interactions between the ILs and SO_2.

In their work, Wang et al. [2011] described a method for the multiple-site capture of SO_2 involving the use of azole-based ILs. Traditional SO_2 chemisorption is based on the strong interaction between the gas and electronegative oxygen ions in the anion of IL. Differently from physical absorption, chemical absorption often has a high reaction enthalpy and so high energy is required for the step of desorption. The increase of number of interaction sites between the IL and SO_2 would improve the absorption capacity

and would reduce the absorption enthalpy . For this reason, the investigation of a way to obtain highly efficient and reversible ILs with multiple sites for the capture of SO_2, is highly interesting. In this regard, the authors showed that by exploiting reactivity of multiple electronegative nitrogen atoms of the anion in azole-based ILs, an extremely high SO_2 absorption capacity could be achieved . Furthermore, the absorption enthalpy was facilely tuned ensuring excellent reversibility (28 recycles). The azole-based ILs which were studied were prepared by the acid-base neutralization between tetrazole (Tetz) or imidazole (Im) and a solution of phosphonium hydroxide in ethanol. By working with $[P_{66614}]$[Tetz] and $[P_{66614}]$[Im] the effect of SO_2 pressure on the absorption was investigated: the molar ratios of SO_2 decreased from 3.72 to 1.54 and 4.80 to 2.07 respectively, when pressure decreased from 1.0 to 0.1 bar. However, even at low pressure the absorption capacity was significantly greater than 1:1 stoichiometry. Instead the absorption capacity decreased significantly as the temperature increased. These results indicated that regeneration could be achieved by heating or bubbling N_2 through the IL. Absorption/desorption cycles were carried out operating at 20 °C for absorption phase and at 80 °C under a N_2 flow for desorption phase. $[P_{66614}]$[Tetz] showed a steady absorption capacity step by step, and high absorption and desorption rates . $[P_{66614}]$[Im] showed an absorption capacity higher than $[P_{66614}]$[Tetz] ($\sim$4.5 mol SO_2/mol IL vs $\sim$3.5 mol SO_2/mol IL), but the desorption of SO_2 was not complete: $\sim$0.7 mol SO_2/mol IL remained. The authors attributed the high SO_2 absorption capacities for these ILs to the electronegative nitrogen atoms in the anion which might contribute to multiple-site interactions with SO_2 and to substantiate their idea, they performed theoretical calculations using the Gaussian 03 program .The results obtained showed that the interactions in [Tetz]-SO_2 and [Tetz]-2SO_2 are mainly chemical interactions, with absorption enthalpies larger than 50 $kJ \cdot mol^{-1}$. So an absorption capacity of $\sim$2 mol SO_2/mol IL could be achieved at low pressure, such as the experimental results already showed; multiple-site interactions between the electronegative nitrogen atoms and the sulfur atom with positive charge in the acidic SO_2 gave the possibility to absorb more than 4 mol SO_2/mol IL . Furthermore, to explain the effect of the anion on the desorption of SO_2, Wang et al. [2011] calculated the absorption enthalpy for the [Im]SO_2, [Im]2SO_2, [Im]3SO_2, and [Im]4SO_2which revealed the significantly stronger interaction of gas with [Im] than with [Tetz] and as a result the greater difficulty for separate SO_2 from $[P_{66614}]$[Im] than from $[P_{66614}]$[Tetz]. Thus, the authors concluded that process involving these ILs with multiple sites rappresented a very promising way for SO_2 capture.

Other azole-based ILs were studied more recently by Chen et al. [2015]. Particularly, in this case the analysis focused on the influence of the anions

basicity in the capture of SO_2 from flue gas, where the concentration of SO_2 is only 2000 ppm. It was seen that strong basicity led to high SO_2 absorption capacity but also an high desorption residue. On the contrary, weak basicity gave a low desorption residue but also a low SO2 absorption capacity . For instance, $[P_{66614}][Triz]$ with strong basicity was characterized by an SO_2 absorption capacity of 1.22 and a desorption residue of 0.89 mol SO_2 per mol IL while, for $[P_{66614}][DCA]$ with weak basicity, the SO_2 absorption capacity and desorption residue were 0.09 and 0 mol SO_2 per mol IL, respectively. For this reason in conclusion, the IL $[P_{66614}][Tetz]$, wich had moderate basicity, was considered to give the best performance with an absorption capacity and desorption residue were 0.87 and 0.06 mol SO_2 per mol IL, respectively.

Recently, Shannon et al. [2014] investigated the effects of functionalizing the imidazole ring positions with alkyl and oligo(ethylene glycol) groups on the SO_2 absorption capacity. The authors claimed that SO_2 absorption occurs via both chemical and physical mechanisms. According to their findings, chemical binding produced a relatively stable 1:1 SO_2- imidazole complex, which can be released under vacuum at moderate temperature ($\sim$100 °C), yielding the original neat solvent; on the other hand, the physically dissolved SO_2 can be readily removed at ambient temperature under vacuum. At 25 °C and 21 psia, the highest overall SO_2 absorption was obtained with $PEG_2 - Im$ and $PEG_2 - MIm$, which absorb respectively 3.11 and 2.93 mol equiv of SO_2 per imidazole mole. Indeed, the presence of ether groups can promote additional non-covalent associations with SO_2 as the lone pairs of the ether oxygen exhibit interactions with the electron-poor sulfur atom in SO_2. The use of $PEG_2 - Im$ and $PEG_2 - MIm$ in the neat form may not be the most practical application for conventional SO_2 removal process, due to the formation of viscous liquids/gels or solids in the equipment. However, these imidazoles could be used in solution with a nonreactive co-solvent such as dimethyl ethers of polyethylene glycol (DMPEG) so as to maintain a low-viscosity liquid phase while taking advantage of the large SO_2 loading capacities of the imidazoles.

Zeng et al. [2014] investigated a series of thermally stable pyridinium-based ionic liquids for SO_2 capture. Among all ILs considered, $[C_4Py][SCN]$ showed at ambient conditions, the highest absorption capacity (0.841 g SO_2/g IL) and selectivity for SO_2/CO_2, SO_2/N_2 and SO_2/O_2.Furthermore after five cycles of absorption and desorption, this IL kept unchenged its absorption performance. By using FT-IR and NMR spectroscopy, Quantum Chemical calculation and Molecular Dynamic (MD) simulation, the authors demonstrated that the physical absorption occured in pyridinium-based ILs for SO_2 capture. Moreover these analysies proved that anion played a predominant role than cation in SO_2 absorption, and so that the higher absorption capacity of SO_2 in $[C_4Py][SCN]$ is mostly attributed to the stronger electrostatic interaction

between$[SCN]^-$ and SO_2. The authors concluded that the pyridinium-based ILs had great potential for SO_2 capture applications.

Extrapolating and reworking data from tables and graphics reported in the cited lecterature studies, it was possible to compare some SO_2solubility values for the different ILs. These values are collected in Table 10.4.

Another way to exploit the properties of ILs for the separation of SO_2 mixtures is by using them as liquid membranes. This application seems very promising especially for the implementation of discontinuous operations. Furthermore the high absorption capacity and selectivity for SO_2 combined with non-volatility makes ILs perfect candidates as liquid membranes for this separation process. However, this solution does not currently show a sufficient technological maturity for the application at the industrial scale. Jiang et al. [2007] provided the first insight into the permeability and selectivity of SO_2 in supported ionic liquid membranes. Five imidazolium-based ILs supported by hydrophilic polyethersulfone (PES) were considered; the support had the following specifications: 0.22 µm pore size, 80% porosity, 150 µm thickness and 64 cm^2 cross-sectional area. At 20 kPa of SO_2 driving force, [EMIm] $[BF_4]$ showed the highest SO_2 permeability, 9350 ± 230 Barrers[2], whereas [BMIm] $[PF_6]$ had the lowest SO_2 permeability, 5200 ±117 Barrers. Indeed, the relative SO_2 permeability between the supported ionic liquid membranes tested appeared to be related to the viscosities of the ILs: the permeability increased with decreasing viscosity. The experimental results showed that the SILMs not only offered a very good permeability of SO_2, but also a very high SO_2/CH_4, SO_2/CO_2 and SO_2/N_2 selectivity. Therefore, the SILM process may be expected to have potential application in improving or replacing traditional chemical absorption processes for the separation and recovery of SO_2 from a flue gas stream or a gas mixture. By using hydrophilic polyvinylidene fluoride (PVDF) -0.20 µm pore size and 129 µm thick- and hydrophobic polyvinylidene fluoride -0.22 µm pore size and 125 µm thick- Luis et al. [2009] carried out a comparison between the permeability of air,CO_2 and the mixture SO_2/air in order to highlight the facilitated flux of CO_2 and SO_2. Absorption and desorption experiments of SO_2 in several ILs were carried out and [MIm] [acetate] and [BIm] [acetate] were selected due to their high affinity towards SO_2; furthermore, because these IL have a very low viscosity at ambient temperature, which is of great importance when a high diffusivity of the gas through the liquid is desired. The results showed a completely reversible absorption. Permeation tests showed that [BIm] [acetate] had the

[2]Barrer is a non-SI unit of gas permeability (specifically, oxygen permeability) used in the contact lens industry. It is a bulk property. It is named after Richard Barrer. $1\,\text{Barrer} = 3.348 \cdot 10^{-19}\text{kmol}\,\text{m}\,\text{m}^{-2}\text{s}^{-1}\text{Pa}^{-1}$.

Table 10.3: *List of some ionic liquids considered in the literature for SO2 absorption*

Ionic Liquid	Eq Abs.[1]	Abs. Kin.[2]	Des.Kin.[2]	Plant [3]	Ref	Notes
[BMIm] [Cl]	*	*			a,b	* only cationic part of Ionic liquid
[BMIm] [OAc]	*	*			a,b	
[BMIm] [BF_4]	*	*			a,b	[1] Test of absorption and desorption
[BMIm] [$MeSO_4$]	*	*			a,b	
[BMIm] [$MeSO_3$]	*	*			a,b	[2] Kinetic Analysis of absorption/desorption
[BMIm] [PF_6]	*	*			a,b	
[BMIm] [HSO_4]	*	*	*		a,b	[3]Simulation of a plant for SO_2absorption
[EMIm] [$EtSO_4$]	*	*	*	*	a,c,d	
[$OH(CH_2)_2NH_3$][formate]	*	*	*		e	a:Kim et al. [2007]
[$OH(CH_2)_2NH_3$][lactate]	*	*	*		e	b:Lee et al. [2008]
[$OH(CH_2)_2NH_3$][acetate]	*	*	*		e	c:Kim et al. [2008]
[$(OH(CH_2)_2)_3NH$][formate]	*	*	*		e	d:Shin et al. [2012]
[$(OH(CH_2)_2)_3NH$][lactate]	*	*	*		e	e:Yuan et al. [2007]
[$(OH(CH_2)_2)_3NH$][acetate]	*	*	*		e	f:Wang et al. [2011]
[$(OHCH_2OCH_2NH_2$][formate]	*	*	*		e	g: Jin et al. [2011]
[$(OHCH_2OCH_2NH_2$][acetate]	*	*	*		e	h: Tian et al. [2014]
[$(OHCH_2OCH_2NH_2$][lactate]	*	*	*		e	i: Shang et al. [2011]
[P_{66614}][Tetz]	*	*	*		f,q	l: Shannon et al. [2014]
[P_{66614}][Im]	*	*	*		f	m: Zeng et al. [2014]
[TMG][lactate]	*	*			g	n: Anderson et al. [2006]
[MEA][lactate]	*	*			g	o: Huang et al. [2008]
[N_{2222}][lactate]	*	*	*		h	p: Lei et al. [2013]
[BMIm][lactate]	*	*	*		h	q: Chen et al. [2015]
[TMG][PHE]	*	*	*		i	
[TMG][TE]	*	*	*		i	
[TMG][Im]	*	*	*		i	
PMIm*	*				l	
DMIm*	*				l	
$PEG_1 - Im$*	*				l	
$PEG_1 - MIm$*	*				l	
$PEG_2 - Im$*	*				l	
$PEG_2 - MIm$*	*				l	
[C_4Py][SCN]	*	*	*		m	
[HMIm] [Tf_2N]	*				n	
[HMPy] [Tf_2N]	*				n	
[TMG][BF_4]	*				o,p	
[TMG][Tf_2N]	*				o,p	
[$TMGB_2$][Tf_2N]	*				o,p	
[TMGPO][BF_4]	*				o,p	
[$TMGPO_2$][BF_4]	*				o,p	
[P_{66614}][Triz]	*				q	
[P_{66614}][DCA]	*				q	

Table 10.4: SO_2 *solubility in some ILs*

IL	P_{so_2}[atm]	T [°C]	mole ratio [mol SO_2/mol IL]
[BMIm] [Cl]	0,7	50	∼1.66
[BMIm] [OAc]	0,7	50	∼1.36
[BMIm] [BF_4]	0,7	50	∼0.45
[BMIm] [$MeSO_4$]	0,7	50	∼0.78
[BMIm] [$MeSO_3$]	0,7	50	∼0.86
[BMIm] [PF_6]	0,7	50	∼0.35
[BMIm] [HSO_4]	0,7	50	∼0.19
[EMIm] [$EtSO_4$]	0,7	50	∼0.95
[$OH(CH_2)_2NH_3$][formate]	1	50	∼0.12
[$OH(CH_2)_2NH_3$][lactate]	1	50	∼0.21
[$OH(CH_2)_2NH_3$][acetate]	1	50	∼0.16
[$(OH(CH_2)_2)_3NH$][lactate]	1	50	∼0.1
[$(OH(CH_2)_2)_3NH$][acetate]	1	50	∼0.08
[$(OHCH_2OCH_2NH_2$][formate]	1	50	∼0.06
[$(OHCH_2OCH_2NH_2$][acetate]	1	50	∼0.07
[$(OHCH_2OCH_2NH_2$][lactate]	1	50	∼0.09
[P_{66614}][Tetz]	1	50	∼2.27
[P_{66614}][Im]	1	50	∼3.27
[TMG][PHE]	1	50	∼1.94
[TMG][TE]	1	50	∼2.08
[TMG][Im]	1	50	∼2.77
[TMG][lactate]	1	20	∼1.95
[MEA][lactate]	1	20	∼0.99
[TMG][BF_4]	1	20	∼0.56
[TMG][Tf_2N]	1	20	∼0.54
[$TMGB_2$][Tf_2N]	1	20	∼0.61
[TMGPO][BF_4]	1	20	∼0.61
[$TMGPO_2$][BF_4]	1	20	∼0.67
[N_{2222}][lactate]	1	100	∼1.23
[BMIm][lactate]	1	100	∼1.10
[C_4Py][SCN]	1	25	∼2.55
[HMIm] [Tf_2N]	1	25	∼0.48
[HMPy] [Tf_2N]	1	25	∼0.62
PMIm	1.5	25	∼2.64
DMIm	1.5	25	∼2.69
$PEG_1 - Im$	1.5	25	∼2.46
$PEG_1 - MIm$	1.5	25	∼2.7
$PEG_2 - Im$	1.5	25	∼3.11
$PEG_2 - MIm$	1.5	25	∼2.93

highest permeability of SO_2 in both membranes, with a higher value ($33.6\pm 0.1{\cdot}10^{-11}$ m^2/s) in the membrane made of hydrophilic polyvinylidene fluoride. The highest selectivity CO_2/air and 10 vol% SO_2 − air/air was reached with the SILM composed of [MIm] [acetate] and hydrophilic PVDF.

In the same context of $SO_2 - CO_2$ separation, Huang et al. [2014] carried out SO_2 permeation tests on supported liquid membranes using carboxylate-based ionic liquids. Acetate and proprionate anions bound to $[N_{2224}]$, which was the cationic part in every IL tested, are alkaline and their strong affinity with SO_2 in the presence of H_2O is undoubtful. However, dimalonate, dimaleate and diglutarate anions are weakly acidic because they are half deprotonated and there is a free carboxylic acid group remaining. Since the pK_{a_1} value of H_2SO_3 is smaller than those of malonic acid, maleic acid and glutaric acid, such acids can still react with SO_2 in the presence of H_2O, as shown by the following reactions:

$$R - COO^- + H_2O + SO_2 \rightarrow R - COOH + HSO_3^-$$

$$HOOC - R - COO^- + H_2O + SO_2 \rightarrow HOOC - R - COOH + HSO_3^-$$

The permeability of SO_2 in the five SILMs increased with the increase of SO_2 partial pressure, whereas the permeability of N_2, and CO_2 proved fairly stable with pressure. As are result, the selectivity of SO_2/CH_4, SO_2/CO_2 and SO_2/N_2 increased with the partial pressure of SO_2. Significantly different SO_2 permeabilities were observed in the five SILMs. Tests carried out with $[N_{2224}]$[dimaleate] showed that the temperature positively affected the SO_2 permeability. The results at 40 °C displayed that$[N_{2224}]$[acetate] had the higest permeability at different conditions of pressure (about 16000 Barrers for a SO_2 partial pressur of 0.1 bar) while the lowest permeability of SO_2 was obtained by $[N_{2224}]$[diglutarate] ($\sim$ 700 Barrers for a SO_2 partial pressure of 0.1 bar). Several factors influenced the permeation of SO_2 in IL, but it was reasonable to assume that $[N_{2224}]$[diglutarate] exhibited the lowest permeability of SO_2 primarily due to its extremely large viscosity; $[N_{2224}]$[dimaleate] displayed the second lowest permeability of SO_2 -about 3000 Barrers considering a SO_2 partial pressur of 0.1 bar- mainly due to its relatively low absorption capacity for SO_2; indeed, the pK_{a_1} value of maleic acid is only slightly larger than that of H_2SO_3.

In their very recent work, Li et al. [2015] employed a mesoporous molecular sieve MCM-41 (Mobil Composition Matter No 41) as support material to prepare a novel absorbent (MCM-41-[TMG][lactate]). [TMG][lactate] is believed to be a potential medium for SO_2 removal, because it is characterized

by a large SO_2 absorption capacity (0.725 mol SO_2/mol IL, at 30 °C and ambient pressure). However, when is used in pure unsupported form, this IL exhibits unsatisfactory SO_2 absorption rate and incomplete desorption, mainly due to its very high viscosity and irreversible chemical reactions with SO_2. Differently, the supported form MCM-41-[TMG][lactate]-x% (x is a measure of amount of [TMG][lactate] in the absorbent) showed a significantly different and interesting behavior. Indeed, the results obtained by Li et al. [2015] indicated that MCM-41-[TMG][lactate] exhibited improved absorption kinetics with an initial absorption rate (average during the first 10 min of test), much higher than that of [TMG][lactate] for each loading considered, except in the case of MCM-41-[TMG][lactate]-50% and MCM-41-[TMG][lactate]-60% for which the value is instead comparable. Moreover, desorption (regeneration) efficiency proved to be better compared to the unsupported form. As an example, SO_2 could be easily stripped out of MCM-41-[TMG][lactate] by heating at 90 °C under vacuum, allowing MCM-41-[TMG][lactate]-10% to maintain at 95% of the initial capacity after 10 cycles of regeneration. The authors mainly attributed the better performance of the supported IL to the increase of gas-liquid interface ensured by the porous support matrix. This explanation is clearly compatible with the enancement of absorption kinetics, but further investigation is required to understand the effect of the solid matrix on the regeneration efficiency.

Another interesting result is that TMGL loading is one of the most critical influencing factors for SO_2 absorption performance. In the paper, [TMG][lactate] loadings in the range 10%-60% were considered at 30 °C. The experimental results showed that the highest capacity of absorption and absorption rate were obtained with 10% loading, followed in the order by 40%, 30% and 20%. With excess loadings of 50% and 60%, much smaller values of initial absorption rate were observed compared to all other cases; the limited duration of the tests does not allow to assess with certainty the maximum absorption capacity corresponding to these higher loadings.

To explain these results, the authors considered that when the loading increases, the dimensionality of the system increases from a 2D-like structure (a single layer coating the pore surface) to a 3D-like structure (the pore filled with IL) in which the IL tends to recover its bulk properties. Hence MCM-41-[TMG][lactate]-10%, which contains small amount of [TMG][lactate], presented a very porous structure and could be consedered as a 2D-like structure. In this case, an appreciable porosity was still preserved and this may be beneficial for the physical adsorption. Instead with loading higher than 10% the structure was considered as three-dimensional; thus since the bulk pure [TMG][lactate] shown larger absorption capacity than the supported ionic liquids, MCM-41-[TMG][lactate]-40% shown the highest absorption ca-

pacity -after MCM-41-[TMG][lactate]-10%- followed by the 30% and 20% loading formulations. The reason for the unsatisfactory absorption rate obtained with MCM-41-[TMG][lactate]-50% and MCM-41-[TMG][lactate]-60% was that the pore channel was blocked by ILs which made molecular SO_2 more difficult to diffuse into ILs.

However the interpretations given by the authors require further clarifications.

Moreover, the performance of MCM-41-[TMG][lactate] was investigated under different conditions, including absorption temperature, SO_2 concentration and vapor concentration of simulated flue gas. Results showed that H_2O had almost no influence on the SO_2 absorption by MCM-41-[TMG][lactate]-40% especially at high temperature. However the SO_2 absorption performance was unsatisfactory at high temperature and low SO_2 concentration.

The literature on the supported IL mentioned above (both for SILMs and SSP) is summarized in Table 10.5. In this table the type of tests carried out for each sample are also specified:

- tests on absorption capacity and desorption efficiency;
- evaluation of absorption/desorption rate;
- analysis of SO_2permeability through the membranes;
- evaluation of membranes ability to allow the selective SO_2 passage, in the presence of other gases.

SILPs could be used to separate SO_2 in a fixed bed sorption column with regeneration operating in temperature/pressure swing mode.

In order to be considered as suitable for SO_2separation, the following IL properties appear as the most important:

- high SO_2 absorption capacity: this is clearly required, regardless of the specific process used for the separation.
- Full regenerability: (nearly) complete SO_2 desorption even after several absorption/desorption cycles. Loss of adsorption capacity during the early cycles can be accepted provided that the residual capacity stabilizes over the cycles and is high enough.
- high SO_2 diffusivity: see viscosity.
- low viscosity: for ILA, this is important to reduce the pumping power; for all processes, it is important because it is inversely related to the diffusivity of SO_2 in the IL, which must be as high as possible to ensure good mass transfer kinetics.

Table 10.5: *List of some supported ionic liquids considered in literature for* SO_2 *separation*

Ionic Liquid	Support	Abs. Eq.[1]	Abs. Kin.[2]	Perm.[3]	Select.[4]	Ref.
[EMIm] [BF_4]	PES	*		*	$\frac{SO_2}{N_2}, \frac{SO_2}{CH_4}, \frac{SO_2}{CO_2}$	a
[BMIm] [BF_4]	PES	*		*	$\frac{SO_2}{N_2}, \frac{SO_2}{CH_4}, \frac{SO_2}{CO_2}$	a
[BMIm] [PF_6]	PES	*		*	$\frac{SO_2}{N_2}, \frac{SO_2}{CH_4}, \frac{SO_2}{CO_2}$	a
[HMIm] [BF_4]	PES	*		*	$\frac{SO_2}{N_2}, \frac{SO_2}{CH_4}, \frac{SO_2}{CO_2}$	a
[BMIm] [Tf_2N]	PES	*		*	$\frac{SO_2}{N_2}, \frac{SO_2}{CH_4}, \frac{SO_2}{CO_2}$	a
[MIm] [ace]	Hydrophilic PVDF	*		*	$\frac{SO_2}{air}$	b
[BIm] [ace]	Hydrophilic PVDF	*		*	$\frac{SO_2}{air}$	b
[MIm] [ace]	Hydrophobic PVDF	*		*	$\frac{SO_2}{air}$	b
[BIm] [ace]	Hydrophobic PVDF	*		*	$\frac{SO_2}{air}$	b
[N_{224}][acetate]	PES			*	$\frac{SO_2}{N_2}, \frac{SO_2}{CH_4}, \frac{SO_2}{CO_2}$	c
[N_{224}][propionate]	PES			*	$\frac{SO_2}{N_2}, \frac{SO_2}{CH_4}, \frac{SO_2}{CO_2}$	c
[N_{224}][dimalonate]	PES			*	$\frac{SO_2}{N_2}, \frac{SO_2}{CH_4}, \frac{SO_2}{CO_2}$	c
[N_{224}][dimaleate]	PES			*	$\frac{SO_2}{N_2}, \frac{SO_2}{CH_4}, \frac{SO_2}{CO_2}$	c
[N_{224}][diglutarate]	PES			*	$\frac{SO_2}{N_2}, \frac{SO_2}{CH_4}, \frac{SO_2}{CO_2}$	c
[TMG][lactate]	MCM-41	*	*			d

[1] Test of absorption/desorption
[2] Kinetic Analysis of absorption/desorption
[3]Permeance test
[4] Permselectivity test

a: Jiang et al. [2007]
b: Luis et al. [2009]
c: Huang et al. [2014]
d: Li et al. [2015]

Table 10.6: *Properties of influence for the processes involving ILs*

Property	Separation Processes		
	ILA	Permeation through SILMs	Fixed-bed sorption on SILPs
SO_2 Abs. Capacity	⋆ ⋆ ⋆	⋆ ⋆ ⋆	⋆ ⋆ ⋆
Regenerability	⋆ ⋆ ⋆	⋆ ⋆ ⋆	⋆ ⋆ ⋆
Viscosity	⋆	⋆ ⋆ ⋆	⋆ ⋆
SO_2 diffusivity	⋆	⋆ ⋆ ⋆	⋆ ⋆
Thermal stability	⋆ ⋆	⋆	⋆ ⋆
Cost	⋆ ⋆ ⋆	⋆	⋆
Ease of massive production	⋆ ⋆ ⋆	⋆	⋆
H_2O abs. capacity	⋆	⋆ ⋆	⋆ ⋆
Importance: ⋆ ⋆ ⋆ high, ⋆ ⋆ medium, ⋆ low			

- high thermal stability/ciclability; may be important for processes involving teperature swing for regeneration (ILA, fixed-bed sorption on SILP)
- low cost and ease of massive production. Important for liquid absorption processes, which may require hundreds of liters (depending on the plant capacity) of IL circulating in the columns.
- low affinity for water vapor: steam may be used as sweep gas in membrane operations or for the regeneration of a SILP. In bot cases, water absorption can result in the dilution of the IL and contamination of the separated gas phase.

These features affect the choice of the ionic liquid depending on the separation process considered, as show in Table 10.6.

10.2.2.2 Comparison between ILs absorption and water absorption for SO_2/O_2 separation

Two of most promising ILs proposed by literature, [BMIm] [$MeSO_4$] and [EMIm] [$EtSO_4$] , have been considered to perform some process calculations and compare the results with a more conventional water absorption process. Firstly, the absorption capacity of both liquids was compared with water: figure 10.5 shows absorption isotherm data for the three liquids at 40°C. It is apparent that SO_2 has a comparable solubility in the two ionic liquids, while the solubility in water is dramatically lower.

Table 10.7 shows performance and energy consumption data for an absorption column with 4 theoretical stages attaining 99% SO_2 recovery using

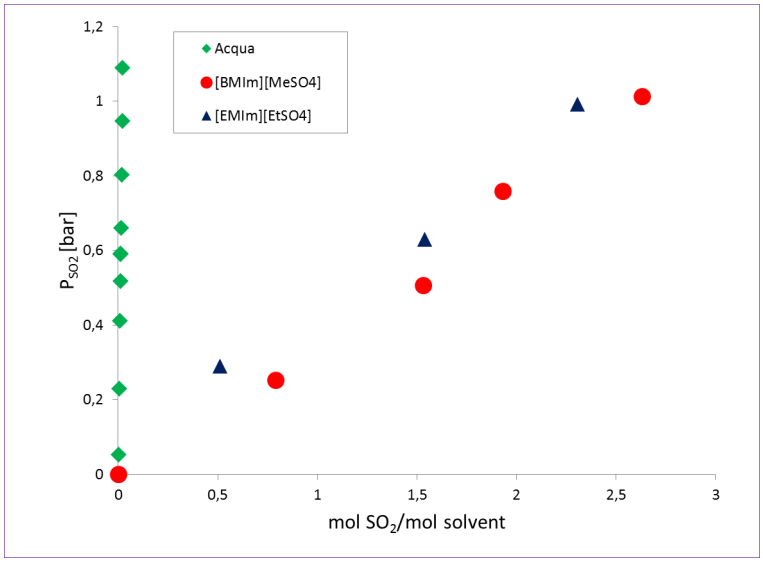

Figure 10.5: SO_2 *absorption equilibrium data for water and two ILs at 40°C.*

Table 10.7: *Operating conditions and energy consumption of an absorption column with 4 theoretical stages attaining 99%* SO_2 *recovery with different liquid solvents.*

Solvent	Temperature [°C]	Pressure [atm]	Solvent rate [mol/molSO_2]	Compression [kJ/mol SO_2]	Pumping [kJ/mol SO_2]
H_2O	30	1	100.5	-	-
	30	2	52.5	3.6	0.16
	30	5	24.3	8.2	0.3
	30	7	18.9	9.9	0.35
	40	1	134.3	-	-
	40	5	30.6	8.5	0.37
	40	7	23.3	10.1	0.43
[BMIm][$MeSO_4$]	30	1	0.83	-	-
	40	1	1.1	-	-
[EMIm][$EtSO_4$]	30	1	1.13	-	-

water or one of the selected ionic liquids as solvent. Energy consumption is estimated with the following assumptions:

- both inlet fluid phases (i.e. gaseous SO_2 /O_2 mixture to be separated and liquid solvent) available at atmospheric pressure;
- mechanical efficiency is 80% and 60% for compression and pumping, respectively;
- only pressure head is considered and pressure drop in the column and piping is neglected.

As a consequence, energy consumption is estimated only for operating pressures above 1 atm. Geometric head could slightly affect the power needed for liquid pumping; however, the incidence of the pumping power on the total consumption is always very small.

It is apparent that the use of ionic liquids potentially allows to meet the same specifications with much lower solvent rates and operating pressures. It is worth noting that the figures reported in Table 10.7 account only for the absorption step. A higher energy input is clearly required if the regeneration step is also included in the calculation. For ionic liquids this extra energy can be provided as low temperature heat. As an example, for [BMIm] [$MeSO_4$] regeneration can be carried out at 100-130°C. Assuming to operate absorption at 40°C and 1 atm, about 30 kJ/mol SO_2 are required to bring the ionic liquid to the regeneration temperature (SO_2 solution heat was assumed to be balanced between the absorption and desorption column; IL heat capacity was estimated based on the values reported by Huang et al. [2008], Rabie [2012].

10.2.3 Membrane separation

Selectively permeable membranes can be used to separate SO_2/O_2mixtures. Compared to other gas separation processes, membrane operations are in general easier to be run discontinuously, which, as pointed out earlier, is a very interesting feature for the application considered here. Basically, two types of membranes can be used in this case:

- SO_2 permeable membranes
- O_2 permable membranes

Few data are available for SO_2 permeable membranes. These membranes include, in addition to innovative ionic liquid supported membranes already

discussed above, polymeric membrane. As for polymeric membranes, polyacrylate and cellulose triacetate single-layer and composite membranes were considered for SO_2 separation [Kuehne and Friedlander, 1980]. However the authors concluded that such membranes can be used for laboratory preparations but are not suitable for industrial application.

As for the former type of membranes, the application of high-temperature oxygen conductors to SO_2/O_2 separation in the context of the sulfur family of thermochemical cycles has been previously studied [He et al., 2013, Atkin et al., 2011]. More specifically, yttria-stabilised zirconia (YSZ) dense membranes were considered.

Two possible approaches to the implementation of such membranes were proposed:

- integrated membrane reactor: the membranes (typically in tubular form) are installed in the reactor and operate in parallel with the catalyst. O_2 is continuously removed from the reaction space, which allows to separate one reaction product and push the conversion at the same time. With this configuration, higher conversions can be attained without recycling unreacted components and the whole reaction/separation system is more compact. However, the construction of an integrate membrane catalytic reactor poses several technological challenges related to the membrane/catalyst coupling;

- standard catalytic decomposition reactor followed by O_2 separation downstream of the reactor and retentate recycling. This configuration is less compact and efficient but easy to implement because it involves building and running a conventional catalytic reactor.

It is worth noting that YSZ membranes work at high temperatures (comparable to SAC), therefore, if the membrane is not integrated in the reactor, it must be installed immediately downstream of the SAC. Due to the temperature level required, there are important issues related to the discontinuous operation of the membrane for the specific application considered here. Indeed, the ceramic material of the membrane cannot withstand the daily thermal cycling of the SAC. Furthermore, Atkin et al. [2011] observed a decrease of O_2 permeability during the tests, which suggests that also stability issues due to the presence of SO_2 are present.

For all the reasons discussed above, the use both of oxygen and SO_2 conductors and in the SOL2HY2 process was discarded.

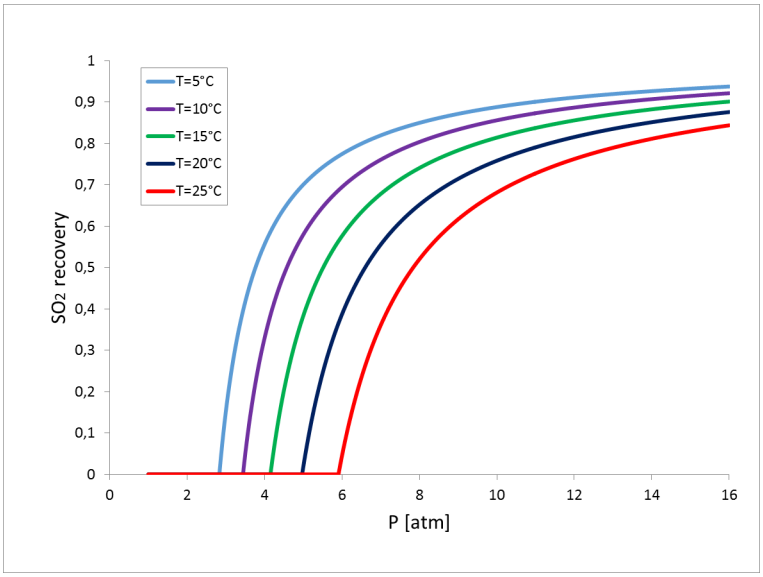

Figure 10.6: *Liquid* SO_2 *recovery upon single stage compression followed by phase separation*

10.2.4 Sulfur dioxide liquefaction

Since O_2 is far above its critical temperature at ambient conditions while SO_2 is not, it is in principle possible to liquefy and separate SO_2 from O_2 by compression.

For a single step compression followed by phase separation, Figure 10.6 and Figure 10.7 show SO_2 recovery and SO_2 contamination (i.e. molar fraction) in the gas phase, respectively. Obviously, both parameters benefit from a pressure increase; however, even after compressing the gas up to 16 atm, the specifications on both SO_2 recovery and O_2 purity are far from being met if the operation is carried out at a close to ambient temperature. Indeed, in order to attain 99% SO_2 recovery at 16 atm, the temperature should be about -39°C. Therefore the use of a refrigerant would be required.

A further increase of the pressure could be possible; however it should be considered that the final storage pressure will hardly exceed 10 atm: according to Louie [2005], a typical mechanical design pressure for SO_2 storage tanks is 15.2 atm, and the actual operating pressure for a maximum operating temperature of 50 °C is about 8 bar.

It is worth noting that the above calculations on separation performance are based on a very simplified model of the operation: single stage compression and only SO_2 and O_2 (molar ratio 1:0.5) in the inlet stream; however, the main conclusions remain basically unchanged if a more realistic model

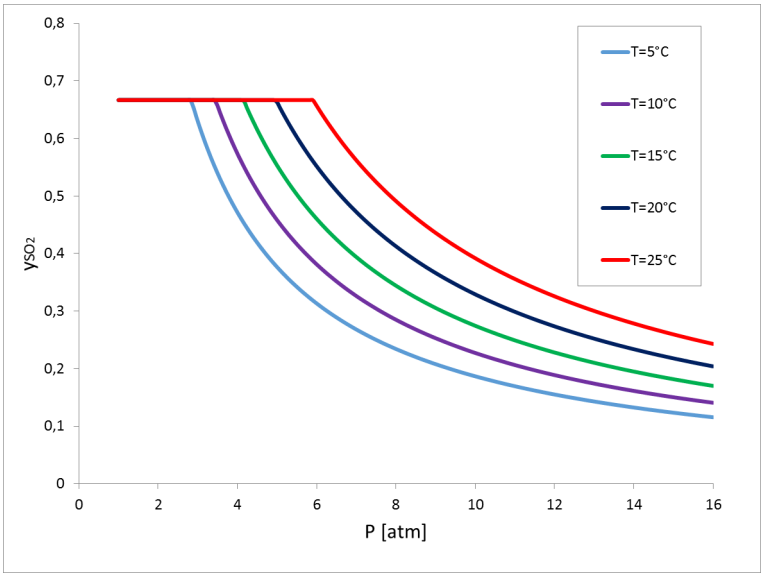

Figure 10.7: SO_2 *mole fraction in the gas stream after a single stage compression followed by phase separation.*

(more compression stages) of the process is considered.

Figure 10.8 shows the Aspen One flowsheet developed for the multi-stage compression; the conditions considered are: intercooled staged compression (4 stages) and inlet stream saturated with water, according to the composition of outlet stream of SAC section . The operating and performance parameters for the staged compression are reported in Table 10.8. It is clear that, in order to achieve an acceptable SO_2 recovery, either the operation have to be carried out at low temperature by using a refrigerant, or the outlet gaseous stream have to be further treated by another SO_2 recovery process

Table 10.8: *Operating parameters and performance of* SO_2 *staged compression and liquefaction.*

Parameter	Units	Value	Note
Feed temperature	°C	25	
Feed pressure	bar	1	
Stage compression ratio	-	2	
Number of stages	-	4	
Interstage cooling temp.	°C	25	
SO_2 recovery	%	83.6	stream 16
O_2 purity	%	75.9	stream 15
specific consumption	kJ/molSO_2	16.9	80% mech. efficiency

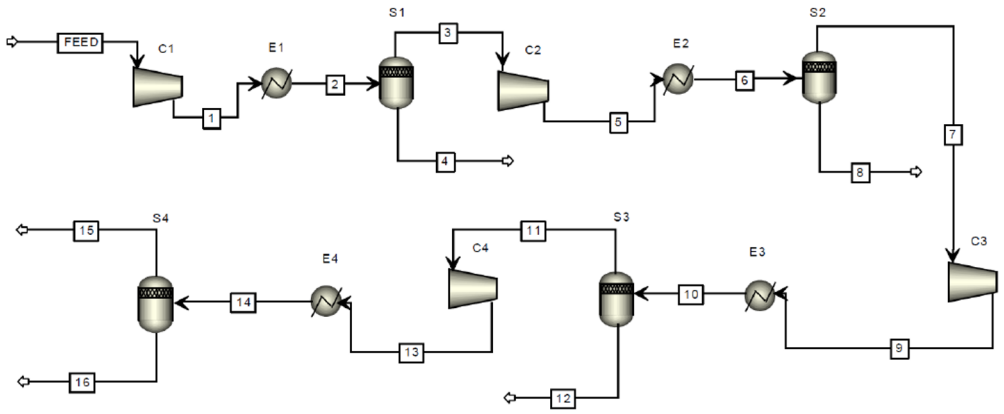

Figure 10.8: *Flowsheet of* SO_2/O_2 *separation by intercooled staged compression*

such as liquid absorption.

10.3 Process selection and flowsheet development

Even if the more innovative processes like ionic liquid absorption or membrane separation appear very promising, especially for the possible discontinuous operation, they do not yet show a sufficient degree of technological maturity to be considered for the industrial application in the SOL2HY2 plant. Hence, water absorption and refrigerated SO_2 liquefaction represented the most suitable processes because they are based on conventional equipment solutions which can be reliably designed and scaled up. Particularly, due to SO_2 liquefaction downstream of the gas separation units being in any case required in the SOL2HY2 process to allow, by storage solutions, the integration between the discontinuous operating regime of SAC and the continuous one of SDE, the SO_2 liquefaction method was selected.

However, as it was resulted in the previous paragraph about SO_2 liquefaction, although operating at high pressure by intercooled staged compression, in order to achieve an acceptable SO_2 recovery, either the use of a refrigerant, or another SO_2 recovery process to treat the outlet gaseous stream, was necessary. In both these options the overall cost of the operation was significantly increased, but in the refrigerated compression method there is the possibility, due SO_2 can be easly condensed and has high heat of evapo-

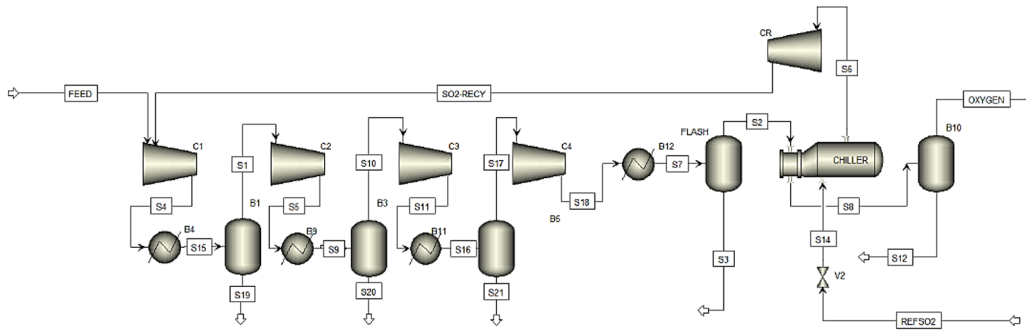

Figure 10.9: *Flowsheet for* SO_2/O_2 *separation block*

ration, to use the same liquid SO_2 available in the plant as refrigerant fluid. For this reason the SO_2 "self-refrigerated" liquefaction has been chosen in the final configuration.

The Figure 10.9 shows the resulting final flowsheet. The gas mixture coming from SAC and SO_3 separation (FEED) undergoes staged compression up to about 18 bar. Water is separated after the first stages of compression, while a part of the liquid SO_2 is recovered at the last stages (S21 and S3). SO_2 recovery is further pushed by lowering the temperature of the residual SO_2/O_2 stream (S2) to about -40°C (S8). To that end, liquid SO_2 from the storage tank (REFSO2) is boiled under vacuum and used as heat sink. The pressure set up for REFSO2 is 5 bar (not 8 bar as in the storage tank), wich is the vapour pressure of SO_2 at an intermediate operating temperature of about 40°C. The final fraction of liquid SO_2 is thus recovered (S12). SO_2 vapour formed in the chiller is recompressed to ambient pressure and recycled to the first stage of the compressor together with the feed. The main operating conditions and performance figures of the process are reported in Table 10.9 .

Table 10.9: *Operating parameters and performance figures for the* SO_2 *"self-refrigerated" liquefaction process.*

Parameter	Units	Value
Feed temperature	°C	25
Feed pressure	bar	1
Discharge pressure	bar	17.7
Number of stages	-	4
Interstage cooling temp.	°C	30
Chiller pressure	bar	0.2
SO_2 recovery	%	99
O_2 purity	%	97.7
specific consumption	kJ/molSO_2	20.7

Chapter 11

Evaluation of energy requirements and process efficiency

11.1 Final block diagram of the process

The conclusions drawn in the previous chapters for each process block are summarized in the detailed block diagram reported in Figure 11.1. The diagram also shows the energy input required by each block in terms of medium (<550°C) and high (>600°C) temperature heat or power.

The selected process solutions are briefly reminded below:

- SA concentration is performed by evaporation with vapor recompression; The inlet SA solution weight concentration (ω_c^0) and the outlet SA solution weight concentration (ω_c^f) for the concentration section, are respectevely set at 20% and 75%. Indeed, this combination of concentration values is advantageous in term of global consumption and process efficiencies, as it will be shown in the Section 11.2.

- High-temperature SAC is carried out by reactant pre-heating at 1000°C, followed by SO_3 decomposition in an adiabatic reactor (Chapter 9)

- SO_3 separation is operated by fractionated condensation (Chapter 9)

- SO_2/O_2 is operated by "self-refrigerated" SO_2 liquefaction (Chapter 10)

Figure 11.1 shows that the plant is divided in two main sections characterized by a different operating regime: the *continuous section* groups the plant units that are operated round-the-clock, while units in the *discontinuous section*

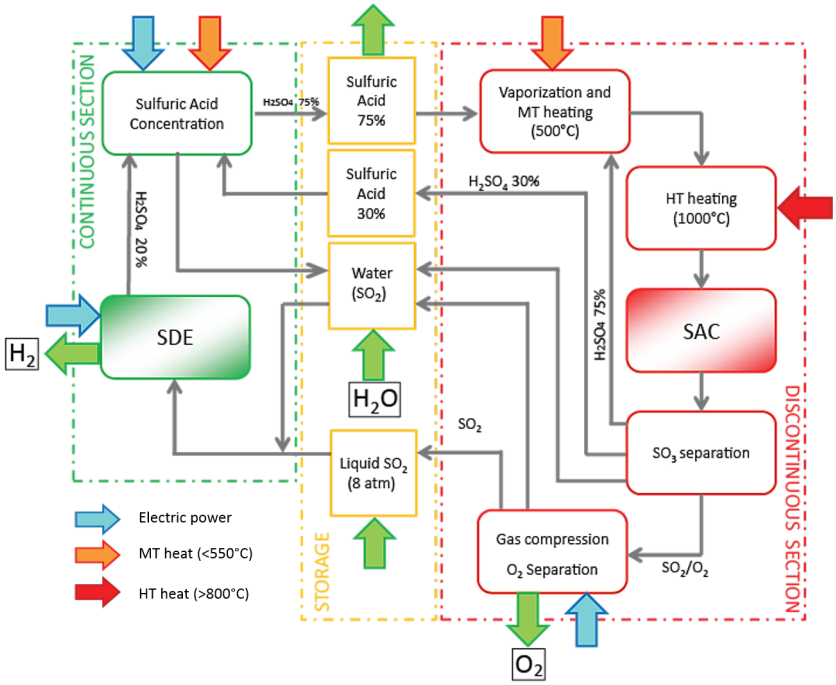

Figure 11.1: *Final block diagram for SOL2HY2 process.*

are operated only when the solar radiation is available (8 h per day) and are started-up and shut-down daily. The reason for this is related to the integration of the proposed HyS process with concentrating solar thermal plants and will be discussed in Section 13.1

In design conditions for closed cycle operation, the two sections have the same daily average throughput; therefore, due to the shorter operating time, the istantaneous throughput of the discontinuous section is higher (double) than that of the continuous section. Liquid storage tanks allow to connect the two sections despite the different operating regimes.

11.2 Energy requirements and process efficiency

The total consumption of SOL2HY2 process, can be evaluated on the basis of single sections contributions. In the Table 11.1the thermal (MT and HT) and electrical energy demand are listed, considering two values for the inlet H_2SO_4 solution to SAC section (ω_c^f), 50 and 75 %wt, starting from a sulfuric acid feed to Concentration section (ω_c^0) both of 20 %wt and 13 %wt.

For almost similar needs in terms of electric power and HT heat, the

Table 11.1: *Consumptions of each process block.*

ω_c^0= 20 %wt						
Process block	ω_c^f=75%wt			ω_c^f=50%wt		
	MT heat [kJ/mol]	HT heat [kJ/mol]	Electric Power [kJ/mol]	MT heat [kJ/mol]	HT heat [kJ/mol]	Electric Power [kJ/mol]
SDE*	-	-	273.4	-	-	273.4
SA concentration	99.9	-	75	84.9	-	61.2
SAC +SO_3separation	206.1	196.37	-	395.8	197.1	-
SO_2/O_2 separation	-	-	20	-	-	20
TOTAL	306	196.37	368.4	480.7	197.1	354.6

ω_c^0= 13 %wt						
Process block	ω_c^f=75%wt			ω_c^f=50%wt		
	MT heat [kJ/mol]	HT heat [kJ/mol]	Electric Power [kJ/mol]	MT heat [kJ/mol]	HT heat [kJ/mol]	Electric Power [kJ/mol]
SDE*	-	-	259.4	-	-	259.4
SA concentration	130	-	75	107.5	-	61.2
SAC +SO_3separation	206.1	196.37	-	395.8	197.1	-
SO_2/O_2 separation	-	-	20	-	-	20
TOTAL	336.1	196.37	354.4	503.3	197.1	350.6

* The information related to SDE has been provided by Research Grouping Aalto Korkeakoulusäätiö (Aalto University Foundation), being the partner within the framework of SOL2HY2 project specialist about the Electrolyte Section

combination of ω_c^0= 20 %wt and ω_c^f=75 %wt, as concentration specifications, determines the minor consumption of MT heat.

On the basis of the calculated consumptions was possible to evaluate the thermochemical and solar-to-Hydrogen efficiencies of plant.

The thermochemical efficiency is generally defined as the ratio of generated H_2 lower heating value and energy input to process. It can be expressed as:

$$\frac{1}{\eta_{TOT}^{tc}} = \frac{\chi_{SO_2}}{\eta_{SS}^{tc}} + \frac{1}{\eta_{SDE}^{tc}} \tag{11.1}$$

where

- $\chi_{SO_2}$is the SO_2 fraction converted to H_2=1 assuming there are no losses of SO_2 in the cycle;

- η_{SS}^{tc} is the thermochemical efficiency of the sulfuric section,expressed as:

$$\eta_{SS}^{tc} = \frac{\chi_{SO_2} LHV_{H_2}}{Q_{ss}} \tag{11.2}$$

with $Q_{ss} = Q_{MT} + Q_{HT}$ (=MT heat + HT heat of Table 11.1) and LHV_{H_2}=H_2 lower heating value;

- η_{SDE}^{tc} is the electrochemical efficiency of electrolyzer, expressed as:

$$\eta_{SDE}^{tc} = \frac{LHV_{H_2}}{2F\Delta V_{SDE} \frac{1}{\eta_{th\to el}} \frac{1}{\eta_{SDE}^{el}}} \tag{11.3}$$

with LHV_{H_2}= Lower Heat Value of Hydrogen , F= Faraday constant, ΔV_{SDE}= potential to Electrolyzer (Table 7.2 in the Chapter 7), $\eta_{th\to el}$= thermal to power efficiency and η_{SDE}^{el}= Electrolyzer efficiency.

The solar-to-hydrogen efficency instead, takes in account that the thermal source of process is solar energy, and so has been calculated as:

$$\frac{1}{\eta_{sol\to H_2}} = \frac{\chi_{SO_2}}{\eta_{SS}^{tc}\eta_{SS}^{CSP}} + \frac{1}{\eta_{SDE}^{tc}\eta_{MT}^{CSP}} \tag{11.4}$$

where

- η_{SS}^{CSP} is the weighted average efficiency of the solar capture thecnologies, expressed as:

Table 11.2: *Assumptions for efficiences evaluation. The the information related to SDE has been provided by Research Grouping Aalto Korkeakoulusäätiö (Aalto University Foundation).*

Symbol of parameter	Value
$\eta_{th\rightarrow el}$ [%]	42
η_{HT}^{CSP} [%]	40
η_{MT}^{CSP} [%]	52
η_{SDE}^{el} [%]	90
F [C/eq]	96480
LHV_{H_2}[kJ/mol]	240

$$\eta_{SS}^{CSP} = \frac{Q_{MT}\eta_{MT}^{CSP} + Q_{HT}\eta_{HT}^{CSP}}{Qss} \tag{11.5}$$

where η_{MT}^{CSP} is the MT CSP efficiency and η_{HT}^{CSP} the HT CSP efficiency.

It is necessary to remember that in the SOL2HY2 process has been set that MT heat was provided using molten salts as HTF and storage medium (with possible backup) and Solar tower proved the HT heat.

The values of all parameters mentionated above are listed in Table 11.2.

.

By implementing the equations 11.1,11.2,11.3,11.5 and 11.4 has been possible to calculate the efficiences of the process both for ω_c^f=50%wt and for ω_c^f=75%wt, considering ω_c^0 both of 20%wt and 13%. The results are shown in Table .

Also in terms of efficiencies, the combination of ω_c^0= 20 %wt and ω_c^f=75 %wt, as concentration specifications, provides generally the best result.

Table 11.3: *Process efficiencies.*

ω_c^0=20 %wt		
Efficiency	Value [%] for ω_c^f=50%wt	Value [%] forω_c^f=75%wt
η_{SS}^{tc}	35.4	47.7
η_{SDE}^{tc}	31.8	31.8
η_{TOT}^{tc}	16.75	19.08
η_{SS}^{CSP}	48.5	47.3
$\eta_{sol\rightarrow H_2}$	8.4	9.5
ω_c^0=13 %wt		
Efficiency	Value [%] for ω_c^f=50%wt	Value [%] forω_c^f=75%wt
η_{SS}^{tc}	34.3	45.9
η_{SDE}^{tc}	33.4	33.4
η_{TOT}^{tc}	16.5	18.78
η_{SS}^{CSP}	48.6	47.4
$\eta_{sol\rightarrow H_2}$	8.3	9.4

Chapter 12

Sizing and costing of the chemical plant equipment

12.1 Sizing of main plant equipment

All the main plant equipment included in the flowsheets developed in the previous chapters have been sized.

For the evaluation has been set up a value of H_2SO_4transformed equal to 15 mol/s, which corrisponds to 15 mol/s of transformed $SO_2$and to 15 mol/s of produced H_2.

The sizing have been performed by using spreadsheet prepared specifically for each kind of equipment, on the basis of guidelines known in the context of engineering design [Peters et al., 2002].

For the heat exchangers, tube and shell configuartion was assumed and their design were performed differently depending on exchange with or without phase change occurred. Particularly, in the case of phase change for fluids involved in the exchange, the "Zone analysis" was employed to calculate the heat transfer coefficient [Kern, 1950]).

The storage tanks of $SO_{2(l)}$ and H_2SO_4 , required to couple the continuous and discontinuos sections of the plant have also been taken into account and sized. In so doing, a storage period equal to 16 h has been considered.

For its sizing, the SO_3 decomposition reactor has been modeled as a PFR.

12.1.1 Sulfur trioxide decomposition reactor

For sizing the decomposition reactor, mass and heat balances have been considered for an adiabatic PFR :

- Mass balance

$$\frac{F^0_{SO_3}}{S}\frac{\mathrm{d}X_{SO_3}}{\mathrm{d}z} = k^v_{STD} P y_{SO_3}(1-\eta_{STD}) \tag{12.1}$$

- Heat balance

$$\sum F^0_i h^0_i = \sum F_i h_i \tag{12.2}$$

with $F_i = F^0_{SO_3}(s_i + \nu_i X_{SO_3})$, hence

$$\sum s_i h^0_i = \sum s_i h_i + \sum \nu_i X_{SO_3} h_i$$

$$0 = \sum s_i \int_{T_{in}}^{T} c_{p_i}\,\mathrm{d}T + X_{SO_3}\Delta_{STD}h$$

$$\bar{c}_p = \sum s_i c_{p,i}$$

$$0 = \int_{T_{in}}^{T} \bar{c}_{p_i}\,\mathrm{d}T + X_{SO_3}\Delta_{STD}h$$

for nearly constant $\bar{c}_p$ (in calculations c_p and $\Delta_{STD}h$ as been assumed constant and their values equal to those at 850°C)

$$\bar{c}_p(T - T_{in}) + X_{SO_3}\Delta_{STD}h = 0 \tag{12.3}$$

By introducing a serie of adimensional terms, as

$$\tilde{T} = \frac{T - T_{ad}}{T_{in} - T_{ad}}; \tilde{z} = \frac{z}{L}$$

$$\delta_{STD} = \frac{\Delta_{STD}h}{\bar{c}_p(T_{in} - T_{ad})}, Da = \frac{k^{v0}_{STD}\exp(-\alpha)PV_{cat}}{F^0_{SO_3}}, \vartheta = \frac{T_{in} - T_{ad}}{T_{in}}, \alpha = \frac{E_a}{RT_{in}}$$

where T_{ad} is the adiabatic reaction temperature, and combining the equations 12.1 and 12.3 results:

$$\frac{\mathrm{d}X_{SO_3}}{\mathrm{d}\tilde{z}} = Da\,\exp\left(-\alpha\frac{\vartheta\left(1-\tilde{T}\right)}{1-\vartheta\left(1-\tilde{T}\right)}\right) y_{SO_3}(1-\eta_{STD})$$

$$(\tilde{T}-1) + \delta_{STD}X_{SO_3} = 0 \quad \Rightarrow \tilde{T} = 1 - \delta_{STD}X_{SO_3}$$

$$\frac{\mathrm{d}X_{SO_3}}{\mathrm{d}\tilde{z}} = Da\,\exp\left(-\alpha\frac{\vartheta\delta_{STD}X_{SO_3}}{1-\vartheta\delta_{STD}X_{SO_3}}\right) y_{SO_3}(1-\eta_{STD})$$

$$\int_0^{X_{SO_3}} \frac{\mathrm{d}X_{SO_3}}{\exp\left(-\alpha\frac{\vartheta\delta_{STD}X_{SO_3}}{1-\vartheta\delta_{STD}X_{SO_3}}\right) y_{SO_3}(1-\eta_{STD})} = Da$$

with Damkoler number calculated at the maximum temperature.

From Da definition it is possible to calculate the catalyst mass as

$$\frac{Da\, F^0_{SO_3}}{k^{m0}_{STD}\, \exp(-\alpha)\, P} = M_{cat}$$

and so to evaluate the reactor size, by considering a calculated bulk density for the catalyst of 0.87 kg/l.

12.2 Costing of main plant equipment

Based on the equipment sizing discussed in previous paragraph the costing of each equipment has been performed, in order to estimate the required investment costs for the whole plant.

For this economical evaluation, the cost charts[1] reported in the Peters et al. [2002] book for all the different equipments, have been used.

Since the available informations were related to 2002 and expressed in \$, Cost Index have been used to discount the values at 2016 (particularly 567 for the year 2016 and 396 for 2002 as reported by ChemicalEngineeringOnline [2016]), and to switch from \$ to € a value of 1.13 was assumed as conversion factor [Ilsole24ore, 2016].

In Table 12.1specifications and costs of the main equipment are reported for a hydrogen production by closed cycle (CC) of 15 mol/s .

The SDE has not been included in Table 12.1 but the estimation for its specific cost (81 €/per mole of H_2 generated) has been provided by Research Grouping Aalto Korkeakoulusäätiö (Aalto University Foundation).

[1] A cost chart for an equipment is a graph indicating the cost as a function of "cost attribute". The "cost attribute" is the main feature of the equipment and is different depending on the equipment type: i.e. the power for compressors, the diameter for columns, area for heat exchangers.

Table 12.1: *Size and cost of equipment considering an hydrogen production of 15 mol/s.*

Equipment	Duty $[kW]$	Calculated Area $[m^2]$	Calculated diameter $[m]$	Calculated Volume $[m^3]$	Cost1(2016) $[k\$]$	Cost2 (2016) $[k€]$	Ref. in Peters
Concentration section (Figure 8.4)							
Compressor C	1170,4				1320,73	5960,8	F.12-28
Exchanger E1	582,0	9,3			6,81	16,9	F.14-19
Exchanger E2	13742,1	229			262,37	580,5	F.14-33
Column D			1,3		12,69	57,3	F.15-15
Reboiler	1508,3	30			96,14	212,7	F.14-33
Reboiler (bis)	1508,3	30			87,48	193,5	F.14-33
SAC and SO_3separation sections (Figure 9.5)							
Exchanger E1	12960	285			295,53	653,8	F.14-33
Exchanger E2	9270,9	183			465,28	1029,4	F.14-33
Exch. E2 (bis)	9270,9	183			232,53	514,4	F.14-33
Exchanger E3	14337	2160			226,71	561,8	F.14-19
Exchanger E4	497,3	49			11,34	28,1	F.14-19
Exchanger E5	5881,5	91			24,92	91	F.14-29
Reactor AD-R				5,2	184,53	369,1	F.13-15
SO_2/O_2separation section (Figure 10.9)							
Compressor 1→17.66 atm	838,9				422,11	1905,1	F.12-28
Compressor 0,2→1 atm	75				207,39	936	F.12-28
Chiller	259,2	15			61,12	135,2	F.14-33
Exchanger	48,6	9,3			6,81	16,9	F.14-19
Storage tanks							
Storage tank H_2SO_4				56,45	83,71	167,4	F.12.55
Storage tank SO_2				45,45	83,71	167,4	F.12.55

The specification (bis) is for the option where molten salts are used as hot fluid for the exchange.
The column titles (Cost1) and (Cost2) are related respectively to equipment made with material cheaper material (CS e SS) and with more expensive material (as NI Alloy o Aisi 316).
The abbreviations SS and CS mean respectively Stainless Steel and Carbon Steel.
"F." in the references column means "Figure"

Chapter 13

Techno-economic assessment of the solar HyS process in selected scenarios

13.1 Integration of the HyS process with solar technologies

As already detailed in Section 11.1, the HyS process defined in this work requires three main types of energy input: power, medium temperature (<550°C) heat and high-temperature (>600°C) heat. All such types of energy input could in principle be provided by different Concentrating solar thermal (CST) or concentrating solar power (CSP) technologies.

Figure 13.1 illustrates the general approach proposed in this work to integrate the flowsheets developed for the HyS plant with CST and photovoltaic (PV) technologies, in order to power the process with renewable energy. Such approach may be summarized as follows:

- For the supply of **medium-temperature (MT) heat**, a parabolic trough CSP (Concentrated Solar Power) plant using solar salt (i.e. 60:40 w/w $NaNO_3/KNO_3$ mixture) as heat transfer and storage medium was considered. The CPS plant has a solar field (SF) of the same type as the Archimede plant in Priolo Gargallo (Italy) and Akesai Solar Thermal Power Plant (China, under development) [Maccari et al., 2016]. A number of 8 h of daily operation are assumed with 16 h of heat storage in order to potentially allow for continuous operation (in design conditions) for the process units that rely on this type of energy input. A set of trough loops connected in parallel with 6 collectors per loop is considered for the MT solar field.

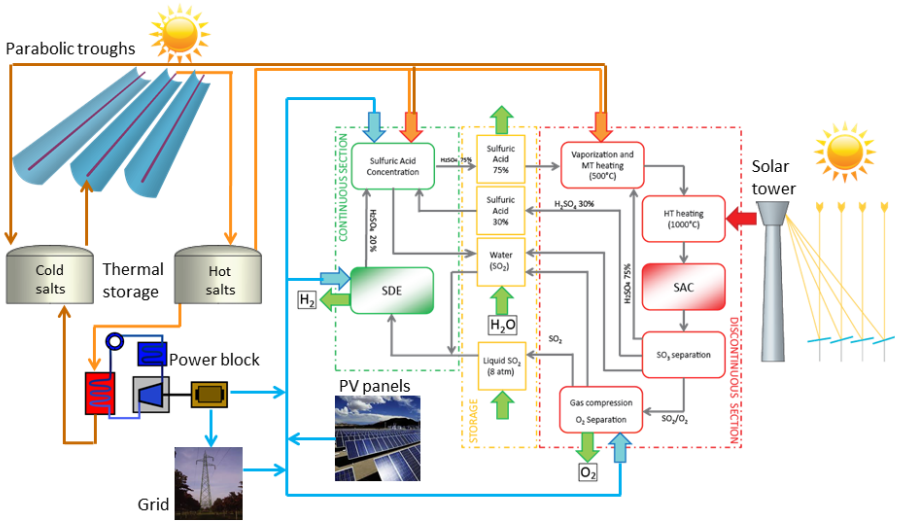

Figure 13.1: *General approach followed for the integration of the HyS process .*

- A central receiver (solar tower) system was considered to provide **high-temperature (HT) heat**, which is only needed for SA decomposition. Since no consolidated thermal energy solution is available today for the temperature required for SAC (1000°C), 8 h of daily operation and no heat storage are considered in this case. Therefore, SAC and, consequently, SA vaporization and unreacted SO_3 separation are assumed to operate discontinuously, only at daytime.

- Three options were considered, alone or in combination, to supply the **power** required by the process:

  - The simplest option is to draw electricity from the grid, which entails lower plant complexity and investment costs at the price of a lower share of renewable energy in the produced hydrogen[1].
  - A second option is the inclusion of a power block in the parabolic trough solar plant. The PB (and solar field) can be sized to fulfill the energy requirement of the HyS plant only or oversized to allow

[1]It should however be considered that in several countries a non-negligible share of the grid electricity is produced with renewable energy sources.

grid export. This clearly increases the share of renewable energy in the produced hydrogen (up to 100%), but also increases the production costs.

– Finally, the integration of a PV (PhotoVoltaic) plant was also considered. The implementation of this technology can help increasing the renewable energy share at a lower price compared to CSP. However, due to the lack of efficient and cost-effective electric storage solutions (for long storage duration), powering the plant with PV alone is not possible.

The proposed integration scheme affects the operating regimes of the units of the HyS plant:

- SA decomposition (SAC) requires HT heat, which is provided by the central receiver system. This process block must therefore operate discontinuously (8 h per day) when the solar reasource is available.

- As a consequence, SA vaporization and SO_2/O_2 separation were also set to work discontinuously (when SAC is in operation) in order to avoid to store of gaseous products upstream and downstream of the SAC section.

- Other plant equipment such as the SDE and SA concentration units are operated continuously for a higher capacity factor and, most of all, to avoid daily start-up and shutdown operations, which this type of units can hardly afford. This is possibile considering that SA concentration requires MT heat ($< 200°C$) and the parabolic trough plant is equipped with a thermal energy storage system.

13.2 Open cycle operation

If an external SO_2 source is available, the continuous (low-temperature) section of the HyS can be oversized compared to the discontinuous section, leading to a higher production of hydrogen and sulfuric acid. In this case, the SA in excess of the SAC capacity can be sold as a co-product of the HyS plant, possibly improving the process economics.

It is worth noting that SO_2 is a waste product in some smelting and gas purification processes. Hence, in appropriate location SO_2 could be available at little or no cost; furthermore, SO_2 could be obtained also by Sulfur burning obtaining at the same time heat can be exploited in the process. Also the

Sulfur is a waste product in some processes such as desulphurisation for petroleum products, hence same considerations made for SO_2 apply.

To quantify the percentage of the hydrogen produced by an external SO_2 source compared to the total hydrogen output, a variable defining the *extent of cycle opening* (OC) has been defined:

$$\text{OC}=\frac{Produced\,hydrogen\,flowrate\,by\,open\,cycle}{Total\,produced\,hydrogen\,flowrate} \tag{13.1}$$

If OC = 0, the HyS plant operates in fully closed cycle, all the SA produced by SDE is is decomposed in the SAC and only hydrogen is obtained as main product[2]. If OC = 1, the plant operates in open cycle as in the OOC process (Section) . If $0 < \text{OC} < 1$ the cycle is partially open.

13.3 Heat backup by sulfur burning

When the heat collected by the CST plant is not sufficient to reach the target hydrogen production, the sulfur burning process 13.2 is a possible way to provide a heat backup avoiding the use of a fossil source, and obtaining a valuable co-production of SO_2.

$$S_{rhomb} + O_2 \rightleftharpoons SO_2 \quad (\Delta H = 9,3\,\text{MJ/kg}) \tag{13.2}$$

The general practice in commercial plants is to use liquid sulfur at 140-150°C [Müller, 2012]: at these temperature levels, the viscosity of sulfur is low enough to spray it through nozzles and to ensure the intimate mixing with the combustion air, which is essential for complete combustion. Currently, in industry, sulfur combustion furnaces with burners for atomizing liquid sulfur are used and their size is dependent on the type and efficiency of the burner used [Müller, 2012].There are three different burner type available on the market: pressure-nozzle burners; two-component burners and rotary burners;the rotary burner (Lurgi's LURO Burner) is nowadays the conventional solution for large plants. The throughput can be varied continuously from the rated capacity down to 20% or less without appreciable change in atomizing intensity. Therefore this burner design can also be used for low sulfur flow rate (as required in the present analysis). Other advantages of this technology [Outotec, 2013] are: single burner capacity up to 35 t/h of liquid sulfur; operational range comprised between 15 to 110% of the nominal sulfur load; high operating quality also during load changes; small furnace due to excellent atomization; easy and fast removal of the burner.

[2]Oxygen is clearly produced together with hydrogen. However, the explotation of the oxygen stream produced by the water splitting process was not considered in this work.

Since part of the heat released by combustion is typically required for preheating air and sulfur streams, as well as for the evaporation and decomposition of sulfur [Müller, 2012], only a fraction of the total heat of reaction (50%) has been considered available for the heat backup. As the sulfur combustion produces SO_2 - which represents a reacting component of the HyS process - it is highly convenient to use it to feed the SDE unit, thus opening the HyS cycle.

13.4 Definition of the scenarios considered

13.4.1 Plant sizing criteria

The chemical plant has been sized for a nominal H_2 production by CC (Closed cycle) of 15 mol/s, a reference plant capacity set in the SOL2HY2 project. For scenarios with partially open cycle (OC) operation, the capacity is higher and depends on the extent of cycle opening.

For the CST plant, different sizing criteria were considered:

- solar field sized as to collect the thermal power required by the chemical plant to produce 15 mol/s of hydrogen under peak insolation conditions (average DNI during the month with the highest insolation). Consequently, the actual solar thermal energy production is not sufficient to allow the nominal H_2 production by CC over the year. In this case, it is possible to reach the target CC capacity by heat integration (e.g., by sulfur burning).

- solar field sized as to collect the thermal power required by the chemical plant to produce 15 mol/s of hydrogen over the year

When a PB is present, the solar field size is increased accordingly.

For the scenarios with PV integration, the PV plant has been sized to fulfill the power requirement in the peak conditions. Hence, also in this case like for the Solar Plant, integration options have been contemplated: supply by grid or CSP.

13.4.2 Plant locations

The desert of Tabernas, near Almeria (Spain, 36.84 N 2.47 E) has been chosen as the reference location of the plant, mainly for its high irradiation level, which made it a suitable site within Europe. Furthermore, in this place a very important Research Centre on solar tecnologies (Plataforma Solar de Almeria) is located.

Table 13.1: *Summary of scenarios envisaged considering a total production of* H_2 *of 22 mol/s,* H_2SO_4 *concentration to the decomposition unit of 75%wt (starting from a 20%wt* H_2SO_4 *solution), solar plant designed on the peak radiation and Almeria as plant location.*

Scenario	Power block in CSP plant	PV integration	Sulfur burning	Off-grid
A, A1	NO	NO	NO	NO
B, B1	NO	YES	NO	NO
C	NO	NO	YES	NO
D	NO	YES	YES	NO
E	YES	NO	NO	NO
F	YES	YES	NO	NO
G	YES	YES	NO	YES

Finally, to evaluate the impact of location on plant performance in terms of the share in renewable energy and the H_2 cost, other installation sites have been included in the assessment:

- Atacama (Chile, 23.52 S 69.08 W)
- Ben Guerir (Morocco, 32.14 N 7.58 E)
- Alghero (Italy, 40.56 N 8.32 E)

For each location, hourly DNI data of a typical year were collected from Meteonorm database. In order to simplify the computational burden, an average day was considered for each month.

13.4.3 Plant configurations

On the basis of considerations made previously about sizing criteria and location of plant, different scenarios have been envisaged and compared.

In Table 13.1such scenarios are summarized, considering total production of H_2 equal to 22 mol/s, H_2SO_4 concentration to the decomposition unit equal to 75%wt (starting from a 20%wt H_2SO_4 solution), solar plant designed on the peak radiation and Almeria as plant location.

Specifically:

- in the scenarios A the electrical energy is supplied only from grid and thermal energy only from CST plants. Since the CS plant is designed on peak radiation the nominal H_2 production by CC (15 mol/s) can not be acheived in the scenario A unless the CS plant is oversized (scenario A1);

- in the scenarios B the electrical energy is drawn from the grid and PV thecnology, and thermal energy only from CST plant. Since the CST plant is designed on peak radiation the nominal H_2 production by CC (15 mol/s) cannot be acheived in the scenario B unless the CS plant is oversized (scenario B1);

- in scenario C the electrical energy is supplied only from grid, and thermal energy from CS plants and S heat backup;

- in scenario D the electrical energy is supplied from grid and PV thecnology, and thermal energy from CS plants and S heat backup;

- in scenario E the electrical energy and thermal energy are provided from CSP (Solar Trough + PB). Even if the yearly average electric production can sustain the HyS plant requirement, grid connection is required to buffer (through grid import/export) the different level of power production during the year;

- in scenario F power and thermal energy are provided by CSP (Solar Trough + PB). Furthermore PV integration is envisaged for the electricity supply and the grid connection is required;

- in scenario G the electrical energy and thermal energy are provided from CSP (Solar Trough + PB). In this configuration the solar plant is oversized to ensure enough power supply for the HyS plant throughout the year so that grid connection is not required. As a consequence, during the higher insolation times, the CSP plant will produce excess energy that will have to be dumped or used locally for other applications (if possible).

For each of these scenarios the achievement of set up H_2 total production (22 mol/s) is obtained by opening cycle; the percentage of OC necessary for this purpose is different depending on the different configurations envisaged.

13.5 Methodology

In order to evaluate the global performance of the different configurations and finally indentify the best one, a dedicated spreadsheet has been developed and used. The main Input and Output of this spreadsheet are summarized in Figure13.2 .

The H_2 cost evaluation performed by this calculation tool comes from a combination of several cost input:

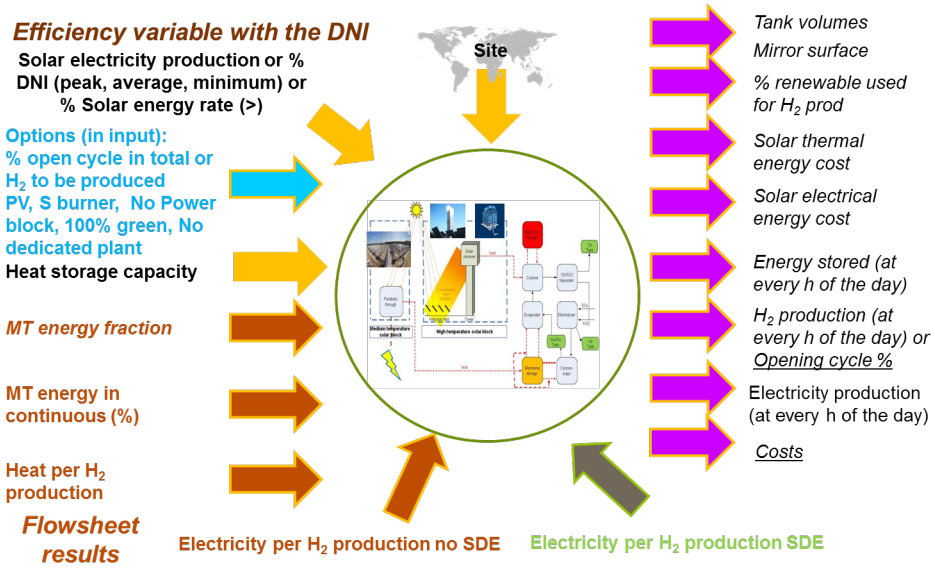

Figure 13.2: *Input and Output of spreadsheet employed for process analysis*

- Plant cost. The total capital investment has been evaluated on the basis of the detailed sizing of SOL2HY2 plant equipment, reported in the previous Chapter 11, obviously also considering the direct, indirect and general installation costs on Purchased Equipment (PE) and the operating costs of the plant (Operation and Mantainance, Annuity factor..). Moreover, for some scenarios the cost of Sulfur burning Liberatore et al. [2017] and/or PB has been also included in the computation.

- Thermal energy cost (MT and HT). All the energy, at medium and high temperature, required for the process has been calculated and the cost for its production by CSP has been evaluated.

- Power cost. For the evaluation, the cost of electrical energy from the grid has been considered and depending on the considered scenarios, also that for power from PV technology and/or from PB has been added.

All the main assumptions (in addition to those one of previous Table 11.2) made for the economical assessment are detailed in Table . The costs associated with the parabolic trough plant have been estimated with the same approach followed by Sau et al. [2016].

Table 13.2: *Main assumptions for economic evaluation.*

	Value
Direct solar radiation time [h]	8
Solar plant working time [d]	365
Power production if the solar plant is not dedicated [MWe]	50
Total Thermal renewable daily energy production HT [%]	100
Collection surface of the collector [m^2]	566.4
Number of collectors for a loop	6
Field specific cost [€/m^2]	2.5
Mirror field specific cost [€/m^2]	210
Foundation cost for each collector [€]	11000
Cost of Solar Salt [€/kg]	0.9
Melter, pumps, electrical systems specific [€/m^2]	1700
Power block specific [€/kWh_e]	850
Grid power specific cost [€/kWh_e]	0.06
Solar plant control, installation, engineering, building factor [% PE*]	25
Contingencies [% PE]	8
Insurance [% PE]	2
General facility factor [% PE]	10
Operation and Mantainence [% capital investment]	4
Annuity Factor (lifetime 30 y, discount factor 8%) [% capital investment]	11.3
Sulfur Burner parameters	
S LHV (solid) [MJ/kg]	9.4
Burner efficiency [%]	50
S specific cost [€/kg]	0.0001
Burner cost [k€]	1000
PhotoVoltaic parameters	
Specific cost [€/kW]	1000
Operation and Mantinence [%]	4
Annuity Factor (lifetime 15 y, discount factor 8%) [% capital investment]	9.6
PV efficiency [%]	15
PV losses [%]	20

*PE = Purchased equipment

Table 13.3: *Summary of results for the case studies of Table 13.1*

	A	A1	B	B1	C	D	E	F	G
MT Mirror Surface [ha]	2.0	2.7	2.0	2.7	2.0	2.0	16.3	13.3	18.14
HT Mirror Surface [ha]	2.1	2.7	2.1	2.7	2.1	2.1	2.1	2.1	2.1
Target H_2 by CC [mol/s]	15	19.2	15	19.2	15	15	15	15	15
H_2 by CC without S backup [mol/s]	11.44	15	11.44	15	11.4	11.4	15	15	15
H_2 by S heat backup [mol/s]	0	0	0	0	3.6	3.6	0	0	0
H_2 by CC with S backup [mol/s]	N/A	N/A	N/A	N/A	15	15	15	15	15
SO_2 by S burning [mol/s]	0	0	0	0	5.95	5.95	0	0	0
H_2 by OC [mol/s]	10.6	7.0	10.6	7.0	7.0	7.0	7.0	7.0	7.0
Total H_2 production [mol/s]	22	22	22	22	22	22	22	22	22
% of H_2 produced with OC	48.0	32.0	48.0	32.0	32.0	32.0	32.0	32.0	32.0
H_2 cost [€/kg]	8.7	8.8	8.7	8.8	8.5	8.4	12.8	11.9	11.5
H_2 cost with H_2SO_4 revenues [€/kg]	7.6	8.0	7.6	8.0	7.7	7.6	12.0	11.1	10.7
% renewable energy used	44.7	50.3	51.5	55.8	44.7	51.5	100	100	100

13.6 Results and discussion

The results obtained for the scenarios listed in Table 13.1 are summarized in Table 13.3 .

By comparing the results for scenarios A and B it can be seen that, as expected, the integration of PV for electricity production (case B) provides a significant improvement in terms of share of renewable energy (RE%), with very close H_2 production costs. It is worth noting that the values of RE% reported in Table 13.3 are conservative since they are obtained by assuming that the grid electricity is 100% non-renewable; actually, depending on the plant location, up to about 40% of the grid electricity is obtained from renewable energy sources. In the scenarios A and B the solar heat collected does not allow to achieve the target H_2 production by CC (11.44 mol/s are possible instead of 15 mol/s) and the total target H_2 production capacity (22 mol/s) is achieved by OC production. On the other hand, the use of backup heat provided by sulfur burning (case C) allows to reach the target CC H_2 production together with a reduction of the hydrogen production costs. Combination of PV integration with sulfur burning without a power block in the concentrating solar thermal plant (scenario D) leads to the lowest H_2 production costs, even if H_2 is not entirely produced with RES. The RE% can be increased up to 100% by including a power block in the concentrated solar plant, which fulfils the whole power demand for H_2 production (scenarios E, F; grid exchange to compensate the different level of power production during the year is however considered). This options entails higher H_2 production

costs (see scenarios E and A), which can however be reduced by about 8% with the PV integration (scenario F), because the required mirror surface of CSP is lower. Finally, an additional totally off-grid scenario (G) was also considered. In this case, the CSP plant was sized as to ensure the required power supply throughout the year, resulting in a plant about 30% larger (see scenarios F-G); however, the H_2 cost is similar if excess power production during the high irradiation times is employed locally for other uses (as reported in the table). On the other hand, if excess power cannot be used, the price of H_2 would raise to 13.9 €/kg (including SA sale revenues).

The difference between A and A1 (or B and B1) is in the actual production of the closed cycle, in fact in the scenarios A, B, C, ...,G the closed cycle target is 15 and the full target 22, but since in A and B the target is not reachable with solar heat heat only, the cycle has been opened up to 48% to reach 22 mol/s; on the other hand in A1 the solar mirror surface has been increased to reach the closed cycle target.

It is worth to note that the H_2 production costs reported in Table 13.3 are conservative because they are obtained by assuming a cost for SO_2 and sulfur from external sources of 0.01 €/(mol SO_2) and 0.0032 €/(mol S), respectively; furthermore, no revenue for selling the sulfuric acid is considered. As an example, in the scenario D, the H_2 cost would drop to 6.5 €/kg instead of 8.4 €/kg if S and SO_2 are available for free (as a waste or byproduct of other processes), and 5.7 €/kg if H_2SO_4 can be sold at about 50 €/ton.

The effect of plant location on performance has been evaluated. For this purpose, the scenario with the lowest H_2 production costs (D) was assessed for different plant locations. The results are summarized in Table 13.4 . The lowest costs are obtained for the Atacama site, thanks to the highest and most uniform solar irradiation, which reduces the required solar plant size. It is worth noticing that the increase of the average energy production leads to a higher H_2 capacity by the HyS closed cycle; consequently the heat backup required is reduced together with the percentage of energy and SO_2 produced by S burning.

Hence, the synergistic action of PV and S burning process coupled with CS technology leads to promising performance of the SOL2HY2 cycle for the hydrogen production, with an estimated cost between 8 and 9.2 €/kg of hydrogen produced (7.2-8.4 €/kg if the sale of H_2SO_4 surpluse is considered), with also a satisfactory share value of "no fossil source" energy supplied to process. Furthermore, this cost is consistent with the current targets set by the Fuel Cells and Hydrogen Joint Undertaking (FCH-JU) for the hydrogen production by high temperature water splitting [FCH-JU, 2014], which are 10, 8 and 6 €/kg for the years 2017, 2020 and 2023, respectively.

By starting from the scenario A1, in which electrical energy is supplied

Table 13.4: *Comparison of different solar plant locations.*

	Almeria	Alghero	Atacama	Ben Guerir
MT Mirror Surface [ha]	2.0	2.4	1.7	2.0
HT Mirror Surface [ha]	2.1	2.3	1.7	2.0
Target H_2 by CC [mol/s]	15.0	15.0	15.0	15.0
H_2 by CC without S backup [mol/s]	11.44	9.6	12.6	12.3
H_2 by S heat backup [mol/s]	3.6	5.4	2.4	2.7
H_2 by CC with S backup [mol/s]	15.0	15.0	15.0	15.0
SO_2 by S burning [mol/s]	5.9	9.1	4.1	4.5
H_2 by OC [mol/s]	7.0	7.0	7.0	7.0
Total H_2 production [mol/s]	22	22	22	22
% OC (in term of H_2)	31.9	31.9	31.9	31.9
H_2 cost [€/kg]	8.4	9.2	8.0	8.3
H_2 cost with H_2SO_4 revenues [€/kg]	7.6	8.4	7.2	7.5
% renewable energy	51.5	48.1	55.0	53.1
% "no fossil source" energy	63.4	66.3	63.1	62.0

from grid only and thermal energy only from CST plants, the effect of increasing the Solar power share from 0 to 100% by including a progressively bigger PB in the CST plant was investigated. The results are reported in Table 13.5. for fully closed cycle (capacity 15 mol/s) and partially open cycle operation (capacity 22 mol/s); more specifically, the performance is assessed in terms of H_2 production cost and solar-to-hydrogen efficiency, which is defined ratio of the higher heating value of the produced hydrogen to the solar energy used (collected Direct Normal Irradiance, DNI). This definition is straightforward and meaningful only for closed-cycle full-solar scenarios, i.e. when both the heat and power requirements are fulfilled with solar energy and water is the only feedstock used (bold face figures in the table). If other energy and/or material streams (e.g., grid electricity and/or SO_2) are fed to the process, other metrics should be used to assess the efficiency. However, an attempt was made to produce comparable efficiency figures also for these cases; to that end, the three definitions reported Table 13.3 were considered. Table 13.5 shows that, clearly, the increase of CSP share increases H_2 production cost up to more than 13 €/kg, but allows to reach up to 100% renewable hydrogen.

The prices obtained for 100% renewable hydrogen producing using only power and heat from CST plants are quite high. This may also be related to the relatively small plant capacity considered. Therefore, in order to asses the economies of scale that can be attained with higher plant capacity, the results presented in Table 13.5 have been reassessed for a plant with a doubled

Table 13.5: *Effect of solar power share on Solar-to-hydrogen efficiency and hydrogen cost. Lower plant capacity.*

Cycle opening %	Solar power share, %	Solar-to-hydrogen efficiency, %			H_2 Cost, €/kgH_2	
		1	2	3	Without acid sales	With acid sales
0% (Production of hydrogen only) H_2 produced by plant: 15 mol/s	0	26.68	19.85	11.23	9.45	Not applicable
	20	16.75	14.31	9.97	10.23	Not applicable
	40	13.22	12.01	9.42	11.23	Not applicable
	60	10.92	10.36	8.99	12.22	Not applicable
	80	9.54	9.31	8.69	13.03	Not applicable
	100 (Full solar)	**8.44**	**8.44**	**8.44**	**13.85**	Not applicable
32% (Co-production of $H_2$and H_2SO_4) H_2 produced by plant: 22 mol/s	0	38.92	24.51	12.81	8.82	8.04
	20	22.63	17.57	11.50	9.56	8.78
	40	17.06	14.50	10.89	10.46	9.68
	60	14.03	12.60	10.46	11.24	10.45
	80	11.67	10.97	10.06	12.11	11.32
	100 (Full solar)	10.33	9.99	9.81	12.76	11.98

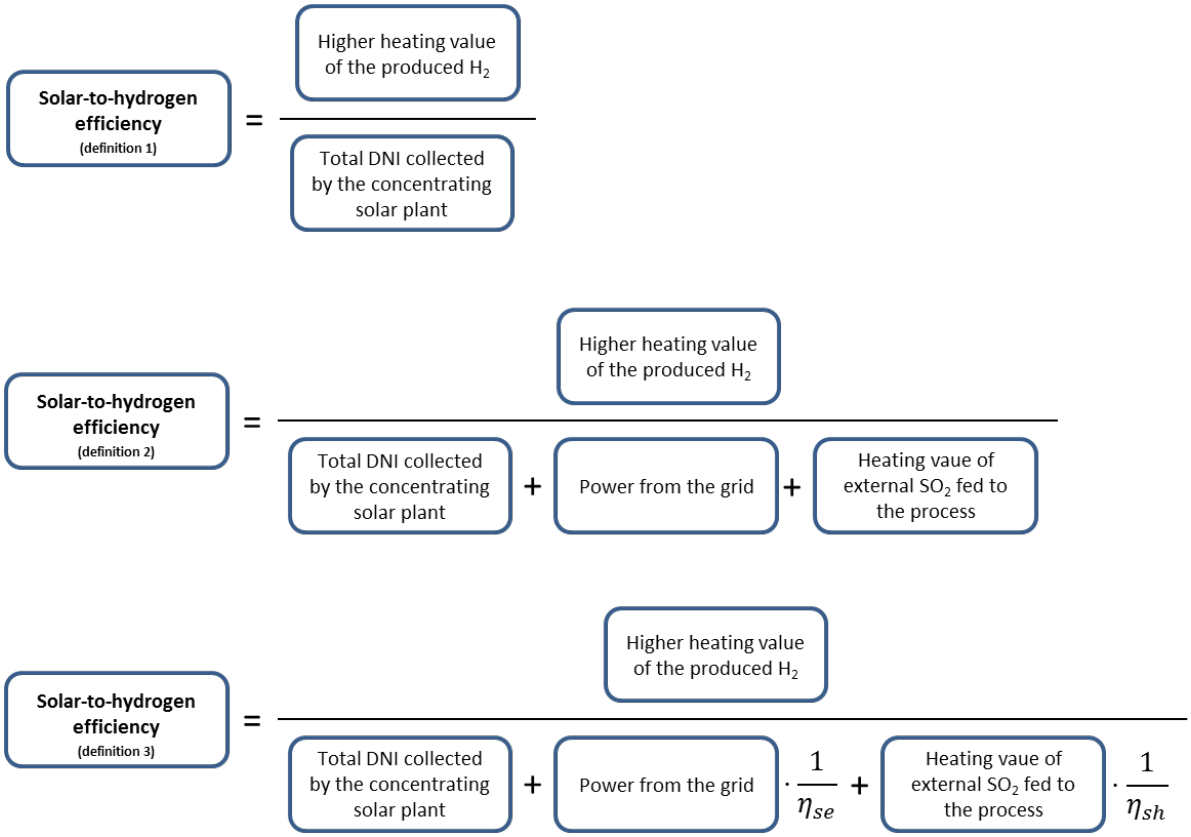

Figure 13.3: *Three different definitions for the Solar-to-hydrogen efficiency. In all definitions collected DNI stands for Direct Normal Irradiance. In definition 3, solar-to-heat (η_{se}) and solar-to-electricity (η_{sh}) conversion efficiencies were introduced in order to obtain a "solar equivalent" of other energy forms fed to the process. The values considered are η_{se}=0.25 and η_{sh}= 0.65, based on the peak performance of a concentrating solar thermal plant; however, these values are somewhat arbitrary and the meaningfulness of this third definition may be argued.*

capacity. The results are reported in Table 13.6 . It can be seen that doubling the plant capacities entails a reduction in hydrogen production costs ranging from 3.5% to 14%, with a price for 100% renewable hydrogen 12.53 €/kg. Obviously for the scenarios where co-production of H_2 and H_2SO_4 has been envisaged (OC=32%), the hydrogen production cost is reduced if revenues coming from SA sales are accounted for.

Table 13.6: *Effect of solar power share on Solar-to-hydrogen efficiency and hydrogen cost. Higher plant capacity.*

Cycle opening %	Solar power share, %	Solar-to-hydrogen efficiency, %			H_2 Cost, €/kgH_2	
		1	2	3	Without acid sales	With acid sales
0% (Production of hydrogen only) H_2 producing by plant: 30 mol/s	0	25.92	19.32	10.95	8.94	Not applicable
	20	17.53	14.87	10.22	9.37	Not applicable
	40	13.95	12.61	9.78	10.24	Not applicable
	60	11.77	11.09	9.46	11.02	Not applicable
	80	10.18	9.91	9.19	11.79	Not applicable
	100 (Full solar)	**8.99**	**8.99**	**8.99**	**12.53**	Not applicable
32% (Co-production of $H_2$and H_2SO_4) H_2 producing by plant: 44 mol/s	0	39.83	24.93	12.96	8.49	7.68
	20	23.60	18.15	11.76	8.97	8.18
	40	18.18	15.28	11.29	9.72	8.93
	60	14.78	13.22	10.93	10.45	9.67
	80	12.60	11.76	10.65	11.13	10.34
	100 (Full solar)	11.01	10.62	10.42	11.78	10.99

Comparison with other Thermochemical cycles

In order to evaluate the perfomance of Solar-HyS Cycle studied in the present work, a comparison in terms of process efficiency and H_2 production cost with other solar-thermochemical cycles analyzed in literature has been carried out.

Particularly, the performances of the following four thermochemical cycles have been considered: the ZnO/Zn, Fe_3O_4/FeO and Fe_2O_3/Fe_3O_4 cycles which were assessed by Charvin et al. [2008] and the Sulfur-Iodine cycle instead analyzed by Liberatore et al. [2012].

For all of these thermochemical cycles (powered by concentrated solar energy) both a process analysis and an economical assessment have been carried out by authors, exactly as been done for the HyS cycle in the present work.

It is worth recalled that the value of thermochemical efficiency estimated for the Solar HyS process which represents, in addition to H_2 production cost, the parmeter to be compared is equal to 19% (considering in the computation the LHV and not HHV of H_2). As regard to H_2 production cost, the reference value to bear in mind for a plant capacity of 30 mol/s of H_2 (about 216 kg/h or 5.2 ton/d) ranges from 8.94 to 12.53 €/kg H_2, according to the value of solar power share in the process: the upper end of range corrisponds to a fully "Solar" H_2 production with all electrical power (and not only the thermal one) needed for the process supplied by concentrating solar plant (integrated to a power block). The best price of H_2 calculated for the solar HyS cycle in the present work, i.e. 8 €/kg H_2, is not considered as reference value for the comparison since it corresponds to an optimal scenario of analysis where the cycle is partially open and not completly closed like in the configurations envisaged by... and.. for the other thermochemical cycles considered.

The ZnO/Zn, Fe_3O_4/FeO and Fe_2O_3/Fe_3O_4 cycles (Appendix B) belong to family of metal oxide-based thermochemical cycles and were chosen as objects of analysis by Charvin et al. [2008] for the large amount of available data on the reactions involved, their level of development and chiefly because

the 2 and 3 step metal oxide cycles are the most attractive thermochemical cycles for high efficiency hydrogen production. Generally for each of these cycles, high temperatures are required for the endothermic reaction involved in the processes and these temperatures can be provided by concentrated solar energy. Hence, the objectives of the authors were to carry out the process analysis and an economic assessment for hydrogen production from two step and three step thermochemical cycles driven by concentrated solar energy.

The process analysis for each cycle started by mass and energy balances for a hydrogen production of 1 mol/s. Then, improvements were assumed for the most energy consuming steps of process by providing inner energy recoveries. Finally a simple flow sheet was realized and on the basis on it evaluating the process efficiency was possible. Particularly, the thermochemical cycle efficiencies resulted for ZnO/Zn, Fe_3O_4/FeO, Fe_2O_3/Fe_3O_4 were respectively about 43, 35 and 36 % (considering in the computation the HHV of H_2).

Furthermore, coupling of the thermochemical process with a solar tower plant providing concentrated solar energy was considered to scale up the system and carry out the economical assessment.

The cost evaluation was conducted from a spreadsheet edited by DOE (Department of Energy, USA) by assuming two different scales of solar tower corresponding to hydrogen productions of 50 kg/h and 250 kg/h and as location for the plant installation Seville.

The analysis of Charvin et al. [2008] was based on a 40 year life time plant (against 30 years set up for solar HyS cycle) with a start up fixed in 2030. Because of important investment costs for solar concentrating systems, the most important assumption was the internal rate of return, set up in this work equal to 10% (against 8% set up for solar HyS cycle). A price of 150 \$/m^2 was used for heliostats (against 210 €/m^2 set up for solar HyS cycle) and 1 \$/m^2 for land (against 2.5 €/m^2 set up for solar HyS cycle) .

Based on these and other assumptions, the total cost of hydrogen produced by the ZnO/Zn thermochemical cycle coupled with a solar tower ranged from 7.98 \$/kg to 14.75 \$/kg H_2 for 250 kg/h and 50 kg/h H_2 capacities, respectively.

Finally, for the three step Fe_2O_3/Fe_3O_4 cycle the H_2 production cost resulting was of 8.4 \$/kg, considering a plant capacity of 250 kg/h.

Comparing the results of Charvin et al. [2008]'analysis with those obtained for the HyS cycle, can be seen that the thermochemical efficiencies shown by the 2 and 3 step metal oxide cycles were quite higher than that of Hybrid-Sulfur one. This because in the HyS cycle envisaged in the present work, a great weight on the global energy balance is assumed by the power required to operate the SDE in the design condition (to see Chapter 7). This

also affects the final cost of H_2. However it is worth noting that the cost evaluation depends heavily by economical assumptions made and particularly by plant capacity considered, and so when there are differences of this kind between two economical assessments (like in this case) the comparison is not very rightful. Furthermore, the metal oxide cycles are processes operationally more complex than HyS cycle .

As anticipated above, for the comparison also the Sulfur-Iodine cycle has been considered. This thermochemical cycle (Appendix B.0.3) , which belongs to Sulfur-based cycles like the HyS one, is widely considered one of the most promising thermochemical processes and it has been studied by several important research groups in the world.

Particularly, Liberatore et al. [2012] provided an energy assessment and a preliminary design of an industrial plant for the production of 100 tons/day of hydrogen by sulfur-iodine thermochemical cycle. The authors started from analysis of each section in order to define a final flow sheet on the basis of which the process efficiency was estimated. The thermochemical efficiency resulting for a chemical plant configuration where the maximum internal thermal recovery was realized was of about 18.5% (considering in the computation the LHV of H_2)

Afterwards, an economic analysis was performed to assess the hydrogen production cost, with the assumption to power the process by solar energy. For this purpose, since the energy requirements are at two temperature levels (1123 K and under 773 K), the adoption of an integrated solar plant which applied two solar collection technologies was hypothesized by authors exactly like has been done for the HyS cycle in the present work. Hence, a central tower was envisaged to supply the mean temperature duties and produce the electrical energy, while a parabolic trough plant was considered for the higher temperature duties; Sicily (Italy) was selected as hypothetical site for the plant installation. In addition, a backup furnace, using fossil fuel, was integrated to ensure the plant work also in the long low irradiation periods.

Starting from the solar plant capacities, thermal and electrical energy cost have been assessed considering a lifetime of 30 years and a discount rate of 5%. A lot of other assumptions were necessary, between them: the cost of the land was supposed equal to 2 €/m^2 , the active solar field (mirror surface) cost was assumed equal to 140 €/m^2, for the salts a prize of 0.57 €/kg (against 0.9 €/kg set up for solar HyS cycle) was considered and finally the cost for the electrical energy production by power block was set equal to 700 €/kWh_e (against 850 €/kWh_e set up for solar HyS cycle).

In order to evaluate the chemical plant cost, the price of each equipment provided was assessed as if it was built of carbon steel and at room pressure; then the obtained value was multiplied by some corrective factors taking

into account the right material and pressure, like has been done within the assessment of Solar-HyS cycle. The annuity of the chemical plant cost was assessed, imposing a lifetime of 30 years (equal to value set up for solar HyS cycle) and a discount rate of 5% (against 8% set up for solar HyS cycle).

The final hydrogen cost derived by assessement was about 8.7 €/kg.

In this case, comparing the results of Liberatore et al. [2012]' analysis with those obtained for the HyS cycle, can be seen that the thermochemical efficiencies of the two cycles are similar with a slightly better value for the HyS cycle. As regard to H_2 cost, the value estimated for the Sulfur-Iodine cycle seems to be more convinient than that calculated for the HyS cycle considering a share of renewable energy employed in the process of 80%, i.e. 11.79 €/kg ; this value can be considered as the reference because for the economical assessement of S-I cycle the authors considered an energy backup by fossil fuel equal to 20% of the whole request in the process. However, is worth noting that many economical assumptions done for the analysis of Hybrid-Suldur process are more conservative than those considered for the Sulfur-Iodine one. Furthermore, Liberatore et al. [2012] based their work on a plant capacity of 100 ton/d of H_2, much higher than that set up for the hybrid thermochemical cycle, i.e. 5.2 ton/d, and this obviously affect the cost evaluation.

On the basis of all that has been above, the performance of Solar-HyS thermochemical cycle can be considered quite satisfactory: even if these seems to be worse than those shown by some metal oxide-based cycles, which however present operating issues, they are definitely comparable with those of other Sulfur-based cycles and are in line with the current target set by the Fuel Cells and Hydrogen Joint Undertaking (FCH-JU) for the hydrogen production by high temperature water splitting at year 2017, i.e. 10 €/kg. Furthermore, as has been shown in previous chapter the H_2 cost by HyS cycle can be further decreased by envisaging specific configurations (partially opened cycle, integration of sulfur burning and photovoltaic thecnologies,..).

Conclusions

The present work has been developed within the framework of European project SOL2HY2, whose ENEA was a partner, and concerned the study of Hybrid-Sulfur cycle powered by Concentrated Solar Energy.

After a preliminary study of HyS cycle, the activity has focused specifically on the theoretical and experimental assessment of a crucial step of this cycle, i.e. the high-temperature sulfuric acid decomposition. In this context, the choice and development of the catalyst for the SO_3 decomposition reaction has represented a fundamental part of the work. The choice of the catalyst has taken into account the features required for the use in a high temperature adiabatic reactor subjected to daily thermal cycles, as expected for the specific application considered. In comparison with other catalysts suggested in the literature, Fe_2O_3 supported by $\gamma - Al_2O_3$ pellets has exhibited, in the operating conditions of interest, better or similar performance in terms of stability and activity with a greater cost-effectiveness, lower toxicity and the guarantee of easier and cheaper large-scale production. More specifically, the catalyst was tested in a laboratory reactor under realistic operating conditions (temperature 925-1000 °C, pressure 1-3 atm, WHSVs 22-33 h^{-1} and feed sulfuric acid concentration 50 % w/w). The catalyst showed a notable catalytic activity (about 70% at 1000°C), and a good stability over a total of more than 100 hours on stream, even including several stand-by phases in which the catalyst was subjected to thermal cycling from operating to room temperature.

The results obtained have been processed to analyze the reaction kinetics. Particularly, in order to determine the kinetic parameters of the reaction, a simple reactor model was used and the reaction rate was evaluated by assuming the SO_3 decomposition as an elementary equilibrium reaction, which led to a calculated activation energy of about 148 kJ/mol. The catalyst developed can be used as-is in a prototype or full scale reactor in the same range of operating conditions explored in the experimental campaign; therefore, the kinetic expression obtained can be used to design and predict the performance of an actual SO_3 decomposition reactor. Indeed, such expression

was used by DLR to design the demo SO_3 decomposition reactor developed within the SOL2HY2 project.

Moreover, the catalyst production procedure was upscaled in order to provide all the catalyst used in the demo reactor (about 20 kg); in so doing, the procedure has been carefully adjusted to ensure a good support coating, and therefore catalytic activity, without being costly and time expensive in case of larger-scale production.

The PhD project also involved active participation (for a period of three months) to the latest phases of the installation demo plant in DLR's solar tower in Juelich, Germany. During this period, some preliminary on-sun tests were also performed in cooperation with DLR's staff. Such tests were aimed at the thermal characterization of the solar receiver-reactor system for sulfuric acid decomposition and were carried out without catalyst in the system. The obtained results were crucial to identify issues in the original plant configuration and were used to suggested modifications to the plant layout, which were implemented by DLR in a subsequent experimental stage.

The second part of the PhD work has been focused on the process analysis and techno-economic assessment of the Solar-powered Hybrid-Sulfur cycle. In this context, the HyS process was studied block-wise in order to identify the best process options for each part of the plant. AspenPlus flowsheets where developed for all process blocks and used to simulate the plant operation in order to determine the energy required for hydrogen production. The total energy consumption of the proposed process is 870 kJ/mol of produced hydrogen, corresponding to an efficiency in excess of 32% (HHV). In particular, three energy types are required by the process: power (42%), high-temperature heat (23%) and medium-temperature heat (35%), which gives a thermochemical efficiency in excess of 19%.

Furthermore, the sizing and costing of main equipment employed in the process has been carried out in order to allow the final economical evaluation of process. Different options for the integration the HyS plant with CST systems have been identified. The possibility to integrate other energy sources, such as heat obtained through sulfur burning and PV thecnologies, has also been considered.

The economic performance of the solar HyS plant was assessed in several scenarios including different plant locations and combinations of (renewable and conventional) energy sources. Plant capacities in the range of 2.6 to 7.6 t/d of hydrogen were considered. Hydrogen production costs in the range 8 €/kg and about 13 €/kg have been found, with the highest values corresponding to 100% renewable hydrogen. The lowest prices are obtained with the synergistic use of PV, heat from sulfur burning process and CST tech-

nology, which leads to promising performance of the SOL2HY2 cycle for the green hydrogen production. The costs obtained are still high compared to conventional hydrogen production processes like methane steam reforming, but are in line with the current targets set by the Fuel Cells and Hydrogen Joint Undertaking (FCH-JU) for the hydrogen production by high temperature water splitting. Furthermore the cost analysis carried out is based on some conservative hypoteses. Firstly, valorization of oxygen co-produced with hydrogen is not considered. Furhtermore, SO_2 and S from external sources required in some process configurations are assumed to be bought at market prices, while for some plant locations such chemicals could be available at a much lower or even at no cost.

Appendix A

The thermodynamics of high temperature section

A.1 Thermodynamic properties of pure compounds

The components in the sulfuric section of the plant are H_2O, H_2SO_4, O_2, SO_2 and SO_3.

A.1.1 Specific heat

Three sources [N.I.S.T, 2011, Sandler, 2005, Poling et al., 2007] have been selected from literature to evaluate the cp of pure compounds. In Table A.1 are reported the thermodynamic properties of pure compounds; the parameters a, b,c, d ,e and f appear in the cp expression:

$$c_p = a + bT + cT^2 + dT^3 + e\frac{1}{T^2} + fT^4 \ \ [^{kJ}/_{(\mathrm{mol\,K})}] \tag{A.1}$$

The figures A.1,A.2,A.3,A.4 andA.5 show comparisons between data resulted from the different references.

From the graphs it is noted that the data are generally in agreement: the exceptions are represented by the specific heat of the SO_2 supplied by Poling et al. [2007] and that of the SO_3 supplied by Sandler [2005]. For this study the data of N.I.S.T [2011] have been used as reference.

A.1.2 The vapor pressure of sulfuric acid

The analysis on the vapor pressure of sulfuric acid has been performed, and the curves provided by the AspenPlus simulator were compared with those

Table A.1: *Thermodynamic properties of pure compounds*

Compound	Reference*	$\triangle G_0$	$\triangle H_0$	a	$b \cdot 10^2$	$c \cdot 10^5$	$d \cdot 10^9$	e	$f \cdot 10^{11}$	T_{min}	T_{max}
		$[^{kJ}/_{\mathrm{mol}}]$	$[^{kJ}/_{\mathrm{mol}}]$							K	K
H_2O	1	-228.75	-241.83	30.092	0.6832	0.6793	-2.5345	82139	0	298	1200
	2	-228.6	-241.8	32.218	0.192	1.055	-3.593	0	0	273	1800
	3	-	-	4.395	-0.4186	1.405	-15.64	0	0.632	50	100
O_2	1	0	0	31.322	-2.024	5.787	-36.506	-7374	0	100	700
	1	0	0	30.032	0.8773	-0.3988	0.7883	-741599	0	700	2000
	2	0	0	25.46	1.519	-0.715	1.311	0	0	273	1800
	3	-	-	3.63	-0.179	0.658	-6.01	0	0.179	50	1000
SO_2	1	-300.03	-296.84	21.430	7.4351	-5.7752	16.3554	86731	0	298	1200
	2	-300.2	-296.8	25.762	5.791	-3.809	8.607	0	0	273	1800
	3	-	-	4.417	-0.2234	2.344	-32.71	0	1.393	50	1000
SO_3	1	-486.67	-395.77	24.025	11.9461	-9.4387	26.9624	-117517	0	298	1200
	2	-371.1	-395.7	16.393	14.573	-11.193	32.402	0	0	273	1300
	3	-	-	3.426	0.6479	1.691	-33.56	0	1.590	50	1000
$H_2SO_{4(g)}$	1	-653.41	-735.13	47.289	19.0331	-14.8129	43.866	-740016	0	298	1200
*1 = N.I.S.T [2011], 2 = Sandler [2005] and 3 = Poling et al. [2007]											

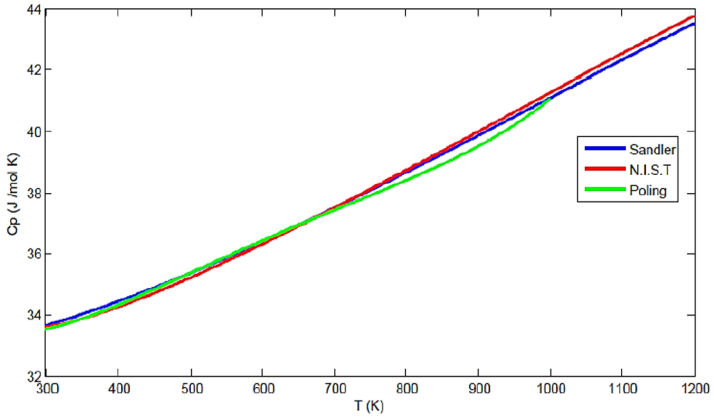

Figure A.1: *Specific heat of* H_2O *vs temperature according to different references*

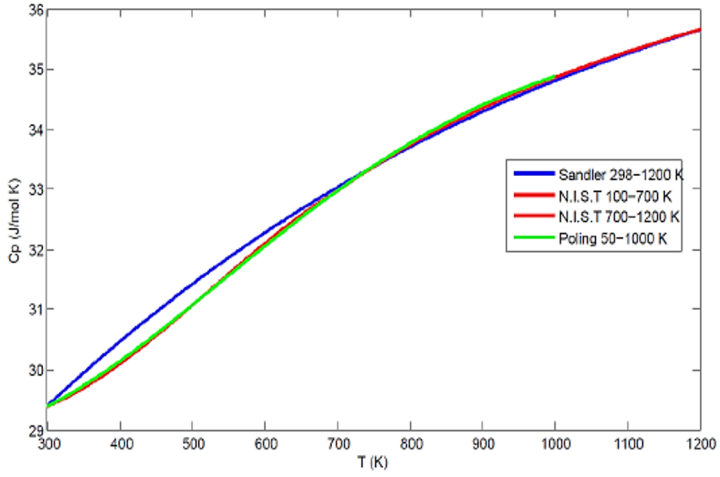

Figure A.2: *Specific heat of* O_2 *vs temperature according to different references*

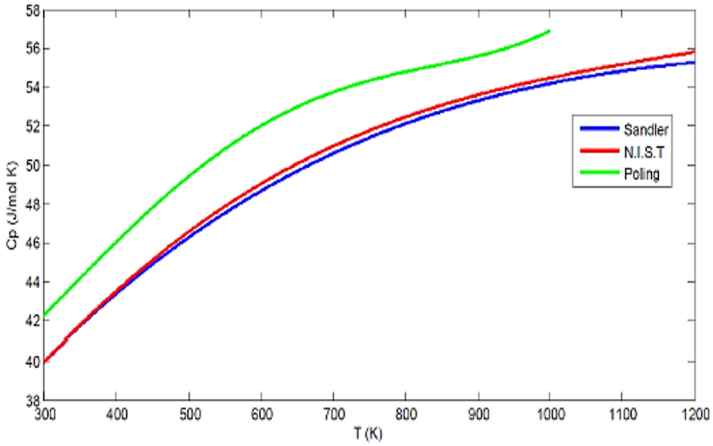

Figure A.3: *Specific heat of* SO_2 *vs temperature according to different references*

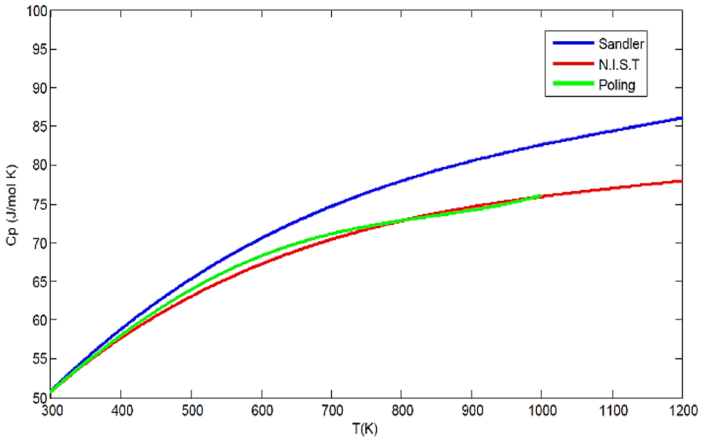

Figure A.4: *Specific heat of* SO_3 *vs temperature according to different references*

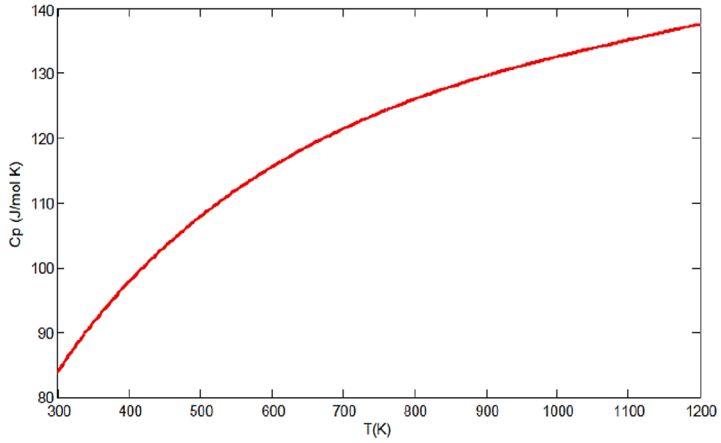

Figure A.5: *Specific heat of* H_2SO_4 *vs temperature according to N.I.S.T [2011]*

obtained from the vapor pressure expressions provided by literature:

- Aspen Plus simulator:

$$\ln p_s(T) = \left(37.6059 - \frac{11216.33992}{T} - 0.0119987T\right)$$

with p_s in bar e T in K;

- Wuster [1979]

$$\ln p_s(T) = \left(11.5836 - \frac{6678.84}{T - 56.1263}\right)$$

with p_s in bar e T in K;

- Bosen and Engels [1988]

$$\ln p_s(T) = \left(13.4515 - \frac{8107.94}{T - 9.26851}\right)$$

with p_s in bar e T in K.

The three correlations are compared in Figure A.6 and are quite consistent.

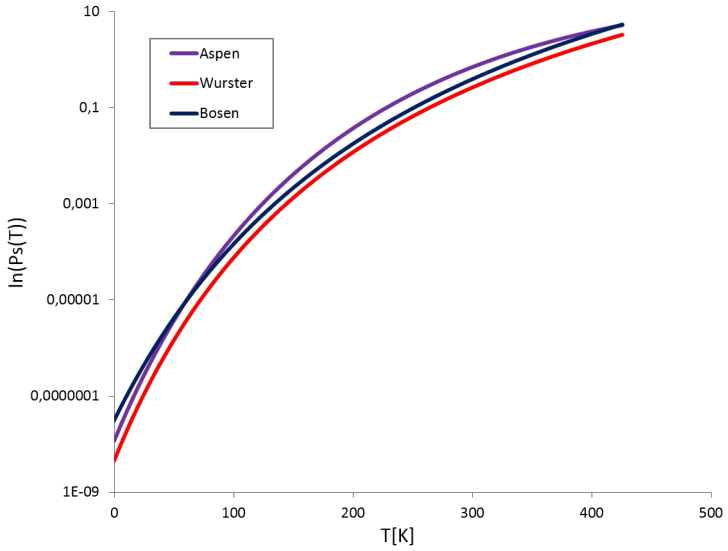

Figure A.6: *Vapour pressure of sulfuric acid*

A.2 Thermodynamic properties of mixtures

A.2.1 The $H_2SO_4 - H_2O$ system

The $H_2SO_4 - H_2O$ system has an azeotrope at 98%wt of sulfuric acid.

In the liquid phase, the following dissociations depend on the operating conditions of T, P and concentration:

$$H_2SO_4 \rightleftharpoons SO_3 + H_2O \tag{A.2}$$

$$H_2SO_4 + H_2O \rightleftharpoons HSO_4^- + H^+ \tag{A.3}$$

$$HSO_4^- + H_2O \rightleftharpoons SO_4^{-2} + H^+ \tag{A.4}$$

In the vapour phase, the following dissociation occurs:

$$H_2SO_4 \rightleftharpoons SO_3 + H_2O \tag{A.5}$$

The Reaction A.5 is increasingly shifted to the right when the temperature rises. In addition, the components will be divided into two phases based on physical equilibrium. Table A.2 reports the collected experimental data for this system.

Table A.2: *Experimental data of Boiling pressure as function of weight fraction of water, for the* $H_2SO_4 - H_2O$ *system.*

Source	T [°C]
Perry[1]	100<T<350
Gmitro[2]	T=100; T=200; T=350
Taransekov[3]	T=100
Burt[3]	140<T<350
Wurster[4]	T=25; T=500
[1]Poling et al. [2007]	
[2]Gmitro and Vermeulen [1964]	
[3]Bosen and Engels [1988]	
[4]Wuster [1979]	

Generally, the experimental data are in agreement with each other, as shown by figures A.7,A.8 and A.9. At high temperatures (T=320°C), data begin to deviate for low concentrations of sulfuric acid.

The process simulations with the related material and energy balances have been performed with Aspen Plus simulator. Among all the thermodynamic models available in the simulator library, the ElecNRTL method has been used. This model is a deviation of the classic NRTL (no random two liquid), specific for electrolytic systems; however, the thermodynamic data inside model code for the system $H_2SO_4 - H_2O$ are valid for temperatures below 300°C and for low concentrations of sulfuric acid. Hence, the ElecNRTL method uses an additional package of thermodynamic data which takes into account the strong non-ideality of system in some specific temperature and pressure ranges. For temperatures higher than 300°C, a model that considers the la electrolytic dissociation of H_2SO_4 into ion pair rather than ion, and that simulates the formation of SO_3 and H_2O at high concentrations in liquid sulfuric acid [Mathias and Brown, 2003] exists. This model employes four different chemistry on the basis of operating conditions:

- Diluted sulfuric acid :

$$H_2SO_4 + H_2O \rightleftharpoons H_3O^+ + HSO_4^-$$

$$HSO_4^- + H_2O \rightleftharpoons H_3O^+ + SO_4^{-2}$$

- Diluted sulfuric acid at high temperature:

$$H_2SO_4 + H_2O \rightleftharpoons 2IONPAIR$$

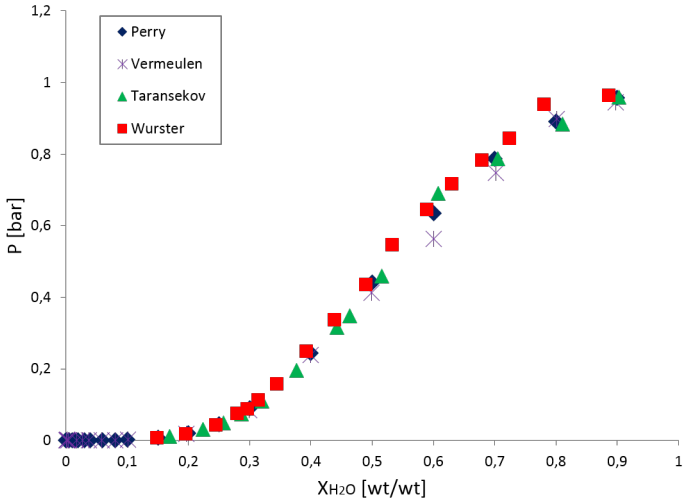

Figure A.7: *Experimental data of boiling pressure of* $H_2SO_4 - H_2O$ *system at T=100°C, by different references.*

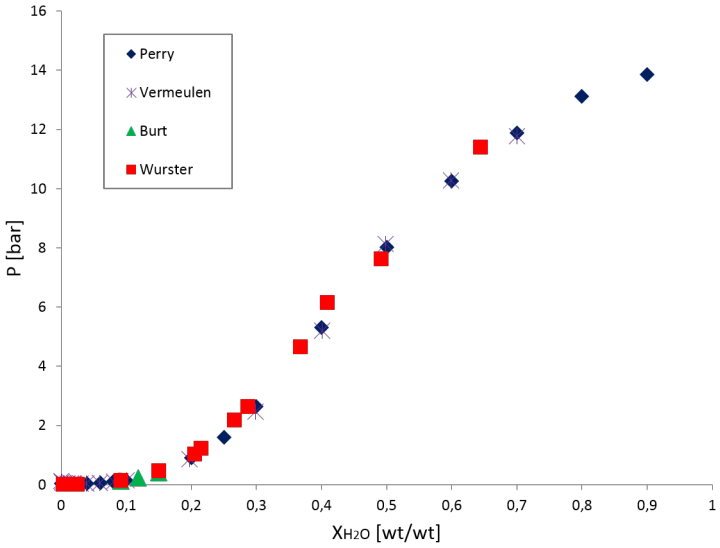

Figure A.8: *Experimental data of boiling pressure of* $H_2SO_4 - H_2O$ *system at T=200°C, by different references.*

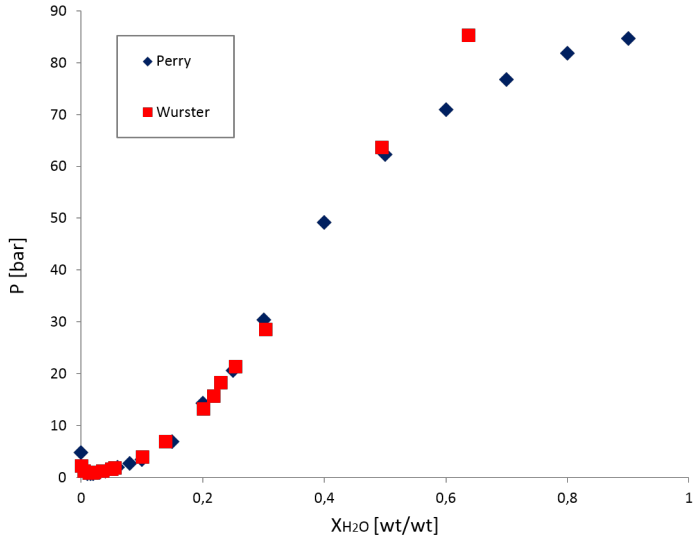

Figure A.9: *Experimental data of boiling pressure of* $H_2SO_4 - H_2O$ *system at T=320°C, by different references.*

- Concentrated sulfuric acid:

$$H_2SO_4 + H_2O \rightleftharpoons H_3O^+ + HSO_4^-$$

$$HSO_4^- + H_2O \rightleftharpoons H_3O^+ + SO_4^{-2}$$

$$SO_3 + H_2O \rightleftharpoons H_2SO_4$$

- Concentrated sulfuric acid at high temperature:

$$SO_3 + H_2O \rightleftharpoons H_2SO_4$$

$$H_2SO_4 + H_2O \rightleftharpoons 2\text{IONPAIR}$$

For the comparison of literature data and those provided by Aspen, the most suitable chemistry for temperature, pressure and composition was taken into account. The selected model follows well the experimental data found in the literature for the temperature and sulfuric acid concentration ranges considered for process in this work (Figures A.10, A.11 and A.12) . The model differs from the experimental data of Perry close to azeotropic concentration (98%wt), increasingly with temperature rising and diluted sulfuric acid solutions at high temperatures. However, the model assumed is based on the experimental data presented in Wuster [1979] and Gmitro and Vermeulen [1964]; by comparing the results it can seen that curve provided by Aspen follows very well the general trend, in the concentration range of interest.

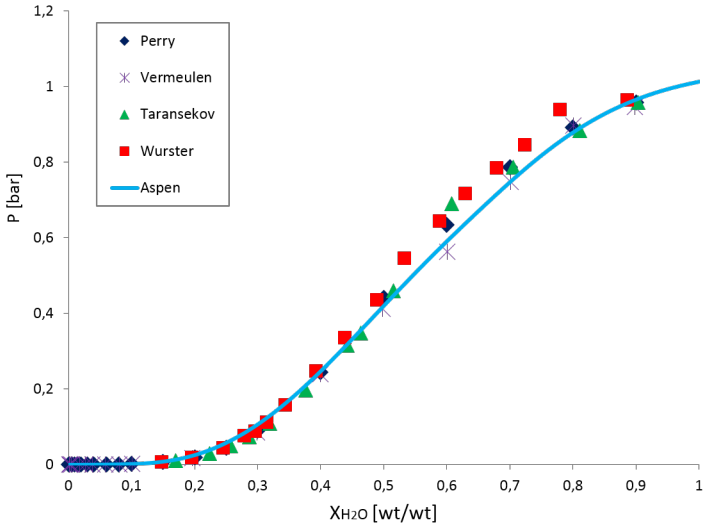

Figure A.10: *Comparison between experimental data and results by Aspen model at 100°C.*

The model is unsuccessfu close to the azeotrope where differs from the experimental data, because it does not take into account the dissociation of the sulfuric acid in the vapor phase, and hence even the contribution of the reaction products to the total pressure which results underestimated, near the pure sulfur acid. For temperatures up to 300- 320 ° C and for concentrations up to 90-95%wt the chemistry 1 (diluted sulfuric acid) was the most suitable for interpreting experimental data and has been therefore used in this work for higher temperatures was necessary to use chemistry 2 (diluted high temperature sulfuric acid).

The ElecNRTL model is valid for the liquid phase; to describe the vapour phase, AspenPlus makes use of the Redlich-Kwong equation. In the context of the $H_2SO_4 - H_2O$ system, a comparison was also made between the curves related to mixing entalpy of mixture; for this comparison, the curves provided by Perry's Chemical Engineers' Handbook [Poling et al., 2007] were used.

A.2.2 Vapor-liquid equilibrium of the $H_2O - SO_2$ system

The SO_2 in water, can dissociate to a certain extent according to its concentration, the presence of other ions and the solution pH [Rabe and Harris, 1963, Mondal, 2007, Shaw et al., 2011]. Moreover, the dissociation affects SO_2 solubility [Krissmann et al., 1998]. The liquid-vapour equilibrium of

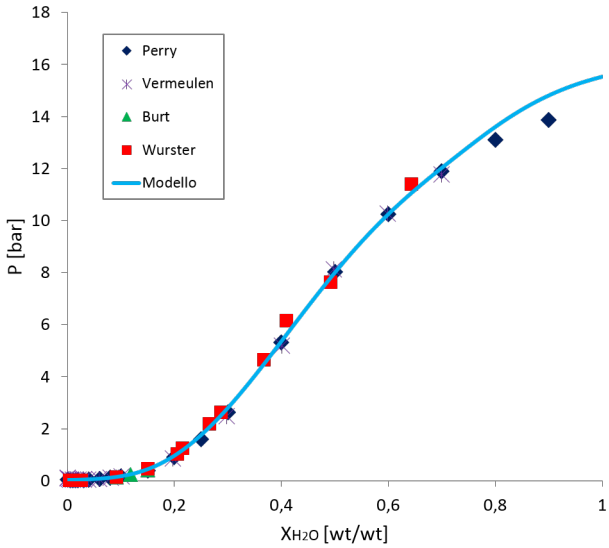

Figure A.11: *Comparison between experimental data and results by Aspen model at 200°C.*

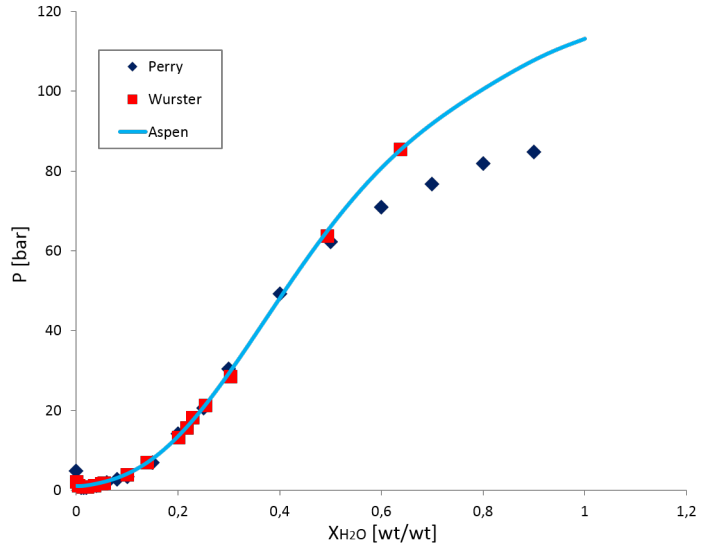

Figure A.12: *Comparison between experimental data and results by Aspen model at 320°C.*

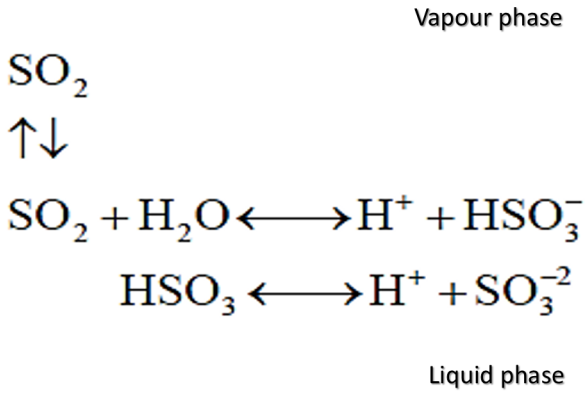

Figure A.13: *Physical and chemical equilibrium in the* $H_2O - SO_2$ *system.*

this system consists of two contributions (Figure A.13): physical equilibrium and that chemical one linked to dissociation of SO_2 in water:

$$SO_2 + H_2O \rightleftharpoons HSO_3^- + H^+$$

$$HSO_3^- \rightleftharpoons SO_3^{-2} + H^+$$

The total amount of dissolved SO_2 in terms of molality m is:

$$m = m_{SO_2} + m_{HSO_3^-} + m_{SO_3^{-2}}$$

When the outside pressure exceeds the vapour pressure, a liquid phase of SO_2 forms due to the miscibility gap of $H_2O - SO_2$ system [Maass and Maass., 1928, Shaw et al., 2011]; when the temperature rises, the SO_2 solubility decreases.

Rabe and Harris [1963] studied the vapour pressures of $SO_2 - H_2O$ solutions at temperatures between 30 and 80 ° C.

For the Henry constant they suggested the expression:

$$\ln(H) = \left(\frac{2581.1}{T} - 9.3595\right) \tag{A.6}$$

with T in K.

Mondal [2007] studied experimentally SO_2 absorption in water at temperatures in the range 293-333 K , and SO_2 pressures in the range 0.447-0.963 kPa.

For the Henry constant he suggested the expression:

$$\ln(H) = \left(\frac{3715.2}{T} + 16.765\right) \tag{A.7}$$

The experimental values of Mondal [2007] and literature up to 1 kPa are consistent with those predicted by equation A.7.

Shaw et al. [2011] studied and modeled the SO_2 solubility in water at temperatures in the range 25-40 °C, and SO_2 pressures in the range 0.2-3.6 atm. They compared the values resulting from their model both with their experimental results and with those of previous experimental works. The model is in line with experimental results at 40 °C, expecially at pressures lower than 3 atm, but at 25 ° C it is not consistent with the experimental data already at 1.5 atm. The authors suggested that this deviation at 25 °C could result from the formation of a second liquid phase not provided by the model, or that the model was not able to properly estimate molecular interactions at high pressures. At pressures above 1-1.5 atm, there were very few experimental data available in literature, particularly at 25 °C.

By the works of Rabe and Harris [1963], Mondal [2007], Shaw et al. [2011], it may be concluded that a linear model such as Henry's law well predicts the solubility of SO_2 at pressures below 1-1.5 atm.

The experimental data collected by Shaw et al. [2011] and the trend obtained with the AspenPlus model have been compared (Figure A.14) and are fairly consistent.

At low pressures, the AspenPlus model is consistent with the experimental data of Rabe and Harris [1963] in all the temperature range (30-80°C) .

At high pressures, the data by Rumpf and Maurer [1992] were used as references, because the authors studied the SO_2 solubility in water at pressures up to 2.5 MPa in the temperature range 293.15-413.15 K. Rumpf and Maurer report that unmixing of two liquid phases does not occur in this operating condition range. The experimental data are in line with Aspen Plus predictions (Figure A.16) .

Rumpf and Maurer [1992] distinguish the Sulfur dioxide solubility in *true* and *overall* values. "Overall" values are the experimental ones and refer to the total amount of SO_2 dissolved, both in molecular and ionized forms. "True" values are calculated and refer to molecular SO_2 only. It should be emphasized that AspenPlus calculations for the $SO_2 - H_2O$ system have been performed by using the NRTL model without taking into account SO_2 dissociation; despite this, the model follows the experimental data satisfactorily. The Henry costant adopted for this system in AspenPlus is given by expression:

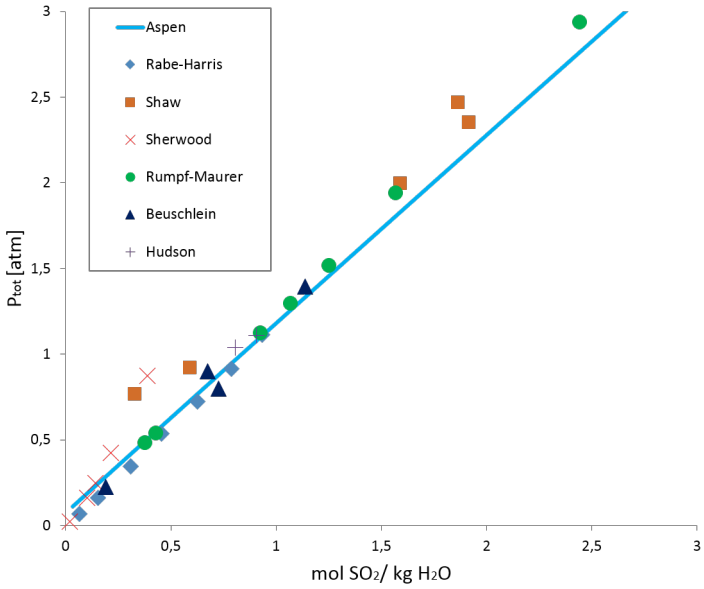

Figure A.14: *Comparison between the experimental data collected in the Shaw et al. [2011] work and those resulted by Aspen model.*

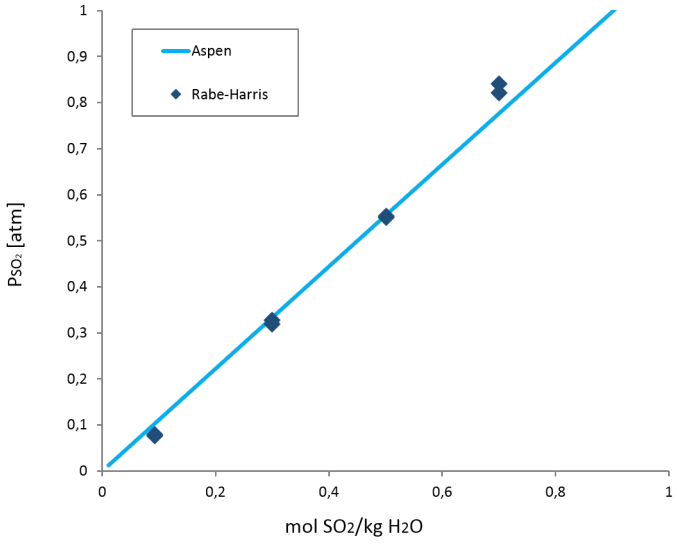

Figure A.15: *Comparison between the experimental data provided by Rabe and Harris [1963] and those resulted by Aspen model.*

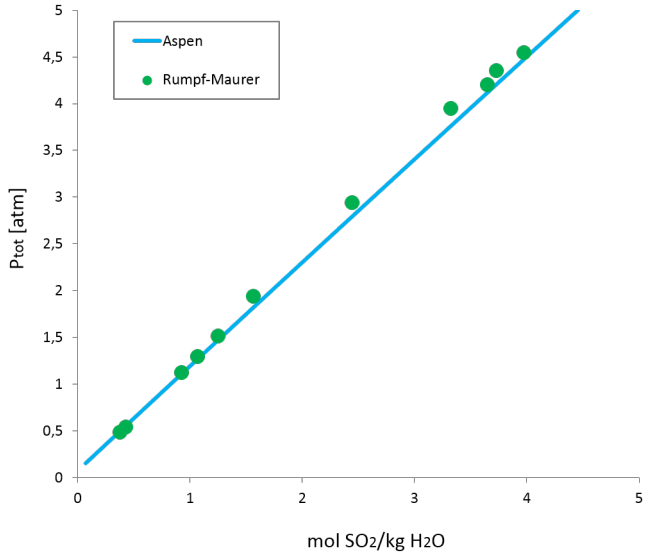

Figure A.16: *Comparison between the experimental data provided by Rumpf and Maurer [1992] and those resulted by Aspen model.*

$$\ln(H) = \left(26.5647 + \frac{2872.96}{T} - 0.30288\ \ln(T)\right)$$

with T in K and H in $\mathrm{N\,m^{-2}}$.

A.2.3 Liquid-liquid equilibrium of the $H_2O - SO_2$ system

The $H_2O - SO_2$ system presents a miscibility gap. For the assessment of this system, the works of Maass and Maass. [1928], Hanson and Butcher [1957] (Table A.3) and Spall [1963] have been taked in account and by using their experimental data (Table A.4), the parameters for the NRTL model have been calculated.

In the tables A.3 and A.4 the superscript "a" represents the aqueous phase and the superscript "b" represents the sulfur phase, while the subscript "1" refers to the H_2O component and the subscript "2" to theSO_2 component.

By setting :

$$\alpha = 0.2$$

$$\tau_{12} = A_{12} + \frac{B_{12}}{T}$$

Table A.3: *Experimental data for the mixture* $H_2O - SO_2$ *in liquid-liquid equilibrium.*

T(°C)	P(atm)	x_1^a	x_2^a	x_1^b	x_2^b
10	2.19	0.916	0.084		
16	2.69	0.915	0.085		
16.5	2.76	0.915	0.085		
18	2.89	0.914	0.086	0.136	0.864
22	3.34	0.913	0.087		
27	3.91	0.913	0.087		
29.7	4.14	0.911	0.089		
42.9	5.49	0.907	0.093		
50.5	6.26	0.904	0.096		
65	7.75	0.9	0.010		

Table A.4: *Experimental data for the mixture* $H_2O - SO_2$ *in liquid-liquid-vapour equilibrium.*

T(°C)	P(atm)	x_1^a	x_2^a	x_1^b	x_2^b	y_1	y_2
58	10	0.911	0.089	0.163	0.837	0.006	0.994
95	25	0.85	0.15	0.3	0.696	0.028	0.972

$$\tau_{21} = A_{21} + \frac{B_{21}}{T}$$

and by fitting the data, the following results have been obtained for the NRTL model:

$$A_{12} = 2.5917$$

$$A_{21} = -1.9747$$

$$B_{12} = -209.698$$

$$B_{21} = 999.935$$

from which the miscibility gap in Figure A.17 results.

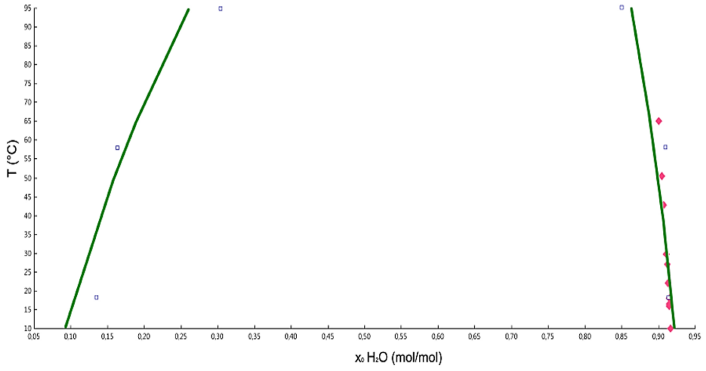

Figure A.17: *Miscibility gap of* $H_2O - SO_2$ *system in the liquid state.*

A.2.4 The $H_2O - H_2SO_4 - SO_2$ system

From the literature it turns out that for the $H_2O - H_2SO_4 - SO_2$ system, when the sulfuric acid concentration in water is high, the SO_2 solubility inside mixture is mainly of a physical nature, while in less acidic solution the chemical component of solubility, linked to the reactions of hydrolysis or other reactions with any species present in the solution, is not negligible.

Hayduk et al. [1988] reported the solubility data for SO_2 in a solution at 97 %wt of sulfuric acid, in the temperature range 298.2-323.2 K and for partial pressure of SO_2 from 10 to 25 kPa. The authors concluded that the Henry law could be employed to predict solubility at 293 and 298K, but for higher temperatures there are deviations to consider. They suggested a Henry-like law, which defined the linear relationship between the molar fraction of the dissolved gas (x_p) and the partial pressure of the gas P:

$$P = H\, x_p$$

Hayduk et al. [1988] have found that SO_2 has a minimum of solubility at 85%wt of sulfuric acid, which corresponds to the equimolar concentration of sulfuric acid and water.

Govindarao and Gopalakrishna [1993] studied the $H_2O - H_2SO_4 - SO_2$ system at low concentrations of sulfuric acid (< 2.815 m), at partial pressur of SO_2 in the range 190-1575 Pa and at temperatures in the range 30-80 °C. They concluded that for acid concentration higher than 0.37 m, the Henry law is effective because SO_2 exists mainly in the molecular form; while at low concentrations the dissociation or hydrolysis reactions of SO_2 influence the solubility, which is not a linear function of SO_2 partial pressure. Regard-

ing the Henry constant dependency on temperature, the authors used the equation:

$$\ln(H) = 27.92 - \frac{3785.9}{T}$$

Govindarao and Gopalakrishna [1993] suggested that this expression for Henry law could be extended up to acid concentrations less than 37 m (78.5 %wt); at higher concentrations the Sulfur dioxide begins to dissolve and another expression that takes into account both the concentration of the acid and the temperature had to be used.

Zhang et al. [1998] studied the SO_2 solubility in sulfuric acid solution for concentration in the range 60-96 %wt, for temperatures from 298 to 393 K and partial pressure of SO_2 in the range 96-258 kPa.

The authors descovered that a modified version of Henry's law could be used to predict solubility in this concentration range. The Henry's constant heavily depended on temperature and reached its maximum value for a sulfuric acid concentration of about 79%wt. Zhang et al. [1998] concluded that the assumption of ideal these was valid under those operating temperatures and partial pressures.

On the basis of the mentioned literature, it can be concluded that Henry formulations can be used to predict the solubility of SO_2 in solutions containing sulfuric acid between 22 and 79%wt, on condition that external pressure does not exceed the SO_2 vapor pressure. At low concentrations, SO_2 dissociation improves the solubility (chemical solubility). At higher concentrations the minimum solubility is reached and moreover, the solubility increases as a function of the sulfuric acid concentration.

A.3 Thermodynamic properties of reactions

The main chemical reactions occurring in the high-temperature section of process are the H_2SO_4 decomposition (Reaction A.8) and the SO_3 decomposition (Reaction A.9).

$$H_2SO_4 \rightleftharpoons SO_3 + H_2O \tag{A.8}$$

$$SO_3 \rightleftharpoons SO_2 + {}^1/_2O_2 \tag{A.9}$$

The thermodynamic properties of such reactions were obtained from enthalpy and free energy of formation of pure components involved in the reaction at standard conditions.

The change of the reaction enthalpy with temperature was determind by the Kirchoff's law:

Table A.5: *Thermodynamic properties of reactions*

Reaction	Reference*	$\triangle G_0^{rx}$	$\triangle H_0^{rx}$	$\triangle a$	$\triangle b \cdot 10^2$	$\triangle c \cdot 10^5$	$\triangle d \cdot 10^9$	$\triangle e$	$\triangle f \cdot 10^{11}$
		$[kJ/\text{mol}]$	$[kJ/\text{mol}]$						
Reaction 3.3	1	-62.01	97.53	6.8278	-6.4038	6.0536	-19.4384	704638	0
	2	53.71	97.63	1.3217	-4.2681	4.675	-15.0573	740016	0
Reaction 3.4	1	186.64	98.93	13.0666	-5.5227	6.5568	-28.8601	200561	0
	1	186.64	98.93	12.4216	-4.0723	3.4641	-10.2129	-166551.5	0
	2	70.9	98.9	22.099	-8.0225	7.0265	-23.1395	0	0
*1 = N.I.S.T [2011] and 2 = Sandler [2005]									

$$\Delta H^{rx}(T) = \Delta H_0^{rx} + \int_{298.15}^{T} \Delta c_p \mathrm{d}T \tag{A.10}$$

The Δc_p in the Kirchoff's expression is calculated according to the following expression:

$$\Delta c_p = \Delta a + \Delta bT + \Delta cT^2 + \Delta dT^3 + \Delta e\frac{1}{T^2} + \Delta fT^4 \ \ [kJ/(\text{mol K})] \tag{A.11}$$

and the parameters a, b, c, d, e and f are listed in Table A.5 with ΔH_0^{rx}, wich is also appears into expression A.10.

The trend of equilibrium constant with temperature was obtained by integration of van't Hoff isobar:

$$\ln K(T) = \ln K(298.15) + \int_{298.15}^{T} \frac{\Delta H^{rx}}{RT^2}\mathrm{d}T$$

The value of K at T =289K is given from expression :

$$K(T) = \exp \frac{-\triangle G_0^{rx}}{RT}$$

and $\triangle G_0^{rx}$ is reported in Table A.5.

Appendix B

Thermochemical cycles considered for the comparison

B.0.1 ZnO/Zn cycle

The reactions characterising of ZnO/Zn cycle are the following:

$$Zn + H_2O_{(g)} \rightarrow ZnO + H_2 \tag{B.1}$$

$$ZnO \rightarrow Zn_{(g)} + {}^1/_2O_{2\,(g)} \tag{B.2}$$

The H_2 is produced by the Hydrolysis of Zinc (Reaction B.1) together with the ZnO, which can be reduced at high temperature, 2000 K, to form Oxygen and Zn to recycle in the process (Reaction B.2) .

Unfortunately, a cooling of gas products (600-2000 K) of Reaction promotes the reverse reaction of Zinc oxide reduction which can occur giving back ZnO as shown by Reaction B.3:

$$Zn_{(s)} + {}^1/_2O_{2(g)} \rightarrow ZnO \tag{B.3}$$

.

Hence, a quenching device must be connected to the reactor outlet where Reaction B.2 occurs in order to reduce the recombination (negligible below 600 K) and to limit the formation of ZnO. The average recombination rate measured in a rotating solar reactor was about 39% [Mu¨ller R, Schunk L, Meier A, Steinfeld A. Solar thermal dissociation of zinc oxide in a directly-irradiated rotary reactor. Proceedings of 13th SolarPACES Symposium, Ref. B2-S9, 2006, Seville, Spain.].

Furthermore, the Reaction B.1 is not complete due to the formation of a layer of ZnO at the surface of the particles, which blocks the diffusion of steam

into the core of the particles and stops the reaction. In literture, the highest conversion rate was obtained when Zinc was vaporized at 1023 K, condensed as nanoparticles and then hydrolyzed [Wegner K, Ly HC, Weiss RJ, Pratsinis SE, Steinfeld A. In situ formation and hydrolysis of Zn nanoparticles for H2 production by the 2-step water-splitting thermochemical cycle. Int J Hydro Energy 2006;31:55–61]. With such a process, a complete hydrolysis can be assumed.

B.0.2 Iron oxide cycles

The reactions characterising the Fe_3O_4/FeO cycle are the following :

$$3FeO + H_2O_{(g)} \rightarrow Fe_3O_4 + H_2 \tag{B.4}$$

$$Fe_3O_4 \rightarrow 3FeO + {}^1/_2O_2 \tag{B.5}$$

Similarly to ZnO/Zn cycle, a passivation phenomenon is encountered during FeO hydrolysis (Reaction B.4) due to the formation of an oxide layer. Thus, the chemical conversion of direct hydrolysis is limited to 75% at 850 K[Charvin P, Abanades S, Flamant G, Lemort F. Two step watersplitting thermochemical cycle based on iron oxide redox pair for solar hydrogen production. Energy 2007;32:1124–33.].

However, unlike the ZnO/Zn cycle, this cycle and in general the iron oxide cycles are "non volatile" cycles because the reduced oxide remains in a condensed state. Thus, the chemical equilibrium of Reaction B.5 is displaced toward FeO formation until complete reduction at about 1900 K.

Furthermore, in this cycle the recombination reaction of oxide (i.e. the reverse reaction of Reaction B.5) it is not favoured like in the ZnO/Zn cycle because the Oxygen can be easly swept out of the reactor where reaction 2 occurs, by injecteing a continuous flow of inert gas which separates the gas phase from the solid phase produced.

Concerning the Fe_2O_3/Fe_3O_4 three step cycle, the reactions characterising are:

$$Fe_3O_4 + 2KHO \rightarrow 2KFeO_2 + H_2 \tag{B.6}$$

$$2KFeO_2 + H_2O \rightarrow Fe_2O_3 + 2KOH \tag{B.7}$$

$$3Fe_2O_3 \rightarrow 2Fe_3O_4 + {}^1/_2O_2 \tag{B.8}$$

The Fe_3O_4 hydrolysis is possible when using a better oxidizing compound than water. The reaction between Fe_3O_4 and melted sodium or potassium hydroxide generates hydrogen and a mixed oxide (Reaction B.6 which occurs at 673 K). This mixed oxide is reactive at low temperature (373 K) with water like shown in the Reaction B.7. These two reactions can be generally assumed complete.

The hematite (Fe_2O_3) reduction into magnetite (Fe_3O_4), i.e. the Reaction B.8, can be considered complete at 1600 K for the same reasons why the Reaction B.5of Fe_3O_4/FeO cycle is complete.

B.0.3 The sulfur-iodine thermochemical cycle

The S-I cycle is based on three main reactions carried out at three different temperature levels (low, medium and high temperature):

- acids production reaction (called Bunsen, exothermic at 293-393 K):

$$2H_2O + I_2 + SO_2 \rightarrow H_2SO_4 + 2HI$$

- decomposition of HI (endothermic at 573-773 K):

$$2HI \rightarrow I_2 + H_2$$

- Sulfuric acid decomposition (endothermic at 1073-1173 K):

$$H_2SO_4 \rightarrow H_2O + SO_2 + \frac{1}{2}O_2$$

In Figure B.1 the process scheme provided by Liberatore et al. [2012] for a S-I cycle powered by Solar energy is reported.

Since the H_2SO_4 dissociation requires heat at high temperatures, a solar tower central receiver can be suitable to provide the energy for the reactor.

The produced SO_2 is sent to the Bunsen section in a reactor containing iodine and water to obtain a two-phases liquid stream as output: H_2SO_4-rich light phase and a heavier phase containing the produced HI. The heavy phase, constituted of HI, H_2O and a large quantity of I_2 is treated in a decomposition section (HI decomposition) where, after a purification step necessary to remove the I_2 , the H_2 is produced . The H_2SO_4 phase, instead, after purification and concentration, is sent to the H_2SO_4 decomposition reactor.

The hydrogen production continuity, in spite of the solar source intermittence, is ensured by the SO_2 storage set downstream the solar receiver.

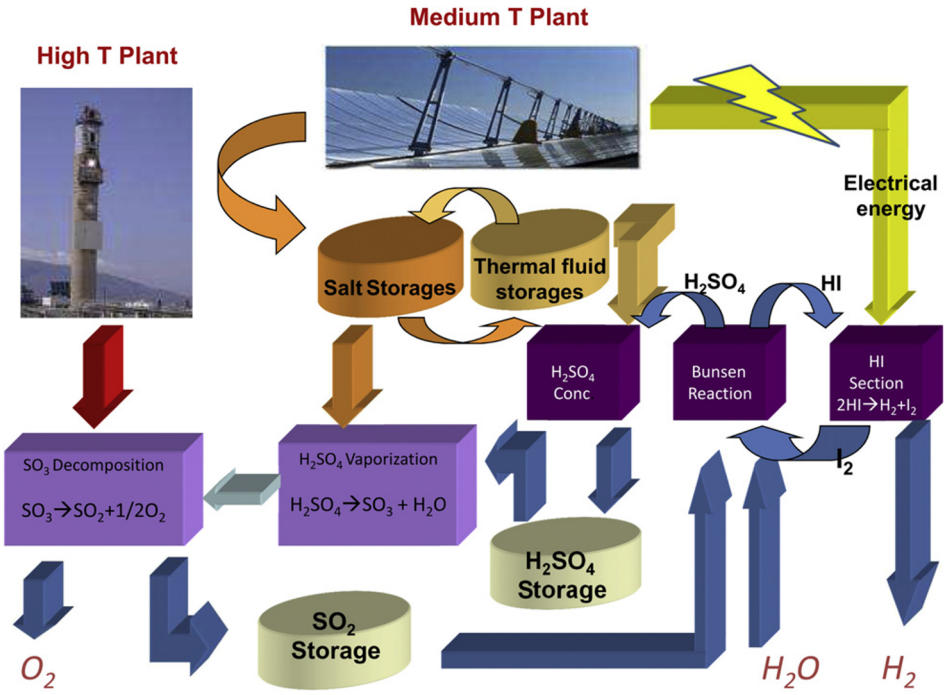

Figure B.1: *Base scheme of the SI cycle fed by two different solar technologies.*

Through the H_2SO_4 storage, indeed, it is possible to mismatch the high-temperature H_2SO_4 decomposition from the lower-temperature hydrogen production. In the scheme proposed in Figure B.1, in fact, the use of two solar plants is considered: a solar central tower plant and a solar trough plant with a molten salt storage system working at indicative maximum temperatures of 1200 K and 823 K, respectively.

Bibliography

Aalto-University. Consistent model for water and charge transport over membrane in sulphur dioxide depolarized electrolyzer conditions, 2014. URL `https://sol2hy2.eucoord.com/Deliverables/body.pe`.

Haznan Abimanyu, Kwang-Deog Jung, Ki-Won Jun, Jinsoo Kim, and Kye Sang Yoo. Preparation and characterization of fe/cu/al2o3 composite granules for so3 decomposition to assist hydrogen production. *Applied Catalysis A: General*, 343(1):134–141, 2008.

altenergymag. The history of hydrogen, 2009. URL `http://www.altenergymag.com`.

Jessica L Anderson, JaNeille K Dixon, Edward J Maginn, and Joan F Brennecke. Measurement of so2 solubility in ionic liquids. *The Journal of Physical Chemistry B*, 110(31):15059–15062, 2006.

Renato A Antunes, Mara CL De Oliveira, Gerhard Ett, and Volkmar Ett. Carbon materials in composite bipolar plates for polymer electrolyte membrane fuel cells: A review of the main challenges to improve electrical performance. *Journal of Power Sources*, 196(6):2945–2961, 2011.

ArchimedeSolarEnergy. Parabolic trough, 2017. URL `www.archimedesolarenergy.it`.

DC Astholz, K Glänzer, and J Troe. The spin-forbidden dissociation-recombination reaction so3->so2+o. *The Journal of Chemical Physics*, 70(5):2409–2413, 1979.

Ian Atkin, Rachael H Elder, Geoffrey H Priestman, Derek C Sinclair, and Raymond WK Allen. High temperature oxygen separation for the sulphur family of thermochemical cycles-part i: Membrane selection and flux testing. *international journal of hydrogen energy*, 36(17):10614–10625, 2011.

AM Banerjee, MR Pai, K Bhattacharya, AK Tripathi, VS Kamble, SR Bharadwaj, and SK Kulshreshtha. Catalytic decomposition of sulfuric acid on mixed cr/fe oxide samples and its application in sulfur-iodine cycle for hydrogen production. *International Journal of Hydrogen Energy*, 33(1):319–326, 2008.

Vincenzo Barbarossa, Sergio Brutti, M Diamanti, S Sau, and Giovanni De Maria. Catalytic thermal decomposition of sulphuric acid in sulphur-iodine cycle for hydrogen production. *International journal of hydrogen energy*, 31(7):883–890, 2006.

S.Z. Baykara. Experimental solar water thermolysis. *International Journal of Hydrogen Energy*, 29(14):1459 – 1469, 2004.

G.E Beghi. A decade of research on thermochemical hydrogen at the joint research centre, ispra. *International Journal of Hydrogen Energy*, 11(12): 761 – 771, 1986.

A. Bosen and H. Engels. Description of the phase equilibrium of sulfuric acid with the nrtl equation and a solvation model in a wide concentration and temperature range. *Fluid Phase Equilibria*, 43(2-3):213–230, 1988.

Nicolas Bayer Botero, Dennis Thomey, Alejandro Guerra Niehoff, Martin Roeb, Christian Sattler, and Robert Pitz-Paal. Modelling and scaling analysis of a solar reactor for sulphuric acid cracking in a hybrid sulphur cycle process for thermochemical hydrogen production. *International Journal of Hydrogen Energy*, 41(19):8008–8019, 2016.

LE Brecher, S Spewock, and CJ Warde. The westinghouse sulfur cycle for the thermochemical decomposition of water. *International Journal of Hydrogen Energy*, 2(1):7–15, 1977.

Lee E Brecher and Christopher K Wu. Electrolytic decomposition of water, June 1975. US Patent 3,888,750.

RD Brittain and DL Hildenbrand. Catalytic decomposition of gaseous so3. *J. Phys. Chem.;(United States)*, 87(19), 1983.

Lloyd C Brown, Gottfried E Besenbruch, RD Lentsch, Ken R Schultz, JF Funk, PS Pickard, AC Marshall, and SK Showalter. High efficiency generation of hydrogen fuels using nuclear power. *General Atomics Report GA-A24285*, page Q4, 2003.

S Brutti, L Bencivenni, G De Maria, V Barbarossa, S Sau, and D Diamanti. Gas phase dissociation of sulfuric acid. *The Journal of Chemical Thermodynamics*, (38):1292–1300, 2006.

Sergio Brutti, Giovanni De Maria, Giovanni Cerri, Ambra Giovannelli, Bruno Brunetti, Patrizia Cafarelli, Elvio Semprin, Vincenzo Barbarossa, and Antonio Ceroli. Decomposition of h2so4 by direct solar radiation. *Industrial & Engineering Chemistry Research*, 46(20):6393–6400, 2007.

Dicle Celik and Meltem Yildiz. Investigation of hydrogen production methods in accordance with green chemistry principles. *International Journal of Hydrogen Energy*, 2017.

Ching Chue Chan. The state of the art of electric, hybrid, and fuel cell vehicles. *Proceedings of the IEEE*, 95(4):704–718, 2007.

Patrice Charvin, Abanades Stéphane, Lemort Florent, and Flamant Gilles. Analysis of solar chemical processes for hydrogen production from water splitting thermochemical cycles. *Energy Conversion and Management*, 49 (6):1547–1556, 2008.

ChemicalEngineeringOnline. Economic indicators, 2016. URL `http://www.chemengonline.com`.

chemistryexplained. Hydrogen, 2017. URL `http://www.chemistryexplained.com/elements/C-K/Hydrogen.html`.

Kaihong Chen, Wenjun Lin, Xini Yu, Xiaoyan Luo, Fang Ding, Xi He, Haoran Li, and Congmin Wang. Designing of anion-functionalized ionic liquids for efficient capture of so2 from flue gas. *AIChE Journal*, 61(6):2028–2034, 2015.

Hector R. Colon-Mercado and David T. Hobbs. Catalyst evaluation for a sulfur dioxide-depolarized electrolyzer. *Electrochemistry Communications*, 9(11):2649–2653, 2007. ISSN 1388-2481. doi: http://dx.doi.org/10.1016/j.elecom.2007.08.015.

Claudio Corgnale and William A Summers. Solar hydrogen production by the hybrid sulfur process. *International Journal of Hydrogen Energy*, 36 (18):11604–11619, 2011.

DP Davies, PL Adcock, M Turpin, and SJ Rowen. Stainless steel as a bipolar plate material for solid polymer fuel cells. *Journal of power sources*, 86(1): 237–242, 2000.

Ibrahim Dincer and Canan Acar. Review and evaluation of hydrogen production methods for better sustainability. *International journal of hydrogen energy*, 40(34):11094–11111, 2015.

ENEA. Idrogeno energia del futuro. Opuscolo online, 2003. URL `http://www.infea.basilicata.it/op23.pdf`.

energy.gov. Hydrogen production:thermochemical water splitting, 2017a. URL `https://energy.gov`.

energy.gov. Maricopa solar power dish plant, 2017b. URL `https://energy.gov`.

eniscuola. Utilizzi dell'idrogeno, 2011. URL `http://www.eniscuola.net/Home/Energia/Idrogeno`.

FCH-JU. Multi annual work plan 2014-2020, 2014.

MM Gasik, J Virtanen, and A Santasalo-Aarnio. Improved operation of so2 depolarized electrolyser stack for h2 production at ambient conditions. *International Journal of Hydrogen Energy*, 42(19):13407–13414, 2017.

Fred Gelbard, James C Andazola, Gerald E Naranjo, Carlos E Velasquez, and Andrew R Reay. High pressure sulfuric acid decomposition experiments for the sulfur-iodine thermochemical cycle. 2005.

A. Giaconia, L. Turchetti, G. Monteleone, B. Morico, G. Iaquaniello, K. Shabtai, M. Sheintuch, D. Boettge, J. Adler, V. Palma, S. Voutetakis, A. Lemonidou, M.C. Annesini, M. Den Exter, and H. Balzer. Development of a solar-powered, fuel-flexible compact steam reformer: The comethy project. *Chemical Engineering Transactions*, 35:433–438, 2013. cited By 14.

Alberto Giaconia, Salvatore Sau, Claudio Felici, Pietro Tarquini, George Karagiannakis, Chrysoula Pagkoura, Christos Agrafiotis, Athanasios G Konstandopoulos, Dennis Thomey, Lamark de Oliveira, et al. Hydrogen production via sulfur-based thermochemical cycles: Part 2: performance evaluation of fe2o3-based catalysts for the sulfuric acid decomposition step. *International journal of hydrogen energy*, 36(11):6496–6509, 2011.

Daniel M Ginosar, Harry W Rollins, Lucia M Petkovic, Kyle C Burch, and Michael J Rush. High-temperature sulfuric acid decomposition over complex metal oxide catalysts. *International journal of hydrogen energy*, 34 (9):4065–4073, 2009.

John Irving Gmitro and Theodore Vermeulen. Vapor-liquid equilibria for aqueous sulfuric acid. *AIChE Journal*, 10(5):740–746, 1964.

Maximilian B Gorensek. Hybrid sulfur cycle flowsheets for hydrogen production using high-temperature gas-cooled reactors. *international journal of hydrogen energy*, 36(20):12725–12741, 2011.

Maximilian B. Gorensek, John A. Staser, Thomas G. Stanford, and John W. Weidner. A thermodynamic analysis of the so2/h2so4 system in so2-depolarized electrolysis. *International Journal of Hydrogen Energy*, 34 (15):6089–6095, 2009.

V. M. H. Govindarao and K. V. Gopalakrishna. Solubility of sulfur dioxide at low partial pressures in dilute sulfuric acid solutions. *Industrial and Engineering Chemistry Research*, 32(9):2111–2117, 1993.

Engin Gürtekin. Biological hydrogen production methods. *Department of Environmental Engineering Firat University, Turkey, Akademic Platform*, 2014.

C. Hanson and K. L Butcher. Miscibility of liquid sulphur dioxide and water. *Chemistry and Industry*, pages 1509–1510, 1957.

Walter Hayduk, Haruki Asatani, and Benjamin C. Y. Lu. Solubility of sulfur dioxide in aqueous sulfuric acid solutions. *Journal of Chemical and Engineering Data*, 33(4):506–509, 1988.

Guanghu He, Rachael H Elder, Derek C Sinclair, and Ray WK Allen. High temperature oxygen separation for the sulphur family of thermochemical cycles-part ii: Sulphur poisoning and membrane performance recovery. *International Journal of Hydrogen Energy*, 38(2):785–794, 2013.

Jun Huang, Anders Riisager, Peter Wasserscheid, and Rasmus Fehrmann. Reversible physical absorption of so2 by ionic liquids. *Chemical Communications*, (38):4027–4029, 2006.

Jun Huang, Anders Riisager, Rolf W Berg, and Rasmus Fehrmann. Tuning ionic liquids for high gas solubility and reversible gas sorption. *Journal of Molecular Catalysis A: Chemical*, 279(2):170–176, 2008.

Kuan Huang, Xiao-Min Zhang, Ya-Xin Li, You-Ting Wu, and Xing-Bang Hu. Facilitated separation of co2 and so2 through supported liquid membranes using carboxylate-based ionic liquids. *Journal of Membrane Science*, 471 (0):227 – 236, 2014.

Ilsole24ore. Finanza & mercati, 2016. URL `http://www.ilsole24ore.com`.

H Ishikawa, E Ishii, I Uehara, and M Nakane. Catalyzed thermal decompositon of h2so4 and production of hbr by the reaction of so2 with br2 and h2o. *International Journal of Hydrogen Energy*, 7(3):237–246, 1982.

Py Jean-Pierre and Capitaine Alain. Hydrogen production by high temperature electrolysis of water vapour and nuclear reactors. *World Hydrogen Energy Conference; Lyon (France)*, 2006.

Ying-Ying Jiang, Zheng Zhou, Zhen Jiao, Lei Li, You-Ting Wu, and Zhi-Bing Zhang. So2 gas separation using supported ionic liquid membranes. *The Journal of Physical Chemistry B*, 111(19):5058–5061, 2007.

Meijin Jin, Yucui Hou, Weize Wu, Shuhang Ren, Shidong Tian, Li Xiao, and Zhigang Lei. Solubilities and thermodynamic properties of so2 in ionic liquids. *The Journal of Physical Chemistry B*, 115(20):6585–6591, 2011.

George Karagiannakis, Christos C Agrafiotis, Alexandra Zygogianni, Chrysoula Pagkoura, and Athanasios G Konstandopoulos. Hydrogen production via sulfur-based thermochemical cycles: Part 1: Synthesis and evaluation of metal oxide-based candidate catalyst powders for the sulfuric acid decomposition step. *International journal of hydrogen energy*, 36 (4):2831–2844, 2011.

George Karagiannakis, Christos C Agrafiotis, Chrysoula Pagkoura, Athanasios G Konstandopoulos, Dennis Thomey, Lamark de Oliveira, Martin Roeb, and Christian Sattler. Hydrogen production via sulfur-based thermochemical cycles: Part 3: Durability and post-characterization of silicon carbide honeycomb substrates coated with metal oxide-based candidate catalysts for the sulfuric acid decomposition step. *International journal of hydrogen energy*, 37(10):8190–8203, 2012.

Donald Q. Kern. *PROCESS HEAT TRANFER*. McGRAW-HILL INTERNATIONAL BOOK COMPANY, 1950.

Chang Soo Kim, Gyeong Taek Gong, Kye Sang Yoo, Honggon Kim, Byoung Gwon Lee, Byoung Sung Ahn, Kwang Deog Jung, Ki Yong Lee, and Kwang Ho Song. Novel separation process of gaseous mixture of so2 and o2 with ionic liquid for hydrogen production in thermochemical sulfur-iodine water splitting cycle. 2007.

Chang Soo Kim, Ki Yong Lee, Gyeong Taek Gong, Honggon Kim, Byung Gwon Lee, and Gwang-Deog Jung. Sulfur dioxide separation and recovery with ionic liquid absorbents. In *The 2008 Annual Meeting*, 2008.

Tatsuya Kodama and Nobuyuki Gokon. Thermochemical cycles for high-temperature solar hydrogen production. *Chemical reviews*, 107(10):4048–4077, 2007.

VN Kovalev, VE Soroko, AF Petropavlovskii, and EV Vasko. Catalytic decomposition of sulfur (vi) oxide under elevated pressure, 1986.

VN Kovalev, AV Forsov, VE Soroko, and NV Kuzovkina. Estimate of the lifetime of catalysts based on chromium (iii) oxide and chromites in gaseous media containing sulfur oxides and oxygen. *Journal of applied chemistry of the USSR*, 64(1):175–177, 1991.

R.J Kriek, J Rossmeisl, S Siahrostamib, and M.E Björketun. H2 production through electro-oxidation of so2: identifying the fundamental limitations. *Physical Chemistry Chemical Physics*, (20), 2014.

Jorg Krissmann, M. Aslam Siddiqi, and Lucas Klaus. Thermodynamics of so2 absorption in aqueous solutions. *Chemical Engineering and Technology*, 21(8):641–644, 1998.

Donald L Kuehne and Sheldon K Friedlander. Selective transport of sulfur dioxide through polymer membranes. 1. polyacrylate and cellulose triacetate single-layer membranes. *Industrial & Engineering Chemistry Process Design and Development*, 19(4):609–623, 1980.

J.H Kwak, Y Wang, D.M Ginosar, and L.M Petkovic. Catalytic decomposition of sulfuric acid on silicon carbides for sulfur-based thermochemical water splitting cycles. *ACS National Meeting Book of Abstracts*, (232):1, 2006.

Samir Lamouri, Mohamed Hamidouche, Noureddine Bouaouadja, Houcine Belhouchet, Vincent Garnier, Gilbert Fantozzi, and Jean François Trelkat. Control of the γ-alumina to α-alumina phase transformation for an optimized alumina densification. *Boletin de la Sociedad Española de Ceramica y Vidrio*, 56(2):47 – 54, 2017.

Ki Yong Lee, Gyeong Taek Gong, Kwang Ho Song, Honggon Kim, Kwang-Deog Jung, and Chang Soo Kim. Use of ionic liquids as absorbents to separate so2-o2 in thermochemical processes to produce hydrogen. *International Journal of Hydrogen Energy*, 33(21):6031–6036, 2008.

Seoung Young Lee, Heon Jung, Won Joo Kim, Yong Gun Shul, and Kwang-Deog Jung. Sulfuric acid decomposition on pt/sic-coated-alumina catalysts for si cycle hydrogen production. *International Journal of Hydrogen Energy*, 38(14):6205–6209, 2013.

Shuo-Jen Lee, Jian-Jang Lai, and Ching-Han Huang. Stainless steel bipolar plates. *Journal of Power Sources*, 145(2):362–368, 2005.

C Legros, C Carry, P Bowen, and H Hofmann. Sintering of a transition alumina: effects of phase transformation, powder characteristics and thermal cycle. *Journal of the European Ceramic Society*, 19(11):1967–1978, 1999.

Zhigang Lei, Chengna Dai, and Biaohua Chen. Gas solubility in ionic liquids. *Chemical reviews*, 114(2):1289–1326, 2013.

Xiaoshan Li, Liqi Zhang, Ying Zheng, and Chuguang Zheng. So2 absorption performance enhancement by ionic liquid supported on mesoporous molecular sieve. *Energy & Fuels*, 2015.

R. Liberatore, M. Lanchi, and L Turchetti. Hydrogen production by the solar-powered hybrid sulfur process: Analysis of the integration of the csp and chemical plants in selected scenarios. volume 1734, 2016. doi: 10.1063/1.4949208.

Raffaele Liberatore, Michela Lanchi, Alberto Giaconia, and Pietro Tarquini. Energy and economic assessment of an industrial plant for the hydrogen production by water-splitting through the sulfur-iodine thermochemical cycle powered by concentrated solar energy. *International journal of hydrogen energy*, 37(12):9550–9565, 2012.

Raffaele Liberatore, Mariarosaria Ferrara, Michela Lanchi, and Luca Turchetti. Integration of photovoltaic and concentrated solar thermal technologies for h2 production by the hybrid sulfur cycle. In *AIP Conference Proceedings*, volume 1850, page 100013. AIP Publishing, 2017.

SS Lin and R Flaherty. Design studies of the sulfur trioxide decomposition reactor for the sulfur cycle hydrogen production process. *International journal of hydrogen energy*, 8(8):589–596, 1983.

Anu Lokkiluoto and Michael M Gasik. Modeling and experimental assessment of nafion membrane properties used in so2 depolarized water electrolysis for hydrogen production. *International Journal of Hydrogen Energy*, 38(1):10–19, 2013.

Anu Lokkiluoto, Pekka A Taskinen, Michael Gasik, Ilkka V Kojo, Heljä Peltola, Michael H Barker, and Karl-Heinz Kleifges. Novel process concept for the production of h2 and h2so4 by so2-depolarized electrolysis. *Environment, development and sustainability*, 14(4):529–540, 2012.

Douglas K Louie. *Handbook of sulphuric acid manufacturing*. DKL Engineering,Inc., 2005.

P.W.T. Lu. Technological aspects of sulfur dioxide depolarized electrolysis for hydrogen production. *International Journal of Hydrogen Energy*, 8(10): 773 – 781, 1983.

P.W.T. Lu and R.L. Ammon. Sulfur dioxide depolarized electrolysis for hydrogen production: Development status. *International Journal of Hydrogen Energy*, 7(7):563–575, 1982. cited By 27.

Patricia Luis, LA Neves, CAM Afonso, IM Coelhoso, JG Crespo, A Garea, and A Irabien. Facilitated transport of co2 and so2 through supported ionic liquid membranes (silms). *Desalination*, 245(1):485–493, 2009.

Eckhard Lüpfert. *Der Einfluss konzentrierter Solarstrahlung auf die Reaktionsgeschwindigkeit der Abfallschwefelsäure-Spaltung*. PhD thesis, 1996.

Fanhua Ma, Nashay Naeve, Mingyue Wang, Long Jiang, Renzhe Chen, and Shuli Zhao. Hydrogen-enriched compressed natural gas as a fuel for engines. In *Natural Gas*. InTech, 2010.

Carol E. Maass and O. Maass. Sulfur dioxide and its aqueous solutions. i. analytical methods, vapor density and vapor pressure of sulfur dioxide. vapor pressure and concentrations of the solutions. *Journal of the American Chemical Society*, 50(5):1352–1368, 1928.

A Maccari, S Donnola, F Matino, and S Tamano. Archimede solar energy molten salt parabolic trough demo plant: Improvements and second year of operation. *AIP Conference Proceedings*, (1734):100007, 2016.

Paul M Mathias and Lloyd C Brown. Thermodynamics of the sulfur-iodine cycle for thermochemical hydrogen production. *68th Annual Meeting of the Society of Chemical Engineers*, 2003.

Kenneth A Mauritz and Robert B Moore. State of understanding of nafion. *Chemical reviews*, 104(10):4535–4586, 2004.

M.K. Mondal. Experimental determination of dissociation constant, henry's constant, heat of reactions, so2 absorbed and gas bubble-liquid interfacial area for dilute sulphur dioxide absorption into water. *Fluid Phase Equilibria*, (253(2)):98–107, 2007.

M Moritz. Biological methods for obtaining hydrogen. *Chemik*, 66(827):e34, 2012.

Yoshiharu Mukouyama, Mitsunobu Kikuchi, and Hiroshi Okamoto. Appearance of new potential oscillation during hydrogen evolution reaction by addition of na2so4 and k2so4. *Journal of Electroanalytical Chemistry*, 617 (2):179 – 184, 2008.

H Müller. Production from elementar sulfur. *Ullmann's Encyclopedia of industrial chemistry*, pages 77–81, 2012.

Alejandro Guerra Niehoff, Dennis Thomey, Moises A Romero Gonzales, Hans-Peter Streber, Justin Lapp, Martin Roeb, Christian Sattler, and Robert Pitz-Paal. Thermodynamic model of a solar receiver for superheating of sulfur trioxide and steam at pilot plant scale. In *ASME 2016 10th International Conference on Energy Sustainability collocated with the ASME 2016 Power Conference and the ASME 2016 14th International Conference on Fuel Cell Science, Engineering and Technology*, pages V001T10A001–V001T10A001. American Society of Mechanical Engineers, 2016.

N.I.S.T. N.i.s.t chemistry webbook, 2011.

Adam Noglik, Martin Roeb, Christian Sattler, and Robert Pitz-Paal. Experimental study on sulfur trioxide decomposition in a volumetric solar receiver-reactor. *International Journal of Energy Research*, 33(9):799–812, 2009.

JH Norman, GE Besenbruch, LC Brown, DR O'keefe, and CL Allen. Thermochemical water-splitting cycle, bench-scale investigations, and process engineering. Final report, GA Technologies, Inc., San Diego, CA (USA), February 1977-December 31, 1981 1982.

J.A. O'Brien, J.T. Hinkley, S.W. Donne, and S-E. Lindquist. The electrochemical oxidation of aqueous sulfur dioxide: A critical review of work with respect to the hybrid sulfur cycle. *Electrochimica Acta*, 55(3):573 – 591, 2010.

Outotec. Luro2 sulfur burner. *www.outotec.com*, 2013.

Max Stone Peters, Klaus D Timmerhaus, and Ronald E West. *Plant Design and Economics for Chemical Engineers*, volume 4. McGraw-Hill, 2002.

Robert Pitz-Paal, Jürgen Dersch, Barbara Milow, Félix Téllez, Alain Ferriere, Ulrich Langnickel, Aldo Steinfeld, Jacob Karni, Eduardo Zarza, and Oleg Popel. Development steps for parabolic trough solar power technologies with maximum impact on cost reduction. *Journal of Solar Energy Engineering*, 129(4):371–377, 2007.

Bruce E. Poling, Daniel G. Friend, Richard R. Rowley, W. Vincent Wilding, and George H. Thomson. *Perry's Chemical Engineers' Handbook*. McGraw-Hill Companies, 2007.

C Quijada, E Morallón, J.L Vázquez, and L.E.A Berlouis. Electrochemical behaviour of aqueous so2 at polycrystalline gold electrodes in acidic media. a voltammetric and in-situ vibrational study. part ii. oxidation of so2 on bare and sulphur-modified electrodes. *Electrochimica Acta*, 46(5):651–659, 2000.

Allen E Rabe and John F Harris. Vapor liquid equilibrium data for the binary system sulfur dioxide. *Journal of Chemical and Engineering Data*, 8(3):333–336, 1963.

Samuel Liversage Rabie. *SO2 and O2 separation by using ionic liquid absorption*. PhD thesis, North-West University, 2012.

Sergey N Rashkeev, Daniel M Ginosar, Lucia M Petkovic, and Helen H Farrell. Catalytic activity of supported metal particles for sulfuric acid decomposition reaction. *Catalysis today*, 139(4):291–298, 2009.

Shuhang Ren, Yucui Hou, Weize Wu, Qingya Liu, Yunfei Xiao, and Xiaoting Chen. Properties of ionic liquids absorbing so2 and the mechanism of the absorption. *The Journal of Physical Chemistry B*, 114(6):2175–2179, 2010.

Trygve Riis, Elisabet F Hagen, Preben JS Vie, and O Ulleberg. Hydrogen production and storage. *International energy agency technical report*, 2006.

Martin Roeb, Dennis Thomey, Lamark de Oliveira, Christian Sattler, G Fleury, F Pra, P Tochon, A Brevet, G Roux, N Gruet, et al. Sulphur based thermochemical cycles: Development and assessment of key components of the process. *International journal of hydrogen energy*, 38 (14):6197–6204, 2013.

M. Romero and A. Steinfeld. Concentrating solar thermal power and thermochemical fuels. *Energy and Environmental Science*, 5(11):9234–9245, 2012. cited By 144.

Moises Romero, Dennis Thomey, Jan-Peter Säck, Stefan Breuer, Martin Roeb, and Christian Sattler. Joule boosted sulphuric acid compact heat exchanger for solar h2 production. 2014.

E Ruberti. Idrogeno energia per il futuro. *Le Scienze*, 33:385, 2000.

B Rumpf and G Maurer. Solubilities of hydrogen cyanide and sulfur dioxide in water at temperatures from 293.15 to 413.15 k and pressures up to 2.5 mpa. *Fluid Phase Equilibria*, 81:241–260, 1992.

Hino Ryutaro, Yan Xing L, et al. Nuclear hydrogen production handbook, 2011.

Stanley I Sandler. *Chemical, Biochemical and Engineering Thermodynamics*. John Wiley and Sons, 2005.

A Santasalo-Aarnio, A Lokkiluoto, J Virtanen, and MM Gasik. Performance of electrocatalytic gold coating on bipolar plates for so2 depolarized electrolyser. *Journal of Power Sources*, 306:1–7, 2016a.

A Santasalo-Aarnio, J Virtanen, and M Gasik. So2 carry-over and sulphur formation in a so2-depolarized electrolyser. *Journal of Solid State Electrochemistry*, 20(6):1655–1663, 2016b.

Sargent and Lundy LLC Consulting Group. Assessment of parabolic trough and power tower solar technology cost and performance forecasts. Technical report, National Renewable Energy Laboratory., 2003.

S Sau, N Corsaro, T Crescenzi, C D'Ottavi, R Liberatore, S Licoccia, V Russo, P Tarquini, and A.C Tizzoni. Techno-economic comparison between csp plants presenting two di erent heat transfer fluids. *Applied Energy*, 68:96–109, 2016.

Salvatore Sau, Mariarosaria Ferrara, Anna Chiara Tizzoni, and Natale Corsaro. Stability test of catalyst for sac, 2015. URL `https://sol2hy2.eucoord.com/Deliverables/body.pe`.

Dominique Schwartz, Roger Gadiou, Jean-François Brilhac, Gilles Prado, and Ginès Martinez. A kinetic study of the decomposition of spent sulfuric acids at high temperature. *Industrial & engineering chemistry research*, 39 (7):2183–2189, 2000.

JA Serfass, D Nahmias, and AJ Appleby. A practical hydrogen development strategy. *International journal of hydrogen energy*, 16(8):551–556, 1991.

Ying Shang, Hongping Li, Suojiang Zhang, Hui Xu, Zanxia Wang, Li Zhang, and Jianmin Zhang. Guanidinium-based ionic liquids for sulfur dioxide sorption. *Chemical Engineering Journal*, 175:324–329, 2011.

Matthew S Shannon, Adam Christopher Irvin, Haining Liu, Joshua Moon, Michelle Sinclair Hindman, C Heath Turner, and Jason E Bara. Chemical and physical absorption of so2 by n-functionalized imidazoles: Experimental results and molecular-level insight. *Industrial & Engineering Chemistry Research*, 2014.

Andrew C Shaw, Moises A Romero, Rachael H Elder, Bruce CR Ewan, and Ray WK Allen. Measurements of the solubility of sulphur dioxide in water for the sulphur family of thermochemical cycles. *International Journal of Hydrogen Energy*, 36(8):4749–4756, 2011.

Mark B Shiflett and A Yokozeki. Chemical absorption of sulfur dioxide in room-temperature ionic liquids. *Industrial & Engineering Chemistry Research*, 49(3):1370–1377, 2009.

Youngjoon Shin, Heesung Shin, Kiyoung Lee, Jonghwa Chang, and Yongwan Kim. A hybrid-sulfur flowsheet using an ionic liquid absorbent to separate sulfur dioxide from oxygen. *Energy Procedia*, 29:576–584, 2012.

sol2hy2.eucoord. General project information, 2017. URL `https://sol2hy2.eucoord.com`.

SolarThermalMagazine. Gemasolar concentrated solar thermal power plant, 2017. URL `http://www.solarthermalmagazine.com`.

B.C Spall. Phase equilibria in the system sulphur dioxide-water from 25-300°c. *The Canadian Journal of Chemical Engineering*, 41(2):79–83, 1963.

J.A. Staser and J.W. Weidner. Effect of water transport on the production of hydrogen and sulfuric acid in a pem electrolyzer. *Journal of the Electrochemical Society*, 156(1):B16–B21, 2009.

Simon Stone, Clark McPheeters, John Staser, Jai V Jayakumar, and John W Weidner. Gas-phase hybrid sulfur electrolyzer stack. *ECS Transactions*, 35(37):23–33, 2011.

Albert Stwertka. *A Guide to the Elements*. Oxford University Press, 2002.

W. A. Summers. In *Proceedings of DOE Hydrogen Program 2008 Annual Merit Review, Arlington, VA,June 12th*, June 12th 2008.

Hiroaki Tagawa and Takayuki Endo. Catalytic decomposition of sulfuric acid using metal oxides as the oxygen generating reaction in thermochemical water splitting process. *International Journal of Hydrogen Energy*, 14(1): 11–17, 1989.

Dennis Thomey, Lamark de Oliveira, Jan-Peter Säck, Martin Roeb, and Christian Sattler. Development and test of a solar reactor for decomposition of sulphuric acid in thermochemical hydrogen production. *International Journal of Hydrogen Energy*, 37(21):16615–16622, 2012.

Dennis Thomey, Hans-Peter Streber, Alejandro Guerra-Niehoff, Moises Romero, Justin Lapp, Martin Roeb, and Christian Sattler. Development and test operation of a demonstration plant for sulfuric acid splitting at the dlr concentrating solar power tower facility. In *2016 AIChE Annual Meeting Proceeding*, 2016.

Shidong Tian, Yucui Hou, Weize Wu, Shuhang Ren, and Jianguo Qian. Absorption of so2 at high temperatures by ionic liquids and the absorption mechanism. *Bull. Korean Chem. Soc*, 35(9):2791, 2014.

L Turchetti, MA Murmura, G Monteleone, A Giaconia, AA Lemonidou, SD Angeli, V Palma, C Ruocco, and MC Annesini. Kinetic assessment of ni-based catalysts in low-temperature methane/biogas steam reforming. *International Journal of Hydrogen Energy*, 41(38):16865–16877, 2016.

Luca Turchetti, Raffaele Liberatore, Salvatore Sau, and Anna Chiara Tizzoni. Carbon-free production of hydrogen via the solar powered hybrid sulfur cycle: the sol2hy2 project. *CHEMICAL ENGINEERING*, 43:2179–2184, 2015.

Evangelos Tzimas, C Filiou, SD Peteves, and JB Veyret. Hydrogen storage: state-of-the-art and future perspective. *EU Commission, JRC Petten, EUR 20995EN*, 2003.

Congmin Wang, Guokai Cui, Xiaoyan Luo, Yingjie Xu, Haoran Li, and Sheng Dai. Highly efficient and reversible so2 capture by tunable azole-based ionic liquids through multiple-site chemical absorption. *Journal of the American Chemical Society*, 133(31):11916–11919, 2011.

Weize Wu, Buxing Han, Haixiang Gao, Zhimin Liu, Tao Jiang, and Jun Huang. Desulfurization of flue gas: So2 absorption by an ionic liquid. *Angewandte Chemie International Edition*, 43(18):2415–2417, 2004.

Wuster. *Wuster's PhD thesis*. Phd thesis, University of Aachen, 1979.

Lulu Xue, Ping Zhang, Songzhe Chen, and Laijun Wang. Pt-based bimetallic catalysts for so2-depolarized electrolysis reaction in the hybrid sulfur process. *International Journal of Hydrogen Energy*, 39(26):14196–14203, 2014.

Hui Yang, Yanwei Zhang, Junhu Zhou, Zhihua Wang, Jianzhong Liu, and Kefa Cen. Study on cuo-ceo2/sic catalysts in the sulfur iodine cycle for hydrogen production. *International Journal of Energy Research*, 2016.

Ayten Yilmaz, Lusi Hindiyarti, Anker D Jensen, Peter Glarborg, and Paul Marshall. Thermal dissociation of so3 at 1000- 1400 k. *The Journal of Physical Chemistry A*, 110(21):6654–6659, 2006.

A Yokozeki and Mark B Shiflett. Separation of carbon dioxide and sulfur dioxide gases using room-temperature ionic liquid [hmim][tf2n]. *Energy & Fuels*, 23(9):4701–4708, 2009.

Xiao Liang Yuan, Suo Jiang Zhang, and Xing Mei Lu. Hydroxyl ammonium ionic liquids: synthesis, properties, and solubility of so2. *Journal of Chemical & Engineering Data*, 52(2):596–599, 2007.

Shaojuan Zeng, Hongshuai Gao, Xiaochun Zhang, Haifeng Dong, Xiangping Zhang, and Suojiang Zhang. Efficient and reversible capture of so2 by pyridinium-based ionic liquids. *Chemical Engineering Journal*, 251:248–256, 2014.

Qinglin Zhang, Hui Wang, Ivo G. Dalla Lana, and Karl T. Chuang. Solubility of sulfur dioxide in sulfuric acid of high concentration. *Industrial and Engineering Chemistry Research*, 37(3):1167–1172, 1998.

Yanwei Zhang, Hui Yang, Junhu Zhou, Zhihua Wang, Jianzhong Liu, and Kefa Cen. Catalytic decomposition of sulfuric acid over cuo/ceo 2 in the sulfur-iodine cycle for hydrogen production. *International Journal of Hydrogen Energy*, 40(5):2099–2106, 2015.

Nomenclature

CC:	Closed cycle
CSP:	Concentrating Solar Power
CST:	Concentrating Solar Thermal
DNI:	Direct Normal Irradiance
GBILs:	Guanidium Based Ionic Liquids
HT:	High Temperture
HyS:	Hybrid Sulfur
HyS:	Hybrid-Sulfur cycle
ILA:	Ionic Liquid Absorption
ILs:	Ionic Liquids
MT:	Medium Temperture
OC:	Open Cycle
PB:	Power Block
PES:	Polyethersulfone
PV:	PhotoVoltaic
PVDF:	Polyvinylidene fluoride
SA:	Sulfuric acid
SAC:	Sulfuric Acid Cracking
SDE:	Sulfur dioxide Depolaized Electrolysis

SF: Solar field

SILMs: Supported Ionic Liquid Membranes

SILP: Supported Ionic Liquid Phase

TSILs: Task Specific Ionic Liquids